ESL-TR-87-60

A COMPUTATIONAL METHOD FOR EVALUATING MODULAR PREFABRICATED STRUCTURAL ELEMENT FOR RAPID CON— STRUCTION OF FACILITIES, BARRIERS, AND REVETMENTS TO RESIST MODERN CONVENTIONAL WEAPONS EFFECTS

T. KRAUTHAMMER, S. SHAHRIAR

DEPARTMENT OF CIVIL AND MINERAL ENGINEERING
UNIVERSITY OF MINNESOTA
MINNEAPOLIS MN 55455

JULY 1988

FINAL REPORT

MARCH 1985 - SEPTEMBER 1987

APPROVED FOR PUBLIC RELEASE: DISTRIBUTION UNLIMITED

ENGINEERING & SERVICES LABORATORY
AIR FORCE ENGINEERING & SERVICES CENTER
TYNDALL AIR FORCE BASE, FLORIDA 32403

NOTICE

PLEASE DO NOT REQUEST COPIES OF THIS REPORT FROM HQ AFESC/RD (ENGINEERING AND SERVICES LABORATORY). ADDITIONAL COPIES MAY BE PURCHASED FROM:

NATIONAL TECHNICAL INFORMATION SERVICE
5285 PORT ROYAL ROAD
SPRINGFIELD, VIRGINIA 22161

FEDERAL GOVERNMENT AGENCIES AND THEIR CONTRACTORS REGISTERED WITH DEFENSE TECHNICAL INFORMATION CENTER SHOULD DIRECT REQUESTS FOR COPIES OF THIS REPORT TO:

DEFENSE TECHNICAL INFORMATION CENTER
CAMERON STATION
ALEXANDRIA, VIRGINIA 22314

NOTICE

PLEASE DO NOT REQUEST COPIES OF THIS REPORT FROM HQ AFESC/RD (ENGINEERING AND SERVICES LABORATORY). ADDITIONAL COPIES MAY BE PURCHASED FROM:

NATIONAL TECHNICAL INFORMATION SERVICE
5285 PORT ROYAL ROAD
SPRINGFIELD, VIRGINIA 22161

FEDERAL GOVERNMENT AGENCIES AND THEIR CONTRACTORS REGISTERED WITH DEFENSE TECHNICAL INFORMATION CENTER SHOULD DIRECT REQUESTS FOR COPIES OF THIS REPORT TO:

DEFENSE TECHNICAL INFORMATION CENTER
CAMERON STATION
ALEXANDRIA, VIRGINIA 22314

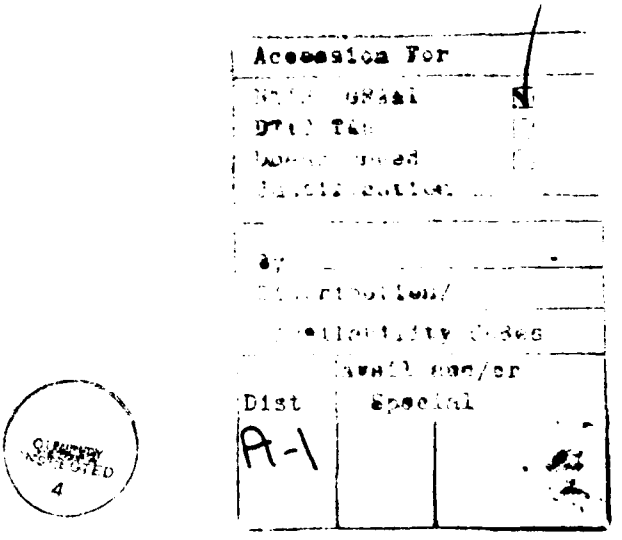

UNCLASSIFIED

SECURITY CLASSIFICATION OF THIS PAGE

REPORT DOCUMENTATION PAGE

Form Approved OMB No. 0704-0188

1a. REPORT SECURITY CLASSIFICATION UNCLASSIFIED	1b. RESTRICTIVE MARKINGS
2a. SECURITY CLASSIFICATION AUTHORITY	3. DISTRIBUTION/AVAILABILITY OF REPORT Approved For Public Release Distribution Unlimited
2b. DECLASSIFICATION/DOWNGRADING SCHEDULE	
4. PERFORMING ORGANIZATION REPORT NUMBER(S)	5. MONITORING ORGANIZATION REPORT NUMBER(S) ESL-TR-87-60
6a. NAME OF PERFORMING ORGANIZATION Department of Civil and Mineral Engineering 6b. OFFICE SYMBOL (If applicable)	7a. NAME OF MONITORING ORGANIZATION Air Force Engineering and Services Center (RDCS)
6c. ADDRESS (City, State, and ZIP Code) University of Minnesota Minneapolis, Minnesota 55455	7b. ADDRESS (City, State, and ZIP Code) HQ AFESC/RDCS Tyndall AFB FL 32403-6001
8a. NAME OF FUNDING/SPONSORING ORGANIZATION Air Force Engineering and Services Center 8b. OFFICE SYMBOL (If applicable) AFESC	9. PROCUREMENT INSTRUMENT IDENTIFICATION NUMBER F08637-85-J-0055
8c. ADDRESS (City, State, and ZIP Code)	10. SOURCE OF FUNDING NUMBERS PROGRAM ELEMENT NO. 62206F; PROJECT NO. 2673; TASK NO. 00; WORK UNIT ACCESSION NO. 39

11. TITLE (Include Security Classification) A Computational Method for Evaluating Modular Prefabricated Structural Element for Rapid Construction of Facilities, Barriers, and Revetments to Resist Modern Conventional Weapons Effects (Unclassified)

12. PERSONAL AUTHOR(S)
Krauthammer, Ted and Shahriar, Shahriar

13a. TYPE OF REPORT	13b. TIME COVERED	14. DATE OF REPORT (Year, Month, Day)	15. PAGE COUNT
Final Technical Report	FROM Mar 85 TO Sep 87	JULY 1988	263

16. SUPPLEMENTARY NOTATION
Availability of this report is specified on reverse of front cover

17. COSATI CODES			18. SUBJECT TERMS (Continue on reverse if necessary and identify by block number)
FIELD	GROUP	SUB-GROUP	
13	02		Protective Structures Weapons Effects Structural Analysis
13	13		

19. ABSTRACT (Continue on reverse if necessary and identify by block number)

The primary purpose of this investigation is to study the behavior of reinforced concrete (RC) structural systems including beams, beam-columns, and slabs subjected to severe localized loads in both the static and dynamic domains. The approach is specifically aimed towards the development of reliable, accurate, and efficient approximate models for predicting the response of RC structural elements in linear and nonlinear domains of behavior. The analytical procedure is based on accurate constitutive models for steel and concrete, principles of equilibrium and geometric compatibility, and rational failure criteria for the RC structural element. In the static domain, the analysis consist of the development of moment-curvature and load-deformation relationships, including, the effects of shear, axial thrust (P-Delta effect), and boundary conditions. A modified model is presented for evaluating the influence of shear in reducing the flexural capacity under static conditions. In the dynamic domain, an approximate evaluation of the response of RC members subjected to impulsive loads. Inelastic response, rate of loading, and the influence of boundary conditions are among the primary variables that are considered. (Continued)

20. DISTRIBUTION/AVAILABILITY OF ABSTRACT	21. ABSTRACT SECURITY CLASSIFICATION	
☐ UNCLASSIFIED/UNLIMITED ☐ SAME AS RPT. ☐ DTIC USERS		
22a. NAME OF RESPONSIBLE INDIVIDUAL Lt Britt Bowen	22b. TELEPHONE (Include Area Code) (904) 283-6225	22c. OFFICE SYMBOL HQ AFESC/RDCS

DD Form 1473, JUN 86 *Previous editions are obsolete.* SECURITY CLASSIFICATION OF THIS PAGE

19. (Continued) In order to verify the effectiveness of the present approach, 29 static cases and 8 dynamic cases are analyzed herein. In nearly all cases, the computed results compared well with the measured experimental data as reported in the literature. The entire numerical procedure is implemented on a personal computer for performing the lengthy computations.

PREFACE

This report was prepared by the University of Minnesota, Department of Civil and Mineral Engineering, Minneapolis, Minnesota, 55455, funded under Contract No FO8635-85-K-0055 by the Air Force Engineering and Services Center, Engineering and Services Laboratory, Tyndall AFB, Florida 32403.

This report summarizes the work done between March 1985 and September 1987. HQ AFESC/RD project officer was Lt. Britt Bowen. The primary investigator at the University of Minnesota was Dr Ted Krauthammer.

This report has been reviewed by the Public Affairs Officer (PA) and is releasable to the National Technical Information Service (NTIS). At NTIS, it will be available to the general public.

This technical report has been reviewed and is approved for publication.

Britt R Bowen
BRITT R. BOWEN, 1Lt, USAF
Project Officer

Robert J. Majka
ROBERT J. MAJKA, Lt Col, USAF
Chief, Engineering Research Division

William S. Strickland
WILLIAM S. STRICKLAND
Chief, Facility Systems and Analysis Branch

Lawrence D. Hokanson
LAWRENCE D. HOKANSON, Colonel, USAF
Director, Engineering and Services Laboratory

(The reverse of this page is blank.)

TABLE OF CONTENTS

TABLE OF CONTENTS
(Continued)

TABLE OF CONTENTS
(Concluded)

LIST OF TABLES

LIST OF FIGURES

LIST OF FIGURES
(continued)

LIST OF FIGURES
(Continued)

LIST OF FIGURES
(Continued)

LIST OF FIGURES
(Continued)

LIST OF FIGURES
(Continued)

LIST OF FIGURES
(Continued)

LIST OF FIGURES
(Concluded)

SECTION I
INTRODUCTION

A. OBJECTIVE

The objective of this investigation is to study the behavior of reinforced concrete structural systems including slabs, beams and beam-columns, subjected to localized loads in both the static and dynamic domains. The approach is specifically aimed to develop of reliable, accurate, and efficient models that can predict the resistance of reinforced concrete structural elements subjected to localized loads from onset of loading all the way to the failure of the element.

B. BACKGROUND

The design of reinforced concrete structural elements subjected to localized loads, such as those generated by blast forces from the detonation of conventional weapons, involves uncertainties with respect to the expected forcing function and the structural behavior. Because of the uncertain nature of such loads, the effect of the applied loads may exceed the strength and/or deformation capacity of the individual structural elements. Generally, more information on the variability of the potential loads and a better understanding of the behavioral response of the structure will reduce the possibility of failure and increase the probability of a structure's survival. Therefore, a knowledge of the expected resistance of the individual elements, as well as the overall performance of the structural system under the given loading condition, becomes important to design process, since this knowledge may give the designer with a more complete overview of the structural performance.

In analysis of reinforced concrete structures, one is often concerned with the actual strength and deformation capabilities of a structural element under a combined state of loading, that is, flexure, shear and axial forces. This issue becomes very critical if the structures are expected to provide protection against modern conventional weapons. The development of reliable analytical/numerical techniques for predicting the structural response is particularly important since it provides the means for controlling the entire structural behavior to be within a desired range. Thus, creating the need for a rational and analytical procedure for predicting the strength and deformation of reinforced concrete structural elements under the effect of severe localized loads.

C. SCOPE

The analytical models, along with the results obtained from the application of the present procedure, are presented in the following sections.

Section II summarizes the existing and relevant information for analysis of reinforced concrete beams subjected to localized static

loads. It includes a background on the material properties and the procedure to compute the moment-curvature relationship for the cross section of a beam or a beam-column. In studying the various modes of failure at the ultimate condition, the lack of the general criteria for failure in reinforced concrete structural elements is discussed. As a result of combining empirical results from previous investigation with the present assumptions about the behavior of the structure at the ultimate condition, an improved model for the failure criteria is also proposed in Section II.

Existing analytical and experimental background on the interaction and influence of shear in reducing the flexural capacity of the reinforced concrete structural elements is studied and discussed in Section II. The truss mechanism analogy, extensive experimental data, and empirical models obtained from the literature, are used to develop a modified model for evaluating the influence of shear in reducing the flexural capacity of the element.

The last part of Section II is devoted to analysis for deriving the load-deformation behavior of the structural element. The computational procedure developed for this purpose accounts for the load-dependent and nonlinear distribution of curvature, influence of the boundary conditions, formation and propagation of plastic zones, and the second-order effect of the axial compressive force.

The behavior and modeling of reinforced concrete members under time-dependent localized load is studied and discussed in Section III. The procedure for obtaining an equivalent dynamic model with nonlinear characteristics is reviewed and is followed by the proposed modified equivalent single-degree-of-freedom (SDOF) model for analysis of reinforced concrete structural elements subjected to high intensity dynamic loads. The modified model accounts for the potential nonlinearities associated with the materials, support conditions, and the dissipation of energy under dynamic conditions. Furthermore, an approximate method is developed for evaluating the shearing response of the elements at the critical locations.

To evaluate the validity and to demonstrate the effectiveness of the present approach, a number of reinforced concrete structural elements tested by other investigations are analyzed in Section IV. In the static domain, these include two groups of reinforced concrete beams and one group of reinforced concrete beam-columns. In the dynamic domain, the analysis is performed for reinforced concrete beams subjected to impact loads, and for reinforced concrete wall slabs subjected to detonation loads of conventional explosive devices. For all cases, the computed results are compared with the available measured experimental data, as reported in the original sources. Additional analytic results and all experimental data from the previous experimental investigations are provided in Appendix B through D.

Section V summarizes the proposed procedure and the results obtained. General conclusions and recommendations for the future

studies are also presented in that section.

(The reverse of this page is blank)

SECTION II
ANALYTICAL MODELING OF STRUCTURAL BEHAVIOR IN THE STATIC DOMAIN

A. INTRODUCTION

The behavior of reinforced concrete beams and beam-columns has been investigated theoretically and experimentally in the past, and a tremendous amount of information on various aspects of the subject is available in the literature. This section provides only the information relevant to the analytical modeling of reinforced concrete structural elements developed through the course of the present investigation. It describes the material models for longitudinal steel and concrete employed in the present study. The behavior of reinforced concrete members subjected to flexure is surveyed briefly, followed by the assumptions and the numerical model used to analyze the flexural resistance of reinforced concrete beams and beam-columns. Study of the previous investigations revealed that none of the available models could provide an accurate description of the failure (collapse) at the ultimate condition. This issue is investigated in the present study, and has resulted in proposed improved models for the failure criteria in reinforced concrete beams. The influence of shear on the flexural behavior with or without the presence of web reinforcement is discussed and a modified method is proposed to account for the influence of web reinforcement on the flexural capacity of deep and slender beams. Also, the effect of axial compressive force on the flexural performance of the cross section is discussed.

B. MATERIAL MODELS

1. Longitudinal Reinforcement

The actual shape of the stress-strain curve for the longitudinal reinforcing bars must be considered in obtaining an accurate estimate of moment and curvature. A typical stress-strain curve for moderate strength steel consists of the three parts (Figure 1): (1) the linear elastic region, (2) the yield plateau, and (3) the strain-hardening region.

Region AB: ($\varepsilon_s < \varepsilon_y$)
In the elastic region, stress is assumed to be proportional to strain by Young's modulus of elasticity,

$$f_s = E_s \varepsilon_s \qquad (1)$$

where, ε_s is the steel strain, ε_y is the yield strain of steel, E_s is the modulus of elasticity for steel, and f_s is the steel stress.

Region BC: ($\varepsilon_y \leq \varepsilon_s < \varepsilon_{sh}$)
In the yield plateau strains increase with no increase in stress up to the beginning of strain hardening. The length of the yield plateau depends on the yield strength of steel. Generally, high strength steel has a shorter yield plateau than low strength steel. The stress-strain relationship for region BC in Figure 1 is as follows:

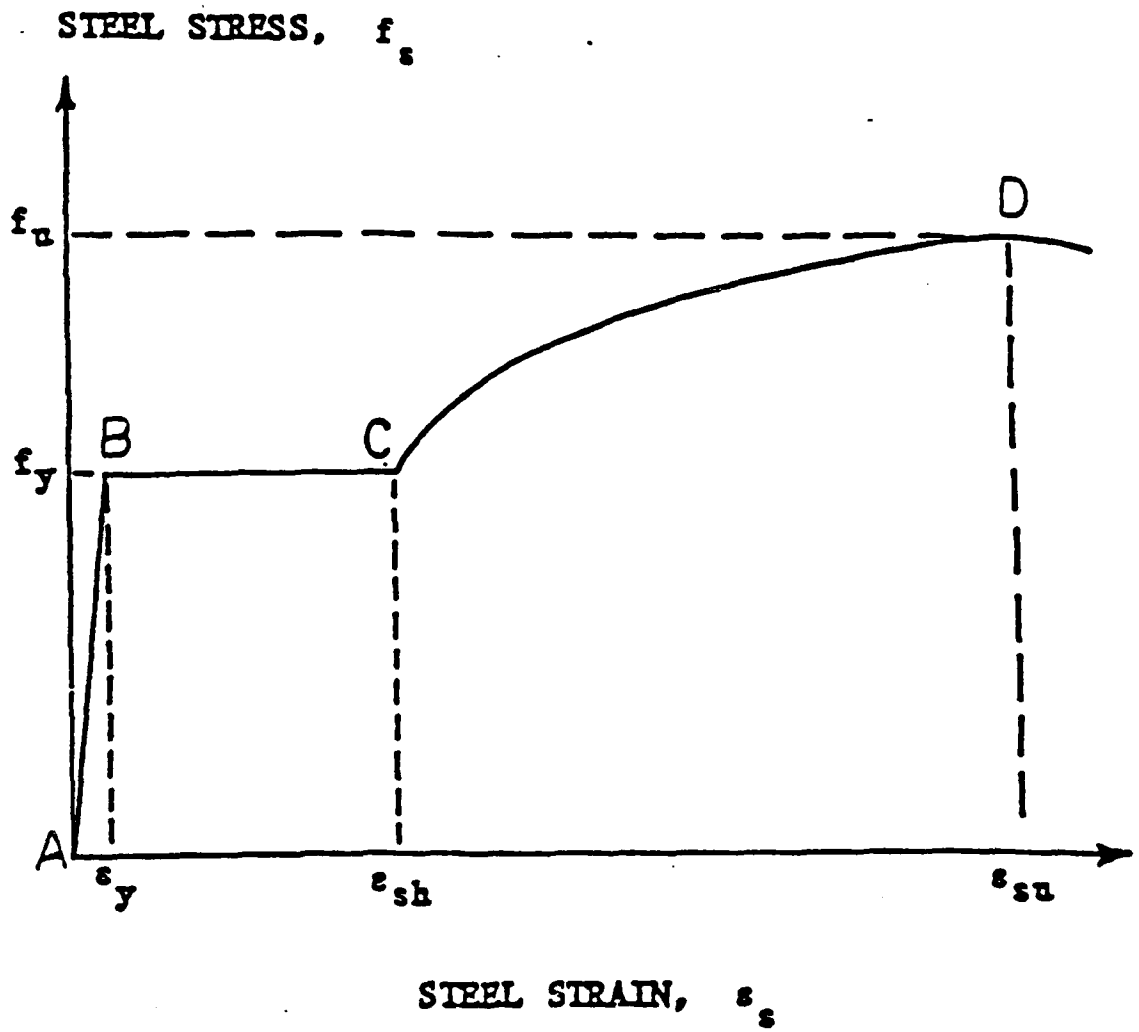

Figure 1. Stress-Strain for Steel.

$$f_s = f_y \qquad (2)$$

where, ε_{sh} is the strain at which strain hardening begins.

Region CD: $(\varepsilon_s \geq \varepsilon_{sh})$

The strain hardening of steel, shown by region CD in Figure 1, has been modeled by Burns and Siess in Reference 1 as follows:

$$f_s = f_y \left[\frac{112(\varepsilon_s - \varepsilon_{sh}) + 2}{60(\varepsilon_s - \varepsilon_{sh}) + 2} + \frac{\varepsilon_s - \varepsilon_{sh}}{\varepsilon_{su} - \varepsilon_{sh}} \left(\frac{f_u}{f_y}\right) - 1.7)\right] \qquad (3)$$

Park and Paulay (Reference 2) proposed a different formulation for region CD:

$$f_s = f_y \left[\frac{m(\varepsilon_s - \varepsilon_{sh}) + 2}{60(\varepsilon_s - \varepsilon_{sh}) + 2} + \frac{(\varepsilon_s - \varepsilon_{sh})(60 - m)}{2(30 + r + 1)^2}\right] \qquad (4\text{-a})$$

where,

$$m = \frac{\left(\frac{f_u}{f_y}\right)(30+r+1)^2 - 60r - 1}{15r^2} \qquad (4\text{-b})$$

$$r = \varepsilon_{su} - \varepsilon_{sh} \qquad (4\text{-c})$$

and

ε_{su} = ultimate strain,
f_u = ultimate stress.

Evaluation of numerical results as reported in Reference 3 has indicated that Equation (4-a) provides better results and thus, it will be used in this study.

2. Unconfined Concrete

The stress-strain relationship for unconfined concrete is normally obtained by standard cylinder tests in the laboratory. The test results in Reference 4 show that plain concrete under uniaxial compression can resist a maximum stress of f'_c (generally known as the uniaxial concrete compressive strength) at a strain of approximately 0.002. From the same test results it has also been found that at strains higher than 0.002, concrete is still capable of providing resistance up to its ultimate useful strain at which it can no longer resist any additional stress.

One of the most realistic stress-strain curves for unconfined concrete has been suggested by Hognestad in Reference 4. Hognestad's model assumes a second-degree parabola between zero strain up to 0.002, where f'_c is reached. Beyond the strain of 0.002, the strain increases to 0.0038, while the stress decreases to $0.85f'_c$. The material model for the unconfined concrete used later for the flexural analysis in this study is very similar to the relationships proposed in Reference 4, except that the ultimate useful strain of concrete is taken as 0.004 instead of 0.0038. Referring to Figure 2, the stress-strain relationship for unconfined concrete, namely the side and top covers in the compression zone of the cross section of beam and beam-columns, is described by the following formulation:

Part 1 : For the strain range $0. \leq \varepsilon_c < 0.002$ (where ε_c is the concrete strain and 0.002 is the strain corresponding to the maximum compressive strength), the stress-strain relationship is parabolic and can be represented by the following expression:

$$f_c = f'_c \left[\frac{2\varepsilon_c}{0.002} - \left(\frac{\varepsilon_c}{0.002}\right)^2\right] \qquad (5)$$

where, f_c is the stress in concrete.

Part 2 : For the strain range $0.002 \leq \varepsilon_c < 0.004$, the concrete stress is assumed to vary linearly from f'_c to $0.85f'_c$ at the strain of 0.004 as follows.

$$f_c = f'_c \left[1 - Z(\varepsilon_c - 0.002)\right] \qquad (6)$$

where, Z is the line slope derived from the above mentioned parameters.

Part 3 : For the strain range $\varepsilon_c > 0.004$, the unconfined concrete cover is assumed to have spalled off, thus resisting no stress.

$$f_c = 0. \qquad (7)$$

Hence, The cover is assumed to contribute to the strength of the section so long as the strain is not larger than 0.004, while at any strain beyond this value, the cover does not resist any stress.

The assumption that the concrete cover in the compression zone would lose strength and eventually spall off has been employed by

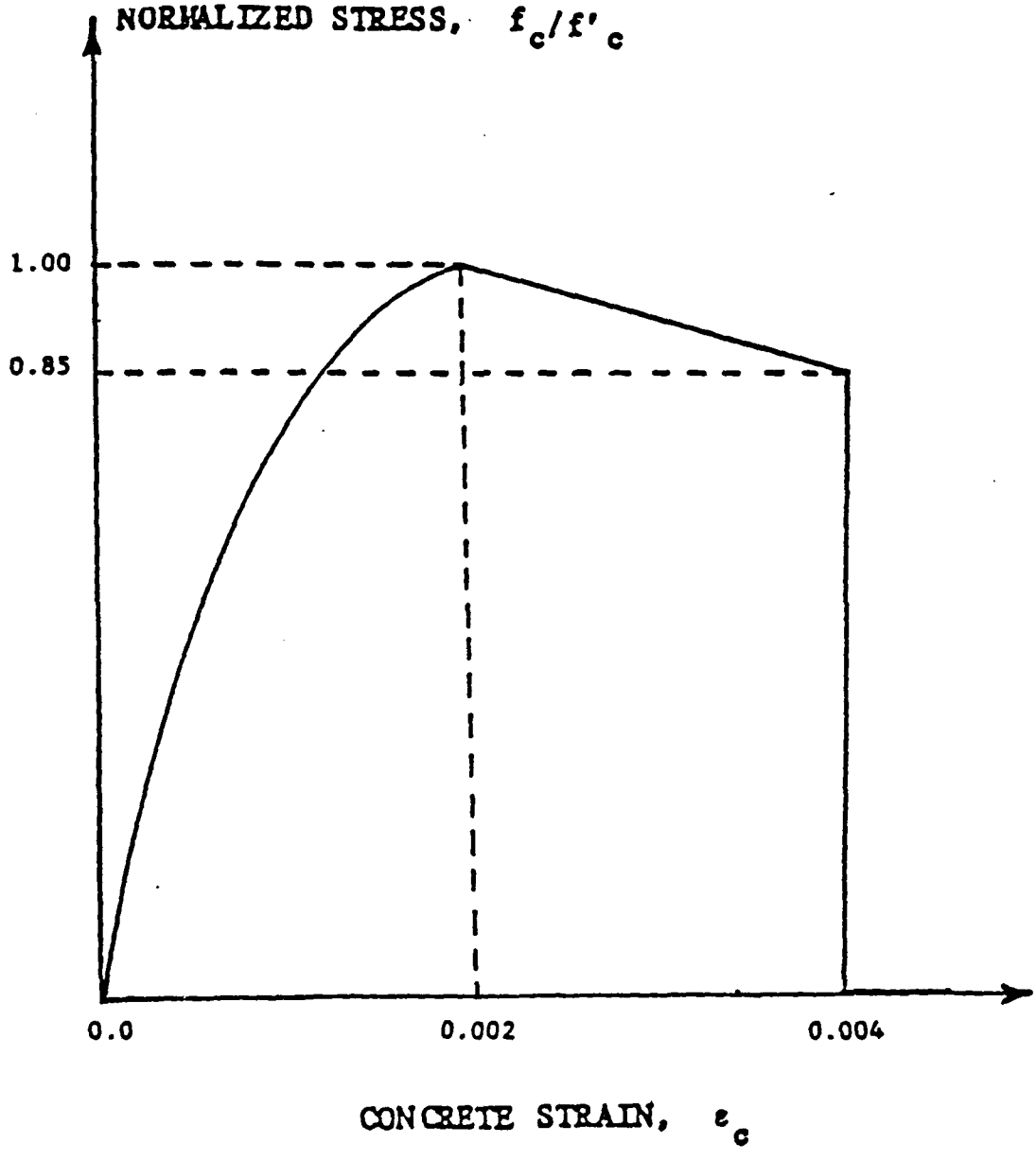

Figure 2. Stress-Strain for Unconfined Concrete.

other investigators. Baker and Amarakone (Reference 5) assumed that spalling occurs at strain of 0.0035, while Blume et al. (Reference 6) chose the spalling strain of 0.004. Krauthammer and Hall (Reference 3) assumed that concrete cover crushes at the strain of 0.004, but it may still resist compressive stresses so long as spalling has not occurred. Furthermore, they assumed that spalling occurs when the strain at the level of the compression longitudinal reinforcement reaches 0.004, but idealized the concrete cover located between the compression reinforcement and the neutral axis to remain on the cross section at strains larger than 0.004 and to resist compressive stresses in the range of between $0.5f'_c$ to $0.85f'_c$.

The maximum usable strain at the extreme compression fiber is taken as 0.003 by the ACI 318-1983 Code (see Reference 7).

3. Confined Concrete

In most reinforced concrete structural elements, concrete is confined by transverse reinforcement in the form of rectangular hoops or spirals. At low stress levels, the confined concrete will resist the applied compressive stresses and deform in a manner similar to unconfined concrete. Due to the internal cracking and crushing of concrete at higher stress levels, lateral deformations in the concrete increase, and the concrete will push against the lateral reinforcement. In response, the lateral reinforcement confines the concrete and improves its stress-strain characteristics. This phenomenon was first observed by Richart et al. (Reference 8) during triaxial compression tests on reinforced concrete cylinders loaded axially and subjected to lateral confining fluid pressure. The experimental results by Richart et al. (Reference 8) and later by Balmer in Reference 9 have indicated that an increase in lateral pressure increases the ultimate strength and ductility of reinforced concrete members.

The behavior of concrete confined by rectangular hoops was studied previously, as reported in the literature (see References 1,5,6,10,11,12, and 13). A brief description of a few material models for concrete confined by rectangular hoops is given in Reference 2.

The stress-strain relationship employed in this study for confined concrete in the compression zone of a beam was originally proposed by Vallenas et al., in Reference 14 for axially loaded compression members, and later modified by Krauthammer and Hall (Reference 3) to represent the behavior of confined concrete in beams or in beam-columns. This stress-strain curve consists of three parts as described below and shown in Figure 3.

Part 1 : For the strain range $0. \leq \varepsilon_c < \varepsilon_o$ where ε_o is the concrete strain corresponding to the maximum stress, the stress-strain relationship is parabolic.

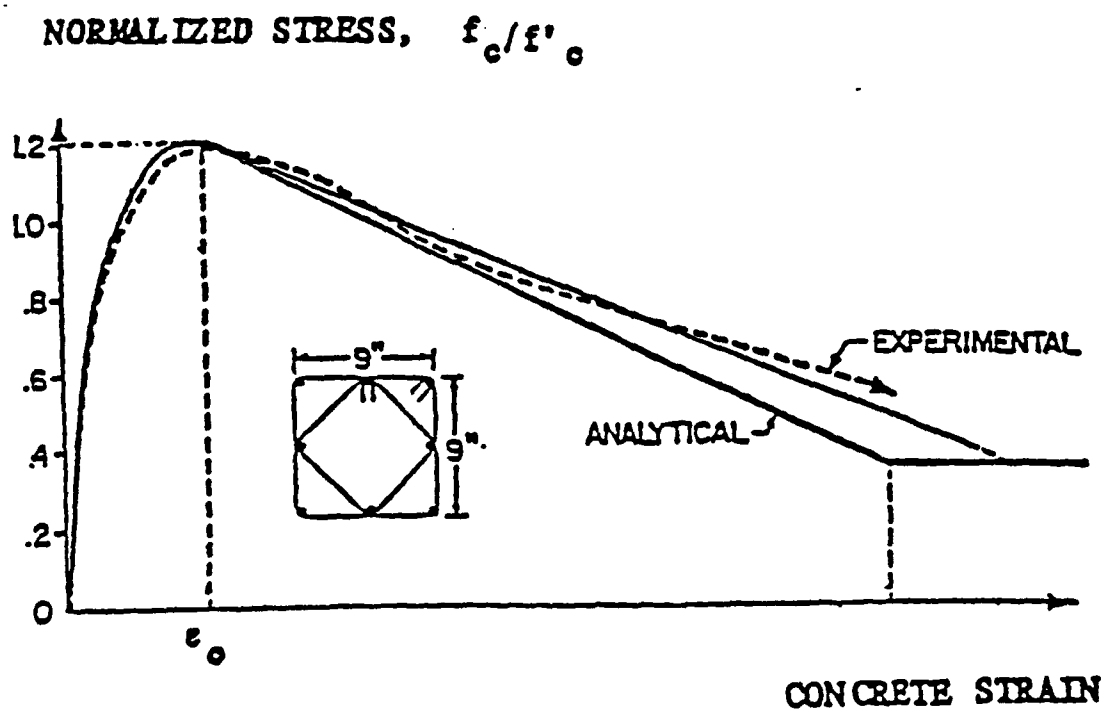

Figure 3. Stress-Strain for Confined Concrete.
(Reference 3)

$$f_c = \frac{\frac{E_c \varepsilon_o}{f'_c}\left(\frac{\varepsilon}{\varepsilon_o}\right) - K\left(\frac{\varepsilon}{\varepsilon_o}\right)}{1 + \left(\frac{E_c \varepsilon_o}{Kf'c} - 2\right)\left(\frac{\varepsilon}{\varepsilon_o}\right)} \tag{8}$$

Part 2 : For the strain range $\varepsilon_o \leq \varepsilon_c < \varepsilon_{0.3K}$, where $\varepsilon_{0.3K}$ is the strain at which the concrete stress is reduced to $0.3Kf'_c$, the stress-strain relationship is linear and described by the following equation:

$$f_c = K\, f'_c\left[1 - 0.8Z\varepsilon_o\left(\frac{\varepsilon}{\varepsilon_o} - 1\right)\right] \tag{9}$$

where, parameters ε_o, K, and Z are given by the following expressions,

$$\varepsilon_o = 0.0024 + 0.005\ \left(1 - \frac{0.734}{h''}S\right)\left(\frac{\rho_r f''_y}{\sqrt{f'_c}}\right) \tag{10}$$

$$K = 1. + 0.0091\ \left(1 - 0.245\,\frac{S}{h''}\right)\left(\rho_r + \frac{D''}{D'}\,\rho'\right)\frac{f''_y}{\sqrt{f'_c}} \tag{11}$$

$$Z = \frac{0.5}{\frac{3}{4}\,\rho_r\sqrt{\frac{h''}{S}} + \left(\frac{3 + 0.002\, f'_c}{f'_c - 1000}\right) - 0.002} \tag{12}$$

Part 3 : The third part of the curve is for strains larger than $\varepsilon_{0.3K}$

$$f_c = 0.3K\, f'_c \tag{13}$$

and,

E_c = elastic modulus of concrete (psi)
h'' = average core dimensions of the confined concrete compression zone measures to the outside of stirrups (inches).
ρ_r = ratio of the volume of confining steel to the volume of the

confined concrete core per unit length of the beam, both in the compression zone,

ρ' = longitudinal compression reinforcement ratio,

f''_y = yield stress of hoops,

S = spacing of hoops (inches),

D" = nominal diameter of hoops (inches),

D' = nominal diameter of longitudinal compression reinforcement (inches)

The above formulation shows that the shape of the stress-strain relationship for confined concrete depends on the parameters ε_o, K, and Z, which depend on the location of the neutral axis. Such a model will provide a unique stress-strain curve for any specific depth of the neutral axis. It is, however, noted in Reference 2 that using such relationship for flexural analysis of beams in which part of the cross section is in tension may be a questionable assumption. The low stress concrete in the tension zone helps to confine the compressed concrete (as discussed in Reference 2) and, for this reason, ρ_x is defined in this study specifically for the compression zone.

C. MEMBERS IN FLEXURE

The methods of evaluating the flexural capacity and curvature of the cross section at various loading stages, as presented in the available literature (References 2,3,15, and 16), is discussed here. In general terms, the procedure is based on a number of assumptions about the behavior of the cross section in bending and employs the stress-strain curves for longitudinal steel and concrete, as discussed earlier. The method was applied successfully in the past (References 2,3, and 16) for the analysis of reinforced concrete beams and beam-columns.

The present numerical model for the flexural analysis of reinforced concrete beams employs the following assumptions:

1. Plane sections before bending remain plane after bending (Bernoulli's principle). This assumption implies that the strains have a linear distribution over the cross section. Experimental results indicated this to be reasonably accurate in analyzing the flexural strength of reinforced concrete members at all stages of loading up to failure. However, in the tensile zone of the cross section, where the bond between steel and concrete may deteriorate, the relative local slip between the tensile reinforcement and the surrounding concrete distorts the validity of this assumption. Although, if the concrete strain is measured across several cracks in that region, Bernoulli's principle would still be valid for the average strain measured in that region, as discussed in Reference 2. In addition, attention must be given to the analysis of deep reinforced concrete beams in flexure, since this assumption is not completely valid for deep cross sections, as discussed in References 2 and 3.

2. Tensile strength of concrete below the neutral axis is ignored. Concrete is weak in tension and cracks at early loading stages, well before the yielding of the tensile reinforcement. Thus, the contribution of concrete below the neutral axis can be reasonably neglected in studying the post-yielding flexural behavior of the member.

3. The stress-strain relationship for steel and concrete is well defined. The longitudinal tensile and compression reinforcement are assumed to behave according to the stress-strain model discussed previously in Section II-B-1. The stress-strain curve for unconfined and confined concrete in the compression zone was also described in Sections II-B-2 and II-B-3, respectively.

The numerical method for obtaining the moment-curvature diagram is straightforward and similar to procedures in References 2,3,16. For any load level that corresponds to a fixed strain in the tensile reinforcement, a location (or distance from the extreme compression fiber) of the neutral axis, kd, is assumed and a linear strain distribution is imposed on the cross section. Then, the concrete compression zone is divided into N1 arbitrary number of layers parallel to the neutral axis (Figure 4). Using the first assumption, the strain at the center of the concrete layer i, ε_{ci}, and the strain for the steel bar j, ε_{sj}, can be obtained. Knowing the stress-strain relationship of steel and concrete, the stresses for each concrete layer i, and steel bar, j, can be computed. These are f_{ci} and f_{si}, respectively. The total compressive force of concrete acting on the cross section, C_c, is obtained by summing the concrete compressive force in all layers.

$$C_c = \sum_{i=1}^{N1} f_{ci} A_{ci} \tag{14}$$

where, A_{ci} is area of the concrete layer i. Also, the compression force in the longitudinal compression steel C_s, is computed as follows:

$$C_s = \sum_{j=1}^{N2} f_{sj} A'_{sj} \tag{15}$$

where, A'_{sj} is the area of the j^{th} compression steel bar and N2 is the number of compression steel bars. Similarly, the net tensile force ,T,

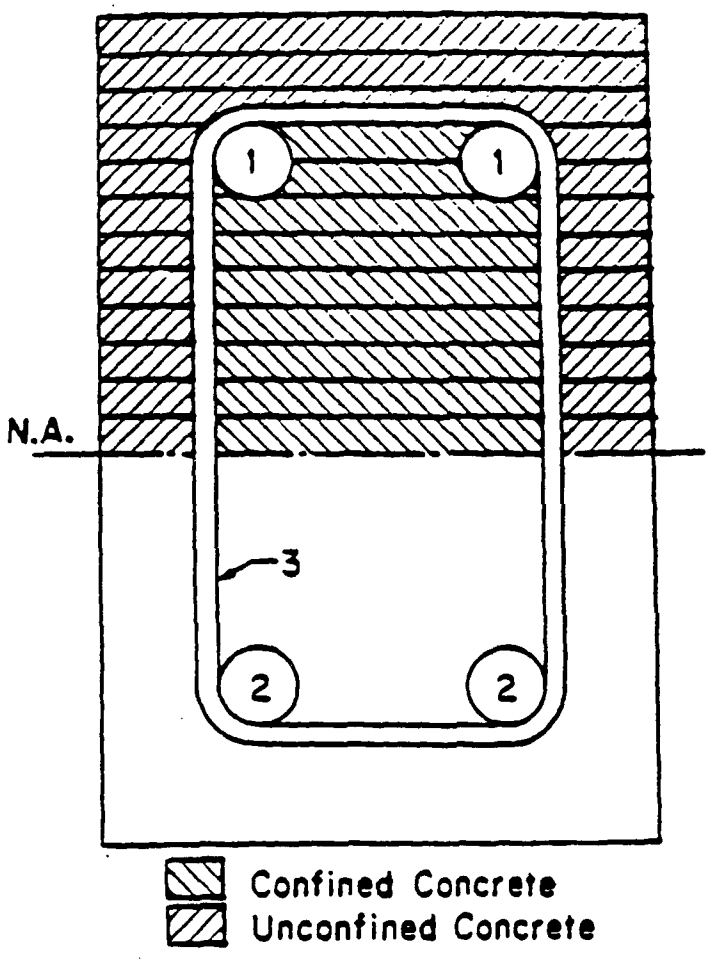

Figure 4. Reinforced Concrete Beam Cross Section and Division of Concrete Area in Compression

acting on the cross section can be given by the following equation:

$$T = \sum_{k=1}^{N3} f_{sk} A_{sk} \tag{16}$$

where, A_{sk} is the area of the k^{th} tension steel bar and N3 is the number of the steel bars in tension. For equilibrium of internal forces, it is required that the sum of all the compressive forces in concrete, C_c, and in the compression reinforcement, C_s, be equal to the sum of the force T in the tensile reinforcement.

$$T = C_c + C_s \tag{17}$$

Equation (17) is the force equilibrium expression of the cross section at any give load level. If Equation (17) is not satisfied for the assumed neutral axis location, an iterative procedure would begin for a new location of the neutral axis (for the same strain in the tensile reinforcement) until equilibrium is obtained to within a small tolerance. The moment and the curvature are subsequently computed for the cross section that is in statical equilibrium.

The moment of all forces can be taken about any arbitrary axis. In this study, the moment is arbitrarily taken about the plastic centroid of the section. The plastic centroid is defined as the centroid of resistance when the entire cross section of the beam is compressed, steel to the yield stress, and concrete to the stress $0.85f'_c$. For a symmetric cross section, this point is the same as the geometric centroid of the section. Referring to Figure 5, the resisting moment of the section may be given by the following expression:

$$M = C_c(d - d" - d_c) + C_s(d - d" - d') + T(d") \tag{18}$$

where,

- d = distance from the extreme compression fiber to the centroid of the tension bars,
- d' = distance from the extreme compression fiber to the centroid of the compression bars,
- d_c = distance from the extreme compression fiber to the centroid of the compression block,
- d" = distance from the centroid of the tension bars to the plastic centroid of the section

The lines of action of forces T, C_s, and C_c are at distances d, d', and d_c from the extreme compression fiber, respectively.

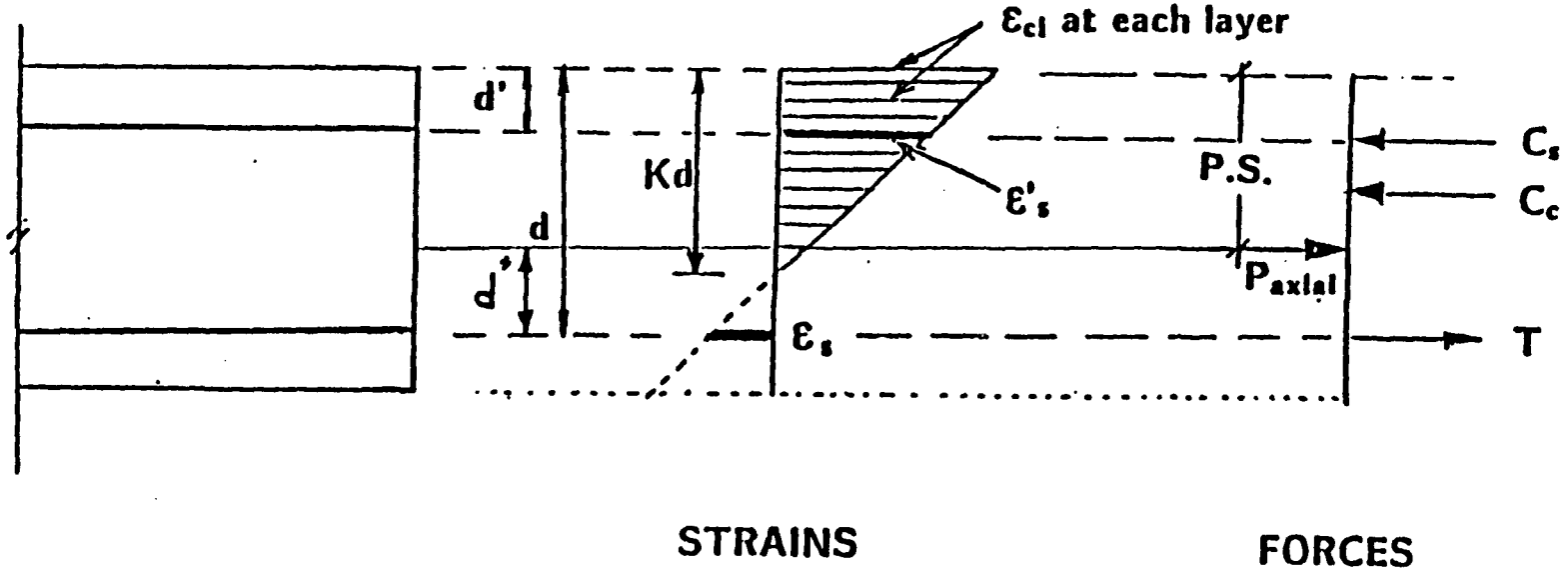

Figure 5. Strain Distribution and Forces in the Cross Section

The curvature of the cross section may be give as follows:

$$\varphi = \frac{\varepsilon_s}{d\text{-}kd} \tag{19}$$

where, ε_s is the strain in the tensile reinforcement and kd is the depth of the neutral axis from the extreme fiber in compression, both corresponding to the same load level.

The entire procedure is repeated for other values of tensile strain (i.e, different load levels) until the failure of the cross section is reached. This will result in a series of moment and curvature values which eventually form the moment-curvature diagram.

1. Failure Modes at the Ultimate

The computation of a complete moment-curvature diagram requires a clear definition of failure in the beam. In this study the words failure and ultimate are used synonymously and they refer to the final collapse loading stage. In general, three different modes of failure are possible in reinforced concrete beams: (a) flexural failure due to the fracture of the longitudinal tensile reinforcement, (b) flexural failure due to concrete crushing in the compression zone of the cross section, and (c) shear failure.

The following discussion describes various possible flexural modes of failure in reinforced concrete beams. Shear failures are discussed later in this section.

The mode of failure and the extent of ductility of the beam at the ultimate curvature depend mostly on the percentage of the longitudinal reinforcement, ρ. If ρ is less than the balanced amount of tensile reinforcement, ρ_b, then the cross section is under-reinforced. Otherwise if ρ is more than ρ_b, the beam is over-reinforced. A distinction between over-reinforced and under-reinforced beams would further require a definition of the balanced amount of reinforcement ratio within the flexural model. The balanced reinforcement ratio ρ_b, can be easily computed. ρ_b can be defined as the amount of longitudinal tensile reinforcement necessary for obtaining equilibrium, i.e. satisfying Equation (17), such that the strain of the tensile steel is at yield, while the concrete strain at the extreme compression fiber is at 0.004. It is also noted that the strain of 0.004 is the ultimate strain for unconfined concrete described in Section II-B-2 and illustrated in Figure 2.

In under-reinforced beams, where the ratio of the percentage of the longitudinal tensile reinforcement to the percentage of the longitudinal compression reinforcement (ρ/ρ') is less than one, the fracture of the tensile reinforcement is usually the predominant mode of failure at collapse (Reference 1). Conversely, if this ratio is

more than unity, concrete failure is expected to occur in the compression zone. Of course, the extent of the ductility would depend on the amount of confining reinforcement and on the ratio of the compression reinforcement present in the beam. Proper confinement of concrete increases its strength and the ductility and may change the flexural mode of failure from compression to tension.

A compression flexural failure in under-reinforced beams is either due to the buckling of the compression bars or excessive decrease in the compressive capacity of concrete. Experimental results (References 1 and 17) have indicated that in most cases the buckling of the compression bars and the loss of strength in concrete both contributed to the ultimate failure of the specimen. It is also noted in Reference 17 that the type of the flexural compression failure depends heavily on the percentage of the compression reinforcement, because specimens with small amounts of compression steel had concrete compression failure and conversely, beams with larger amounts of compression reinforcement failed by buckling of the bars. The results of experiments reported in References 1 and 17 indicated that buckling of the compression reinforcement between two adjacent ties occurred in all beams that exhibited compression type failure. It was also noted that the bars always buckled outward on a horizontal plane, since they were restrained laterally by the surrounding confined concrete and the curvature of the beam prevented the upward buckling of the bars.

Yamashiro and Seiss (Reference 17) proposed a formulation which included the effect of buckling of the compression bars in predicting the ultimate point on the moment-curvature diagram. In their study, they assumed that the ultimate point on the moment-curvature diagram was the point of absolute maximum moment or the point corresponding to the buckling load of the compression bars, whichever occurred first. Moreover, it was assumed that stirrups provided perfect restraint against rotation and displacement, and no lateral restraint was provided by the surrounding concrete. With these assumptions, the idealized buckling stress was proposed according to the following expression:

$$f_{cr} = \frac{\pi^2 E_t}{4\ (S/D')^2} \qquad (20)$$

where, E_t is the tangent modulus and D' is the diameter of the compression bar. Equation (20) implies that the buckling of the bars could occur only after the compression reinforcement has entered into the strain hardening region. Although the criteria selected in Reference 17 for ultimate condition provided adequate computational results, the collapsed members did not seem to follow the assumed behavior. For example, some beams continued to deflect under increasing load after the buckling of the compression reinforcement. Moreover, in case if buckling occurred after reaching the point of the absolute maximum moment, that point did not seem to be the failure of

the beam, since more deformation was observed with increasing loss of strength due to the excessive concrete distress in the compression zone.

Although predicting the flexural mode of failure at the ultimate curvature was of major concern in a number of experimental investigations (see References 1,11,13,17,18,19,20, and 21), no analytical or empirical method was available to relate the flexural failure to geometrical and/or material properties of the member. From information available in the existing literature, an attempt has been made here to establish analytical/empirical failure criteria for reinforced concrete beams and beam-columns that will include rational relationships for the ultimate strain in the materials as a function of the element material and geometric properties. The validity of the proposed formulation will be illustrated later in Section IV, when the analytic results for a number of cases are compared with the measured experimental values.

2. Proposed Failure Criteria for Flexural Failure

The present study ignores the possibility of failure in a beam caused by buckling of the compression reinforcement. Instead, the flexural failure for ductile members at the ultimate curvature is based on the ultimate strain in the tensile reinforcement or the ultimate strain of the confined concrete, whichever occurs first. The ultimate strain of the longitudinal tensile reinforcement, ε_{su}, is the last point on the stress-strain curve of steel as discussed in Section II-B-1. If this strain is reached in the tensile reinforcement before a concrete failure in the compression zone occurs, the beam will be assumed to have failed in tension. Otherwise, if the concrete failure in the compression zone precedes the fracture of the tensile reinforcement, then a compression failure is assumed.

A failure in the confined compression zone depends on two important factors;

1. The ultimate strain of confined concrete in compression,
2. The location on the confined compression zone at which the ultimate strain of the confined concrete must be reached in order to trigger a concrete compression failure.

The following discussion is aimed at illustrating the simulation for a concrete compression failure in ductile members within the flexural model.

The ultimate strain of confined concrete was studied experimentally by a number of investigators (References 5,11,13, and 21). The results of these investigations indicate that the ultimate strain of concrete confined by rectangular hoops depends mostly on the amount and properties of the confining reinforcement. Based on a series of tests on short specimen of confined concrete subjected to axial forces, Chan (Reference 11) suggested the following expression for the ultimate strain of concrete confined by rectangular ties:

$$\varepsilon^c_{cu} = 3\sqrt{\rho'_c/24.5} + \varepsilon^u_{cu} \qquad (21)$$

where, ρ'_c is the ratio of the volume of the lateral reinforcement to the volume of the confined concrete, ε^c_{cu} is the ultimate strain of confined concrete and ε^u_{cu} is the ultimate strain of unconfined concrete taken as 0.004 in this study (see Section II-B-2).

Other investigators (References 11,12, and 21) proposed empirical expressions for the strain of confined concrete at the ultimate curvature. Extensive experimental studies by Corely (Reference 13) on inelastic behavior of reinforced concrete beams under concentrated loads provided the following expression as a lower-bound ultimate strain for concrete confined by rectangular ties:

$$\varepsilon^c_{cu} = 0.003 + 0.02(b/L_z) + (\rho_c\ f''_y/20)^2 \qquad (22)$$

where,

- L_z - distance on the span of the beam from the section of maximum moment to the section of zero moment,
- b - width of the cross section
- f''_y - yield stress of web reinforcement (psi),
- ρ_c - the ratio of the volume of the confining steel (one stirrup plus compression reinforcement) to the volume of the confined core.

In discussing Corley's paper, Mattock (Reference 21) recommended the following simpler relationship, which is independent of the yield strength of web reinforcement, in lieu of the last expression:

$$\varepsilon^c_{cu} = 0.003 + 0.02(b/L_z) + 0.20\ \rho_c \qquad (23)$$

where, all variables are the same as defined above. Equations (22) and (23) (for f'_y = 50 ksi) are shown graphically in Figure 6. These expressions represent a family of curves defining a lower bound for the ultimate strain of confined concrete for the number of beams that tested in Reference 13. These expressions will reduce to 0.003 if the moment is constant along L_z, and if the effect of lateral reinforcement is neglected. Also, for a beam subjected to a single concentrated load at its midspan, L_z would be the same as the shear span of the beam.

After the results of these equations were compared to the experimental data as reported in (References 1 and 17), the simpler model proposed by Mattock and give by Equation (23) was chosen as the basic method for determination of the ultimate strain of confined concrete with the following modifications:

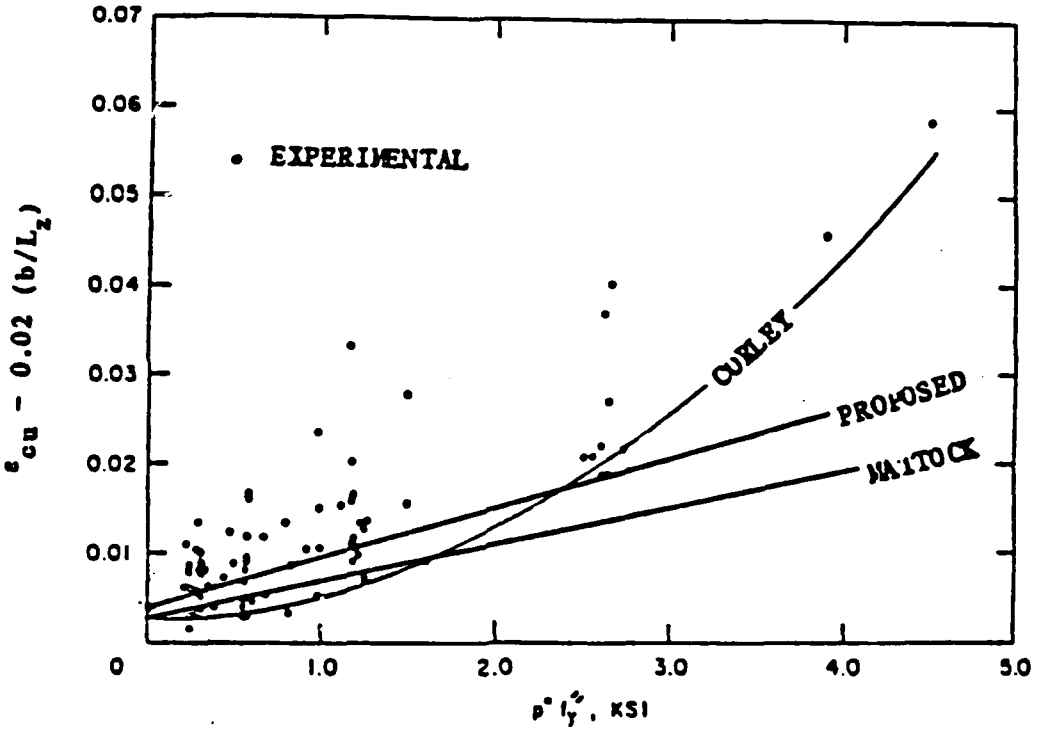

Figure 6. Modified Ultimate Strain of Confined Concrete. (Reference 13)

1. The ultimate strain of unconfined concrete is taken as 0.004 instead of 0.003. This adjustment is primarily for the sake of consistency with the unconfined concrete material model that was previously discusses in Section II-B-2.

2. Equation (23) is only a lower-bound to the ultimate strain of confined concrete. In order to obtain more realistic values, the coefficient 0.2 is replaced by 0.27 (ρ/ρ'). This modification will compensate for the fact that for smaller amounts of compression reinforcement (relative to the amount of tensile reinforcement), the neutral axis at the ultimate curvature is at a lower depth, providing a larger confined compression zone of concrete which is in equilibrium with the tension force in the longitudinal tensile reinforcement, thus allowing the confined concrete to withstand higher strains at the ultimate condition.

The proposed modified equation for the ultimate strain of confined concrete is the following:

$$\varepsilon_{cu}^{c} = 0.004 + 0.02(b/L_z) + 0.27\ \rho_c\ (\rho/\rho') \qquad (24)$$

The parametric range of this equation for the ratio of ρ/ρ' is

$$1.0 \leq \rho/\rho' \leq 1.79 \quad ; \quad \rho' \text{ not equal to } 0.$$

Equation (24) is plotted as well in Figure 6 along with Equations (22) and (23). It can be seen that for equal percentages of tensile and compression reinforcement, the proposed equation predicts values that are close to expressions in References 13 and 21.

As mentioned earlier, the complete formulation of a compression failure criteria would require one to define the level on the confined concrete zone for which the strain at each load step is compared with the ultimate strain of confined concrete. If the strain of concrete at that level exceeds the ultimate strain as obtained from Equation (24) before the tensile reinforcement reaches its fracture strain, the mode of failure is by compression. For beams without the influence of axial compressive force, this level is chosen as follows:

1. If $\rho/\rho' = 1$, the above check is made at the midheight of the confined compression concrete zone,

2. If $1. \leq \rho/\rho' \leq 1.79$, then the check will be made at some point between the midheight of the confined compression zone and the neutral axis, linearly proportional to the ratio ρ/ρ'.

The distance between the neutral axis and the axis at which the

strain is compared against the ultimate strain is denoted by d_c, and can be expressed as following:

$$d_c = \left(\frac{kd - TC - 0.5\,D''}{2}\right)\left(\frac{\rho}{\rho'}\right) \qquad (25)$$

where,

kd = the depth of the neutral axis from the extreme compression fiber,
TC = thickness of the top cover,
D" = diameter of the transverse reinforcement.

According to the above formulation, a failure in the compression zone depends on the ultimate strain of concrete and the equilibrium of forces acting on the cross section, as reflected by the depth of the neutral axis in Equation (25). The parametric range for Equation (25) is the same as for Equation (24).

The preceding model was developed specifically for reinforced concrete members capable of behaving in a ductile fashion. In heavily reinforced concrete members in which the tensile steel content is near (or more than) the balanced amount, failure would be brittle unless the concrete is well confined by transverse reinforcement. A brittle failure occurs because a high tensile force T would require a lower depth of neutral axis and consequently, the concrete would be crushed (if it is not heavily confined) before the yielding of the reinforcement. This situation is characterized by an immediate loss of strength upon reaching the peak flexural moment before the yielding of the tensile steel. In the present analysis, whenever the flexural moment capacity was reduced significantly (due to a large amount of tensile reinforcement or the presence of a high axial compressive force), the peak moment was taken as the ultimate flexural resistance on the moment-curvature diagram and a brittle compression failure would be assumed. On the other hand, if the flexural moment was slowly and consistently increasing to a peak along with yielding of the tensile reinforcement, a ductile compression or tension failure would be assumed to occur as discussed earlier in this section.

D. INFLUENCE OF SHEAR ON THE FLEXURAL BEHAVIOR OF BEAMS

The influence of shear on the performance of reinforced concrete beams has been studied theoretically and experimentally in the last 30 years. Generally, it is well understood that the so called "shear failure" in reinforced concrete beams is a result of bending, shear, and sometimes axial force acting simultaneously. A failure of this kind is usually brittle and it occurs before the structure reaches its ultimate flexural capacity.

To understand the problems associated with shear in reinforced concrete beams, the influence of shear must be first examined in beams without web reinforcement, then in beams with shear reinforcement. The

shear strength of reinforced concrete beams has been investigated by elastic, plastic and empirical models in the literature. In this section, the nature and mechanism of various types of shear failures in reinforced concrete beams are examined separately for beams with or without transverse reinforcement. In addition, two theoretical models proposed in the literature are discussed for providing a rational analytic background for the modified shear model that is proposed later in this section.

1. Shear Failure in Beams without Web Reinforcement

The cracking pattern in a typical simply supported reinforced concrete beam is shown in Figure 7. Potential flexural cracks are initially formed vertically at locations of high bending moment. A combined state of stress due to shear and flexural stresses will cause the formation of secondary or flexure-shear cracks near the interior extremity of one of the initial cracks (Figure 8). From elementary mechanics of materials, the maximum principal tensile stress, f_t, at any point below the neutral axis of the beam is obtained from the following expression:

$$f_{t(max)} = 0.5f_t + \sqrt{(0.5f_t)^2 + v^2} \qquad (26)$$

where, v and f_t are shear stress and flexural stress at that point, respectively. The direction of the principal tensile stress is given by the following expression:

$$\text{Tan } 2\theta = v / (0.5f_t) \qquad (27)$$

where, θ is the angle between the maximum principal stress and the longitudinal axis of the beam, measured in a counter clockwise direction. If the shear stress is small, the principal tensile stress is nearly equal to the longitudinal tensile stress, and its direction is nearly parallel to the longitudinal axis of the beam. On the other hand, if the longitudinal tensile stress is small, the magnitude of the principal tensile stress is nearly equal to the shear stress and it makes an angle of 45 degrees with the longitudinal axis of the beam.

Since concrete is weak in tension, the principal tensile stresses are the major reason for the formation of the initial cracks in reinforced concrete beams as shown in Figure 8. With increasing load, inclined flexure-shear cracks will subsequently develop as an extension of the initial flexural cracks (Reference 22). As shown later in this section, some beams fail immediately after the formation of the inclined cracks, while others may resist higher loads, even after the appearance of the inclined cracks.

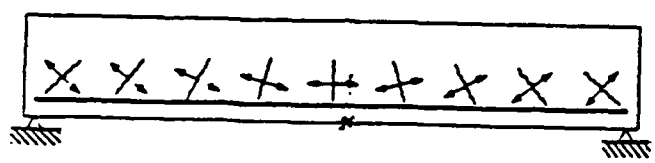

Figure 7. Cracking Pattern in a Simple Beam.
(Reference 79)

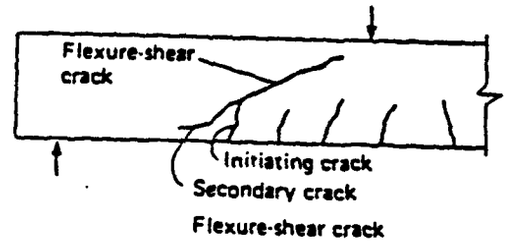

Figure 8. Typical Flexure-Shear Cracks.
(Reference 79)

Upon the formation of the inclined cracks, the shear force in the beam is resisted by the following internal forces (Figure 9):

1. Dowel forces in the flexural reinforcement; V_d
2. The vertical component of the aggregate interlocking shear force along the diagonal crack; V_a
3. Shear across the uncracked concrete in the compression zone; V_c

Thus,

$$V = V_d + V_a + V_c \tag{28}$$

where, V is the applied shear force at the cracked section. It has been reported (Reference 22) that approximately 15-25 percent of the shear force is carried by dowel resistance, 20-40 percent by the concrete in compression zone and 30-50 percent by the aggregate interlocking shear resistance.

These forces contribute to two principal mechanisms of shear resistance, namely, the "beam action" and the "arch action" mechanisms. From basic principles of beam theory, shear force is related to bending moment by the following expression:

$$V = dM/dx \tag{29}$$

where, M is the resisting moment of beam which can be expressed by the following relationship (Figure 9-b):

$$M = (jd)(T + V_d \text{ Cot } \alpha) \tag{30}$$

T is the tensile force in the longitudinal reinforcement, and jd is the vertical distance between T and C in Figure 9-b.

Assuming that the dowel resistance force is ignored, the above expression reduces to the following:

$$M = T(jd) \tag{31}$$

Substituting Equation (31) into Equation (29),

$$V = (d/dx)(T\ jd) = (dT/dx)(jd) + T(d/dx)(jd) \tag{32}$$

If the internal lever arm does not change along the length of the beam, the beam action mechanism of shear resistance can be expressed

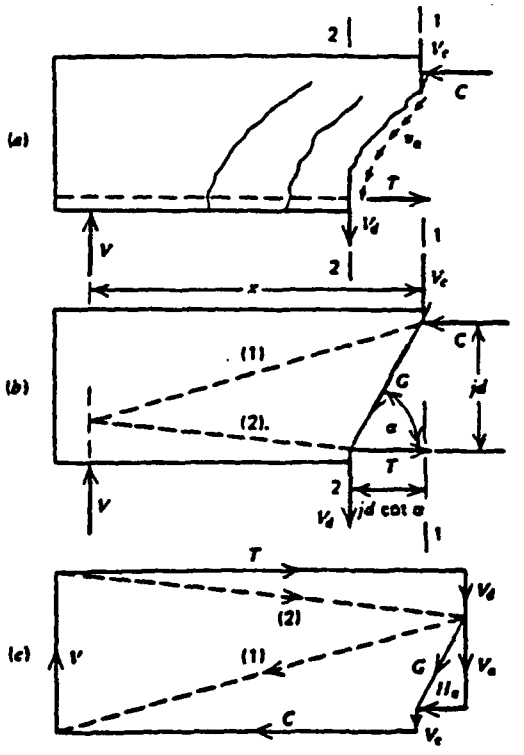

Figure 9. Equilibrium Requirements in the Shear Span of a Beam. (Reference 2)

as:

$$V = (dT/dx)\ (jd) \tag{33}$$

The rate of change in tensile force with distance is called the shear flow which is in turn the bond force between the reinforcement and the surrounding concrete. If the bond force between steel and concrete is destroyed, then the tensile force does not change any more and the beam mechanism is no longer valid. In that case, the inclined compression or arch action will resist the applied shear as follows:

$$V = T\ (d/dx)\ jd \tag{34}$$

Ignoring the aggregate interlocking resistance, from Figure 9-a,

$$T = C \tag{35}$$

where, C is the net compressive force acting on the uncracked concrete. Substituting for T in Equation (34),

$$V = C\ (d/dx)\ jd \tag{36}$$

Thus, the external load is balanced by arch action.

In general, a perfect bond between steel and concrete is uncommon and the necessary bond force for the beam mechanism can not fully develop. Therefore, both mechanisms contribute to shear resistance at the same time and the extent of their individual contribution depends on the internal deformation pattern at various stages of loading as extensively discussed in Reference 2.

The development and growth of the inclined cracks in a reinforced concrete beam depends on the relative magnitude of the shear and flexural stresses. For all practical purposes (see Reference 22), these stresses may be represented by the following expressions:

$$v = C_1\ (V/bd) \tag{37-a}$$

$$f_t = C_2\ (M/bd^2) \tag{37-b}$$

where, d is the effective depth of the beam, b is the width of the web, and C_1 and C_2 are arbitrary coefficients which depend on the

amount of reinforcement, type of steel, type of loading and bond force between steel and concrete. Dividing the second of Equations (37) by the first,

$$f_t/v = C_3 \ (M/Vd) \tag{38}$$

where C_3 is the ratio of C_2 to C_1. For a beam subject to a concentrated load at its midspan, the M/V ratio is the so called shear span, a. Thus,

$$f_t/v = C_3 \ (a/d) \tag{39}$$

It can be seen that the variation in inclined cracking capacity of the beam is a function of a/d, namely the shear span to the effective depth ratio.

Experimental results (References 23 and 24) indicate that when all other parameters are kept constant, the strength of rectangular simply supported reinforced concrete beams depends on the shear span to the effective depth ratio. In general, two different categories of failure may be established:

1. Slender Beams: ($2.5 \leq a/d \leq 7$). Initial flexural cracks are followed by flexure-shear cracks which extend diagonally towards the point of load application. The beam will fail shortly after the formation of the diagonal crack and the subsequent arch mechanism cannot sustain any additional load. Such a crack causes a failure in the beam before its full flexural capacity is developed. This type of failure is known as a "diagonal tension failure."

2. Deep Beams: ($1.0 \leq a/d \leq 2.5$). Failure is either due to the propagation of the secondary crack along the longitudinal reinforcement which in turn results in a loss of bond between steel and concrete, or due to an extension of the inclined crack to the top of the beam which results in crushing of concrete above the upper end of the inclined crack. In fact, this is an arch action failure in which the propagation of the crack reduces the size of the compression zone, causing the compressive stresses to exceed the compressive strength of concrete. This type of failure is known as " shear compression failure." Moreover, in very deep beams in which the a/d ratio is close to one, the failure may also be due to the following reasons:

    a. Anchorage failure of tensile reinforcement.
    b. Crushing of concrete near the reaction point.
    c. Flexural failure either by crushing of the concrete above the tip of the inclined crack or by yielding of the tensile reinforcement.

d. Tension failure of the arch rib accompanied by crushing along the crack.

The ACI 318-1983 Code (Reference 7) provides the following relationship for evaluating the shear strength of reinforced concrete beams without web reinforcement.

$$v_c = \frac{V_c}{bd} = 1.9\sqrt{f'_c} + 2500\,\rho\,\frac{V_u d}{M_u} < 3.5\sqrt{f'_c} \tag{40}$$

All parameters are in pound and inch units, and

$$\rho = A_s/bd$$

$$V_u d/M_u \leq 1.0$$

where,

v_c = shear stress of concrete, (psi)
A_s = area of tensile reinforcement, (inches^2)
b = width of beam, (inches)
d = effective depth of beam, (inches)
V_u = ultimate shear force, (pounds)
M_u = ultimate moment at the section, (pound-inches)
f'_c = compressive strength of concrete (psi)

Equation (40) provides reasonable and acceptable predictions, as discussed in References 22,23,25, and 26 for the flexure-shear cracking load, particularly for beams with shear span-to-depth ratios in the range of 2.5 to 7.

According to the ACI-1983 Code, the following more conservative and simpler equation can be used instead of the previous equation:

$$v_c = 2\sqrt{f'_c} \tag{41}$$

Figure 10 shows a comparison between Equation (40) and Equation (41) with experimental results.

Perhaps the best statistically accepted equations for predicting the shear strength of reinforced concrete beams has been proposed by Zsutty (Reference 27) as follows:

$$v_c = 59\,(f'_c\,\rho\,d/a)^{1/3} \tag{42}$$

Other investigators (Reference 28) have developed similar expressions:

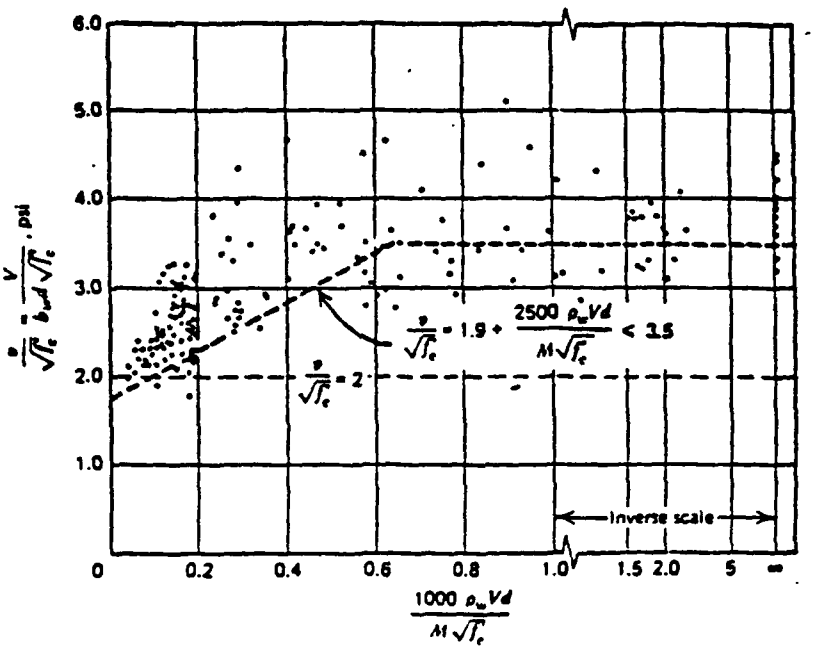

Figure 10. Comparison of Equations (40) and (41) with Experimental Data. (Reference 2)

$$v_c = 12.5\ (100\ \rho\ a/d\ f'_c)^{1/3} \qquad (43)$$

All these statistical studies indicate that unless shear reinforcement is provided, collapse occurs immediately after the formation of the diagonal crack. Moreover, the most significant variables that affect the shear strength of reinforced concrete beams are the longitudinal reinforcement ratio, the tensile strength of concrete, and the shear span-to-effective depth ratio of the beam.

Experimental test results obtained by Kani (Reference 23) and other investigators (Reference 24) indicate that the flexural capacity of reinforced concrete beams with shear span-to-effective depth ratios between one and seven cannot fully develop. Based upon these investigations, it was found that the moment capacity is primarily a function of two variables, namely the percentage of tensile reinforcement and the shear span-to-effective depth ratio. Kani (Reference 23) showed that the influence of the compressive strength of concrete on the shear strength is not significant and can be ignored in the shear failure analysis.

Figure 11 summarizes results obtained by Kani in Reference 23. It can be seen that the ratio of the ultimate moment with shear influence to the ultimate flexural moment without shear influence clearly depends on two variables, namely the tensile longitudinal reinforcement ratio, ρ, and the shear span to the effective depth ratio, a/d. Krauthammer and Hall (Reference 3) studied these results and arrived at the following observations:

1. Regardless of the amount of tensile reinforcement, the minimum capacity falls in the range: $2 \leq a/d \leq 3$.
2. No moment reduction exists for beams with a/d larger than seven.
3. No moment reduction exists for beams with a/d less than unity.

Moreover, it was assumed in Reference 3 that the minimum moment capacity line is comprised of three linear segments parallel to the ρ axis. The following equations have been obtained from Reference 3. These equations were developed by the numerical evaluation of the experimental results in Reference 23 for describing the minimum moment ratio as a function of ρ.

$$0 < \rho < 0.65\% \ : \ \left(\frac{M_u}{M_{fl}}\right)_m = 1.0 \qquad (44\text{-a})$$

$$0.65\% < \rho \leq 1.88\% \ : \ \left(\frac{M_u}{M_{fl}}\right)_m = 1.0 - 36.6\ (\rho - 0.0065) \qquad (44\text{-b})$$

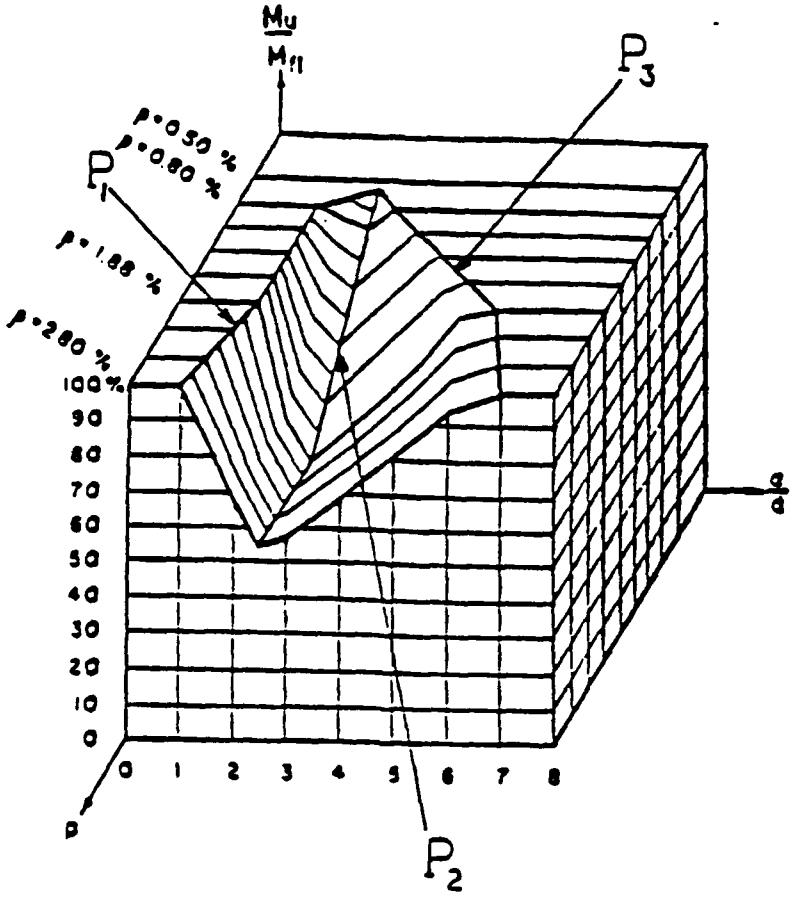

Figure 11. General Model for Shear Influence on Beams Without Web Reinforcement. (Reference 23)

$$1.88\% < \rho \leq 2.88\% \quad : \quad \left(\frac{M_u}{M_{f1}}\right)_m = 0.6 \qquad (44\text{-c})$$

where, $(M_u/M_{f1})_m$ is the minimum ratio of moment capacity of the beam with shear influence to the the maximum flexural capacity of the beam without any shear influence. Using these expressions, it is possible to describe the maximum influence of shear on the flexural moment capacity.

Assuming a straight line relationship on both sides of the minimum moment capacity line (Figure 12), Krauthammer and Hall (Reference 3) also developed the following procedure for computing the influence of shear on moment capacity of reinforced concrete beams without web reinforcement:

1. Define the a/d value of the minimum moment capacity as point P_2 (Figure 12).
2. Define the a/d values on both sides of the minimum point for which the ratio of moment capacity to full flexural capacity is one. These are points P_3 for slender beams and P_1 for short beams in Figure 12.
3. Since two points are defined on both sides of the minimum point, a linear interpolation will give the moment capacity for a specific shear span to the effective depth ratio.

For slender beams,

$$\left(\frac{M_u}{M_{f1}}\right) = 1.0 + \left[\left(\frac{M_u}{M_{f1}}\right)_m - 1\right] \frac{\frac{a}{d} - P_3}{P_2 - P_1} \qquad (45\text{-a})$$

and for deep beams,

$$\left(\frac{M_u}{M_{f1}}\right) = 1.0 + \left[\left(\frac{M_u}{M_{f1}}\right)_m - 1\right] \frac{\frac{a}{d} - P_1}{P_2 - P_1} \qquad (45\text{-b})$$

where, $(M_u/M_{f1})_m$ can be obtained from Equations (44). Point P_2 in Figure 12 is the shear span to the effective depth ratio corresponding to the minimum moment capacity line. P_1 is the shear span to the effective depth ratio below which there is no reduction in the moment capacity (Figure 12) and P_3 is the a/d beyond which there is no loss

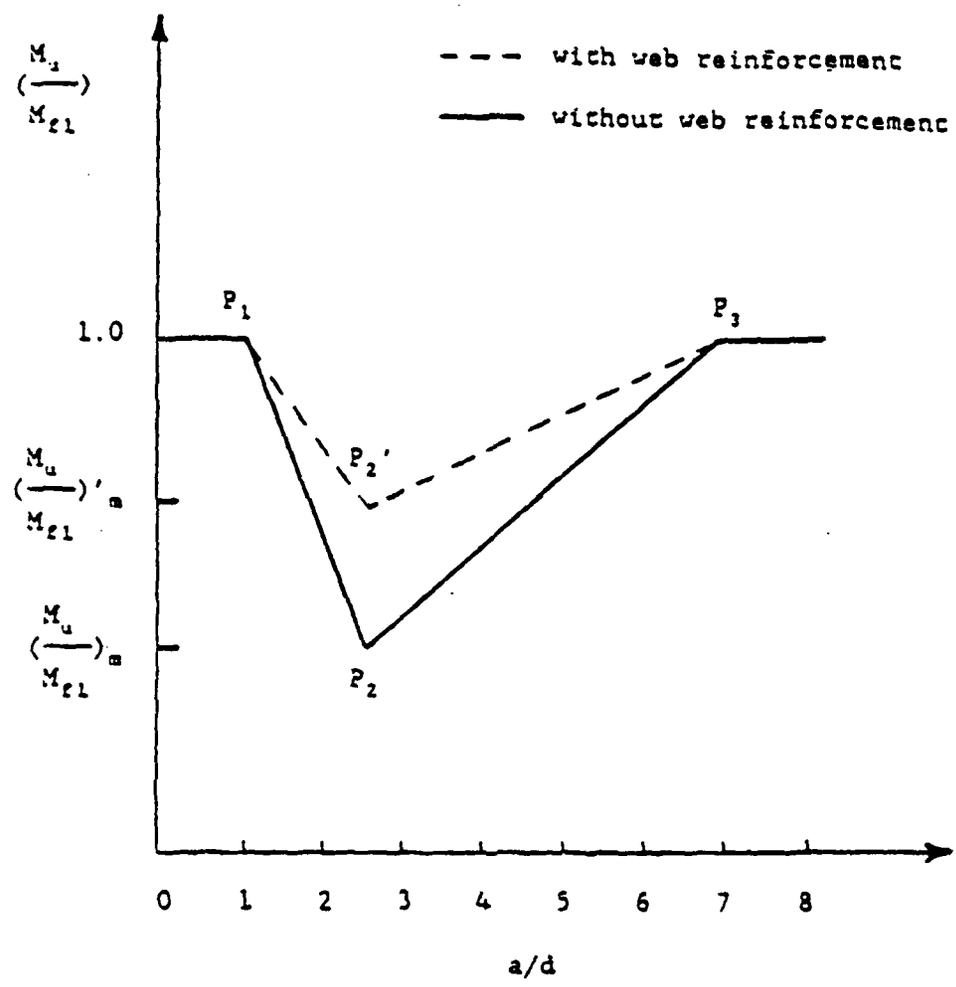

Figure 12. The Present Flexure-Shear Model

of flexural capacity. The numerical values for P_1 and P_3 were taken as one and seven (see Reference 3) for all values of the tensile reinforcement ratio.

2. Modifications for Evaluating the Influence of Shear in Beams without Web Reinforcement

The model and the procedure that is used in the present investigation for beams without transverse reinforcement is in essence the same as that proposed in Reference 3, with the following modifications:

a. From the numerical evaluation of experimental results in Reference 23 as shown in Figure 11, point P_3 may be obtained from the following proposed equation:

$$\rho > 1.88\% \quad : \quad P_3 = 7. \tag{46-a}$$

$$0.65\% \leq \rho \leq 1.88\% \quad : \quad P_3 = 7. + 365.9(\rho - 0.0188) \tag{46-b}$$

Thus, P_3 can be defined as a function of the amount of tensile longitudinal reinforcement. P_1 and P_2 have the same definition as before.

$$P_1 = 1. \tag{47}$$
$$P_2 = 2.5 \tag{48}$$

The procedure for computing the influence of shear in reducing the moment capacity for slender and deep beams without transverse reinforcement is the same as that discussed in the previous section.

b. For over-reinforced sections, shear would not have the same influence on reducing the moment capacity. In an over-reinforced beam, the concrete compression zone is considerably larger at the ultimate curvature, causing a more effective aggregate interlocking mechanism and as a result, the inclined flexure-shear cracks do not propagate as extensively as they would in an under-reinforced beam. This phenomenon is accounted for in the present model by introducing a factor called ORF (Over-reinforcing Factor) defined in the following manner:

$$\rho \leq \rho_b \quad : \quad ORF = 1 \tag{49}$$

$$\rho > \rho_b \quad : \quad ORF = \rho/\rho_b \tag{50}$$

where, ρ is the percentage of the tensile longitudinal reinforcement and ρ_b is the balanced percentage of the tensile

reinforcement defined earlier in Section II-C. ORF is subsequently applied to the minimum moment capacity ratio given earlier in the last section by Equation (45) as follows:

$$\left(\frac{M_u}{M_{f1}}\right)_m = \left(\frac{M_u}{M_{f1}}\right)_m \cdot ORF \leq 1.0 \qquad (51)$$

The expression on the left hand side of Equation (51) is the new moment ratio for the over-reinforced section. The model proposed for over-reinforced beams in shear will be verified later in Section IV by comparing the experimental results with the analytic values as obtained from the present model.

3. Shear Failure in Beams with Web Reinforcement

The improvement in shear capacity of reinforced concrete beams due to the presence of web reinforcement is primarily attributed to the following phenomena:

a. Supporting the longitudinal bars and thus increasing the dowel shear resistance.
b. Enhancing the shear resistance of the aggregate interlocking mechanism by reducing the width of the diagonal cracks.
c. Enhancing the compressive strength of concrete by confinement of concrete.
d. Suppressing tensile stresses across the concrete cantilever blocks.
e. Preventing the breakdown of forces between concrete and tensile reinforcement near the anchorage zone.

Perhaps the most accepted method for computing the shear capacity of reinforced concrete beams is the truss mechanism analogy. Referring to Figure 13, the truss analogy assumes that stirrups act like tension members and the concrete compressive struts act like compression members in the web of the analogous truss. Also, the forces in the bottom and the top chords of the truss are equivalents of the resultant compressive forces in the compression zone and the tensile force in the longitudinal steel,respectively. From equilibrium of forces at joint X:

$$V_s = T_s \, Sin\beta \qquad (52)$$

$$T_s = A_v \, f''_s \qquad (53)$$

where,
V_s = external shear force attributed to stirrups,
T_s = sum of all stirrup forces across the diagonal crack,

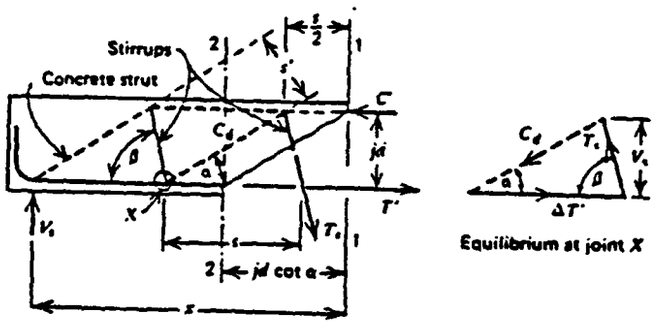

Figure 13. Internal Forces in an Analogous Truss. (Reference 2)

β = angle between stirrups and the longitudinal axis of the beam,
A_v = area of web reinforcement (both legs),
f''_s = stirrup stress.

Also, from the geometry of the truss, spacing between the stirrups, S, can be given as:

$$S = jd\ (\cot\alpha + \mathrm{Cot}\beta) \tag{54}$$

where, α is the angle between the diagonal compressive strut and the longitudinal axis of the beam. From the last two expressions, the tributary shear force per spacing of the stirrups may be given by the following equation:

$$\frac{T_s}{S} = \frac{V_s}{(jd)\mathrm{Sin}\beta(\mathrm{Cot}\alpha + \mathrm{Cot}\,\beta)} = \frac{A_v f''_s}{S} \tag{55}$$

Therefore, the shear stress that must be resisted by a single stirrup may be expressed in the following manner:

$$v_s = \frac{V_s}{b(jd)} = \frac{A_v f''_s}{b\ S}\ \mathrm{Sin}\ \beta\ (\mathrm{Cot}\alpha + \mathrm{Cot}\beta) \tag{56}$$

Assuming that stirrup stresses are beyond their respective yield stresses before a shear failure occurs, the amount of web reinforcement necessary to resist the external shear can be computed from Equation (57) as following:

$$A_v = \frac{v_s}{\mathrm{Sin}\beta\ (\mathrm{Cot}\alpha + \mathrm{Cot}\,\beta)} \left(\frac{Sb}{f''_y}\right) \tag{57}$$

where, f''_y is the yield stress of the web reinforcement.

According to the ACI-1983 Code (Reference 7) the external shear is resisted by both the concrete and the web reinforcement. This implies that

$$v_u = v_c + v_s \tag{58}$$

v_c is given by Equation (40) or (41), and v_u is the ultimate shear stress. Furthermore, the ACI code assumes that the diagonal cracks are to prevail at 45 degrees with respect to the longitudinal axis of the beam. For vertical placement of stirrups, Equation (57) reduces to the following form:

$$A_v = v_s \left(\frac{bS}{f''_y}\right) \tag{59}$$

which is the familiar expression used often in the design of web reinforcement for typical reinforced concrete beams.

The results of shear tests on reinforced concrete beams as reported by the ACI-ASCE joint committee (Reference 22) have indicated that the ACI procedure outlined above is conservative. Moreover, it is clear that the ACI design procedure does not include the interaction of bending in the shear resistance mechanism. Experimental observations have shown that unlike what is assumed in the ACI Design Code, the slope of the diagonal cracks at ultimate is not necessarily 45 degrees, and several investigators (References 25,29, and 30) have developed more accurate methods for the design of web reinforcement.

A procedure was proposed in Reference 3 to account for the contribution of shear reinforcement to the ultimate flexural capacity of slender and deep beams. In that approach point P_2 in Figure 12 is shifted upward to point P'_2 in accordance with the following formulation:

$$\left(\frac{M_u}{M_{f1}}\right)_m' = \left(\frac{M_u}{M_{f1}}\right)_m + \left[1 - \left(\frac{M_u}{M_{f1}}\right)_m\right] \text{Cot } \theta \tag{60}$$

where, θ is the shear crack angle at the failure defined by explicit empirical expressions available in Reference 3 for slender and deep beams as a function of beam geometry, material properties and the amount of web reinforcement. $(M_u/M_{f1})_m'$ is the new position of the minimum moment capacity due to the influence of web reinforcement and it replaces the value of $(M_u/M_{f1})_m$ in the right hand side of Equation (45). Thus, the new moment capacity that includes the influence of shear reinforcement for a specific case can be computed from Equation (45).

In the following two sections, two analytical failure models relevant to the ultimate shear strength in reinforced concrete beams are discussed. The first model (Section II-D-4) was originally developed by Thurlimann (References 31 and 32) and later used to verify test results in Reference 33. The second model (Section II-D-5)

was discussed in Reference 34 which also agreed well with experimental results. The primary purpose of discussing these models is to create a rational explanation for the shear model that is proposed later in Section II-D-6.

4. The Truss Shear-Flexure Interaction Model

A free body diagram of the truss model is shown in Figure 14. As described before, the tension force in the lower chord represents the tension force in flexural reinforcement and the compression force in the upper truss chord is the net compressive force of concrete in flexural compression with any compression reinforcement. The direction of the maximum principal tensile stress is perpendicular to the cracks and the principal compression stresses act in a direction parallel to the diagonal cracks, forming the compressive strut of the analogous truss. The web reinforcement represents the vertical tension ties of the space truss.

This model assumes the following (Reference 33):

1. The longitudinal reinforcement must yield prior to shear failure. Therefore, only under-reinforced beams may be analyzed by this model.
2. The tensile strength of concrete is ignored.
3. Dowel and aggregate interlocking contributions are ignored.
4. Diagonal crushing of concrete does not precede the yielding of the web reinforcement. Thus, it is not necessary to assume an upper bound limit for the concrete stresses in the compressive strut.
5. Longitudinal reinforcement is properly anchored to avoid bond or slip failure.

A moment balance about point O in the free-body diagram of segment AB of the beam shown in Figure 14 gives the following relationship:

$$M = C(jd) - nA_v f''_s \left(\frac{jd}{2} \cot\alpha\right) \qquad (60)$$

where,
n = number of stirrups in the cracked segment AB,
α = angle of the diagonal compression strut at ultimate,
A_v = area of two legs of stirrup,
f''_s = stress in the web reinforcement,
C = compressive force in the upper chord of the analogous truss,
jd = distance between tensile and compressive chords of the analogous truss.

Dividing both sides of the last equation by (jd) and assuming the transverse reinforcement has yielded prior to the failure of the beam (i.e., $f''_s = f''_y$),

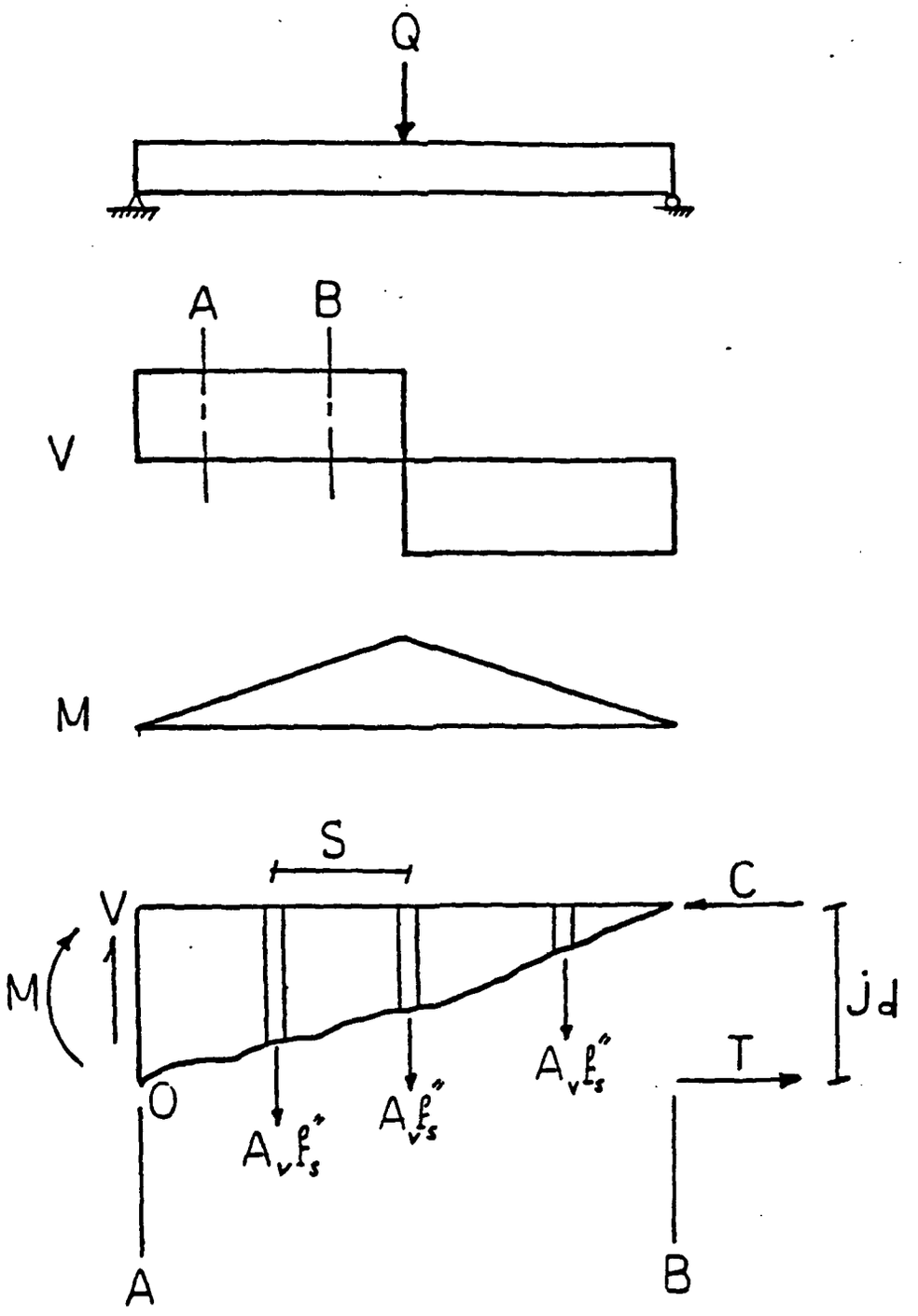

Figure 14. Forces in the Flexure-Shear Truss Model

$$C = \frac{M}{(jd)} + \frac{V_u}{2} \text{Cot}\alpha \tag{61}$$

where, V_u is the ultimate shear at failure. Neglecting the shear capacity of concrete, V_u can be given by the following expression:

$$V_u = nA_v f''_y = \left(\frac{jd}{S}\right) \text{Cot}\alpha \; A_v \; f''_y \tag{62}$$

where, S is the spacing between the vertical stirrups. Therefore, the angle α at ultimate can be obtained from either of the following two equations:

$$\text{Tan}\alpha = \frac{A_v f''_y (jd)}{V_u \; S} \tag{63}$$

or

$$\text{Tan}\alpha = \frac{\rho'' f''_y}{V_u} \tag{64}$$

where, v_u is the ultimate shear stress at failure and ρ'' is defined as the percentage of the web reinforcement. They are given by the following relationships:

$$v_u = \frac{V_u}{b(jd)} \tag{65}$$

$$\rho'' = \frac{A_v f''_y}{Sb} \tag{66}$$

Equation (64) shows that the angle of the diagonal strut at ultimate shear stress is function of the yield strength and the amount of the web reinforcement as well as the ultimate shear stress in the beam.

Substituting for Cotα from Equation (64) into Equation (61),

$$C = \frac{M}{jd} + \frac{V_u^2 S}{2(jd)A_v f''_y} \qquad (67)$$

If the longitudinal tensile reinforcement (lower chord of the analogous truss) has also yielded prior to the failure of the beam, then,

$$M = M_u = (T \text{ or } C)(jd) = A_s f_y (jd) \qquad (68)$$

and,

$$C = \frac{A_s f_y}{jd} + \frac{V_u^2 S}{2(jd)A_v f''_y} \qquad (69)$$

Equation (69) represents the combined effect of bending and shear at failure, provided that both longitudinal and web reinforcement have yielded prior to failure. For the case of pure bending, one can set ($V_u = 0$) in Equation (69). This will give the pure flexural capacity of the beam as

$$V_u = 0 \quad ; \quad M_u = M_{f1} = T(jd) = A_s f_y (jd) \qquad (70)$$

For the case of pure shear (no bending), one can set $M_u = 0$ in Equation (69). This will give the maximum value of shear strength as

$$M_u = 0 \quad ; \quad V_u = V_{us} = \left[\frac{2T(jd)A_v f''_y}{S}\right]^{1/2} \qquad (71)$$

Combining Equations (69), (70), and (71) will result in the basic flexure-shear interaction relationship as follows:

$$\frac{M_u}{M_{f1}} + \left(\frac{V_u}{V_{us}}\right)^2 = 1 \qquad (72)$$

Equation (72) is only valid if both longitudinal and web reinforcement have yielded prior to failure.

Unlike the traditional truss analogy where the angle of

compression strut is always assumed to be 45°, Thurlimann's space truss model is valid for all inclinations of α. However, as the following kinematic analysis will show, the requirement that both web and longitudinal reinforcement yield places certain limitations on the magnitude of the angle α.

The angle of inclination of the concrete strut given by Equation (64) is defined at ultimate (just before failure) and not during the earlier load levels. As the loading increases from the initial cracking, diagonal cracks widen and the orientation of the diagonal compression strut will change until the cracks are so widely open that no further shear transfer by aggregate interlocking can take place across the cracks. At this point the redistribution of internal stresses as well as any further changes in the inclination of the diagonal compression strut stops, thus, causing the failure of the beam.

Thurlimann and others (References 31,32, and 33) introduced limitation on the use of Equation (72). The limitations were primarily based on the magnitude of diagonal tension crack width and the relative strain values in the chords and stirrups. From the kinematic relationship between the strains in the analogous truss members and the width of the crack, it is possible to show that at least analytically, the state of strain in the web of the analogous truss and the longitudinal reinforcement determine the crack width at failure (Reference 33). The assumptions for the kinematic strain model are as follows (Reference 33):

1. The beam is under-reinforced.
2. Concrete in the compression strut is rigid.
3. Deformations are only due to the longitudinal and web reinforcement.
4. At failure, the angle of the principal compressive stress corresponding to the force in the diagonal compressive strut coincides with the angle of inclination of the principal compressive strain.

Consider the state of the strain in the shear field element (Figure 15). Figure 15-a represents the shearing strain due to the elongation of the stirrups and Figure 15-b shows the state of strain due to the deformation of the longitudinal bars. The total shear strain due to the stirrup strain and the longitudinal chord strain is

$$\gamma_T = \gamma_s + \gamma''_s \tag{73}$$

where, γ''_s and γ_s are the shearing strains due to the transverse and longitudinal reinforcement, respectively. From Figures 15-a and 15-b;

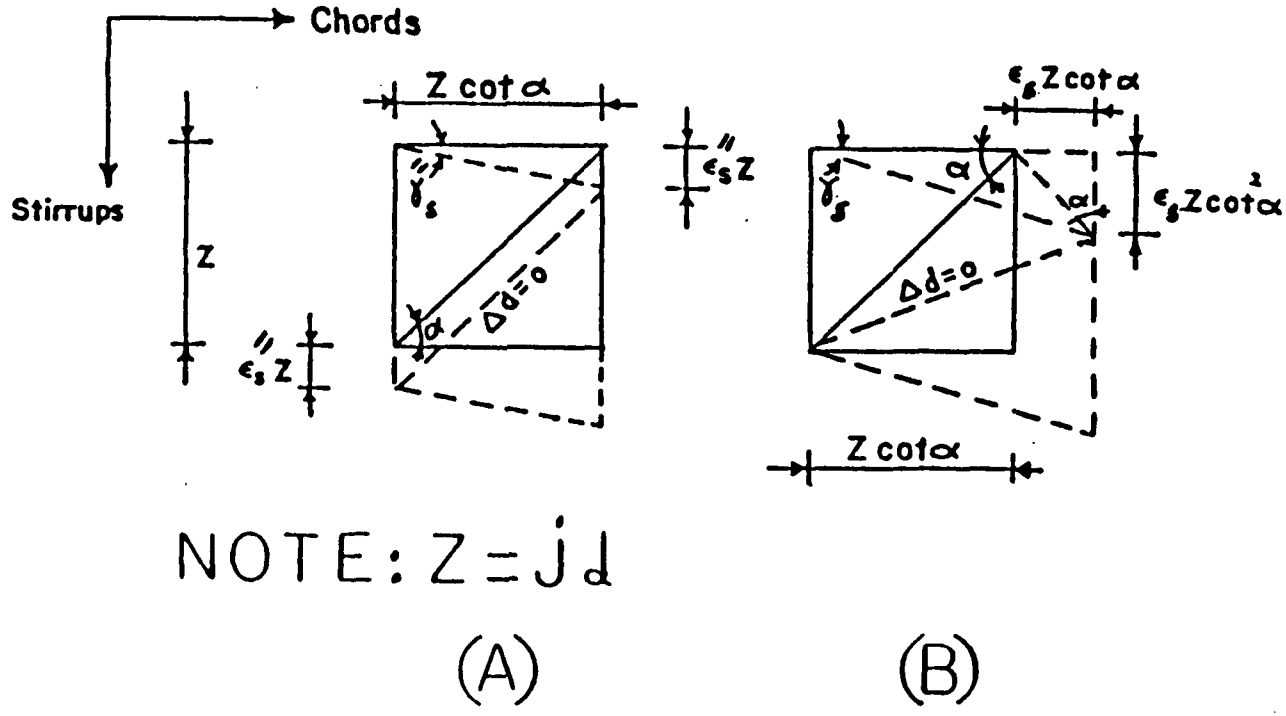

Figure 15. Deformation Diagrams for the Shear Field Element.
(A) Shear Strain Due to Stirrup Strain.
(B) Shear Strain Due to Chord Strain.
(Reference 33)

$$\gamma_s = \frac{\varepsilon_s \, \mathrm{Cot}\alpha}{1 + \varepsilon_s} = \varepsilon_s \, \mathrm{Cot}\alpha \qquad (74)$$

$$\gamma''_s = \frac{\varepsilon''_s \, (jd)}{(jd) \, \mathrm{Cot}\alpha} = \varepsilon''_s \, \mathrm{Tan}\alpha \qquad (75)$$

substituting the last two relationships into Equation (73),

$$\gamma_T = \varepsilon_s \, \mathrm{Cot}\alpha + \varepsilon''_s \, \mathrm{Tan}\alpha \qquad (76)$$

From Figure 16, the relationship between the mean crack strain, ε_{cr}, and the strain in the longitudinal and the transverse direction can be given as follows.

$$\varepsilon_s = \varepsilon_{cr} \, \mathrm{Sin}^2\alpha \qquad (77\text{-a})$$

$$\varepsilon''_s = \varepsilon_{cr} \, \mathrm{Cos}^2\alpha \qquad (77\text{-b})$$

where, the mean crack strain is defined as the ratio of the mean crack width to the spacing between two adjacent cracks. From the last two equations,

$$\varepsilon_{cr} = \varepsilon_s + \varepsilon''_s \qquad (78)$$

Equation (77) can be rearranged in the following form:

$$\frac{\varepsilon_{cr}}{\varepsilon_s} = 1 + \mathrm{Cot}^2\alpha \qquad (79\text{-a})$$

$$\frac{\varepsilon_{cr}}{\varepsilon_s} = 1 + \mathrm{Tan}^2\alpha \qquad (79\text{-b})$$

Assuming that both the transverse reinforcement and the longitudinal reinforcement yield at failure, Equation (79) may be rewritten as follows.

$$\frac{\varepsilon_{cr}}{\varepsilon_y} = 1 + \mathrm{Cot}^2\alpha \qquad (80\text{-a})$$

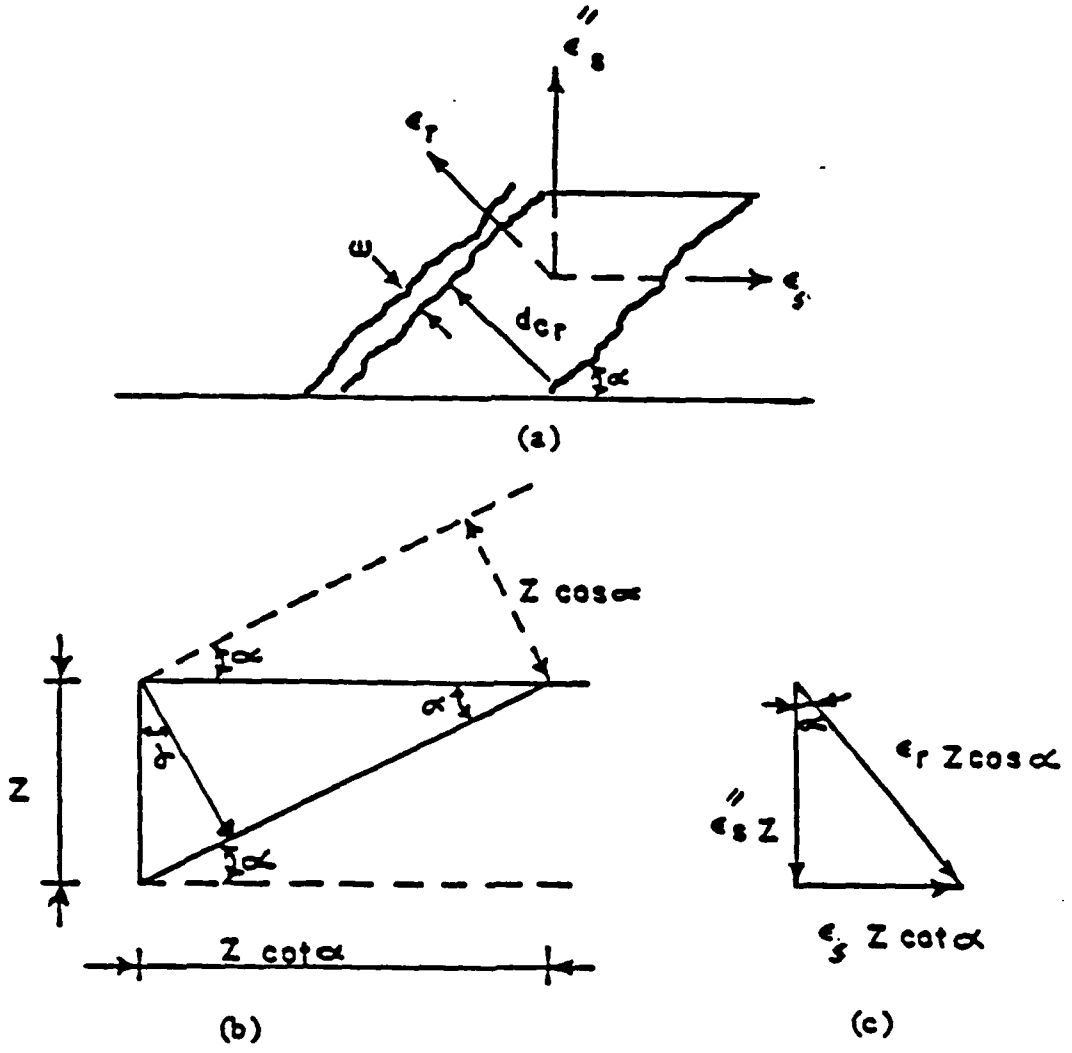

Figure 16. State of Strain in the Diagonal Strut.
(Reference 33)

$$\frac{\varepsilon_{cr}}{\varepsilon_y} = 1 + \text{Tan}^2\alpha \qquad (80\text{-b})$$

Equation (80) are plotted on the same graph in Figure 17. If both the longitudinal and the web reinforcement are at their respective yield points, the mean crack width has the smallest possible value. An angle of inclination that is less than 45° represents a failure in which the transverse reinforcement is strained more than the longitudinal reinforcement and yielding of the chord reinforcement could increase the width of the diagonal crack to the point that no additional shear transfer across the previously formed cracks can take place. Conversely, an angle of inclination greater than 45° represents a failure in which the strain in the transverse reinforcement is less than the strain in the longitudinal reinforcement and yielding of the web reinforcement increases the crack width. Based on experimental observations, it is suggested that the analogous space truss shear-bending interaction model can predict satisfactory results for the following range:

$$26° \leq \alpha \leq 63° \qquad (81\text{-a})$$

$$0.5 \leq \text{Tan}\,\alpha \leq 2.0 \qquad (81\text{-b})$$

These restrictions are introduced to account for the fact that the deformation of the concrete compression strut may alter the validity of Equation (72). Moreover, when the angle α is less than 26°, diagonal crushing of the compression strut may occur prior to the yielding of the flexural reinforcement (Reference 33), thus, placing a limitation on the use of Equation (72).

The limiting values of the angle of compression strut in the space-truss model should not be thought as fixed points (Reference 33). These limits, as for example suggested by Equations (81), only represent the transition between different mechanisms of failure. According to the space truss model, if the angle of the diagonal compression strut at failure is less than 45 degrees, the strain in the web reinforcement is beyond yield. Furthermore, if this angle is less than 26 degrees, the longitudinal reinforcement has not reached its yield strain at the ultimate. This would be an example of a pure shear mechanism in which the influence of shear is expected to cause a premature failure in the beam before the ultimate flexural capacity of the beam is developed. For values of the angle between 26 and 45 degrees, the strain in the transverse steel at the ultimate load is higher than the strain in the longitudinal reinforcement. This is flexure-shear type failure in which the moment capacity of the beam is

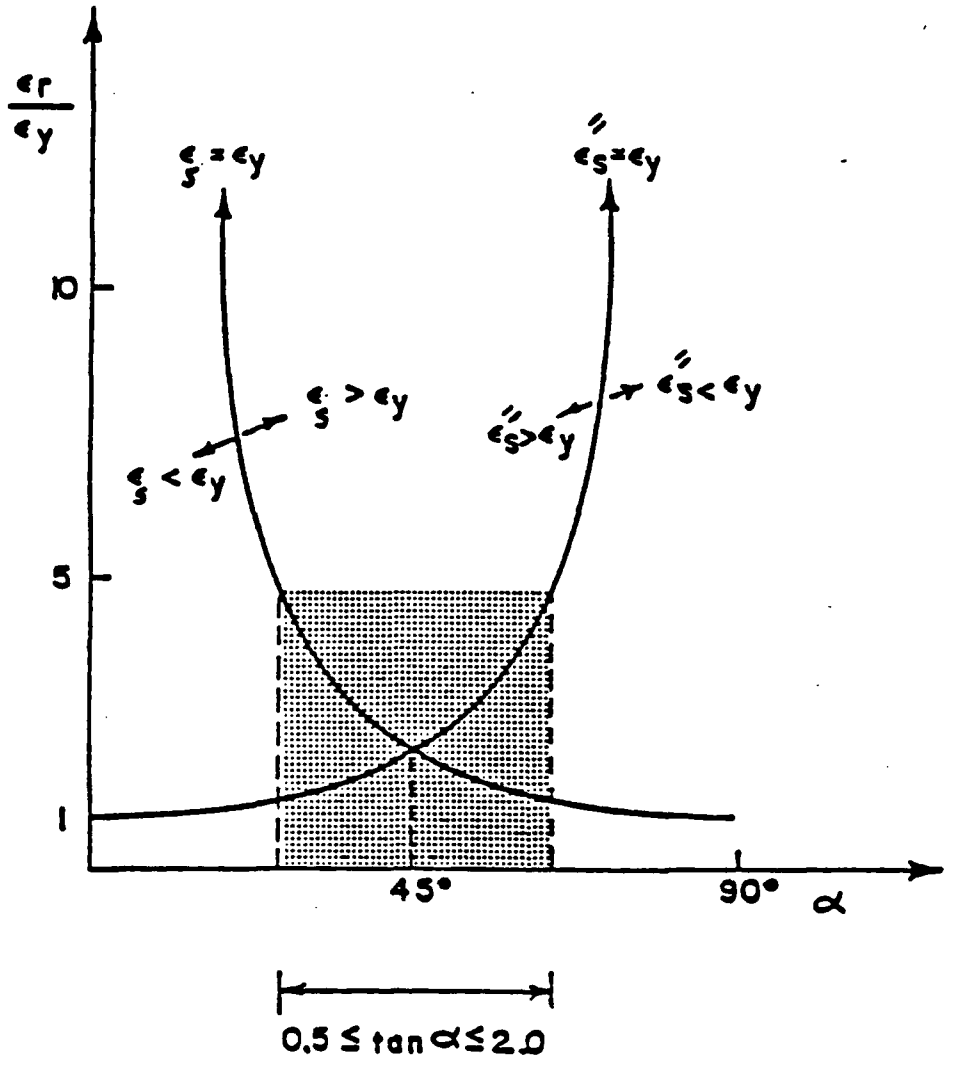

Figure 17. Mean Ratio of Crack Strain to Yield Strain vs. the Angle of Diagonal Strut at Ultimate. (Reference 33)

reduced by the shear influence. The minimum value of the angle for which the full flexural capacity of the beam can be developed is 45°. When Tanα is equal to unity, both the longitudinal and the transverse reinforcement of the shear field element yield. In fact, as shown in Figure 16, when the angle α is 45°, the mean crack width has the minimum possible value, thus, resulting in highest shear strength at the collapse mechanism. For all values of the inclination of the diagonal compression strut greater than 45°, the shear stress in the beam at ultimate must be less than the shear capacity as provided by the transverse reinforcement in Equation (56). In that case, the mode of failure is by flexure and the moment capacity of the beam remains unaffected. Hence, the inclination of the diagonal compression strut can be used as a parameter to relate the influence of shear to the ultimate flexural strength of beams which fall into the critical shear region, namely beams with shear-span to the effective depth ratio between one and seven.

5. Diagonal Tension at the Ultimate Load Condition

The problem of shear in reinforced concrete beams has also been approached by the limit analysis technique as developed presented by Nielsen and presented in Reference 34. This was done by considering an admissible stress field in the web of the reinforced concrete beam. From equilibrium of forces in Figure 18, the compressive force in the diagonal concrete strut can be given by the following expression:

$$D = f_d\, b\, (jd)\, \text{Cos}\alpha = \frac{V}{\sin\alpha} \tag{82}$$

where, f_d is the stress in the diagonal strut defined as:

$$f_d = \frac{V}{b(jd)\, \text{Cos}\alpha\, \text{Sin}\alpha} = \frac{v}{\text{Cos}\alpha\, \text{Sin}\,\alpha} \tag{83}$$

Moreover, the stresses in the x and y directions for the element that is bound by diagonal cracks are as follows (Figure 18):

$$\sigma_x = f_d\, \text{Cos}^2\alpha \tag{84-a}$$

$$\sigma_Y = f_d\, \text{Sin}^2\alpha \tag{84-b}$$

The vertical component of the stress field is in equilibrium with the stirrup forces and therefore,

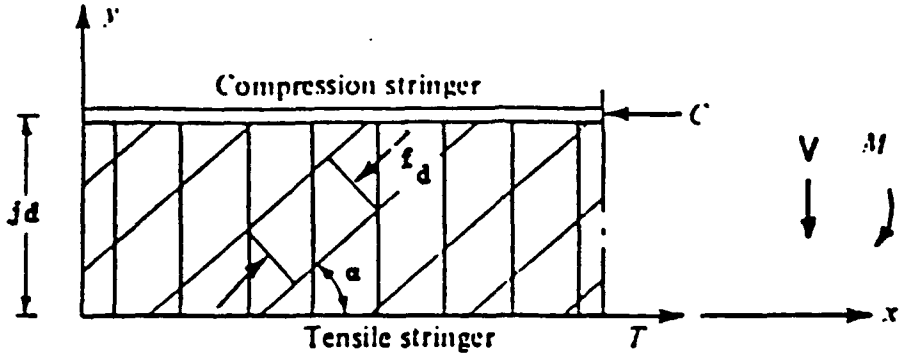

Figure 18. Idealized Stress Field in Beams with Vertical Stirrups. (Reference 34)

$$f_d \, Sin^2\alpha = \frac{A_v f''_y}{b \, S} = \rho'' f''_y \qquad (85)$$

Substituting Equation (83) into Equation (85) and rearranging the terms,

$$Tan\alpha = \frac{\rho'' f''_y}{v} \qquad (86)$$

At the point of collapse, shear is at ultimate (i.e., $v = v_u$)

$$Tan\alpha = \frac{\rho'' f''_y}{v_u} \qquad (87)$$

This is the same as Equation (64) obtained previously from the space-truss analogy. After some algebraic manipulation, it is possible to arrive at the following relationships:

$$Tan\alpha = \left[\frac{\left(\frac{\rho'' f''_y}{f_d}\right)}{1 - \left(\frac{\rho'' f''_y}{f_d}\right)}\right]^{1/2} \qquad (88)$$

$$\frac{v_u}{f_d} = \left[\frac{\rho'' f''_y}{f_d}\left(1 - \frac{\rho'' f''_y}{f_d}\right)\right]^{1/2} \qquad (89)$$

Figure 19 shows plots of the last two equations. It can be seen that when $(\rho'' f''_y)/f_d$ increases from zero to 0.5, the angle of compression strut increases, from zero to a maximum of 45°. Also, when $(\rho'' f''_y)/f_d$ is 0.5, the shear strength is maximum and the angle of the diagonal compression strut is at 45°. This reveals that for any angle greater than 45°, the shear strength of the beam does not increase with increasing the amount of the transverse reinforcement. Nielsen also showed that for values of $(\rho'' f''_y)/f_d$ greater than 0.5, the angle α stays constant at 45°.

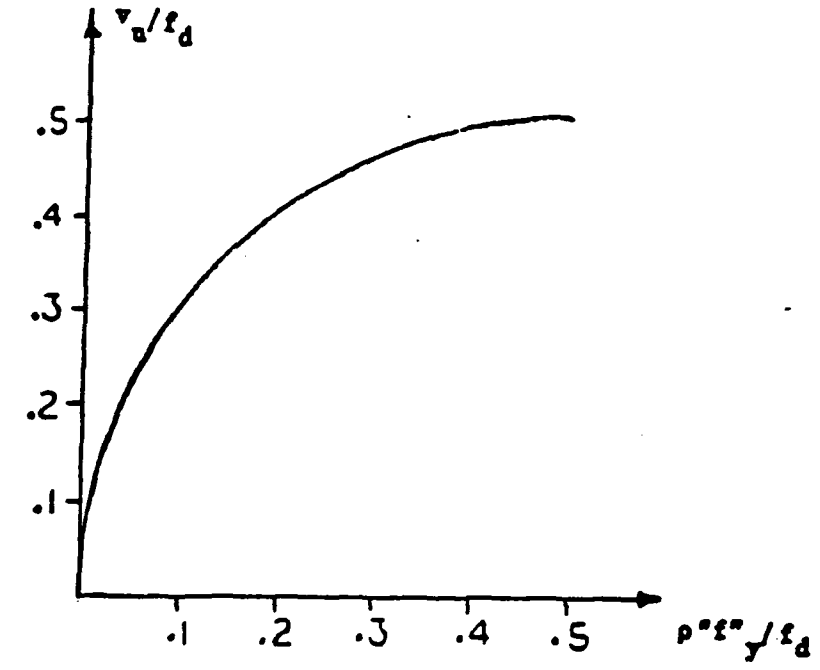

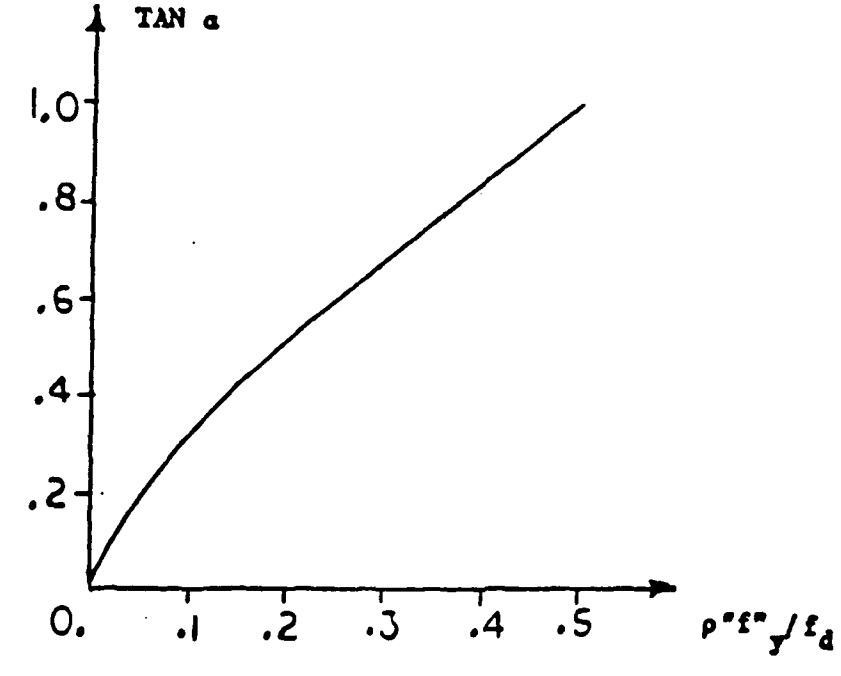

Figure 19. Plots of Equations (88) and (89)

6. A Modified Method to Evaluate the Influence of Shear in Beams with Web Reinforcement

The angle of compression strut with the longitudinal axis of the beam is a good measure for the determination of shear influence in reducing the flexural strength of the beam. This concept was employed here to account for the improvement in the moment capacity ratio of the beams, (M_u/M_{f1}), due to the presence of web reinforcement. For that purpose, the rational approach of the truss mechanism (Sections II-D-3 through II-D-5) was used in conjunction with results of tests from various sources in the literature. The modified method has been developed for rectangular deep beams ($1 \leq a/d \leq 2.5$) as well as rectangular and T slender beams ($2.5 \leq a/d \leq 7$), as follows.

a. Deep Rectangular Beams:

The model proposed here for deep rectangular beams is based on experimental results from a study by Clark (Reference 35), in which the beams were loaded by either a single concentrated load at their midspan, or by two single concentrated loads at their quarter span points.

The following variable defined the influence of the material property and the amount of the web reinforcement:

$$\rho^* = \frac{\rho'' f''_y}{\sqrt{f'_c}} \tag{90}$$

where f'_c is the compressive strength of concrete and ρ'' is the web reinforcement ration, and f_y'' is the yield stress of stirrups. Table A-1 in Appendix A presents the data for the 27 beams which are used in this study. When the product of the variables ρ^* and a/d were plotted against the angle of the compression strut at ultimate, as computed from Equation (87) for 27 beams (Reference 35), the following linear relationship was observed, as illustrated in Figure 20.

$$\alpha = 2.72\ \rho^*\ (a/d) + 4.08 \tag{91}$$

It can be seen that the scatter between data for the 27 points is not large, resulting in a statistical correlation coefficient of 0.91. Moreover, Figure 20 shows that the angle α improves with increasing the amount of web reinforcement. Therefore, the influence of beam geometry and material properties on the angle of diagonal compression strut at failure can be reasonably predicted. The experimental data from which the last expression was obtained fell into the following parametric ranges : $3200 \leq f'_c \leq 4200$ psi, $f''_y = 48$ ksi, $1.57 \leq a/d \leq 2.42$, and $0.0035 \leq \rho'' \leq 0.0096$.

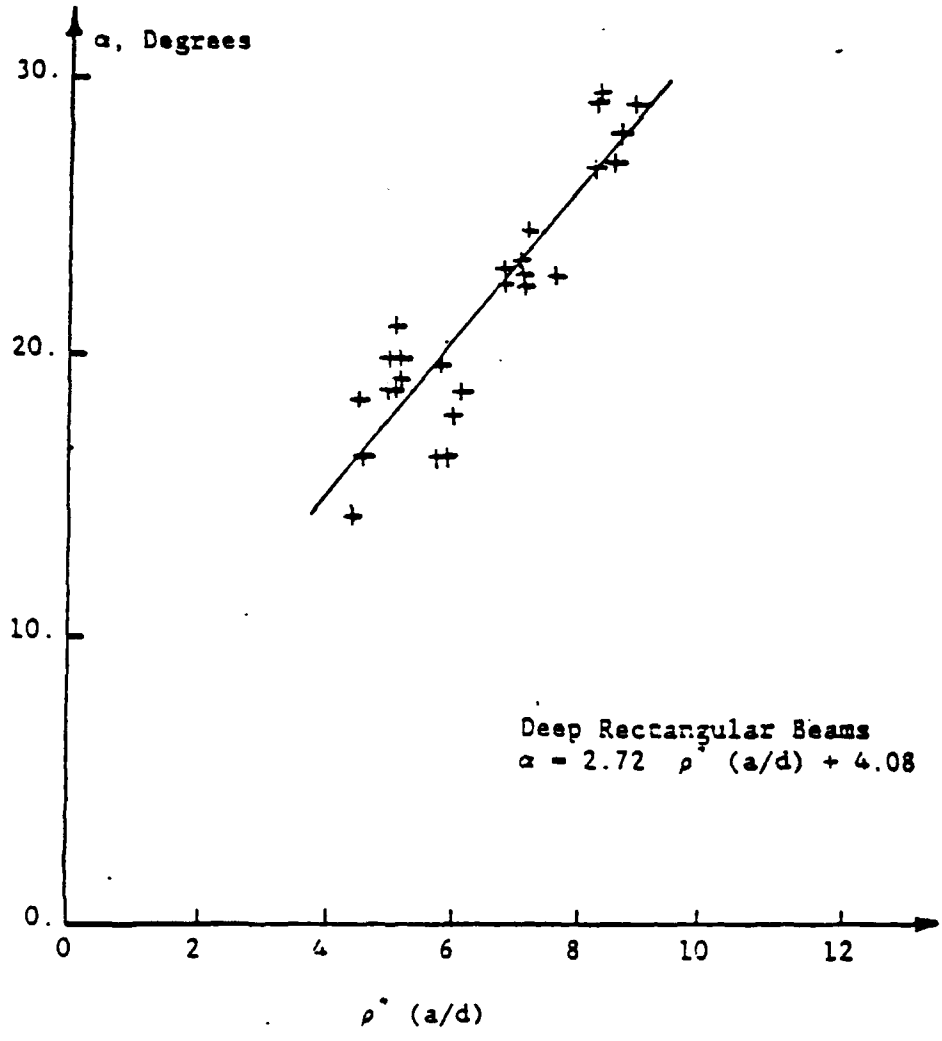

Figure 20. Inclination of the Concrete Compression Struts at Ultimate for Deep Rectangular Beams Based on Experimental Data from Reference 35

b. Slender Rectangular Beams:

The experimental data for the 27 rectangular under-reinforced slender beams used for the derivation of the following formulation were gathered from studies by Burns and Siess (Reference 1), Bresler and Scordelis (Reference 36), Placas and Regan (Reference 28), and Mattock and Wang (Reference 37). These beams were loaded by either a single concentrated force at their midspan or two concentrated loads at quarter span points. In this case it became clear that the variable $\rho^* \sqrt{a/d}$ provided a better correlation to the data than $\rho^*(a/d)$ which was the the better choice for deep beams. When the variable $\rho^* \sqrt{a/d}$ for these beams was computed (Table A-2 in Appendix A) and plotted against the angle of the diagonal compression strut at ultimate, as shown in Figure 21, the following linear relationship was derived.

$$\alpha = 3.06 \ (\rho^* \sqrt{a/d}\ ) + 7.22 \qquad (92)$$

Again, the scatter between the 27 points about the best fitted line was small, reflecting in a correlation coefficient of approximately 0.99, and the properties of the 27 beams used in the last expression fell into the following parametric ranges; $1850 \leq f'_c \leq 6230$ psi ($12.7 \leq f'_c \leq 43$ MPa), $47.2 \leq f_y'' \leq 60.2$ psi ($325 \leq f_y'' \leq 414$ Mpa), $3 \leq a/d \leq 7$, and $0.004 \leq \rho'' \leq 0.001$.

c. Slender T Beams:

Here, the data was obtained from experimental investigations by Placas and Regan (Reference 28) and Mattock et al. (Reference 38) for tests on 29 under-reinforced T beams loaded by a concentrated force at midspan. The data for these beams is documented in Table A-3 in Appendix A. For these cases, the following relationship was derived, as illustrated in Figure 22.

$$\alpha = 1.63 \ (\rho^* \sqrt{a/d}\ ) + 9.55 \qquad (93)$$

The correlation coefficient for Equation (93) is computed as 0.98, and the range of beam parameters were as follows; $1850 \leq f'_c \leq 7840$ psi ($12.7 \leq f'_c < 54$ MPa), $50 \leq f_c'' \leq 52$ ksi ($344.7 \leq f_y'' \leq 358.5$ MPa), $2.5 < a/d < 4.5$, and $0.0017 \leq \rho'' \leq 0.018$.

Unlike the traditional truss analogy where the angle of compression strut, α, at ultimate is assumed to be at 45°, Thurlimann and other investigators (References 29,31,32,33, and 34) developed and verified analytical models that were valid for a wide range of α values. In Sections II-D-4 and II-D-5 it was shown that, at least analytically, when the angle α was at 45°, shear would have no influence in reducing the moment capacity ratio. However, if $\tan\alpha$ was less than unity, the moment capacity ratio would be reduced. Therefore, it is reasonable to expect that α can be chosen as a parameter that can represent the interaction between the shear and

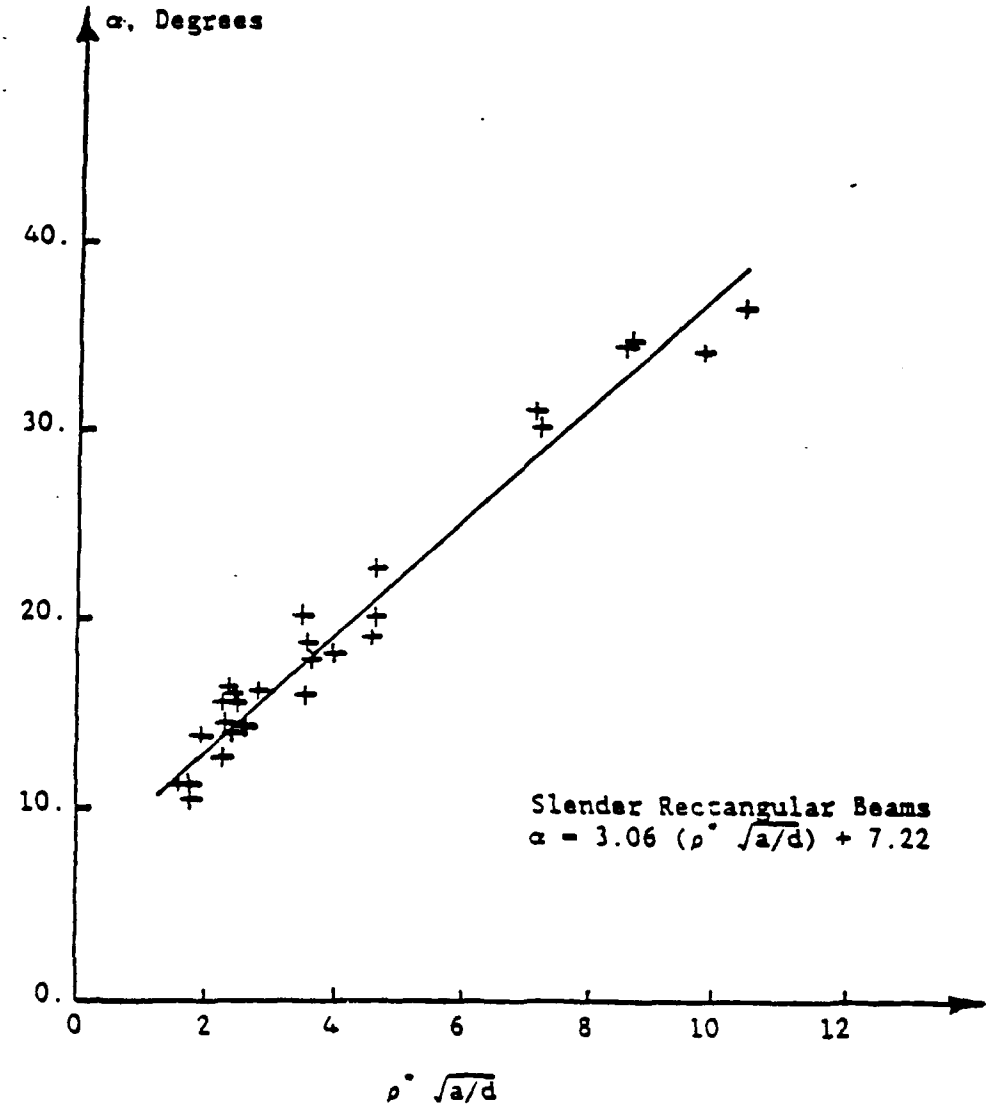

Figure 21. Inclination of the Concrete Compression Struts at Ultimate for Slender Rectangular Beams (Experimental Data from References 1,28,,36, and 37)

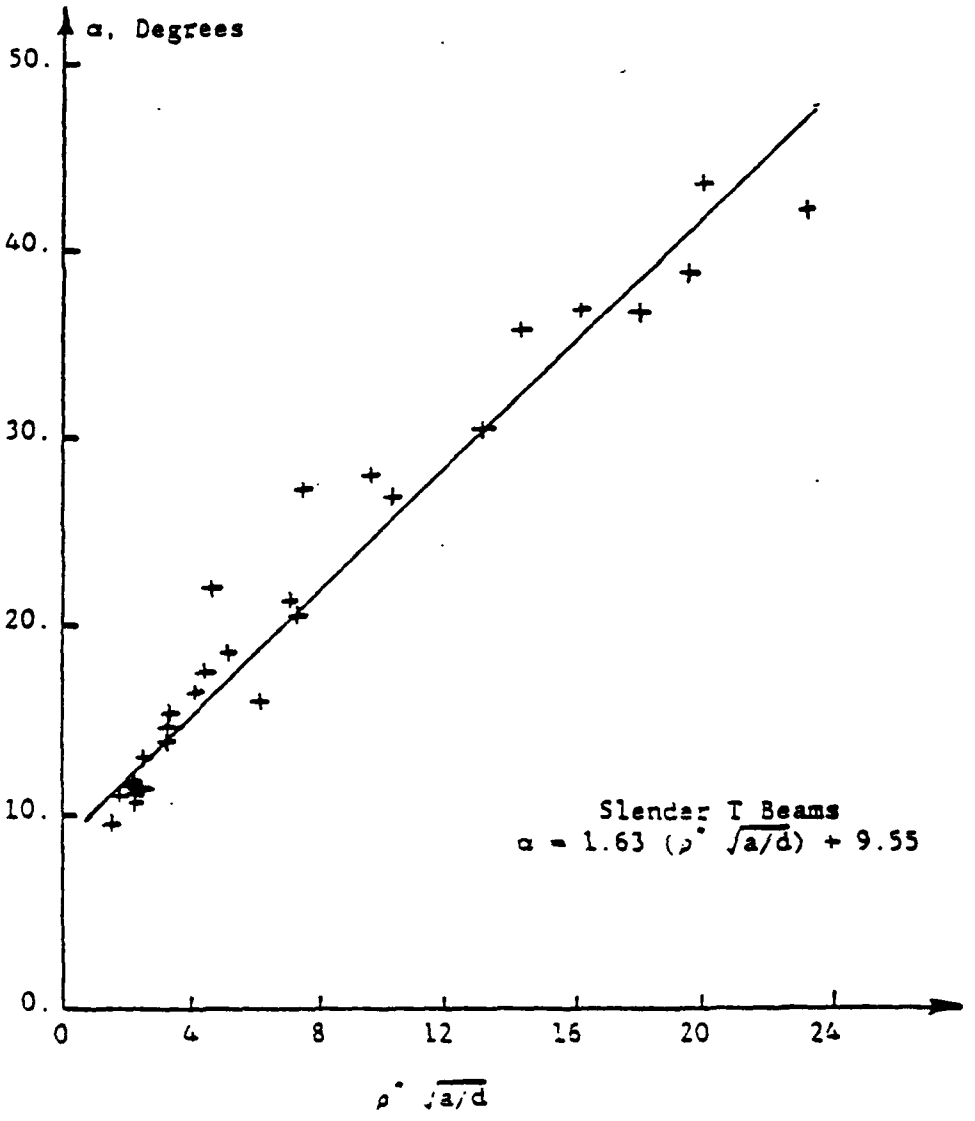

Figure 22. Inclination of the Concrete Compression Struts at Ultimate for Slender T Beams (Experimental Data from References 28 and 38)

flexure. Following in the same direction, it was decided to choose the function "tan α" as the parameter which would represent the effect of shear reinforcement on the ultimate capacity of the beam by varying the value of the minimum moment capacity ratio (point P_2 in Figure 11) as defined next.

$$\left(\frac{M_u}{M_{f1}}\right)'_m = \left(\frac{M_u}{M_{f1}}\right)_m + \left[1.0 - \left(\frac{M_u}{M_{f1}}\right)_m\right] * \tan \alpha \qquad (94)$$

where, $(M_u/M_{f1})'_m$ is the new (enhanced) value of the minimum moment capacity ratio due to the influence of transverse reinforcement. The improvement in the flexural capacity of the member is schematically shown in Figure 11 by shifting the point P_2 upward to a new point P'_2. The present approach is different from the previous study (Reference 3) in which α was defined as the measured angle of shear crack, and the function "cot α" was used for modifying the minimum flexural ratio.

The above procedure can be summarized in the following steps for deep beams and for slender beams,respectively:

1. Deep beams

   a. Compute $\rho^*(a/d)$ for the deep beam.
   b. Using Equation (91), compute the angle α.
   c. Compute the minimum moment capacity $(M_u/M_{f1})_m$ ratio by using Equations (44).
   d. Modify the minimum moment ratio of step 3 by using Equation (94) to account for the improvement in the ultimate capacity caused by the shear reinforcement.
   e. Use the modified minimum moment ratio in Equation (45-b) to obtain the moment capacity ratio of the deep beam, M_u/M_{f1}.

2. Slender Beams

   a. Compute $\rho^*/(a/d)$ for the slender beam.
   b. Compute the angle α from Equation (92) if the beam has a rectangular cross section and from Equation (93) if the cross section is T shaped.
   c. Compute the minimum moment capacity ratio $(M_u/M_{f1})_m$ by using Equations (44).
   d. Modify the minimum moment capacity ratio in accordance with Equation (94) to include the effect of shear reinforcement.
   e. Employ the modified minimum moment ratio in Equation (45-a) to obtain the moment capacity ratio of the beam, M_u/M_{f1}.

Hence, it is possible to represent the influence of shear on the

flexural capacity by SRF (Shear Reduction Factor) as following

$$SRF = \left(\frac{M_u}{M_{fl}}\right) \tag{95}$$

In the previous study (Reference 3), the SRF was applied only to the ultimate moment. Since this study is concerned also with the overall behavior of beams, it is proposed here to multiply all values of the computed moments between zero and failure by the SRF. It must be noted that the concept of SRF, as defined here, was originally developed in Reference 3, but the formulation for the influence of web reinforcement on the flexural capacity of deep and slender beams was different from the proposed procedure, as discussed in Section II-D-3. Furthermore, contrary to the initial assumption that shear deformations were negligible compared to the bending deformations, it was observed later (as discussed later in Section IV) that the computed collapse deflection of beams sensitive to shear (SRF<1) could be increased slightly to account for shear deformations and to obtain better correlation with the available experimental results. Therefore, it is also proposed here to divide all computed curvatures, from zero to the ultimate, by the SRF. Thus, to compute the modified moment-curvature diagram that includes shear effects, one can multiply the moments by the SRF and divide the curvatures by the SRF to obtain the new curve.

E. EFFECT OF AXIAL COMPRESSIVE FORCE ON MEMBERS WITH FLEXURE AND SHEAR

The presence of an axial compressive load acting on the cross section of the beam is accounted for by modifying the equilibrium expression, Equation (17), to the following form:

$$T + P_{axial} = C_c + C_s \tag{96}$$

where T, C_c ,C_s have been defined before and P_{axial} is the constant axial compressive force.

From basic analysis of reinforced concrete beam-columns, it is understood that as long as the magnitude of the axial force is below the balance condition, the result is an enhancement of the moment capacity of the cross section. Furthermore, the effect of axial force on reinforced concrete beams that fall into the critical shear region ($1 < a/d < 7$) is to reduce the tensile stresses and delay the opening of the diagonal tension cracks. The presence of axial force increases the depth of the compression zone and prevents the extension of the cracks far into the compression block.

The ACI 318-83 Design Code suggests the use of the following equation in lieu of Equation (40) to reflect the improvement of the shear capacity in the presence of the axial force:

$$v_c = 1.9\sqrt{f'_c} + 2500\,\rho\,\frac{V_u d}{M_m} \qquad (97)$$

where, V_u is the ultimate shear capacity of the beam and M_m is modified ultimate moment given by the following approximate equation,

$$M_m = M_u - P_{axial}\left(\frac{4h-d}{8}\right) \qquad (98)$$

where, h is the overall depth of the beam. Alternatively, the ACI Code also recommends the following equation to account for the enhancement in shear capacity of concrete with axial force:

$$v_c = 2\left(1+0.0005\,\frac{P_{axial}}{A_g}\right)\sqrt{f'_c} < 3.5\sqrt{f'_c}\left(1+\frac{0.002\,P_{axial}}{A_g}\right)^{1/2} \qquad (99)$$

Mattock and Wang (Reference 37) studied the influence axial compressive force on the shear strength of reinforced concrete beams and concluded that Equation (99) is too conservative. Instead, they recommended the following expression:

$$v_c = 2\sqrt{f'_c}\left(1+\frac{3P_{axial}}{A_g\,f'_c}\right) \le 3.5\sqrt{f'_c} + \frac{0.3P_{axial}}{A_g} \qquad (100)$$

Experimental results obtained by Mattock et al. (References 37,38, and 39) have reconfirmed that increasing the axial compressive force improves the shear capacity of the beam. In addition, it was found that the contribution of the web reinforcement to the ultimate strength of the beam is approximately independent of the magnitude of the axial force.

The increase in the strength of beams caused by the axial force is included in the analytical model proposed in this report. This nonlinear second order effect of axial force is discussed later in Section III-F-4.

F. LOAD-DEFORMATION ANALYSIS OF RC BEAMS AND BEAM-COLUMNS

1. Introduction

Upon obtaining a complete moment-curvature relationship for the cross section of the structural element, including the effects of shear and axial force, it was desired to derive the load-deformation relationship for the element. The primary reasons of this phase of analysis were to obtain a quantitative description of the behavior of the structural element from the onset of loading to the ultimate (collapse) stage under a static loading condition, and to compare that information with the available experimental data. The proposed step-by-step procedure accounts for the nonlinear distribution of the curvatures on the span as well as the possibility of nonlinearities associated with the support conditions.

In addition to the load-deflection relationship, if a dynamic analysis was required, it would be necessary to compute the deformed configuration of the structural element at every load step, and to employ that information for computing the parameters of the equivalent dynamic model. The second major goal of the analysis at this stage was to compute these variables as discussed later in Section III.

The numerical method employed here for deriving the load-deformation relationship from the moment-curvature diagram is based on the following assumptions:

1. The approximate theory for small rotations and deflections is employed. This assumption implies that deformations are small enough so that the slopes and curvatures can be closely approximated by the first and the second derivatives of the deflection curve with respect to the position coordinate. Figure 23 shows the small-deformation and large-deformation solution for the center deflection of a simply supported beam subjected to a concentrated load at midspan. For deflections as high as 15 percent of the beam length, the solutions are not different from each other. This is well within the range of the expected result in the present investigation.

2. The effect of diagonal tension cracks, as a result of excessive shear forces, on the external bending moment diagram is ignored. In the presence of diagonal tension cracks, the tension force in the tensile reinforcement is slightly larger than that predicted by the flexural moment diagram, thus, increasing the distance on the span of the beam over which the curvatures exceed the yield curvature (Reference 2).

3. The influence of bond slip on the rotation and deflection of the beam is also ignored.

Assumptions 2 and 3 lead to conservative solutions, since diagonal tension cracks and the loss of bond between steel and concrete tend to increase the deformations.

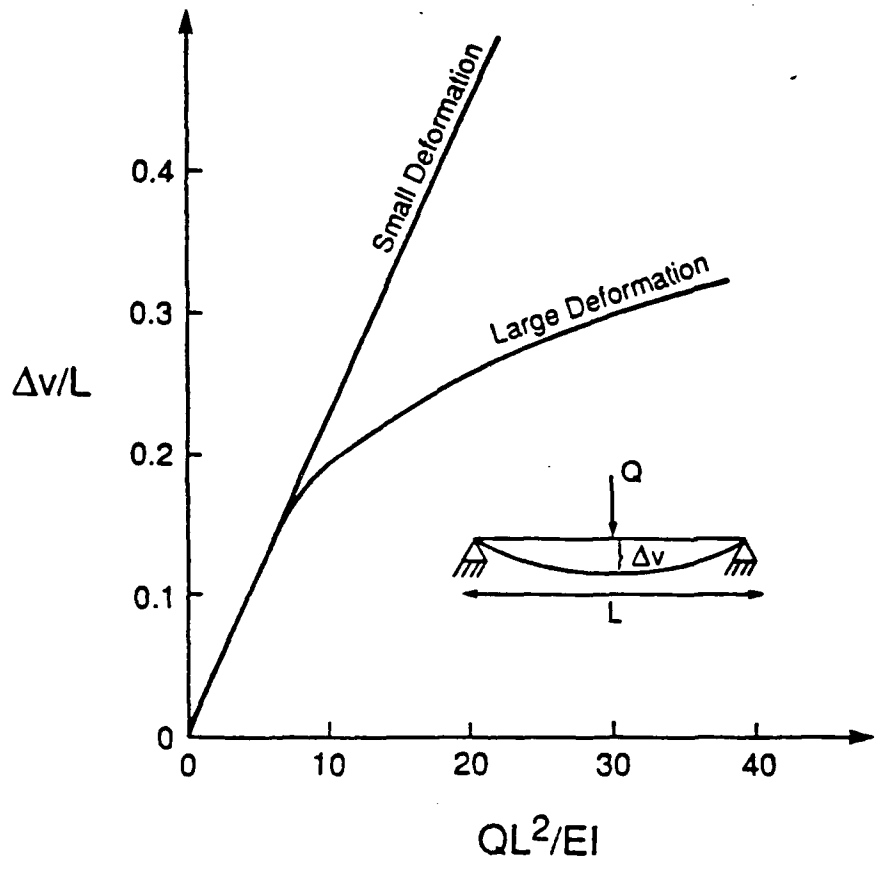

Figure 23. Small Deformation vs. Large Deformation

2. Description of the Present Numerical Method

Since the nonlinear relationship between the resisting moment and the curvature of the cross section is available in a numerical form, closed form analytical solutions for the reactions, moments and deformations are not considered. Because of the nonlinear nature of the moment-curvature relationship and the arbitrary (linear or nonlinear) nature of translational or rotational boundary conditions, reactions and deformations deviate considerably from the solutions of the linear elastic beam theory. In order to obtain the behavior of the beam at all levels of loading, the following formulation has been employed, as presented next.

The general reinforced concrete element under consideration is shown in Figure 24. The load may act at an arbitrary distance, a, from the left support. Moreover, partial linear or nonlinear restraints against rotation and lateral displacement are modeled at the boundaries of the element by rotational and translational springs for which the moment-rotation and force-displacement relationships are assumed to be known. It is also assumed that the complete moment-curvature relationship for the cross section has been computed using the method discussed earlier herein. Knowing the lateral concentrated load, Q at load step i, it is desired to obtain the end moments, end reactions and a numerical solution for lateral deflections at load step i. Referring to Figure 24, the solution methodology can be summarized according to following steps:

a. Divide the beam into N number of elements ; N+1 nodes.

b. Increment the load, Q, by dQ.

c. Assume a moment M_1 at the left support. This moment acts on the rotational restraint and the support at end 1. Also, assume a moment M_2 at the right support. Similarly, this moment will act on the right end of the beam as well as the rotational spring. A very good initial guess would be to choose the end moments obtained form the previous load step.

d. From equations of static equilibrium, obtain the reactions at the left and right supports. The equilibrium equations for the element in Figure 24 can be given by the following expressions:

$$V_1 + V_2 = Q \qquad (101\text{-a})$$

$$V_1 \cdot a + V_2 \cdot (L - a) - M_1 + M_2 = 0. \qquad (101\text{-b})$$

where, V_1 and V_2 are the reactions at the left and right supports, respectively.

e. The displacements at the supports are denoted by Δ_1 and Δ_2. They

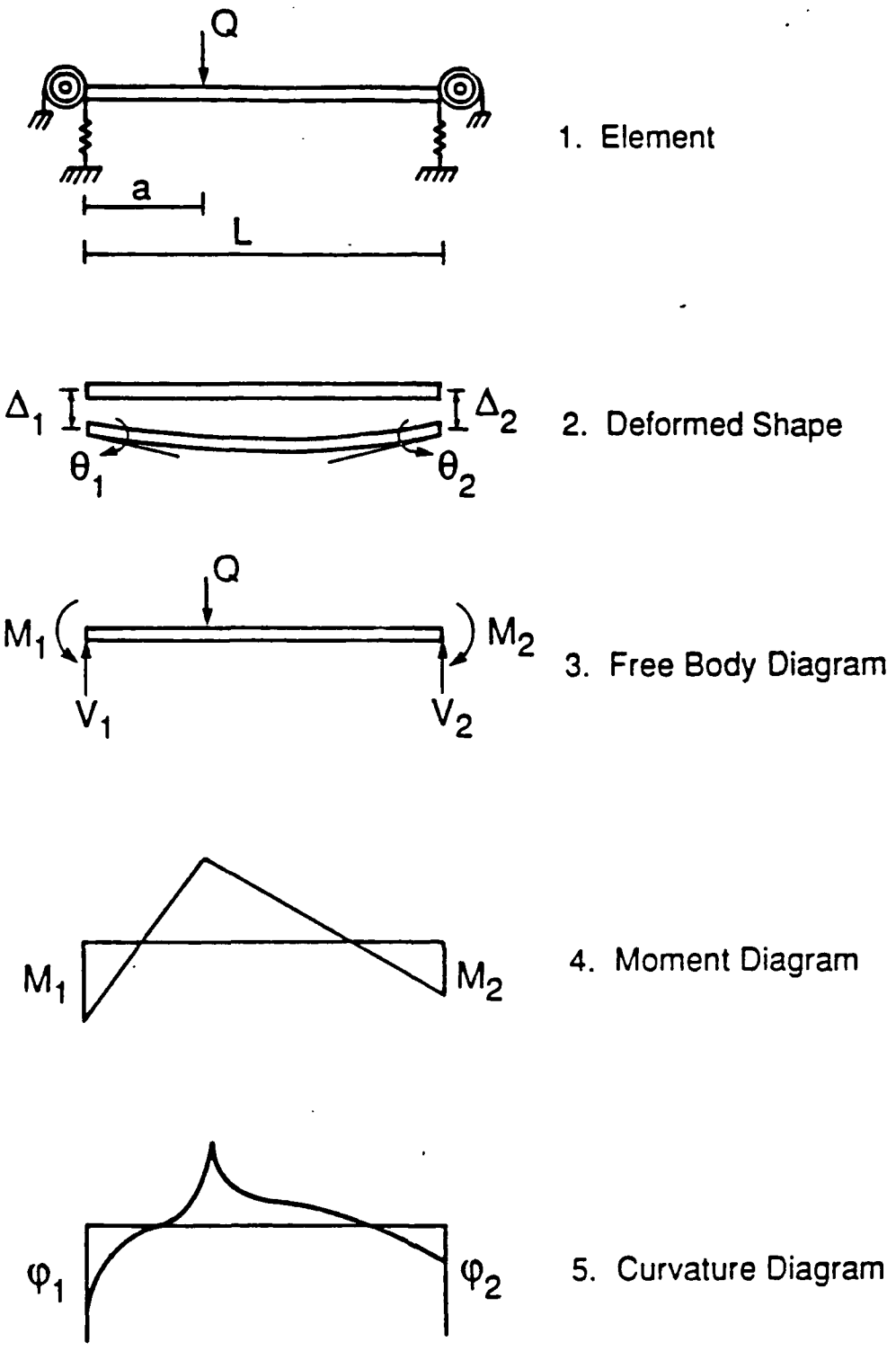

Figure 24. General Element with Variable Boundary Conditions

can be computed from the following expressions:

$$\Delta_1 = f_1 (V_1) \qquad (102\text{-a})$$

$$\Delta_2 = f_2 (V_2) \qquad (102\text{-b})$$

where, f_1 and f_2 are the translational boundary conditions at ends 1 and 2, respectively.

f. Similarly, The rotations at supports are denoted by θ_1 and θ_2 and can be computed from the moment-rotation boundary conditions.

$$\theta_1 = g_1(M_1) \qquad (103\text{-a})$$

$$\theta_2 = g_2(M_2) \qquad (103\text{-b})$$

where, g_1 and g_2 are the functions for rotational boundary conditions at ends 1 and 2, respectively.

g. Knowing the end reactions and the end moments, create the moment diagram by computing the moment at each node.

h. Obtain the curvature diagram, $\phi(x)$, in a numerical form by using the moment diagram in conjunction with the moment-curvature relationship.

i. Compute the slopes at the boundaries from the curvature of the beam by numerical integration of the curvature diagram along the span of the beam as following.

$$\theta'_1 = \int_0^L \phi(x)\, dx \qquad (104\text{-a})$$

$$\theta'_2 = \int_0^L \phi(x)\, dx \qquad (104\text{-b})$$

j. It is now necessary to check for geometric compatibility at the boundaries of the beam. The conditions of compatibility can be expressed by the following expressions for ends 1 and 2, respectively.

$$\theta_1 + (\theta'_1 + \zeta) = 0. \qquad (105\text{-a})$$

$$\theta_2 + (\theta'_2 + \zeta) = 0. \qquad (105\text{-b})$$

where,

$$\zeta = (\Delta_1 - \Delta_2)/ L \qquad (106)$$

ζ is the chord deflection resulting from the differential

displacement at the supports. The only permissible state of equilibrium for the beam is when compatibility conditions, as for example given by Equations (105-a,105-b), are satisfied to within a small tolerance. A value of $1.*10^{-5}$ is chosen in this procedure which provides a reasonable computational speed and accuracy.

k. If Equations (105-a,105-b) are not satisfied, then the end moments, M_1 and M_2 are modified and the iterative procedure, steps 2 through 10, will be repeated until convergence is obtained.

l. In the event that convergence is not reached within an acceptable number of iterations (taken as 50), the load increment, dQ, is reduced and the entire iterative process, steps 2 through 11, will be repeated for the new load.

m. Once equations of equilibrium, i.e., Equations (101-a,101-b), and equations of geometric compatibility, i.e. Equations (105-a,105-b), are satisfied simultaneously within an acceptable tolerance, the rotations and deflections may be computed for every node, j, on the beam for the specific load level.

$$\theta_j = \theta_1 + \int_0^{x_j} \phi(x)\, dx \tag{107}$$

$$\Delta_j = \Delta_1 + \int_0^{x_j} x\, \phi(x)\, dx \tag{108}$$

Where, x_j is the distance between end 1 and node j. Furthermore, once these computations are performed for all nodes, it is possible to obtain the expression for the deflection function, $\Delta(x)_i$, and slope function, $\theta(x)_i$ corresponding to the load step i. The normalized deflected shape function, $\psi(x)_i$, can be obtained in a numerical form by dividing the deflection function by the maximum value of deflection obtained at this step.

$$\psi(x)_i = \Delta(x)_i \,/\, \Delta_{max} \tag{109}$$

This function will be used later in computing the parameters of the equivalent dynamic model (Sections III-F-3, II-F-4, and III-H-2).

n. Steps three through fourteen are repeated for a new load level until the collapse load of the member is reached, i.e., when hinges are formed at the boundaries and under the concentrated load.

The iterative procedure for satisfying the conditions of geometric compatibility for either one of the end moments is bypassed if the moment at that end is known. In other words, iterations

performed on either end moments are required only if the beam is statically indeterminate at that end. For example, a simply supported beam does not require iterations at all, because the value of the moment at the support hinges is always zero. Similarly, upon the formation of the plastic hinge in one location, the moment at that point will be kept constant and equal to the ultimate moment (on the moment-curvature relationship). Beyond this load, any additional increase in load is supported by other parts of the element (redistribution of moments), provided that sufficient ductility is available at the critical sections. The collapse (ultimate) load of the member is reached upon formation of plastic hinges at the critical locations.

Experimental observations (References 1,13, and 17) indicate that the failure of reinforced concrete cross sections seem to occur over a finite length in the vicinity of the critical section. Thus, the formation and propagation of plastic hinges require special attention, and the following assumptions are used in this study to formulate the influence of hinge formation on the behavior of the beam. If the maximum moment in the critical section is less than the yield moment, the beam will be assumed to behave elastically. When the moment at the critical section exceeds the yield moment, a hinge begins to develop. The length of the plastic hinge, L_p, is defined as the distance between the location of the yield moment, M_y, and the maximum moment. The curvature over the length of the plastic hinge will be assumed constant and equal to the magnitude of the curvature at the critical section. This assumption is in fact analogous to the horizontal displacement of the bending moment diagram proposed in (References 40 and 41) to empirically account for the effect of diagonal tension cracks at the critical section. As the load increases, the plastic hinge propagates and may reach its full length. Based on experimental result on simply supported beams subjected to concentrated loads, Corely (Reference 13) proposed the following expression for the full length of a plastic hinge.

$$L_p = 0.5\ d + 0.2\ \sqrt{d}\ \left(\frac{L_z}{d}\right) \qquad (110)$$

where, d is the effective depth of the cross section in inches and L_z is the distance between the critical section to the point of contraflexure in inches. The validity of the present assumptions are investigated later in Section IV, where the analytic results are compared with the experimental findings.

3. Complete Structural Systems

The method outlined above includes the consideration of the boundary conditions for the element under investigation. These conditions may reflect the contribution of the adjoining members and/or connections to the response of the particular loaded element,

and are included in the numerical derivation of the load-deflection relationship and the deflection shape function. The boundary conditions considered in the present study are the following:

a. Simply supported
b. Fully restrained against rotation and displacement
c. Partially restrained against rotation and displacement

If the loaded member is simply supported, the end moments are zero, consequently no iterations are required and the numerical computation of the deformations from the moment curvature relationship is straightforward. The collapse mechanism is reached upon the formation of the first plastic hinge in the span. On the other hand, if the loaded member is fixed at both ends, two sets of iterations must be performed at every load-step until the formation of the first plastic hinge. Provided that sufficient ductility is available at the plastic hinge, the computational procedure for redistribution of moments will continue with one set of iterations until the formation of the second plastic hinge, beyond which the structure is determinate and no iterations are required. In this case, the collapse mechanism is reached upon the formation of the third plastic hinge.

The following two options have been considered for modeling partially restrained members:

1. Employment of rotational and translational springs at the supports for which the linear or nonlinear load-deformation characteristics may be defined by numerical functions. The resistance of the rotational springs is defined by a moment-rotation relationship, $\theta=g(M)$, and the resistance of the translational springs is defined by a load-displacement function, $\Delta=f(V)$. This option could be particularly useful in modeling the interaction of connections (e.g., bond slip in the anchorage zone) with the flexural behavior of element in question.

2. Attachment of the loaded element at its boundaries to a simple linear rectangular frame. The properties of the adjoining elements of the frame, i.e., lengths, moments of inertia and elastic modulus, must be provided. Figure 25 depicts all the possible configurations for which the analysis can be performed. The assumption of frame linearity seems to be rational for cases where concentrated loads are considered in the dynamic domain, since the nonlinear flexural response is primarily governed by the element in question while the effects of adjoining elements decreases as they are further away from the zone of interest. In the event that the analyst might suspect nonlinearities in the frame action, the use of the preceding option is recommended instead.

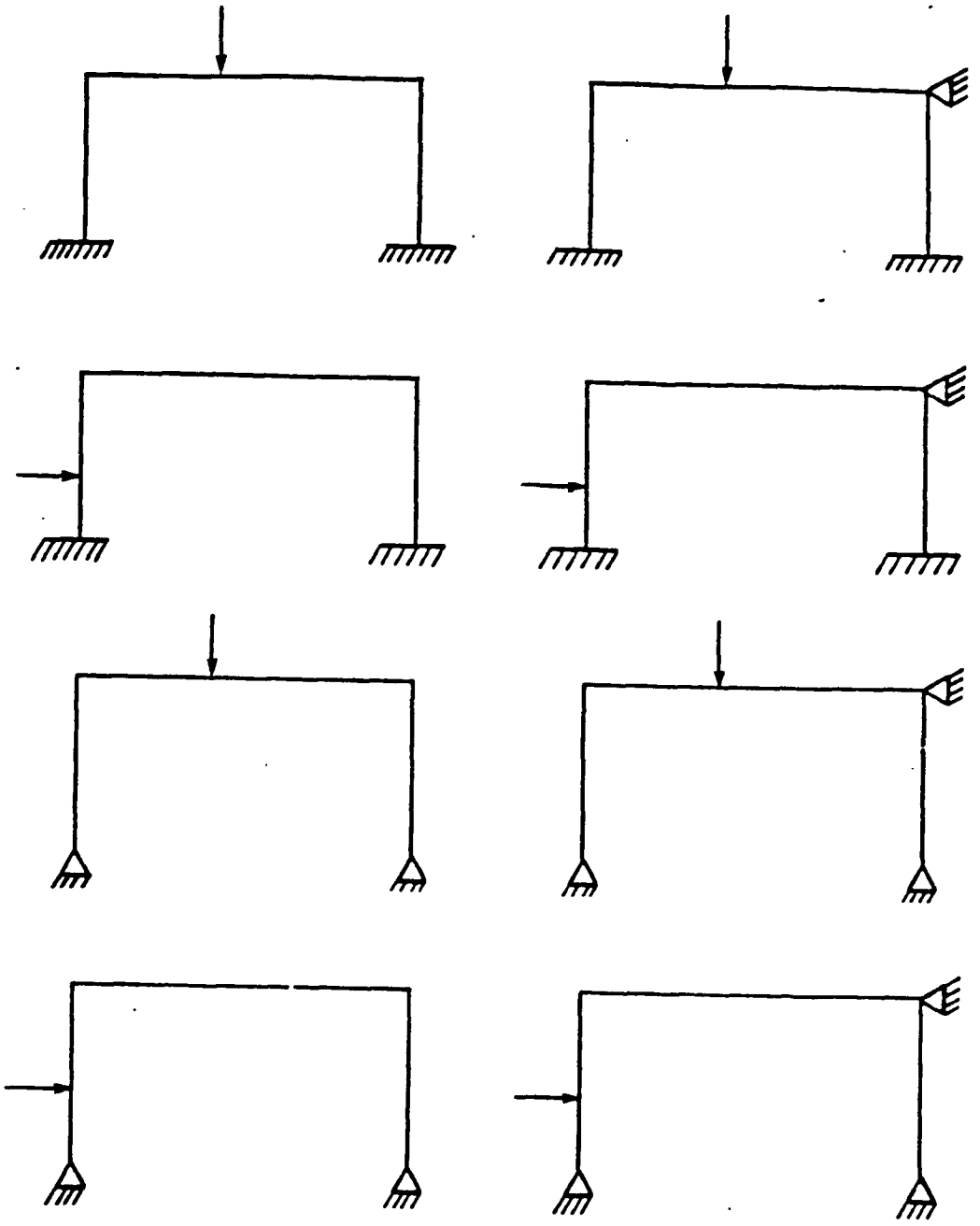

Figure 25. Available Options for Frame Analysis

G. COMPUTER PROGRAM AND FLOW CHART FOR STATIC ANALYSIS

Based on the formulations presented in this section, the computer program, ZCON, for the moment-curvature analysis of the element cross section, and the computer program, LOADDEF, for load-deformation analysis of structural elements were developed. These programs are currently ready for use on IBM AT as well as IBM 4341 computers. The programs were used to analyze a number of experimental cases in which reinforced concrete elements were subjected to severe concentrated loads. The analysis for these cases are provided in Section IV. The contents of the programs ZCON and LOADDEF are illustrated by flow diagrams in Figures 26 and 27, respectively.

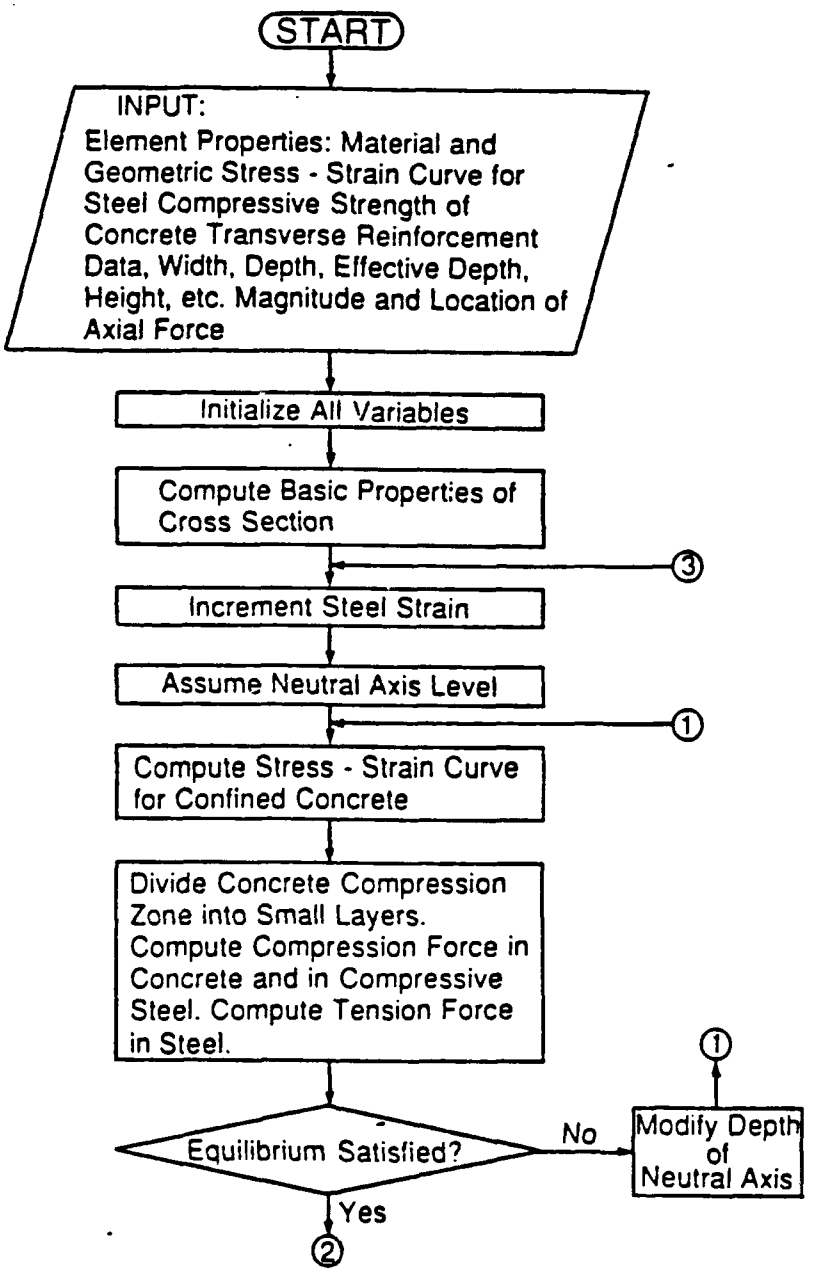

Figure 26. Flowchart for Program ZCON

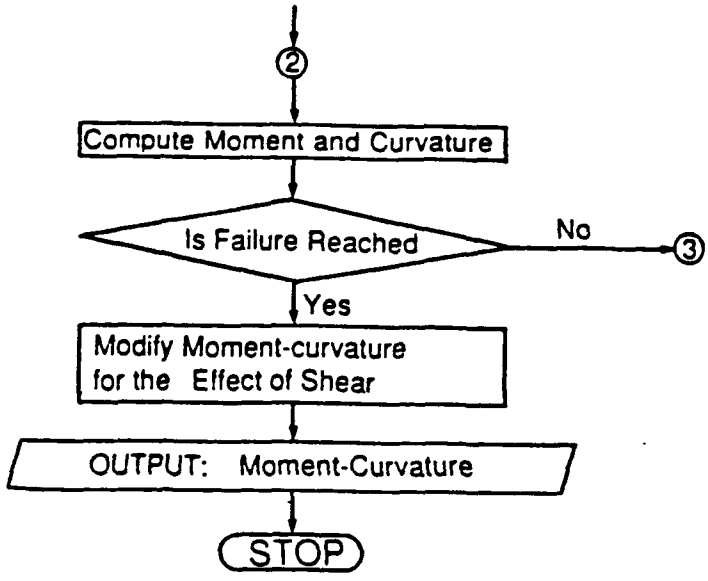

Figure 26. Flowchart for Program ZCON
(concluded)

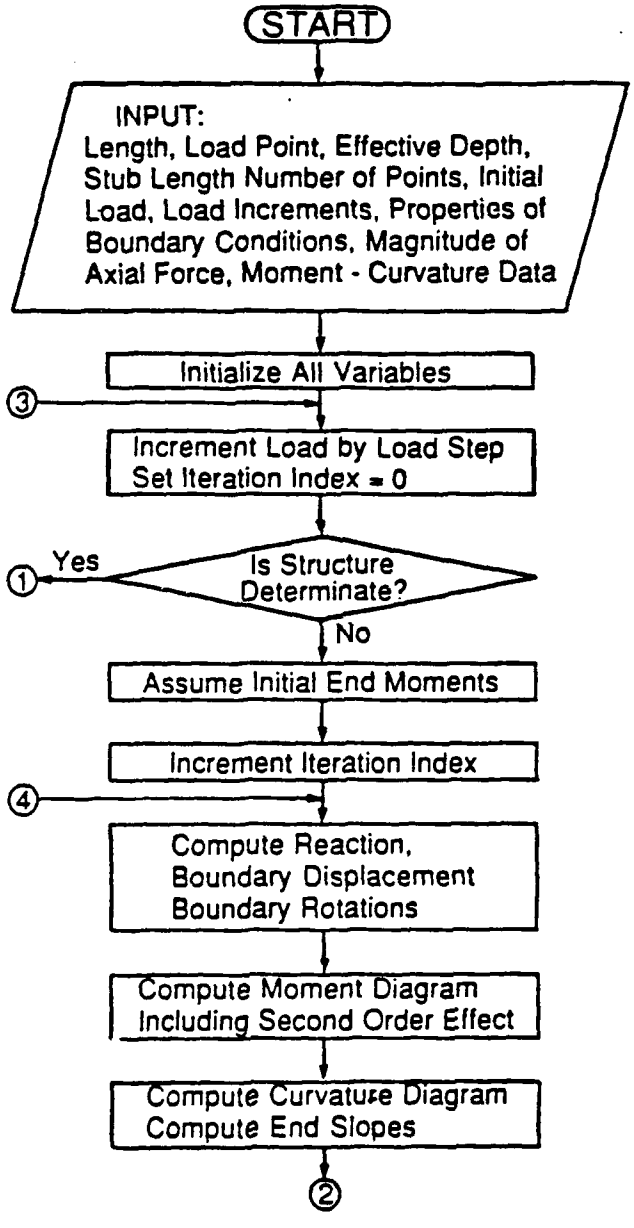

Figure 27. Flow Diagram for Program LOADDEF

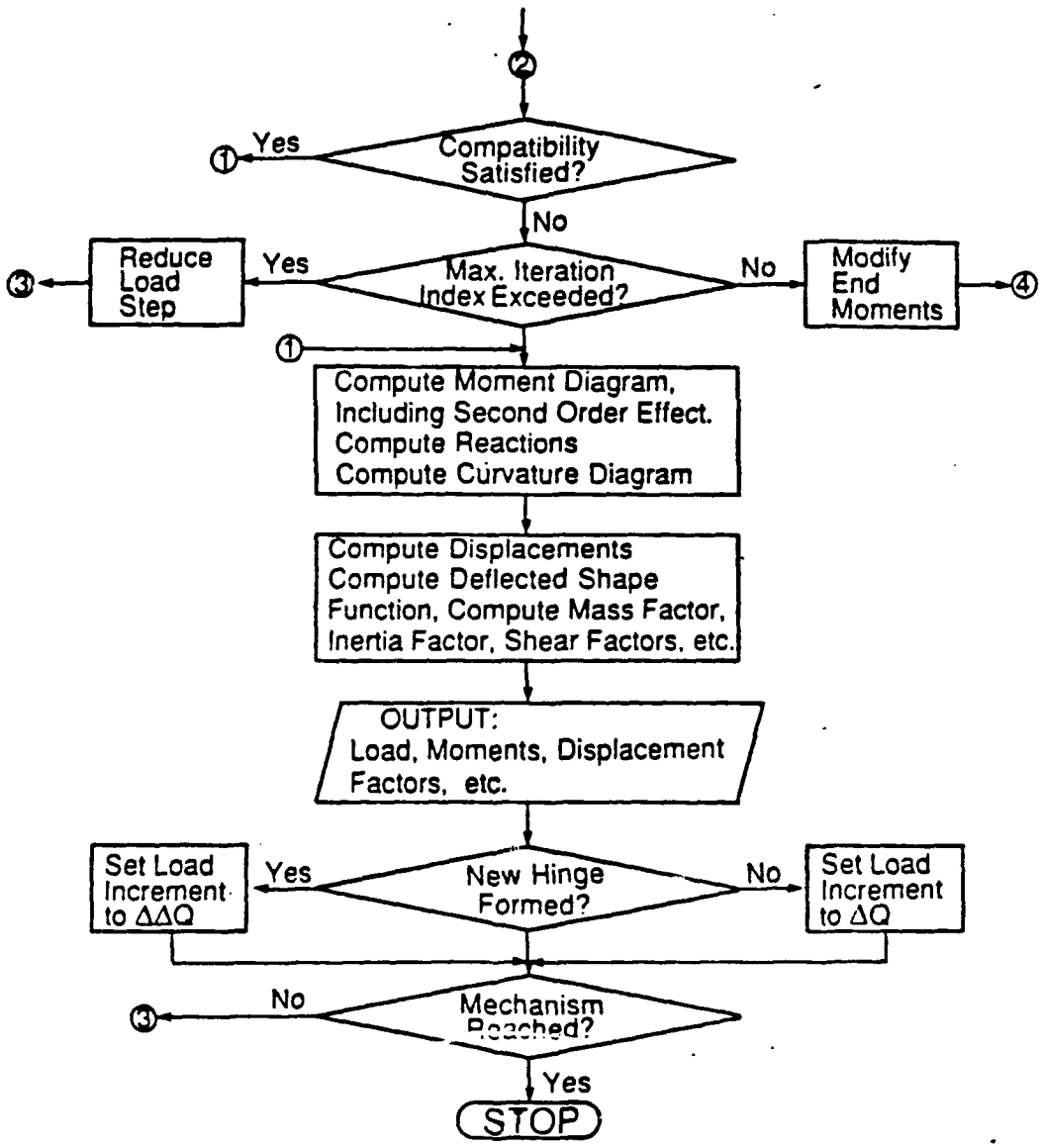

Figure 27. Flow Diagram for Program LOADDEF
(concluded)

SECTION III
ANALYTICAL MODELING OF STRUCTURAL BEHAVIOR IN THF DYNAMIC DOMAIN

A. INTRODUCTION

Since the end of WW II there has been an extensive amount of theoretical and experimental research on the effects of detonations on structures. Most of the research activities were devoted to the dynamic response of structures that were subjected to nuclear blast, and relatively little work was performed on the response of reinforced concrete structures to resist localized effects of conventional weapons. For nuclear detonations it is generally assumed to consider only the variation of load (pressure) with time, since the spatial variation of the load is assumed to be uniform in nature. However, for conventional weapons there is a steep decay of pressure with distance, and the applied loads act only on a small part of the structure or structural element. Thus, it becomes important to study the response of the individual elements which may be subjected to local blast forces arising from a nearby detonation. This study is concerned only with dynamic load sources which act on a relatively small part of the structural members, such as loads generated from a local impact and detonation of conventional weapons.

A reinforced concrete structural element subjected to lateral localized impulsive load is a continuously distributed vibrating body. Theoretically, it consists of a large number of elements, each with specific mass, that are connected to other elements, each having a specific stiffness properties. The mathematical idealization for such an ideal continuous system is by means of a partial differential equation, with independent variables being the position coordinate along the longitudinal axis of the element, and time. The solution of the partial differential equation will depend on the boundary conditions, initial conditions, type and distribution of the loading function, and the mass and stiffness properties of the continuous system (References 42,43, and 44). The closed form solution to the partial differential equation of motion for a vibrating elastic homogenous Bernoulli-Euler beam with simple boundary condition (e.g., clamped, hinged) is available in References 42,43, and 44. The so called 'exact' solutions become increasingly complicated, if not impossible, for beams with arbitrary translational and rotational support conditions. The dynamic response of a reinforced concrete beam is further complicated by the fact that it is a composite structural element with nonhomogenous anisotropic material properties, in which certain highly stressed parts of the beam are likely to experience nonlinear (plastic) deformations, while other parts may still remain elastic.

As Biggs (Reference 42) points out in his book: "rigorous dynamic solutions for vibrating beams are only possible when the loads, stiffness properties, and boundary conditions are simple and convenient mathematical functions. Thus, it is desirable to employ approximate, reliable, and inexpensive techniques to analyze the dynamic behavior of reinforced concrete beams."

One of the most common analytic methods for the analysis of complicated dynamic systems is to discretize the continuous system and concentrate the mass of the beam in a number of lumps, and to connect these lumped masses by springs which are representatives of the stiffness properties of the continuous system. Each lumped mass is associated with a number of prescribed independent displacement coordinates or degrees of freedom (e.g., bending deflection, rotation, axial deformation, etc.). In selecting the degrees of freedom it is very important to choose displacement coordinates which posses significant physical features (e.g., point of maximum deflection). Since the mass of the continuous system is lumped, inertia forces can only be developed at the discrete points. By considering the dynamic equilibrium of each mass, a differential equation of motion can be developed for every degree of freedom, and thus the continuous system is approximated by a multi-degree-of-freedom (MDOF) system. In general, these equations are not independent (static coupling) and an approximate response solution of the system can be obtained by solving the system of differential equations simultaneously.

It is possible, at least theoretically, to create a MDOF system for dynamic analysis of reinforced concrete beams or one-way slabs subjected to impulsive loads. But, because of the arbitrary nature of the support conditions considered in this study, obtaining an accurate description of stiffness properties of the discrete parameter system becomes a very difficult task. More important is the difficulty associated with inclusion of plastic displacements and rotations on the stiffness properties of the springs. These inelastic deformations are load-dependent and occur only at certain highly stressed regions along the longitudinal axis of the member. Furthermore, it becomes necessary to solve a series of coupled, simultaneous and nonlinear differential equations, often in itself a tedious and expensive task. In addition, for blast loads arising from the detonation of conventional weapons, the distribution and magnitude of the applied impulsive loads on the lumped masses is uncertain. Hence, employing a complex MDOF model for dynamic analysis of reinforced concrete members does not seem to be a well justified method.

Another possible approximate technique for solving dynamic problems of this type is to use an advanced numerical approach such as the Finite Element Method. Generally, this method includes certain features of both the discrete MDOF and the generalized distributed coordinate procedure (Reference 44). In this method the beam is divided into an appropriate number of elements, interconnected to each other at nodes, and the displacements of these nodes are the degrees of freedom or the generalized coordinates. By using proper shape functions, the deformations in the structure are expressed as functions of generalized coordinates. Similar to the generalized distributed method, these shape functions must be compatible with the geometric boundary conditions and maintain the internal continuity of the displacements at the nodes. Upon formation of global mass, stiffness, and load vectors, a numerical solution to the set of simultaneous equations may follow.

SECTION III
ANALYTICAL MODELING OF STRUCTURAL BEHAVIOR IN THE DYNAMIC DOMAIN

A. INTRODUCTION

Since the end of WW II there has been an extensive amount of theoretical and experimental research on the effects of detonations on structures. Most of the research activities were devoted to the dynamic response of structures that were subjected to nuclear blast, and relatively little work was performed on the response of reinforced concrete structures to resist localized effects of conventional weapons. For nuclear detonations it is generally assumed to consider only the variation of load (pressure) with time, since the spatial variation of the load is assumed to be uniform in nature. However, for conventional weapons there is a steep decay of pressure with distance, and the applied loads act only on a small part of the structure or structural element. Thus, it becomes important to study the response of the individual elements which may be subjected to local blast forces arising from a nearby detonation. This study is concerned only with dynamic load sources which act on a relatively small part of the structural members, such as loads generated from a local impact and detonation of conventional weapons.

A reinforced concrete structural element subjected to lateral localized impulsive load is a continuously distributed vibrating body. Theoretically, it consists of a large number of elements, each with specific mass, that are connected to other elements, each having a specific stiffness properties. The mathematical idealization for such an ideal continuous system is by means of a partial differential equation, with independent variables being the position coordinate along the longitudinal axis of the element, and time. The solution of the partial differential equation will depend on the boundary conditions, initial conditions, type and distribution of the loading function, and the mass and stiffness properties of the continuous system (References 42,43, and 44). The closed form solution to the partial differential equation of motion for a vibrating elastic homogenous Bernoulli-Euler beam with simple boundary condition (e.g., clamped, hinged) is available in References 42,43, and 44. The so called 'exact' solutions become increasingly complicated, if not impossible, for beams with arbitrary translational and rotational support conditions. The dynamic response of a reinforced concrete beam is further complicated by the fact that it is a composite structural element with nonhomogenous anisotropic material properties, in which certain highly stressed parts of the beam are likely to experience nonlinear (plastic) deformations, while other parts may still remain elastic.

As Biggs (Reference 42) points out in his book: "rigorous dynamic solutions for vibrating beams are only possible when the loads, stiffness properties, and boundary conditions are simple and convenient mathematical functions. Thus, it is desirable to employ approximate, reliable, and inexpensive techniques to analyze the dynamic behavior of reinforced concrete beams."

Just as for the MDOF approach, the drawbacks in using such a technique for the present problem are again the difficulties with an accurate formulation of material behavior for reinforced concrete, and uncertainties about the load. In other words, it is really not worthwhile to perform an elaborate three-dimensional dynamic finite element analysis without both a realistic constitutive material model for reinforced concrete at hand, and an accurate definition of the loading condition. Most dynamic finite element codes do not have a well verified material model which can accurately simulate cracking, post-elastic, and confinement of concrete. Moreover, there are considerable uncertainties with regard to the nonlinear resistance and the loss of stiffness due to the formation and propagation of plastic zones along the span of the beam during vibration.

The use of an advanced approximate technique , such as MDOF, Finite Element, or Finite Difference codes is justified only if it will better represent the behavior of the structure under consideration. Usually, employment of complex analytical techniques is not recommended. In light of the preceding discussion and from the viewpoint of obtaining a practical and justifiable solution to this extremely complicated dynamic problem, employment of an advanced form of a single-degree-of-freedom for dynamic analysis is proposed. The primary reasons for using the SDOF model are as follows:

1. It permits an accurate representation of the material behavior of reinforced concrete members in the analytical scheme. This method is able to account for elastic, smooth transition to inelastic, and the plastic behavior of reinforced concrete members. Such representation considers the effects of confinement and cracking of concrete and the strain hardening of the reinforcing bars, in addition to the effect of the enhancement in material properties of steel and concrete when subjected to short impulsive loads. Above all, the nonlinear behavior of the element, due to the formation and propagation of plastic hinge(s), is incorporated into the vibration analysis.

2. It is possible to incorporate a systematic and consistent method for including the influence of arbitrary linear or nonlinear support conditions. The influence of translational and rotational end conditions on the flexural resistance function of the element in the dynamic domain can be considered.

Although this technique has its own limitations (as discussed in Section III-H-2), it should not be thought of as a poor approximation for predicting the dynamic behavior of reinforced concrete beams under impulsive loads. As Clough and Penzien (Reference 44) point out: "..the quality of results obtained with a SDOF approximation depends on many factors, principally the spatial distribution and time variation of the loading and the stiffness and mass properties of the structure." Moreover, when employing the SDOF approximation for the dynamic analysis of a continuous system like a beam, one must always

be aware of inherent limitations of the approach. For example, determination of dynamic shear forces and bending moments directly from the results of the SDOF analysis yields erroneous results. In that case, additional special steps must be taken for obtaining an adequate solution.

In this section, the procedure for obtaining the equivalent SDOF system for an elastic vibrating beam with simple boundary conditions is discussed. The development of an equivalent SDOF for a beam that theoretically has an infinite number of degrees of freedom requires that certain important idealizations be made regarding the dynamic motion of the structural element. These assumption and the influence of other important parameters such as loading duration, support conditions, damping, resistance, and inertia forces on the solution of the SDOF are studied. In addition, the procedure and limitations for deriving the equivalent dynamic system for a beam with plastic deformations, as reported in the literature, is studied.

One of the most difficult problems in modelling structural elements as SDOF systems is in the flexural interaction of the individual element with others members of the structure. In MDOF modelling of elastic structures, this phenomenon is generally referred to as elastic or stiffness coupling between the structural elements. When modeling the dynamic behavior of the individual element by a SDOF system, one must be aware of this important interaction, since it may have a considerable impact on the quality of the results. The significance of this concept for structural members that are subjected to short impulsive loads is also discussed.

1. Objectives of SDOF Dynamic Analysis

The analytical scheme in this study has been structured as follows:

a. It represents the flexural dynamic response motion of a reinforced concrete structural element (i.e., beam, one-way slab, etc.) by an equivalent SDOF system.

b. It employs an accurate flexural resistance-deformation relationship for the reinforced concrete element in the dynamic analysis. Such relationships take into account internal changes along the element due to the formation of plastic zones. These changes occur as a result of gradual loss of stiffness at highly stressed cross sections, and they affect inertia and resistance forces.

c. It includes the influence of boundary conditions in the SDOF modeling. The proposed resistance-deformation relationship reflects the influence of arbitrary linear or nonlinear support conditions in the form of translational and rotational springs. These end condition reflect the influence of attached structural elements and/or connections on the stiffness properties of the element under consideration. The

importance of stiffness coupling between the individual element and the support structure is also examined for short duration impulsive loads.

d. It considers the energy dissipation and stiffness deterioration of the reinforced concrete element via a hysteresis resistance-displacement relationship which is consistent with previous experimental observations.

e. It incorporates the influence of loading rate on stress-strain properties of concrete and steel.

f. It considers the direct shear resistance of reinforced concrete beams and one-way slabs subjected to localized impulsive loads.

B. THEORETICAL BACKGROUND ON EQUIVALENT SDOF SYSTEMS

The method of approximating the dynamic response of a beam, which in reality is an infinite-degree-of-freedom system, by a SDOF system is discussed thoroughly (see References 42,44, and 45) and reviewed here briefly. In order to derive such an equivalent system, it is necessary to represent the motion in terms of one displacement coordinate, i.e., the maximum displacement of the beam, with some approximate shape function to represent the deflection of the entire beam. Figure 28 shows a beam with arbitrary boundary conditions subjected to a concentrated dynamic load at some arbitrary point j on the span. The SDOF idealization is also shown in Figure 28. The displacement coordinate u_e represents the maximum deflection of the beam, k_e is the equivalent stiffness constant of the spring, and Q_e is the equivalent dynamic load. A common approach to derive the parameters of an equivalent SDOF system is to equate the energies of the distributed and SDOF systems in the following manner.

1. The kinetic energy of the beam, KE_b, and the kinetic energy of the equivalent SDOF system, KE_e, may be expressed by the following two equations:

$$KE_b = 0.5 \int_0^L m_u \, (\partial u/\partial t)^2 \, dx \qquad \text{(111-a)}$$

$$KE_e = 0.5 \, M_e \, (\partial u_e/\partial t)^2 \qquad \text{(111-b)}$$

where, m_u is the mass per unit length of the beam, L is the length of the beam, and u is the displacement of the beam which depends on position and time. For the SDOF, M_e is the equivalent mass and u_e is the displacement of the lumped mass, chosen to be the same as the maximum deflection of the beam. If the displacement function, u(x,t), can be represented by the product of a proper shape function, $\psi(x)$,

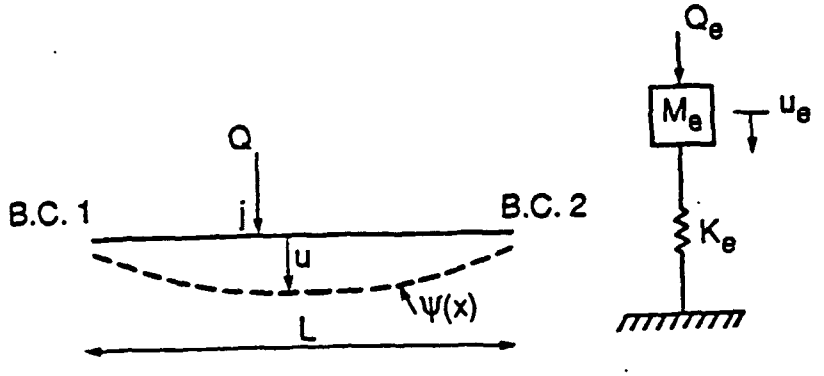

Figure 28. Dynamically Loaded Beam and SDOF Idealization

and a time varying function, G(t), i.e.,

$$u(x,t) = \psi(x)\, G(t) \qquad (112)$$

then, by equating Equations (111-a) and (112-b) it is possible to obtain an expression for the equivalent mass of the SDOF system as follows;

$$M_e = \int_0^L m_u\, \psi\,(x)^2\, dx \qquad (113)$$

The function $\psi(x)$ is normalized with respect to the maximum deflection of the beam and it must be compatible with the geometric end conditions.

2. The strain energy of the elastic beam, U_b, and the strain energy of the equivalent system, U_e, may be given by the following relationships, respectively.

$$U_b = o.5 \int_0^L (EI)_x\, (\partial u^2/\partial x^2)^2\, dx \qquad (114\text{-a})$$

$$U_e = 0.5\, k_e\, u_e^2 \qquad (114\text{-b})$$

Substituting for u(x,t) from Equation (112) into Equations (114) and equating Equation (114-a) to Equation (114-b), the equivalent stiffness constant for the SDOF system may be derived as follows;

$$k_e = \int_0^L (EI)_x\, (\psi(x)")^2\, dx \qquad (115)$$

Here, E is the elastic modulus of the beam, I is the moment of inertia, and $\psi(x)"$ is the second derivative of the normalized shape function with respect to the longitudinal coordinate variable x.

3. The external work on the beam, W_b, and the external work on the SDOF, W_e, may be expressed in the following manner;

$$W_b = Q(t)_j\, u_j \qquad (116\text{-a})$$

$$W_e = Q_e(t)\, u_e \qquad (116\text{-b})$$

where, $Q(t)_j$ is a time dependent concentrated load function acting at point j on the span of the beam, u_j is the displacement of the beam evaluated at point j, and $Q_e(t)$ is the equivalent load of the SDOF system. By equating Equations (116-a) and (116-b) to one another and substituting for u from Equation (112), the equivalent load may be obtained as following;

$$Q(t)_e = Q(t)_j \psi(x)_j \tag{117}$$

where, $\psi(x)_j$ is the shape function ψ evaluated at point j. Thus, the equation of motion for an undamped equivalent SDOF system can be written as

$$M_e \ddot{X} + k_e X = Q_e(t) \tag{118}$$

and the displacement of any point along the longitudinal axis of the beam can be obtained from Equation (112), in which G(t) is the solution of the differential equation of the equivalent system, i.e., Equation (118).

Biggs (Reference 42) derived the parameters of the equivalent system for an elastic beam by employing the shape functions obtained from the application of the load to the beam under static condition. These parameters were presented only to a limited number of cases for which the boundary conditions were simple and the concentrated load was always applied to the center point of the span. Moreover, certain assumed shape functions were provided for the fully plastic range of behavior and it was stated that the lack of a smooth transition from elastic to plastic behavior could introduce errors in the results of a dynamic analysis.

Biggs (Reference 42) proposed another version of Equation (118) by introducing transformation factors as follows;

$$(MF)\, M_t \ddot{X} + (LF)\, K\, X = (LF)\, Q(t) \tag{119}$$

Where, M_t is the actual mass and k is the stiffness of the beam. MF and LF are the mass factor and the load factors defined by the following equations, respectively.

$$MF = M_e/M_t \tag{120-a}$$

$$LF = Q_e(t)/Q(t) \tag{120-b}$$

These factors are often referred to as "the Biggs factors" and they can be computed once the deflected shape function is assumed. In addition, by introducing the concept of a resistance function to replace the stiffness parameters, a more practical form of Equation (119) can be obtained. The resistance function to be used in the dynamic analysis is the relationship between the applied load and the

selected deflection coordinate (where deflection is chosen be equal to that of the equivalent SDOF) under the static application of the dynamic load. The resistance force is the internal force that resists the externally applied load, and hence must be equal to it. For an elastic beam, the resistance force is equal to the product of the equivalent spring stiffness constant and the displacement, i.e., $k_e x$. For an inelastic beam, the resistance R is the restoring force in the spring, and the maximum resistance is the ultimate load the beam can carry under static conditions. Since resistance and the applied load are essentially the same under static conditions, the resistance factor denoted by RF is always the same as the load factor, LF. Hence, the more general form of Equation (118) may be give as follows;

$$MF\ M_t\ \ddot{X} + (LF)\ R(t) = LF\ Q(t) \tag{121}$$

where, R(t) is the time dependent resistance function. If external damping is also introduced by a viscous dashpot, the equation of motion for the equivalent SDOF will have the following form.

$$M_e\ \ddot{X} + C\ \dot{X} + LF\ R(t) = LF\ Q(t) \tag{122}$$

where, C is the external damping constant. More on the effect of damping on structural response is provided in Section III-E-3.

C. EFFECT OF LOAD DURATION ON STRUCTURAL RESPONSE

Since this study is concerned specifically with the dynamic response of structural elements to impulsive loading, it is important to study how the duration of of loading may affect the response of the element. References 42,44, and 46 provide excellent discussion on this subject and a brief review is provided in this section.

Consider the impulse-momentum relationship for the single-degree-of-freedom system,

$$M_e\ X(t) = \int_0^{T_L} (\ Q_e(t) - R(t)\ )\ dt \tag{123}$$

where,
- T_L = duration of the applied load
- $Q_e(t)$ = equivalent applied dynamic load
- $X(t)$ = displacement function
- M = equivalent mass
- $R(t)$ = equivalent resistance

It can be observed that if the loading duration is short compared to the natural period of the system, there is not enough time for the resistance force to develop and therefore, the mass does not displace significantly. In that case, the inertia force provides the primary resistance mechanism to the applied load. Hence, if T_L is small relative to the natural period of the structure, the magnitude of the second term in the integrand of Equation (123) will be small compared

to the first term, and the impulse-momentum relationship may be expressed by the following approximate equation.

$$\dot{X}(t) = 1/M_e \left(\int_0^{T_L} Q_e(t)\, dt\right) \qquad (124)$$

In general, the error in using Equation (124) is negligible if the ratio of the load duration to the natural period of the structure is less than 0.1, as illustrated and discussed in Reference 46.

Biggs (Reference 42) studied the influence of loading duration on the response of elasto-plastic undamped SDOF systems. The results of his work are summarized in Figures 29 and 30 for triangular and rectangular loads,respectively. As the duration of the pulse decreases, the ratio of maximum displacement to the elastic displacement, i.e. y_m/y_{el}, becomes smaller. For example, for an applied force that may be as large as 2.5 times the ultimate static resistance load, if the ratio of the applied triangular pulse to the natural period of the system is 0.2, the response displacement does not even exceed the elastic displacement value.

Baker et al. (Reference 46) point out that it would be unreasonable to generalize and employ this concept in the dynamic analysis of large structures which have many structural and non-structural components. This is because the individual elements of the structure have their own natural periods of vibration, and while the duration of a high-intensity load, such as a blast, may be small relative to the natural period of the overall structure, it may not be short enough when compared to the period of some of the individual members. In that case, considerable localized damage to individual elements may occur, while the entire structure may remain relatively unaffected. This is why it is important to analyze for the dynamic response of the individual structural elements, in addition to studying the overall response of the structure.

D. EFFECT OF STIFFNESS COUPLING

Any structure is ideally a MDOF dynamic system and when a SDOF dynamic analysis of an individual structural element is required, it is often important to be aware of the influence of stiffness (elastic) coupling between the structure and the specific loaded member. Generally, if the impulsive load is applied over a short period of time relative to the natural periods of the coupled system, the effect of stiffness coupling between the loaded member and the support structure on the response of the individual member is not expected to be significantly important.

Baker et. al. (Reference 46) employed a simple example for illustrating the effect of flexibility of the support structure on the response of the loaded element by comparing the maximum response of the two systems, as shown in Figure 31. The first system was a two-degree-of-freedom dynamic model in which the loaded member was

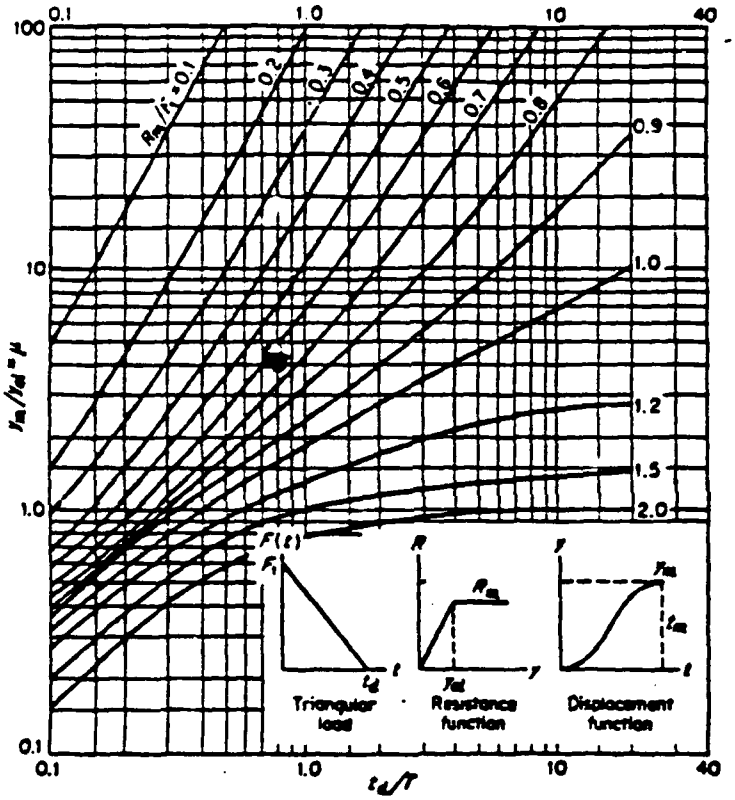

Figure 29. Maximum Displacement of Undamped SDOF Elasto-Plastic System Subjected to Triangular Pulse with Zero Rise Time. (Reference 42)

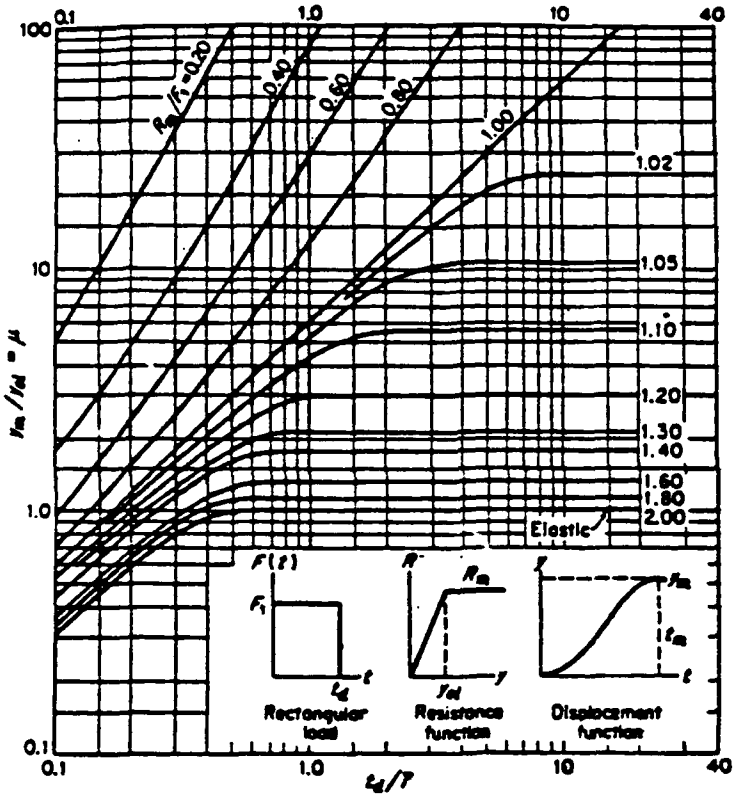

Figure 30. Maximum Displacement of Undamped SDOF Elasto-Plastic System Subjected to Rectangular Pulse with Zero Rise Time. (Reference 42)

416

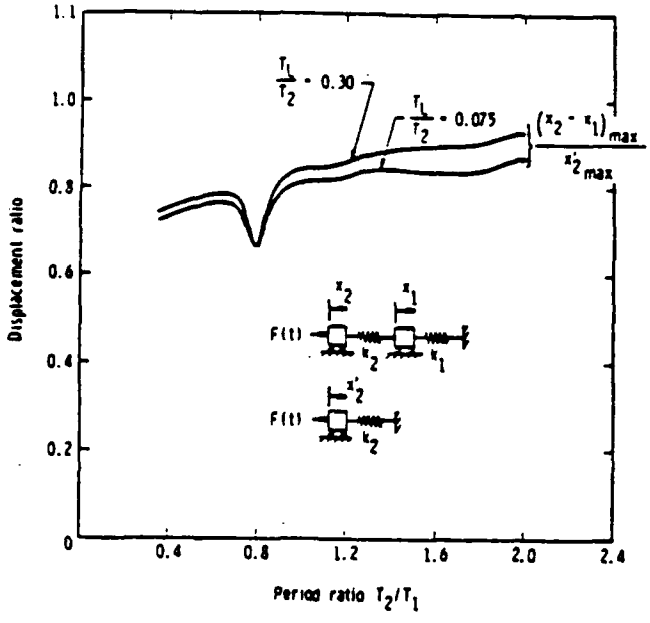

Figure 31. Effect of Support Rigidity on Maximum Displacement. (Reference 46)

supported by an elastic structure, whereas in the second system the loaded element was connected to an infinitely rigid base. The analysis was performed for two different loading durations. In each case a short triangular pulse was applied to the loaded element of each system as shown in Figure 31. The results indicated that the maximum relative elastic deformation of the two masses in the coupled system was generally less than the maximum elastic deformation of the second SDOF system. However, as the stiffness of the support structure increased, the ratio T_2/T_1 increased, and the maximum relative deformation of the coupled system approached the maximum displacement of the second system. Moreover, it was observed that the loading duration did not have much influence, as long as it was small compared to the natural period of the systems.

In most engineering structures, such as frames and buildings, the ratio T_2/T_1 is usually greater than one, thus, reducing the error when a SDOF model is used for estimating the dynamic response of an individual element subjected to short impulsive loads. However, It should be emphasized that such generalization does not hold when the period ratio, T_2/T_1, is considerably less than one, or when the entire structure (as opposed to one element) is subjected to cyclic loadings.

E. NONLINEAR SDOF SYSTEMS FOR ANALYSIS OF RC ELEMENTS

1. Introduction

Dynamic analysis of reinforced concrete structural elements using a linear SDOF model may provide adequate results for loads that cause very little damage to the structure. At higher load levels, particularly beyond the elastic range of response, the material properties and the mechanism of structural behavior and energy absorption of the structural member no longer conform with the assumptions of the linear theory. Thus, the linear differential equation of motion is not sufficient for describing the motion of the vibrating element and a nonlinear dynamic analysis of the structural element becomes necessary.

The nonlinear form of the equivalent SDOF differential equation of motion can be represented as follows:

$$M(x)\ddot{X} + C(x)\dot{X} + R(x) = Q(t) \qquad (125)$$

M(x), C(x), and R(x) are nonlinear functions representing mass, damping, and resistance characteristic of the system. These functions are independent of time. Q(t) is the arbitrary time dependent loading function which is independent of displacement, velocity, and acceleration (Reference 43).

2. NonLinear Response of Structural Components

The primary sources of nonlinear behavior in a reinforced concrete beam are the following:

a. Material nonlinearity
b. Nonlinearity of support conditions
c. Geometric nonlinearity

In the present study geometric nonlinearities (as a result of large deformations) are not included in the analytical scheme. The use of the small deformation theory was justified in Section II, and later in Section IV the range of results will demonstrate the validity of this assumption. However, the significant features of nonlinearities associated with material properties and boundary conditions are considered in the dynamic analysis.

Nonlinearities associated with the inelastic behavior of materials in reinforced concrete affect the dynamic response significantly. In SDOF analysis, it is required to provide a force-deformation function that is representative of the flexural performance of the structural element under the static application of the load, and the effect of important sources of nonlinearity in concrete and steel must be rationally considered in deriving such function. These sources can be summarized as follows:

a. Nonlinear behavior of flexural reinforcement when strained beyond the elastic limit. This includes the range of behavior in the yield plateau and in the strain hardening region.

b. Nonlinear behavior of concrete. The stress-strain relationship for concrete is not linear and thus, a nonlinear distribution of stress must be considered in the concrete compressive zone of the cross section. In addition, confining of concrete by transverse reinforcement can significantly affect the nonlinear ductile behavior of the beam.

c. Nonlinear failure criteria of the cross section in flexure. The failure criteria must properly define the plastic (ultimate) moment beyond which the cross section can not resist additional load, and can only rotate if sufficient ductility is provided.

d. Nonlinear distribution of curvatures along the span of the beam, particularly for deformations beyond the yielding of the reinforcement. This is to account for the gradual spreading of plastic hinges as a result of the concentration of curvatures in the vicinity of highly stressed (inelastic) regions. Since the distribution of the curvature diagram is not linear, it will no longer relate directly to the moment diagram. Hence, for statically indeterminate beams, an iterative step-by-step numerical procedure is required for obtaining the resistance function.

e. Nonlinear damping mechanisms by which energy is dissipated in the dynamic system as a result of plastic deformations. A discussion on this issue, accompanied by a modified proposed model is given in Sections III-E-3 and III-F-2 herein.

f. Nonlinear influence of loading rate on the material properties of steel and concrete. This topic is discussed later in Section III-G.

In addition to including these nonlinearities in the derivation of the load-deflection (resistance) function, it is also necessary to consider the effect of nonlinear deformations on the parameters of the equivalent SDOF model. These parameters depend directly on the displacement shape function, $\psi(x)$. The material nonlinearities affect this function at every load step and thus, the parameters of the nonlinear SDOF system must be modified in accordance with the updated shape function. For example, the equivalent mass of the system, as computed from Equation (113), may not be considered as a constant parameter in nonlinear analyses. Moreover, for beams with axial compressive load, the nonlinear resistance function must be continuously modified at every load step to account for the loss of resistance (increased deflection) due to the second order moments caused by the axial load. The procedure employed in this study for such modifications is presented in Section III-F-4.

3. Mechanisms of Energy Dissipation

Perhaps the most distinguished feature of inelastic dynamic response is the irreversible mechanism by which energy is removed from the dynamic system. In a realistic dynamic analysis of reinforced concrete elements, this phenomenon should be modeled as accurately as possible; i.e., representing a hysteretic process. A hysteresis model is a particular case of structural damping in which the dissipated energy is assumed to be independent of frequency of vibration. The amount of absorbed energy is primarily a function of the extent of inelastic displacement history of the structural element. Although a precise theory on the hysteretic characteristics of reinforced concrete is not available, numerous experimental investigations, particularly in the field of earthquake engineering, have provided valuable insight into the inelastic response of RC elements under repeated loading and unloading conditions. In order to justify the development of the proposed model in Section III-F-2, a brief review of the subject is provided next.

Reference 47 summarizes hysteretic responses of reinforced concrete beams and beam-columns. Typical hysteretic moment-rotation models are shown in Figure 32. Model A is a hysteresis curve commonly used for elements made of structural steel, while Model B, originally developed for reinforced concrete members, consists of a bilinear skeleton curve and it accounts for the loss of stiffness upon reloading.

A typical hysteresis curve for a cantilever reinforced concrete beam with a symmetric cross section and subjected to a concentrated load is shown in Figure 33-a. The loading history of the element is depicted in Figure 33-b. Even though the cross section may be slightly

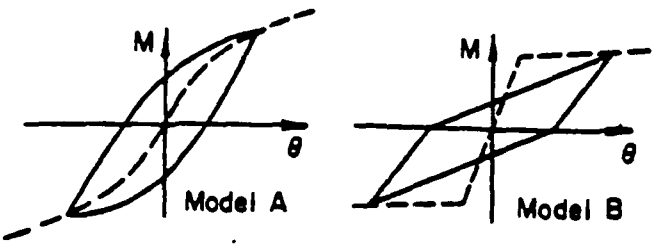

Figure 32. Idealized Hysteretic Models for Ductile Material. (Reference 47)

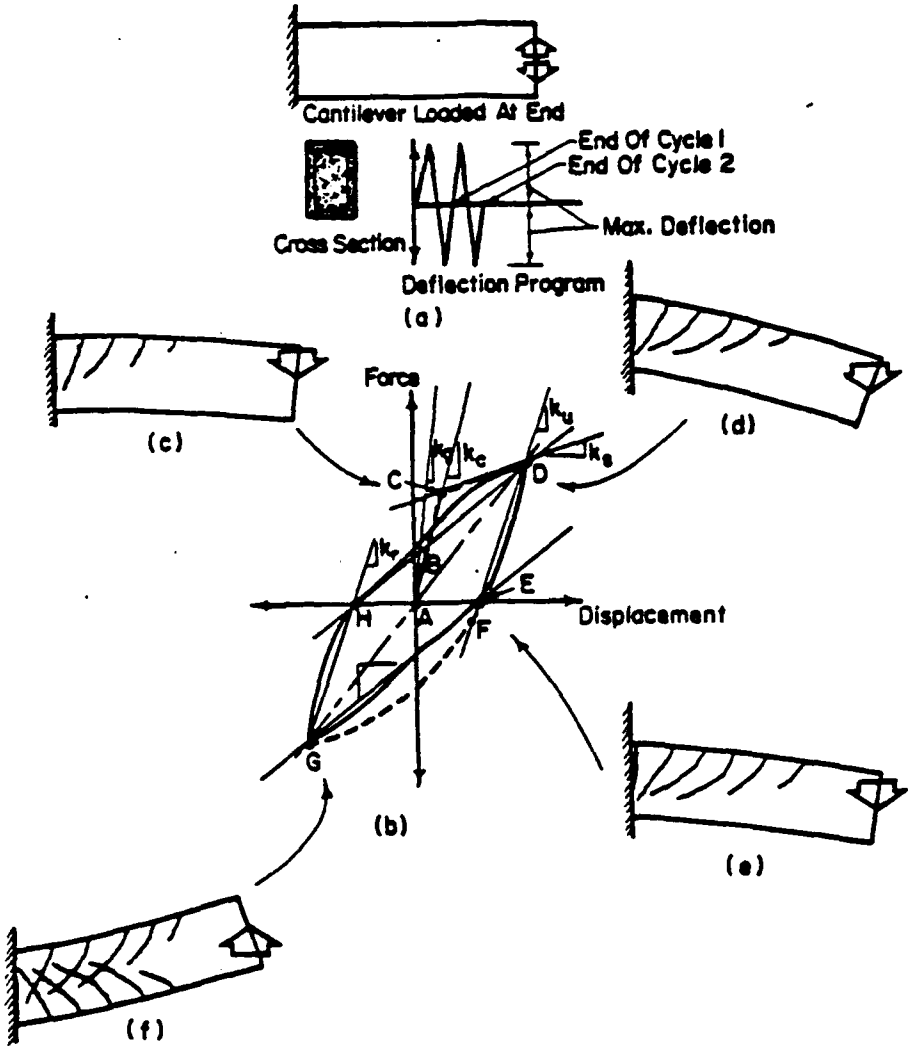

Figure 33. Hysteresis for a Reinforced Concrete Cantilever Beam. (Reference 47)

cracked, the force-displacement relationship is nearly linear from A to C (Figure 33-c). As the load is increased beyond the yield point C, the beam responds inelastically and a plastic hinge begins to develop near the fixed support. The behavior of the beam in region CD is marked by spalling of the concrete cover at the extreme compression fiber near the support, extensive cracking, and further yielding of the tensile reinforcement (Figure 33-d). If the direction of loading is reversed at point D, the beam begins to unload almost elastically to a plastic deformation at point E. If more load is applied in the reverse direction, flexural cracks in the opposite direction will be formed (point F), and the hysteresis curve will proceed to point G. The slope of the curve between points F and G depends on the amount of reinforcement, stress-strain properties of steel, and the extent of crack closure in the compression zone. If cracks do not close, the entire compression force must be carried by the reinforcement. Due to the Bauschinger effect, the compression steel yields at a lower stress that the initial yield stress. At point G, almost all cracks are expected to close in the compression zone. Point G can be thought of as the image of point D in the opposite displacement direction and hence, reloading from G to H is similar to unloading from D to E.

The second loading cycle begins at point H, the cracks begin to close in the original compression side, but since the reinforcement was already strained beyond yield, the Bauschinger effect would considerably reduce the slope of the curve beyond this point. Reference 2 also points out that the formation of flexural cracks in both directions eventually would result in a fully cracked section and consequently, a drastic reduction in the flexural resistance. In addition, the loss of bond between steel and concrete and the presence of high shear distortions at the critical section contribute to further reduction of resistance under repeated loading.

Analytical models are available that reflect the effect of stiffness degradation on the hysteretic response of reinforced beams. Figure 34-a shows the Ramberg-Osgood model in which the skeleton curve is primarily constructed in accordance with the Bauschinger phenomenon. Figure 34-b shows Clough's elasto-plastic degrading stiffness hysteresis relationship in which the loss of stiffness in modeled by a reduction in the slopes of the reloading and unloading line segment. Figure 35 depicts another idealized stiffness degraded model discussed by Sozen (Reference 47), where the slope of the unloading portion, k_u, is related to the initial slope, k_c, by the following relationship;

$$k_u = \hat{a}\, k_c\, \mu^{\hat{a}} \qquad (126)$$

where, μ is the displacement ductility factor at the unloading point and $\hat{a}$ is a material dependent coefficient taken as 0.5. In this model, the slope of reloading for each cycle is obtained by connecting a straight line between the point of plastic deformation on the displacement axis and the point of maximum deformation in the reverse direction.

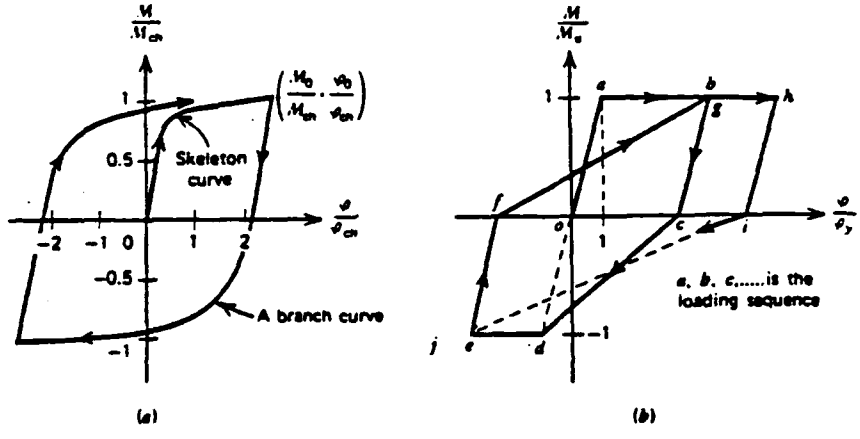

Figure 34. Idealized Hysteretic Moment-Curvature Relationships (a) Ramberg-Osgood Model (b) Clough's Degrading Stiffness Model. (Reference 47)

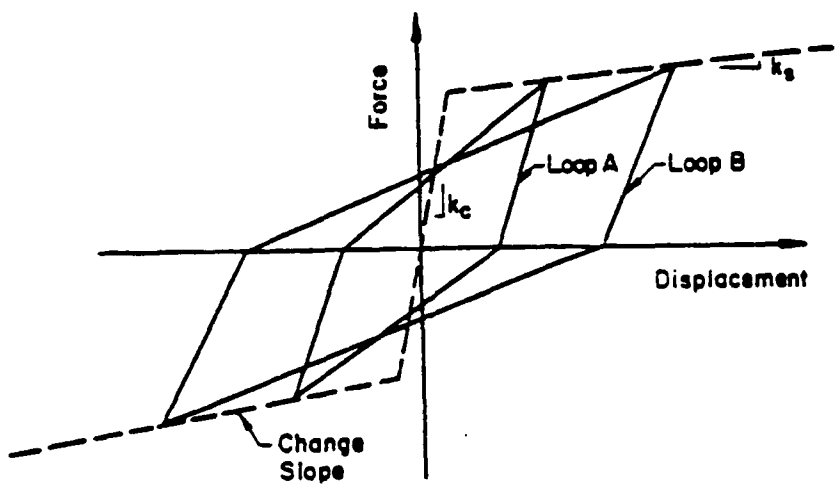

Figure 35. Idealized Hysteresis Loops for Reinforced Concrete Members. (Reference 47)

To obtain a more realistic view of hysteresis problem in reinforced concrete elements, one must also pay close attention to the experimental observations. Figure 36 shows a typical hysteresis load-deformation curve for a simply supported, moderately reinforced concrete beam with a symmetric cross section. The beam was loaded statically for a small number of cycles by a concentrated force at its midspan. The behavior during cycles a,b, and c is nearly elastic. Cycles d and e clearly reflect the influence of cracking and the Bauschinger effect on the response. Figure 37 demonstrates the hysteretic response of a reinforced concrete beam-column joint at the face of the column. In this experiment, the cross section of the beam and the column were both symmetric and well confined. The presence of high shear stresses and the slippage of the tensile reinforcement in the connection core contributed to the deterioration of the assembly under repeated loading cycles. The corresponding joint moment-end deflection curve is shown in Figure 37-b. Additional information on the hysteretic response of RC connection can be found in References 48-52.

F. PROPOSED MODIFIED SDOF MODEL FOR ANALYSIS OF RC ELEMENTS

1. Introduction

In Section II assumptions and the procedure for deriving the moment-curvature diagram and the load-deflection relationship for a rectangular reinforced concrete beam were discussed. Formulation of the moment-curvature diagram included the nonlinearities associated with the behavior of confined and unconfined concrete in the compression zone, inelastic behavior of the longitudinal steel, and failure criteria for the cross section. The procedure for obtaining the numerical load-deflection function from the moment-curvature diagram was also described in Section II. The numerical model included the possibility of translational and rotational end conditions, as well as systematic formulation for the nonlinear distribution of plastic curvatures along the span of the beam. In this section the nonlinear load-deflection relationship serves as the skeleton curve, used to calculate dynamic resistance functions and other parameters of the equivalent SDOF system.

2. Dynamic Resistance Function

The proposed resistance-displacement model shown in Figure 38 is similar to models discussed earlier in Section III-E-3 by Clough (Figure 34-b) and Sozen (Figure 35). Assuming that the cross section of the beam is symmetrically reinforced, the skeleton curve OAC in Figure 38 is the numerical load-deflection function. Unlike the bilinear models proposed by Clough (Reference 53) and Sozen (Reference 47), the present nonlinear function is actually a piecewise multilinear curve and it includes all material and support nonlinearities mentioned earlier in Section III-E. Since a specific closed form mathematical expression is not available, theoretical evaluation of the structural response are not considered and all computations are performed numerically.

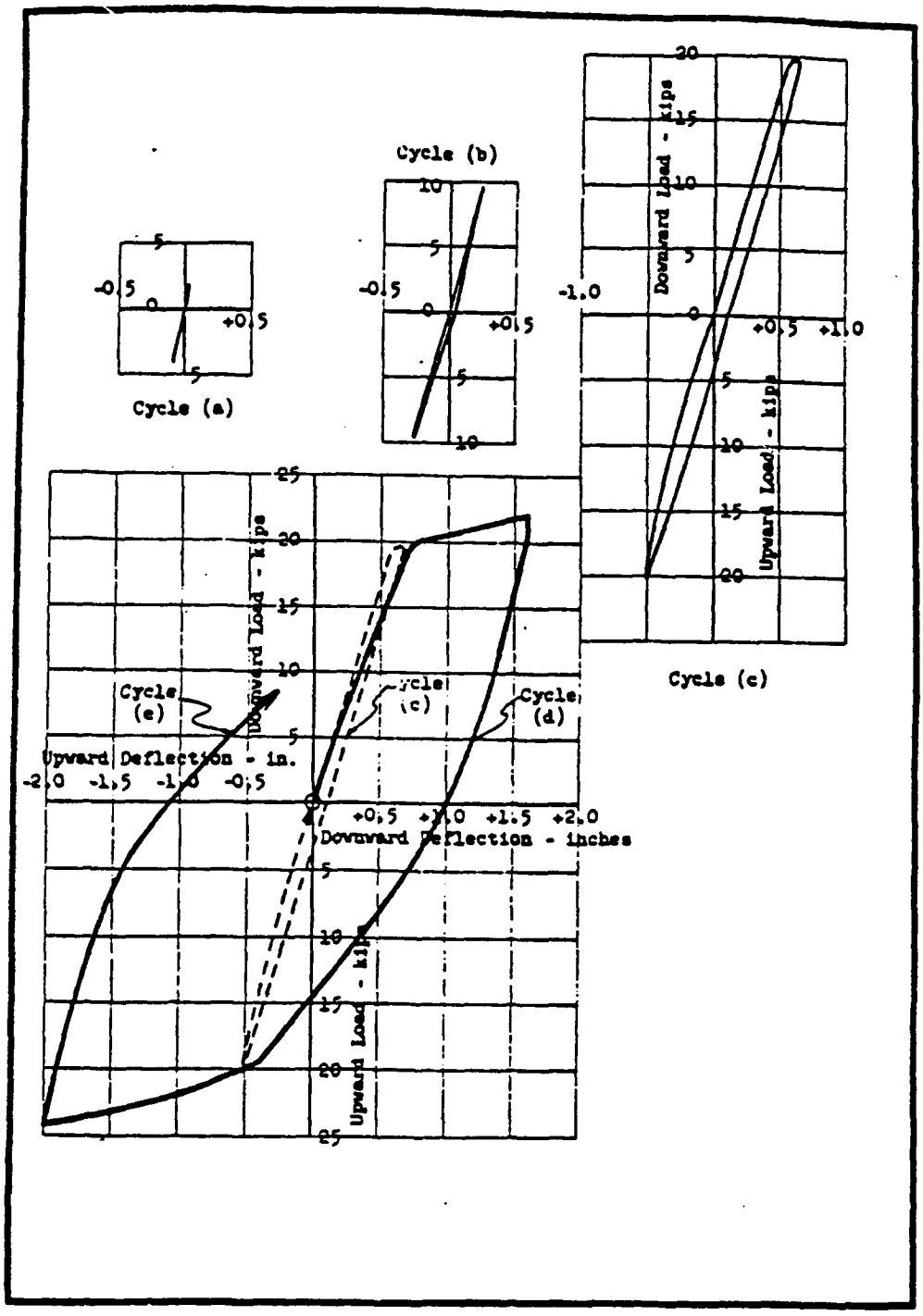

Figure 36. Effect of Load Reversal on the Load-Deflection of a Reinforced Concrete Beam. (Reference 1)

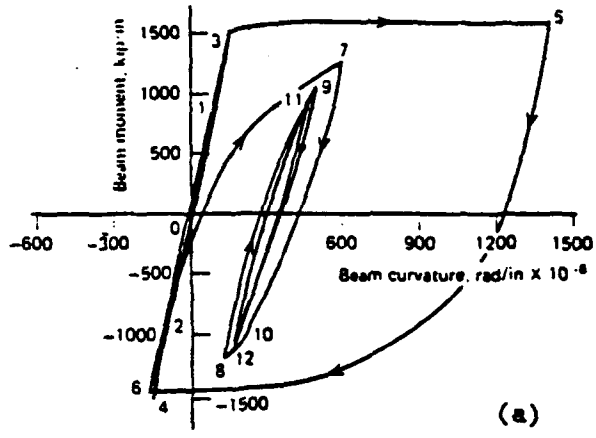

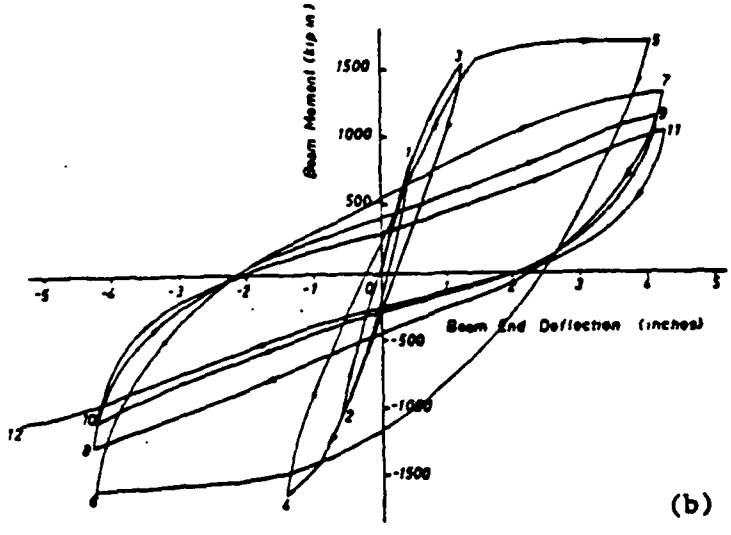

Figure 37. Experimental Observation on the Hysteretic Response of Reinforced Concrete Members
(a) Moment-Curvature for Plastic Hinge
(b) Moment-Deflection.
(Reference 2)

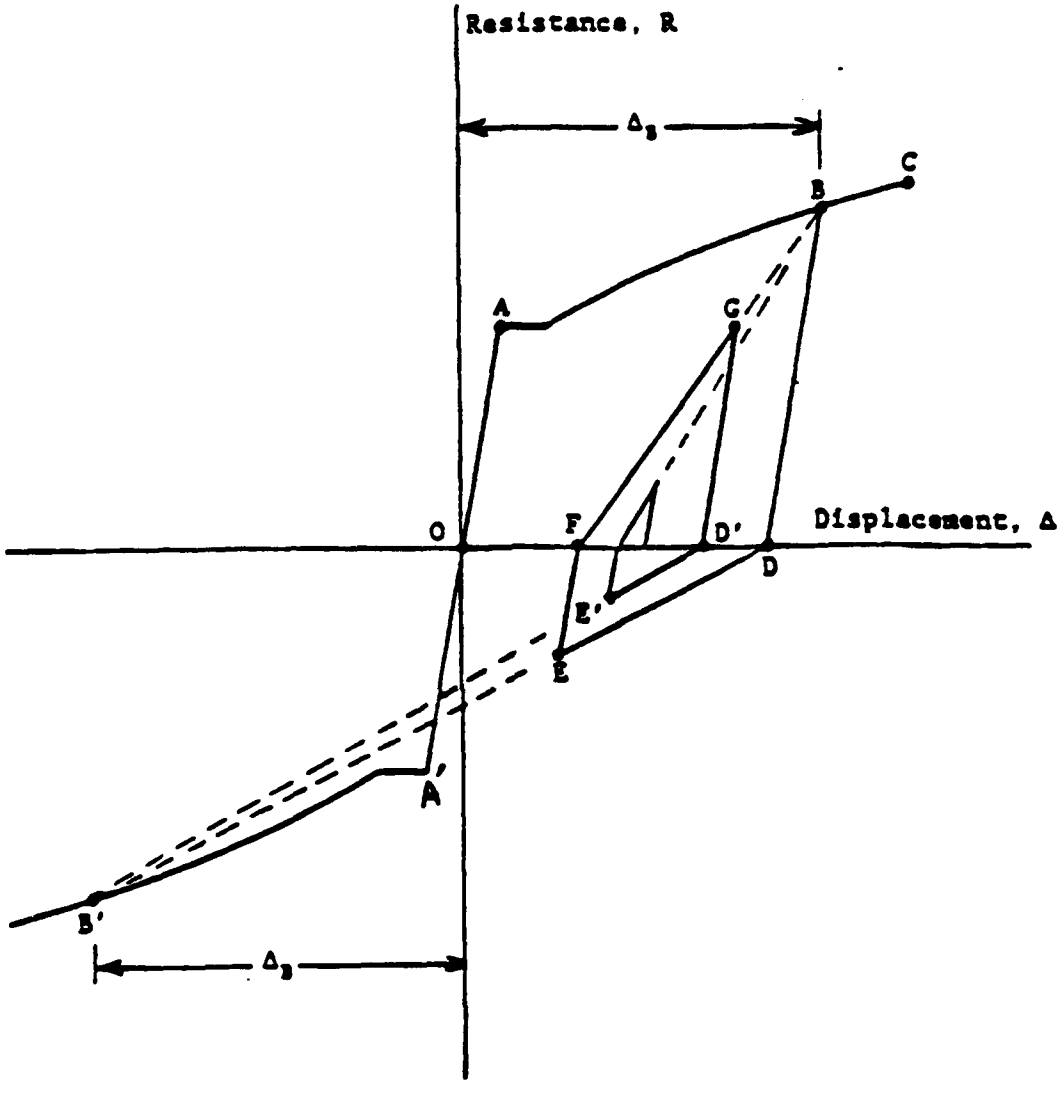

Figure 38. Typical Response of SDOF System. (a) Elastic Response, (b) Inelastic Response.

The proposed dynamic resistance function is described next by using a typical displacement response diagram.

a. Elastic Response

If the maximum dynamic displacement does not exceed the yield displacement, i.e. $\Delta_{max} < \Delta_y$, the behavior of the beam is elastic and oscillation will occur about the zero displacement position (Figure 39-a) or between points A and A' on the resistance-displacement diagram (Figure 38). The beam eventually comes to rest after all energy has been dissipated by external damping.

b. Inelastic Response

If the maximum dynamic displacement exceeds the yield displacement, the beam experiences unrecoverable inelastic deformation. In that case, the beam will come to rest with a residual displacement, after all energy is dissipated by the internal hysteretic damping mechanism as well as the external damping. Referring to Figures 38 and 39-b, the following steps describe the proposed hysteretic behavior and the inelastic dynamic response of the beam;

(1) Upon initial loading, the maximum dynamic deflection increases along the resistance-displacement (R-Δ) curve, exceeds the yield displacement, and reaches a maximum deflection at point B shown in Figures 38 and 39-b.

(2) At point B the displacement begins to decrease and positive unloading of the beam is assumed to occur along a straight line BD in Figure 38.

(3) Once point D is reached, negative unloading follows along line DB'. The slope of the negative unloading segment is the same as that proposed by Sozen (Reference 47); i.e., to choose point B' to be the mirror image of point B on the negative R-Δ diagram. Negative unloading continues until the point of minimum displacement E in Figures 38 and 39-b is reached.

(4) After point E, displacement begins to increase and negative reloading occurs along path EF for the first time. Experimental findings (Section III-E-3) show that the slope of the reloading line is best represented by a straight line until the initiation of positive unloading marks the end of the first complete hysteretic cycle.

(5) The formation of the flexural cracks in both positive and negative directions in conjunction with the Bauschinger effect reduce the strength (stiffness) of the section Clough (Reference 53) and Sozen (Reference 47) acknowledged this

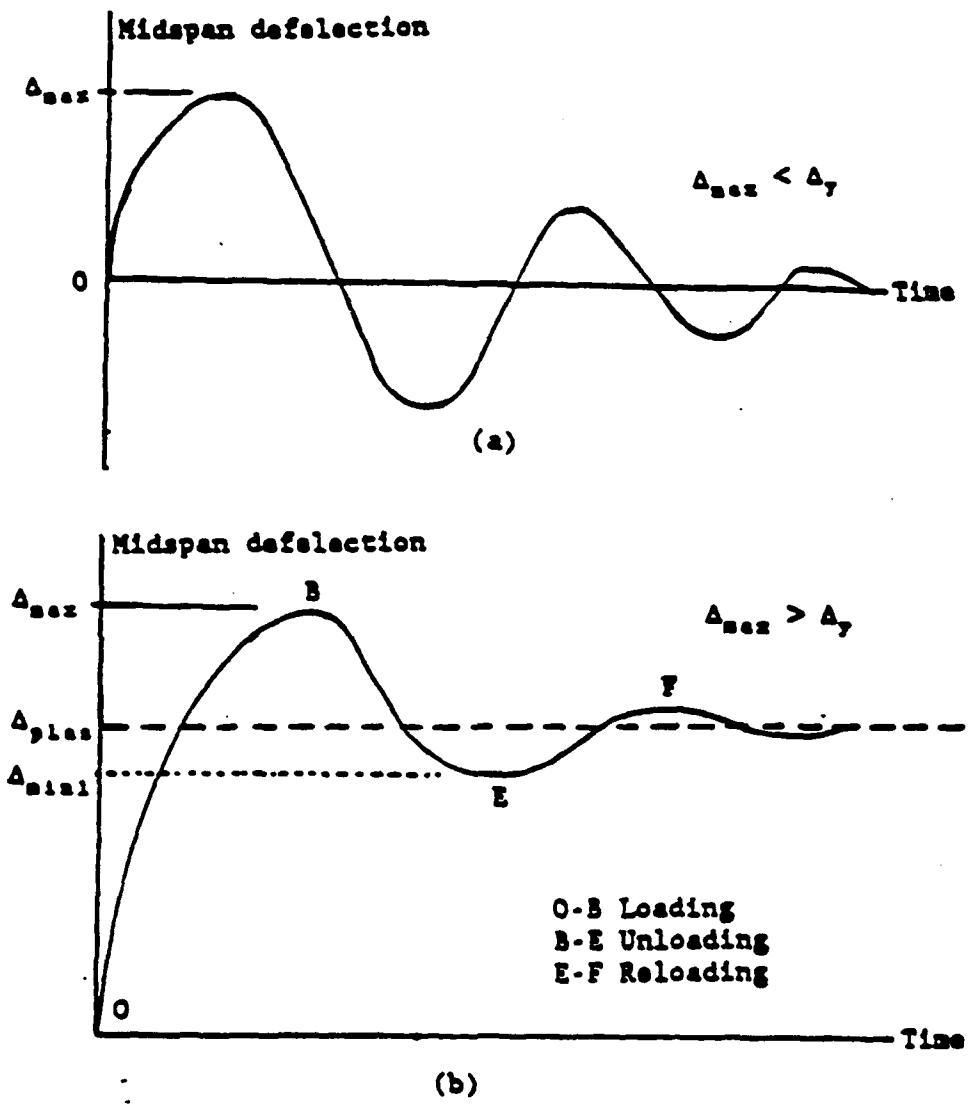

Figure 39. Proposed Modified Resistance-Displacement Model.

fact and proposed models that account for stiffness degradation within the hysteretic model. Here, the slope of the reloading line segment, FG, is taken the same as that proposed by Sozen (Reference 47) i.e., along a line between points F and B by in Figure 38.

(6) If the new maximum deflection does not exceed the maximum value of the previous cycle, unloading is assumed to follow along a straight line from G to D'.

(7) The process of reloading and unloading cycles continues until the beam eventually comes to rest with a residual deflection denoted by Δ_{plas} in Figure 39-b.

The following should be noted about the proposed model:

a. Point C in Figure 38 represents the flexural failure of the beam. If the deflection at any time exceeds the value of the deflection at point C, failure is assumed and the computational process is stopped.

b. The model shown in Figure 38 is constructed for a beam with a cross section that is symmetrically reinforced. For beams with unsymmetrical cross sections two resistance-displacement curves must be provided; one for the positive loading and one for the negative loading.

c. The above discussion it was assumed also that the maximum displacement would be reached during the first positive loading cycle. Such an assumption would often be valid for blast and impact loads but not necessarily for earthquake and other types of dynamic loads. If the nature of loading was such that the maximum deflection exceeded the value at point B or point B' in Figure 38, the displacement should continue to increase on the skeleton curve(s) until either failure or rebounding would occur.

In discussing the effects of energy dissipation, Baker et al. (Reference 46) provide the following reasons for ignoring external damping in the analysis of structures to resist blast loads:

a. The amount of external damping is very small compared with internal (material) damping.

b. Only the first cycle of response is usually of interest and the effect of external damping on the response in the first cycle is negligible.

c. There are considerable uncertainties in estimating the external damping factors. By ignoring damping, results are always more conservative.

Nevertheless, the presence of external damping has been

included by employing a linear viscous dashpot, for which the value of the damping ratio must be known.

3. A Modified Method to Evaluate the Parameters of Equivalent SDOF Model

This study proposes to perform the dynamic analysis by employing a SDOF approximation for the reinforced concrete structural element. The results obtained from a number of studies (References 54,55,56, and 57) show that this technique is a simple and relatively accurate tool for evaluation of the structural response, if proper behavioral models are assumed. Thus, special attention must be devoted to the derivation of the parameters of the SDOF model. The accuracy of the results is extremely sensitive to the formulation and employment of these parameters.

In Section III-B the procedure for computing the equivalent mass and load was discussed. Evaluation of the integral in Equation (113) would result in an equivalent mass for the dynamic system, from which the mass factor as given by Equation (113) could be computed. Also, the concept of Equivalent Load applied to the SDOF system was expressed mathematically by Equation (117). This was presented by Biggs (Reference 42) for a number of cases by assuming an analytical expression for the shape function $\psi(x)$. Those few cases were limited to perfectly elastic or perfectly plastic beams with ideal boundary conditions (e.g., fixed, hinged) and always loaded at the mid-span by a concentrated force. Moreover, there was no attempt to compute the mass and the load factors for the transition period, when the behavior changes from elastic to plastic. The present numerical method, as presented next, removes these restrictions so that a complete array of mass and load factors can be computed for a reinforced concrete beam with arbitrary linear or nonlinear boundary conditions from the initiation of loading to failure.

a. Mass Factor

In Section II the shape function $\psi(x)$ which satisfied the geometric support conditions was obtained in a numerical form for every incremental load level from the onset of loading to the ultimate condition. Therefore, the mass factor at every load step i could be computed by numerical integration over the length of the beam of the right hand side of the following expression

$$MF_i = \left(\int_0^L m_u \, (\psi(x)_i)^2 \, dx \right) / M_t \qquad (127)$$

Where, MF_i is the mass factor at load step i, $\psi(x)$ is the deflected shape function of the beam at load step i, m_u is the mass of the beam per unit length, M_t is the total mass of the beam, and L is the length of the beam.

During the dynamic analysis, the mass factor, MF, is computed for

the specific displacement at every time step by the following linear interpolation equation;

$$MF = MF_i + \left[\frac{MF_{i+1} - MF_i}{\Delta_{i+1} - \Delta_i}\right] (\Delta - \Delta_i) \qquad (128)$$

where, $\Delta_i < \Delta \leq \Delta_{i+1}$

Equation (128) is employed at every time step until rebounding from the maximum inelastic dynamic displacement (point B in Figure 38) takes place. After that time, the mass factor is kept constant and equal to its value computed at point B, since it is assumed that the inelastic deformed shape function does not change considerably after the formation of plastic hinges.

The effects of the arbitrary nature of end conditions and the location of the load on the span of the beam have been incorporated in the development of the deflected shape function, as discussed in Section II. Thus, the present approach removes all limitations mentioned earlier in this section. In addition, the analysis is no longer restricted to perfectly elastic or perfectly plastic beams, since it is possible to compute the mass factor for every displacement during the transition from elastic to plastic.

b. Load Factor

The computation of a load factor follows the same approach used for the mass factor. In the development of the load-deflection diagram the load factor at any load step i is computed according to the following expression

$$LF_i = \psi(x)_{(i,j)} \qquad (129)$$

where, LF_i is the load factor at load step i and $\psi(x)_{ji}$ is the shape function at step i evaluated at point j on the span. For example, the magnitude of load factor for a beam with symmetric boundary conditions and loaded at the midspan by a concentrated force is always unity, because maximum deflection always occurs at the point of load application.

Similar to the development of the mass factor, the array of load factors contains values at every load step i, from the initiation of loading to the ultimate condition. During the dynamic analysis, the load factor at every time step may be computed by a linear

interpolation in the following manner;

$$LF = LF_i + \left[\frac{LF_{i+1} - LF_i}{\Delta_{i+1} - \Delta_i}\right] (\Delta - \Delta_i) \qquad (130)$$

where, $\Delta_i < \Delta \leq \Delta_{i+1}$.

It is important to realize that so long as the end conditions are not different and the load is applied at the center of the span, the magnitude of the load factor does not deviate from unity.

4. Influence of Axial Compressive Force

The effect of an axial compressive force on the moment-curvature and load-deflection behavior was discussed in Section II. From the equilibrium of the cross section, the difference between the net compressive and tensile forces is the axial thrust. In addition, due to considerable lateral deflection of the beam at advanced loading stages, the presence of the axial compressive force introduces an additional secondary external moment (P-Δ effect) into the beam which would result in additional curvature and deflection. In the present approach, a closed form evaluation of the second order effects is not considered because:

a. Numerical models were employed to model material nonlinearities in reinforced concrete and thus, unique load-dependent closed form solutions for the variation of EI, $\psi(x)$, and derivatives of $\psi(x)$ with x are not available.

b. The possibility of including arbitrary linear and nonlinear support conditions were considered by employing numerical models and therefore, the shape function $\psi(x)$ can not be presented in closed form.

Instead, it was decided to modify the nonlinear resistance-deflection relationship (R-Δ curve) to include the effect of axial load, as described next.

In Section II a deflection function Δ(x) which satisfied the the geometric boundary conditions was computed numerically for every incremental load step. Therefore, the second order moment denoted by M′ can be evaluated numerically at every load step i for every point j on the span of the beam by the following expression;

$$M'_{(i,j)} = P_{axial}\, \Delta_{(i-1,j)} \qquad (131)$$

where, P_{axial} is the axial compressive force, i is the load step, and j is the arbitrary point on the span of the beam. The second order moment, M′, is subsequently added to the first order moment to obtain

the modified moment diagram which includes the effect of axial compressive load.

$$M^*_{(i,j)} = M_{(i,j)} + M'_{(i,j)} \qquad (132)$$

where, $M^*_{(i,j)}$ is the moment representing the combined effect of transverse and axial load at point j in step i. The modified moment diagram is subsequently used in conjunction with the moment-curvature relationship to compute the maximum deflection at step i. The modified R-Δ curve obtained from the procedure mentioned above is subsequently employed in the dynamic analysis.

G. EFFECT OF LOADING RATE ON STRENGTH

This study is particularly concerned with the response of reinforced concrete structures subjected to high loading rates such as impact and blast. Under these conditions, the strength and modulus of elasticity of concrete and steel increase significantly. Many experimental investigations were conducted in the past to demonstrate the influence of rate of strain on material properties. Consequently, empirical relationships were developed to model this phenomenon as accurately as possible. Inclusion of this concept into the proposed dynamic model is discussed in Section III-G-1.

In an original experimental study, Watstein (Reference 58) investigated the behavior of plain concrete cylinders subjected to rates of straining ranging from 10^{-6} /Sec. to 10. /Sec. with the corresponding duration of tests ranging from 30. to 0.003 seconds. Under the highest rate of loading, the compressive strength of concrete increased by as much as 85 percent, and the secant modulus increased by 47 percent for weak concrete (2500 psi) and 33 percent for strong concrete (6500 psi). Bazant and Byong (Reference 59) extended the data base by combining the results from several studies (including Watstein's) to obtain empirical relationships between strength and strain rate for plain concrete. A summary of these results are shown in Figure 40. The effect of strain rate on a typical constitutive model for plain concrete is shown in Figure 40-a. Figure 40-b shows that the rate effect does not have much influence on the strain of concrete at peak stress. Figures 40-c and 40-d depict the influence of strain rate on compressive strength and secant modulus respectively.

Soroushian et al. (Reference 60) conducted a similar study in which empirical constitutive models for plain and confined concrete were proposed based on extensive experimental studies by other investigators. In that study, it was found that the influence of loading rate is more pronounced for wet concrete than it is for dry concrete. Moreover, the trend of data showed that the strain of concrete at maximum stress decreased for strain rates smaller than 0.01 /Sec and increased at higher strain rates (Figure 41-a). Figures 40-b, 40-c, and 40-d show the strain rate effect on compressive strength, secant modulus and tangent modulus of concrete as reported in Reference 60.

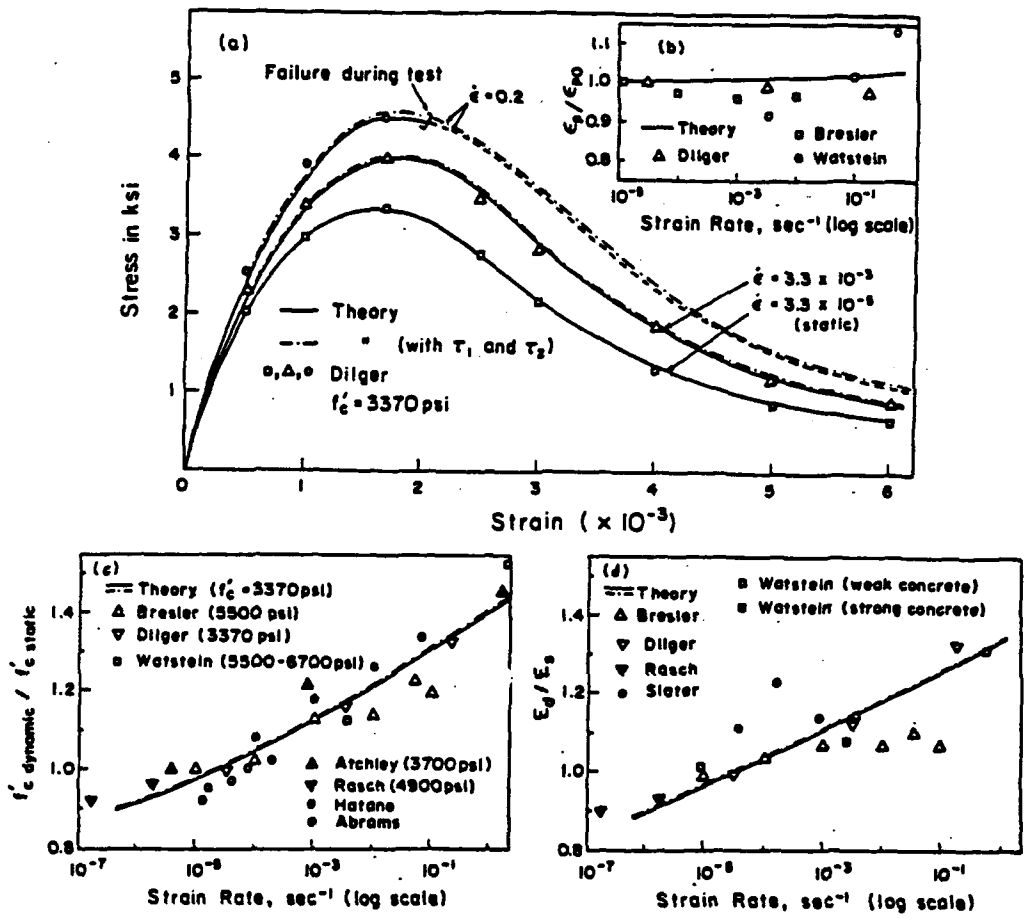

Figure 40. Effect of Strain Rate on Properties of Plain Concrete; (a) Constitutive Model,
(b) Strain at Peak Stress
(c) Maximum Compressive Strength
(d) Secant Modulus of Elasticity.
(Reference 59)

(a)

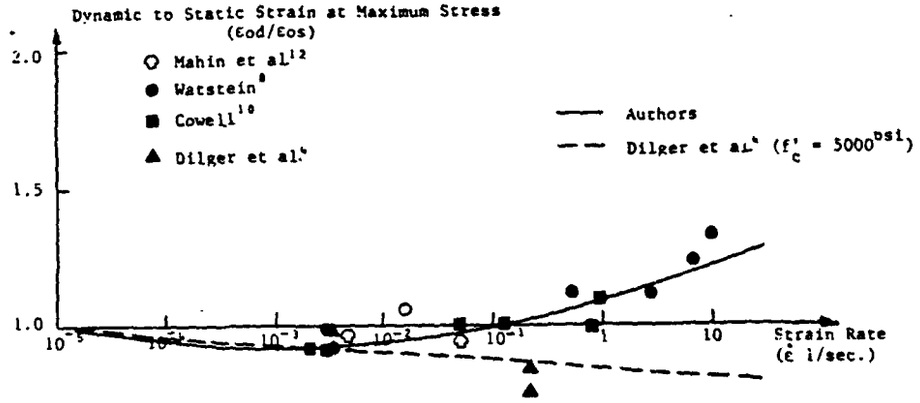

(b)

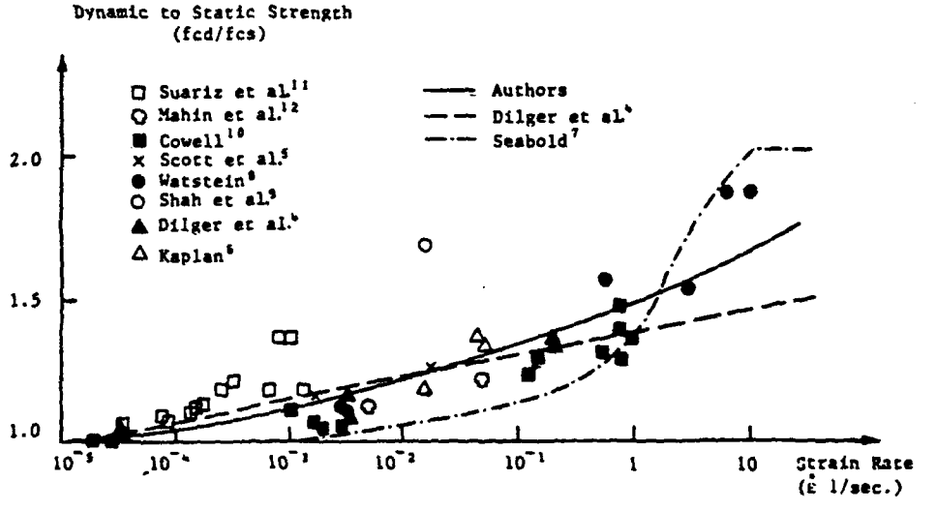

Figure 41. Strain Rate Effect on: (a) Concrete Strain at Maximum Compressive Stress, (b) Maximum Compressive Strength, (c) Secant Modulus of Elasticity, (d) Tangent Modulus of Elasticity. (Reference 60)

(c)

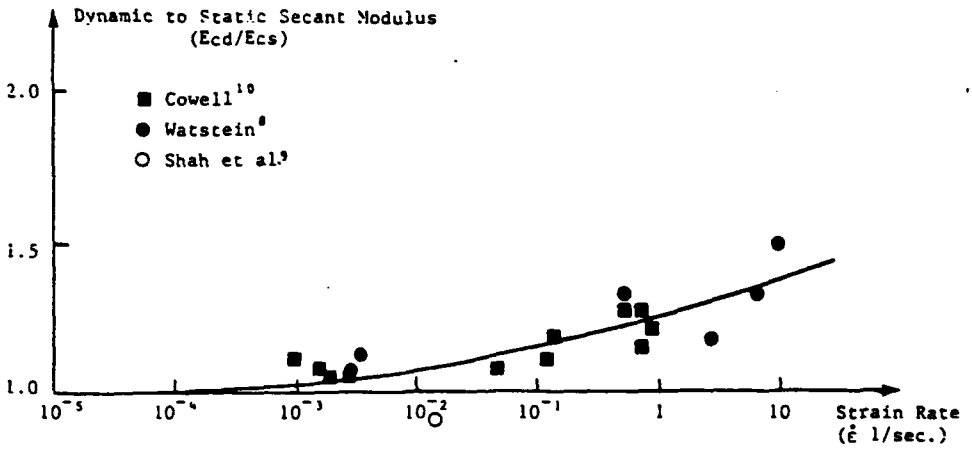

(d)

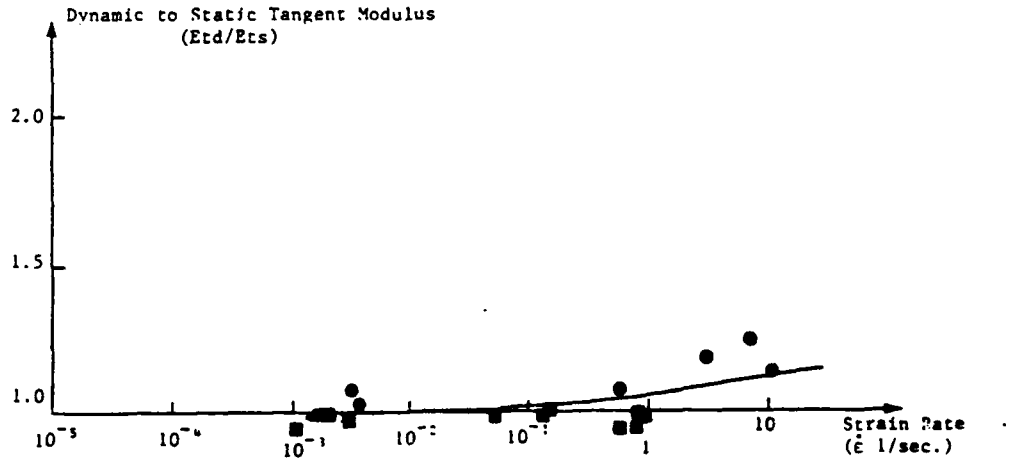

Figure 41. Strain Rate Effect on: (a) Concrete Strain at Maximum Compressive Stress, (b) Maximum Compressive Strength, (c) Secant Modulus of Elasticity, (d) Tangent Modulus of Elasticity. (Reference 60)

(concluded)

Soroushian and Choi (Reference 61) studied the strain rate effects on material properties of structural steel. In that study, extensive experimental data from past investigations were combined to obtain empirical relationships for predicting the strain rate effects on yield strength and ultimate strength of steel (Figure 42). It was concluded that increasing the rate of straining would increase all the characteristic stress and strain values on the constitutive model. But, material properties of steel with high-yield stress demonstrated less sensitivity to high strain rates.

A number of other experimental and analytical investigations focused on predicting the overall enhancement in the strength of reinforced concrete structural elements subjected to dynamic loads applied at high rates. In design for protective structures, Newmark (Reference 62) recommended to increase the yield strength of steel by 30 percent and to increase the compressive strength of concrete by 25 percent. Criswell (Reference 63) found that the strength of reinforced concrete specimens would increase by 18 percent in flexure and 26 percent in shear under dynamic loads. Furlong et. al (Reference 64) observed an increase of 30 percent in flexural strength and an average increase of 37 percent in shear strength in beams subjected to impact loads. Similarly, Seabold (Reference 65) found 20 percent to 30 percent improvement in strength of reinforced concrete beams under dynamic conditions.

Soroushian and Obaseki (Reference 66) employed strain rate dependent constitutive models for concrete and steel to predict analytically the strength of reinforced concrete beams-columns subjected to different strain rates. The results of the computational effort in Reference 66 indicated that closer placement of the longitudinal steel to extreme fibers of the cross section and confinement of concrete increased the strain rate effects. Furthermore, it was reported that increasing the strain rate from 0.000005 /Sec. to 0.05 /Sec. caused an average increase of 25 percent on the axial-flexural strength of the member. However, it was noted that the influence of strain rate would not necessarily induce the same effect on the shear strength of beams. In addition, variations of the strain rate in different sections of the structural element could result in unforeseen and perhaps undesirable redistribution of stresses within the element.

1. Implementation of the Rate Effect into the Analytical Procedure

Since the response of a structural element depends on the dynamic excitation, the strain rate is a time dependent parameter. Therefore, empirical constitutive models developed from constant strain rate test results should only be used for the average rate of straining the material (see Reference 67). In addition, review of the existing state of knowledge on this subject, as presented in the previous section, reveals considerable variabilities in the experimental data. This is particularly true for structural elements

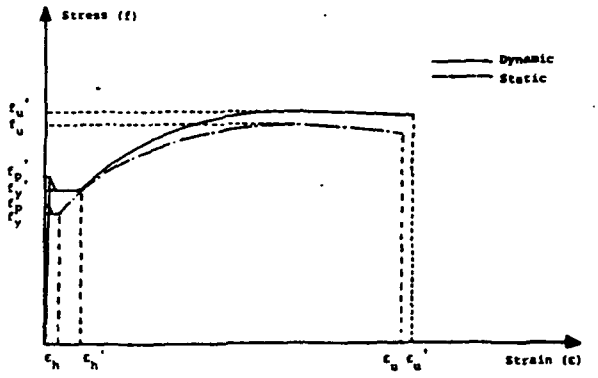

(a)

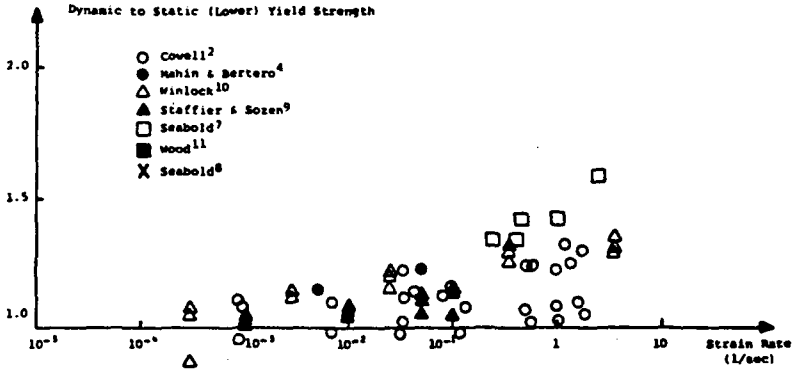

(b)

Figure 42. Strain Rate Effect on Material Properties of Steel: (a) Constitutive Model, (b) Yield Strength, (c) Ultimate Strength. (Reference 61)

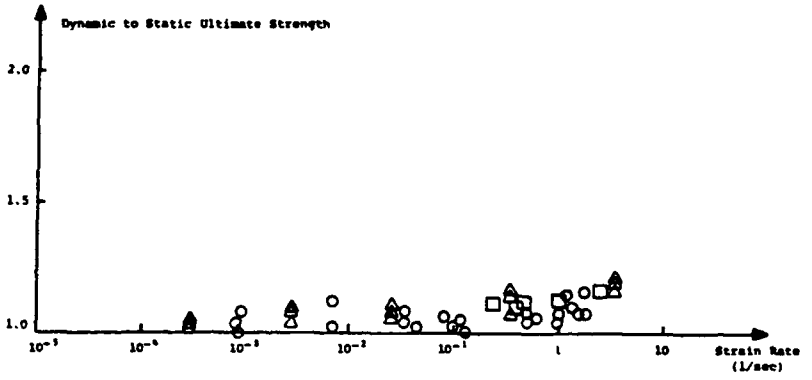

(c)

Figure 42. Strain Rate Effect on Material Properties of Steel: (a) Constitutive Model, (b) Yield Strength, (c) Ultimate Strength. (Reference 61)

(concluded)

subjected to blast and impact loads, since the average rate of straining or loading often exceeds the range of the available experimental data. Such being the case, direct employment of the constitutive models described in the previous section can not be justified.

This study proposs modification of strength properties of steel and concrete by applying the average rate effect enhancement factor to the stress parameters of the material models. Such modification are introduced as follows.

$$f_{ey} = \eta_{sy} f_y \quad (133\text{-a})$$
$$f_{eu} = \eta_{su} f_u \quad (133\text{-b})$$
$$f'_{ec} = \eta_c f'_c \quad (133\text{-c})$$

where, η_{sy}, η_{su}, and η_c are the average material enhancement factors for yield strength of steel, ultimate strength of steel, and compressive strength of concrete respectively. f_{ey}, f_{eu}, and f'_{ec} are the modified yield strength, modified ultimate strength, and modified compressive strength of concrete. The modified values are subsequently utilized to compute the moment-curvature and resistance-displacement relationships using the procedures mentioned earlier in Section II. The modified R-Δ curve is then employed in the dynamic analysis.

Good engineering judgment must be exercised in selecting appropriate values for the enhancement factors. If the average rate of straining is not very high, Figures 41 and 42 may serve as guidelines in predicting the enhancement factors for f_y, f_u, and f'_c. For very high rates of loading (e.g., blast), enhancement of material properties is estimated to be often between 0.2 and 0.4 (References 62-66).

H. ANALYTICAL MODEL FOR DIRECT SHEAR RESISTANCE MECHANISM IN REINFORCED CONCRETE ELEMENTS

1. Analytical Methodology

So far, the dynamic SDOF analysis has been only based on the flexural resistance of the element and it has been assumed that the element would not fail in direct shear. Experimental observations on the dynamic response of shallow-buried reinforced concrete box-type structures to blast loading (as reported in References 67,68, and 69), indicated that in many instances the structure failed in shear at critical locations (e.g., supports) at an early time. The shear failure surface observed in the experiments (see References 68 and 69) looked quite similar to the interface shear failure along the vertical shear plane. This type of failure is commonly referred to as the direct shear failure and is characterized by sliding or large displacements along the interface shear plane. A review of the current state of knowledge on the dynamic shear resistance of one way slabs as reported in References 67-70 indicated that if the dynamic shear resistance was not included in the analytic formulation, and if the dynamic analysis was performed only for evaluation of the flexural

response, it would be possible to grossly overestimate the strength of the member. The possibility of an interface shear or direct shear failure of the element could control the failure mechanism and therefore, should be included in the overall analytical scheme, as presented next.

The analytic approach adapted here is very similar to the model proposed by Krauthammer et. al (Reference 56) and used successfully for the analysis of buried reinforced concrete box-type structures. In this method, two single-degree-of-freedom systems are considered for the overall response of the element to the impulsive excitation. The first is for the evaluation of the flexural response (discussed earlier in this section) and the second is for monitoring the direct shear response at critical locations on the span of the beam (e.g., at the supports or under the concentrated load). The procedure for deriving the parameters of the second (shear) SDOF system are presented in Sections III-H-2 through III-H-4. For each time step, the flexural and shearing responses are computed and compared to their respective failure criterion. If the flexural dynamic displacement exceeds the maximum displacement on the resistance function, a flexural failure is assumed to have occurred. Similarly, if the shear slip at the selected critical location exceeds the ultimate permissible shear displacement (Section III-H-2), a shear failure is assumed and the computational procedure is halted. So, the present highly nonlinear dynamic problem has been approximated by two uncoupled simpler piecewise-linear problems, each represented by a separate nonlinear SDOF system.

Experimental observations as reported in References 68 and 69 indicated that the response of box-type buried reinforced concrete structures subjected to blast loads was controlled by either a direct shear failure mode at the end supports which occurred very early in time, or by a flexural mode where the roof slabs experienced permanent inelastic deformations. From the experimental observations, it was apparent that if the structure happened to fail in shear, there was hardly any significant flexural response. Similarly, in cases that the roof member failed in flexure at much later time, it survived the early high shear forces. Therefore, it would seem reasonable and justifiable to uncouple the direct shear response from the flexural response in the manner discussed above.

Ross (References 67 and 71) investigated the direct shear failure phenomenon in one way reinforced concrete by employing the classical elastic Timoshenko beam model to account explicitly for the shearing deformations when slabs were subjected to distributed impulsive loads. It was found that direct shear failures preceded the flexural failures in all cases examined. This conclusion agreed well with the experimental observations reported by Kiger et al. (Reference 68), thus, further reaffirming the assumption of uncoupling of direct shear and flexural response in the simplified SDOF models.

The nonlinear form of the SDOF differential equation of motion for direct shear analysis can be presented as follows:

$$M_s \ddot{Y} + C_s \dot{Y} + R_s = V(t) \quad (134)$$

where, M_s is the shear mass, C_s is the shear damping coefficient, R_s is the direct shear resistance function, and V(t) is the applied shear force (e.g., dynamic reaction at the support). These parameters are discussed in the following Sections. Y, Y, and Y are the shear displacement, velocity and acceleration, respectively.

2. Dynamic Shear Force

One of the inherent limitations of the SDOF approach is in lack of results for some of the key characteristics responses which may be of great interest to the analyst. One such case is the dynamic reaction. In his book, Biggs (Reference 42) provides the following explanation on this issue:

> "...the dynamic reactions of the real structural element have no direct counterpart in the equivalent one-degree system. In other words, the reaction of the equivalent system, i.e., the spring force, is not the same as the real reaction. This is true because the simplified system was deliberately selected so as to have the same dynamic deflection as the real element, rather than the same force or stress characteristics."

In order to obtain an approximate value of the dynamic reaction of the real structural element, Biggs considers the dynamic equilibrium of forces on the free body of the left half of the elastic simply supported beam (Figure 43) as follows.

$$V\,(61L/192) - M_c - 0.5\,(61L/192 - L/4)\,F = 0. \quad (135)$$

where, V is the dynamic reaction, F is the total dynamic load on the beam, M_c is the dynamic moment at the midspan and L is the length of the beam. Similar to the procedure in Reference 42, it is assumed that the inertia forces have the same distribution as the deflected shape function of the elastic beam under uniform static load. It is further assumed that the relationship between the dynamic bending moment and dynamic resistance is the same as that between the static bending moment and the applied load. Thus, by substituting RL/8 for the M_c it is possible to arrive at the following expression for the dynamic reaction.

$$V = 0.39\,R + 0.11\,F \quad (136)$$

where, R is the time dependent resistance function and F is the time dependent loading function.

Keenan (Reference 70) obtained the 'exact' solution for the support reaction of a simply supported elasto-plastic beam

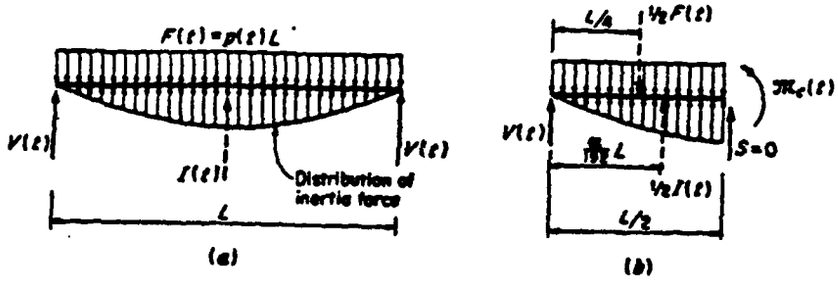

Figure 43. Determination of Dynamic Reaction for a Simply Supported Beam Subjected to Uniform Load. (Reference 42)

subjected to a triangular pulse, and he compared that with the result of Equation (136) for the same load. It was found that the magnitude of the dynamic shear force at the support predicted by Equation (136) would provide an adequate result for all practical purposes. Furthermore, it was stated that the maximum shear stress produced by a blast load can exceed the maximum shear stress produced by the ultimate flexural resistance under static conditions.

Based on a similar procedure, Biggs obtained and documented analytic expressions for the dynamic reaction of beams with different support conditions. However, these cases were always limited to some perfectly elastic or perfectly plastic beams, loaded at the midspan by a concentrated force, with ideal boundary conditions (e.g., hinged or fixed). In addition, it is noted in Reference 42 that the assumed shape function for the plastic domain is not necessarily the actual deformed shape of the beam, and the abrupt transition from the elastic shape to the assumed plastic shape may result in incorrect deviation in behavior of the dynamic model from the actual behavior of the element.

The following formulation removes these restrictions so that the dynamic reactions for a reinforced concrete beam with arbitrary boundary conditions can be approximated at every time step. The procedure, summarized below, assumes that the distribution of the inertia forces is identical to the deformed shape function of the beam (Figure 44).

a. During the computational procedure for the load-deflection relationship, obtain the reactions at each end of the structural element and compute the load proportionality factor γ for each end as follows;

$$\gamma_{1i} = Q(1)_i/Q_i \qquad (137\text{-a})$$

$$\gamma_{2i} = Q(2)_i/Q_i \qquad (137\text{-b})$$

where, $Q(1)_i$ and $Q(2)_i$ are the static reactions of the beam at load step i, Q_i is the load at step i, and γ_{1i} and γ_{2i} are the load proportionality factors at ends 1 and 2 respectively.

b. At every load step j, compute the Inertial Load Factor, IFL, by evaluating the following integral numerically at every load step j.

$$ILF_i = \left(\int_0^L (\psi(x)_i)\, dx\right) /L \qquad (138)$$

where, IFL is the load factor associated with the distribution of the inertial forces and $\psi(x)_i$ is the deflected shape function at load step i.

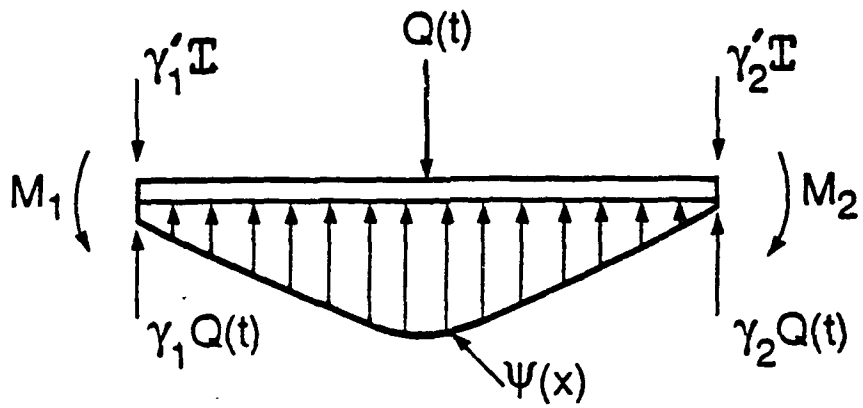

Figure 44. Determination of Dynamic Reaction for a Beam with Arbitrary Boundary Conditions

c. Knowing the distribution of the inertia forces, compute the inertia proportionality factors γ'_{1i} and γ'_{2i} for ends 1 and 2, respectively at every load step i. Since the magnitude of the inertia load is not known at this stage, an iterative procedure for the exact determination of the these factors can not be performed. Therefore, these factors are approximated by using the principles of the linear beam theory. The fact that the peak direct shear response always occurs early in time, before any significant nonlinear flexural response is developed, further justifies this assumption.

d. During the dynamic analysis, the dynamic reaction at either end of the element can be computed at every time step as follows.

$$V_1 = \gamma_{1i} * Q(t) + ILF * \gamma'_{1i} * M_t * X \qquad (139\text{-a})$$
$$V_2 = \gamma_{2i} * Q(t) + ILF * \gamma'_{2i} * M_t * X \qquad (139\text{-b})$$

where, Q(t) is the forcing function, M_t is the mass of the beam and X is the acceleration. Factors γ_{1i}, γ'_{1i}, γ_{2i}, and γ'_{2i} are computed for the specific displacement at every time step by the following linear interpolation equations respectively.

$$\gamma = \gamma_i + \left[\frac{\gamma_{i+1} - \gamma_i}{\Delta_{i+1} - \Delta_i}\right] (\Delta - \Delta_i) \qquad (140)$$

where, $\Delta_i < \Delta \leq \Delta_{i+1}$

where, Δ is the dynamic displacement at the specific time step, and γ is the generic name for inertia and load proportionality factors.

The dynamic reaction obtained is used as the forcing function to derive the second SDOF system which provides the shearing motion response at the critical location. The validity of the present approach is investigated later in Section IV, where the results obtained are compared with experimental data.

3. Direct Shear Resistance Function

The issue of direct interface shear resistance mechanism in reinforced concrete beams has been discussed by Park and Paulay (Reference 2). The present empirical model is based on the investigations by Mattock and Hawkins as modified and documented by Múrtha and Holland (Reference 72), followed by further

modifications by Krauthammer et. al in Reference 56. The original model, shown in Figure 45, is simply a nonlinear relationship between the shear stress and shear slip at the shear interface. The linear segments of the model are described briefly as follows:

a. Line OA: In this region the response in linear elastic up to the point A (Figure 46). The slope of this line is defined by a slip of 0.004 in. and an elastic shear stress limit given by the following expression

$$\tau_e = 165 + 0.157\ f'_c \qquad (141)$$

where, τ_e is the elastic shear stress limit in psi, and f'_c is the compressive strength of concrete in psi.

b. Line AB: The slope of the line in this region is defined by a shear slip of 0.012 in. and a maximum shear resistance, τ_m, given by the following equation.

$$\tau_m = 8\sqrt{f'_c} + \rho_{vt}\ f_y \leq 0.35\ f_c \qquad (142)$$

where, f_y is the yield strength of the reinforcement crossing the shear plane in psi, ρ_{vt} is the of the total reinforcement ratio crossing the shear plane, f'_c is the compressive strength of concrete in psi, and τ_m is the maximum shear stress.

c. Line BC: This segment is defined by a horizontal line where the shear stress remains constant at τ_m, while the shear slip increases to 0.024 in.

d. Line CD: Beyond point C, the shear slip increases with decreasing shear stress down to the limiting shear capacity τ_L, given by

$$\tau_L = (0.85\ A_s\ f'_s\ )\ /A_g \qquad (143)$$

The slope of this segment is given by the following expression.

$$K_u = 2000 + 0.75\ f'_c \qquad (144)$$

e. Line DE: The shear capacity remains constant as the shear slip increases until the failure slip at point E . The slip for the point of failure is defined by the following expression.

$$\Delta_{max} = 2.0\ (e^x - 1)/120 \qquad (145)$$

and,

$$x = 900/\ (2.86\ \sqrt{f'_c}/d_b) \qquad (146)$$

d_b is the bar diameter in inches, and Δ_{max} is the maximum shear displacement at failure in inches.

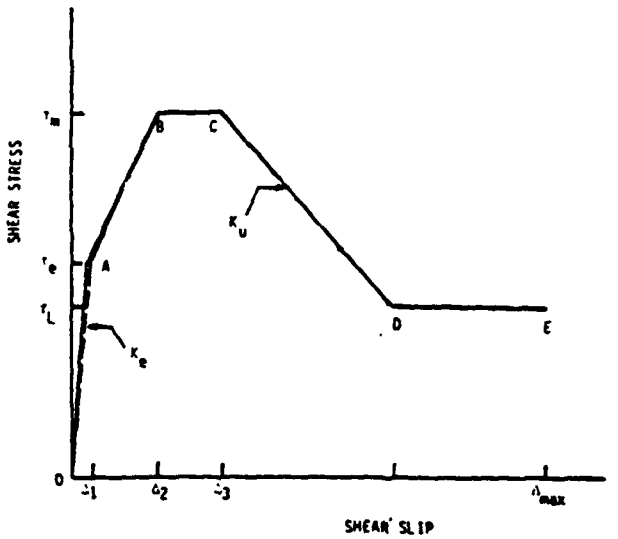

Figure 45. Empirical Model For Direct Shear Stress-Shear Slip Relationship. (Reference 56)

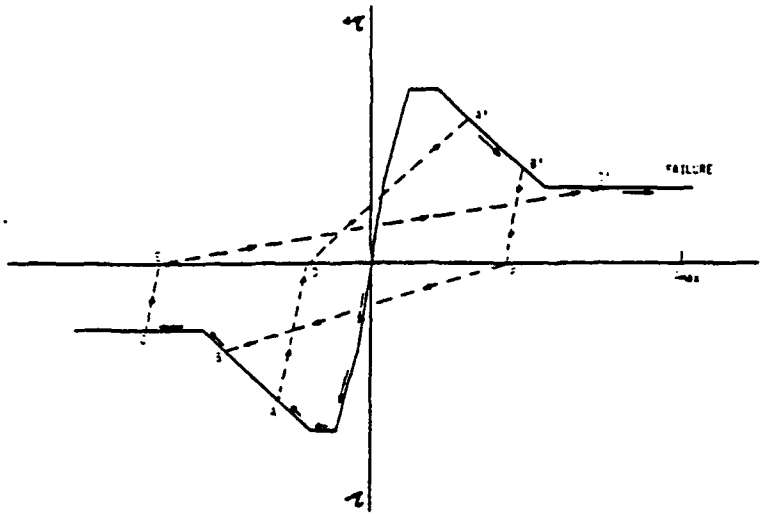

Figure 46. Direct Shear Resistance Envelop and Reversal Loads. (Reference 56)

The model described above is based primarily on the results of experimental investigations as reported in References 72 and 73. The slope of segment OA is based on the assumption that for low values of slip, the effect of dowel action in the flexural reinforcement is negligible, and the compressive strength of concrete can be used as the parameter that relates the shear stress to the shear slip. The maximum shear stress, τ_m, given by Equation (142), is based on the recommendations by ACI Committee 318 in the Proposed Commentary to the ACI Code 318-83. The shear slip values of 0.012 and 0.024 at points B and C are due to experimental observations as reported in Reference 73. Equations (145) and (146) were proposed in Reference 72 based on experimental observations on the relationships between dowel force, slip, and limiting shear capacity.

In order to employ the Hawkins shear model in dynamic analyses, Krauthammer et al. (Reference 56) modified the present model to include the effect of load reversals. This modification is shown in Figure 46 for a slab having the same amount of reinforcement in tension and compression. On initial loading, the shear stress-shear slip will follow the original path until unloading is reached at point A, and followed along a straight line until the point of zero stress, D. Once point D is reached, unloading will follow along line DA'. A' is the mirror image of point A on the opposite (reverse) shear envelope. If the shear displacement continues to increase in the reverse direction, it will follow the curve until the second unloading occurs at B, and the loop is repeated in a similar manner. If the shear slip never exceeds the maximum slip value on either side of the envelope, the system will eventually come to rest with a residual shear deformation. In the event of reloading, the shear displacement is assumed to follow a straight line with a slope equal to the initial loading path (Line OA in Figure 45)

4. Effective Mass in Analysis for Direct Shear Resistance

One of the important parameters in SDOF analyses of structures is to obtain the equivalent mass of the system based on the assumed approximate shape function. In the flexural analysis, the deformation pattern of the beam was obtained numerically at every load step, and subsequently used to compute the mass of the equivalent system. In a similar manner for shear, proper shape functions must be employed in order to characterize the behavior of the total element in accordance with the existing experimental observations. Furthermore, since it is important to investigate the shearing resistance at supports as well as under the concentrated dynamic load, estimates of the equivalent mass must be obtained for both types of analysis, as presented next.

a. Support Shear Failure Mode

Experiment observations on the dynamic shear failure of shallow-buried flat-roofed reinforced concrete structures subjected to blast loading (References 68 and 69) indicated that in nearly all cases of direct shear failure, the roof slab was completely severed and separated from the walls along a vertical shear failure plane at each end of the slab (Figure 47). Due to the uniform nature of loading, it is suspected that the reactions and the shearing resistance were nearly equal at both ends of these slabs and the mode of direct shear failure would resemble the configuration shown in Figure 47. Thus, the entire mass of the beam and the shearing resistance of both supports must be considered in the SDOF dynamic analysis.

Krauthammer et. al (Reference 56) applied the shear SDOF approximation to analyze the experiments reported in Reference 68. It was concluded that the method could effectively predict adequate results, so long as rational models were employed in the analysis.

No experimental data are available on the direct shear resistance of reinforced concrete beams subjected to localized (non-uniform) impulsive loads. However, it is speculated that if the loading is not uniform, direct shear failure at the support (as a result of separation of the roof from the wall) would certainly occur first at the boundary with the highest magnitude of the dynamic shear force, and then perhaps followed by the failure at the other end. In that case, only the shearing resistance of one cross section should be considered in the SDOF analysis, and the mode of failure could be assumed triangular (Figure 48) for which the equivalent mass can be computed as one half of the total mass of the beam.

b. Localized Shear Failure Mode Under the Load

There are only a few studies on which the localized direct shear failure in reinforced concrete elements subjected to impulsive loading were investigated. Ross and Rosengren (Reference 74) and Ross et al. (Reference 75) analyzed generic reinforced concrete slabs for localized shear failure in the vicinity of an explosive device placed in soil directly below the concrete slab. In that study, a static localized hinge mechanism (Figure 49-a) was used with the assumption that failure would cause a volume of the slab (shear mass) to be sheared off without appreciable damage to the other parts of the slab. It was found that the breach radius of the slab (49-b) depended on the magnitude, type, and distribution of the explosive charge and therefore, it would not be possible to predict a general expression for the shear mass for different types of loading conditions.

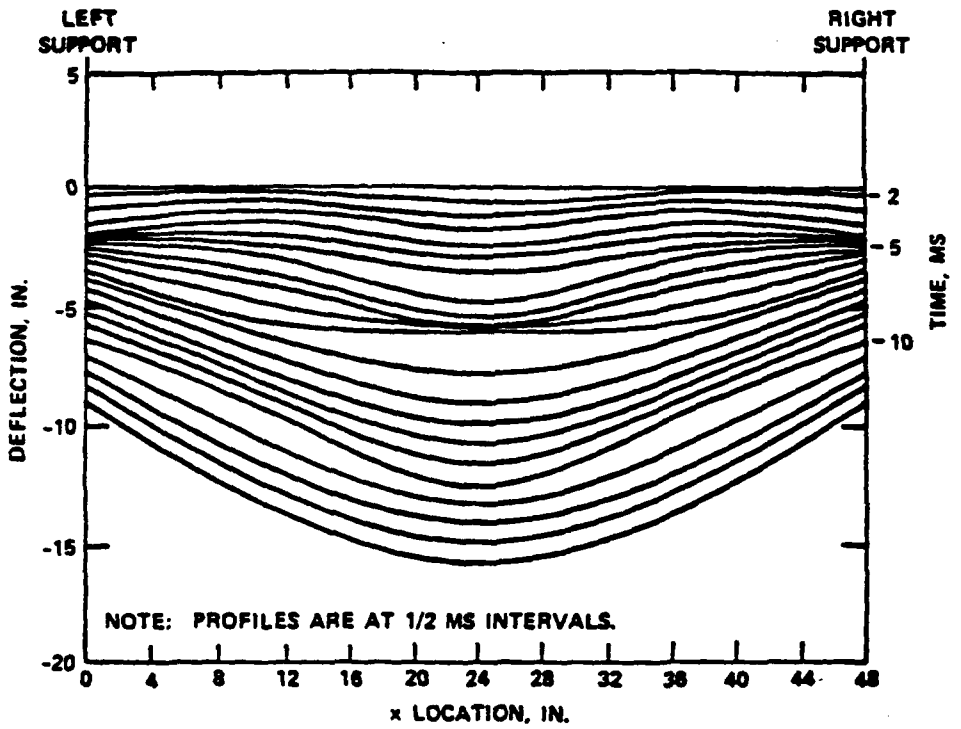

Figure 47. Experimental Observation on Direct Shear Failure. (Reference 68)

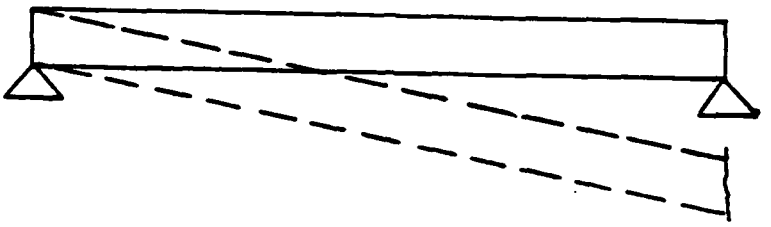

Figure 48. Assumed Mode for Support Direct Shear Failure

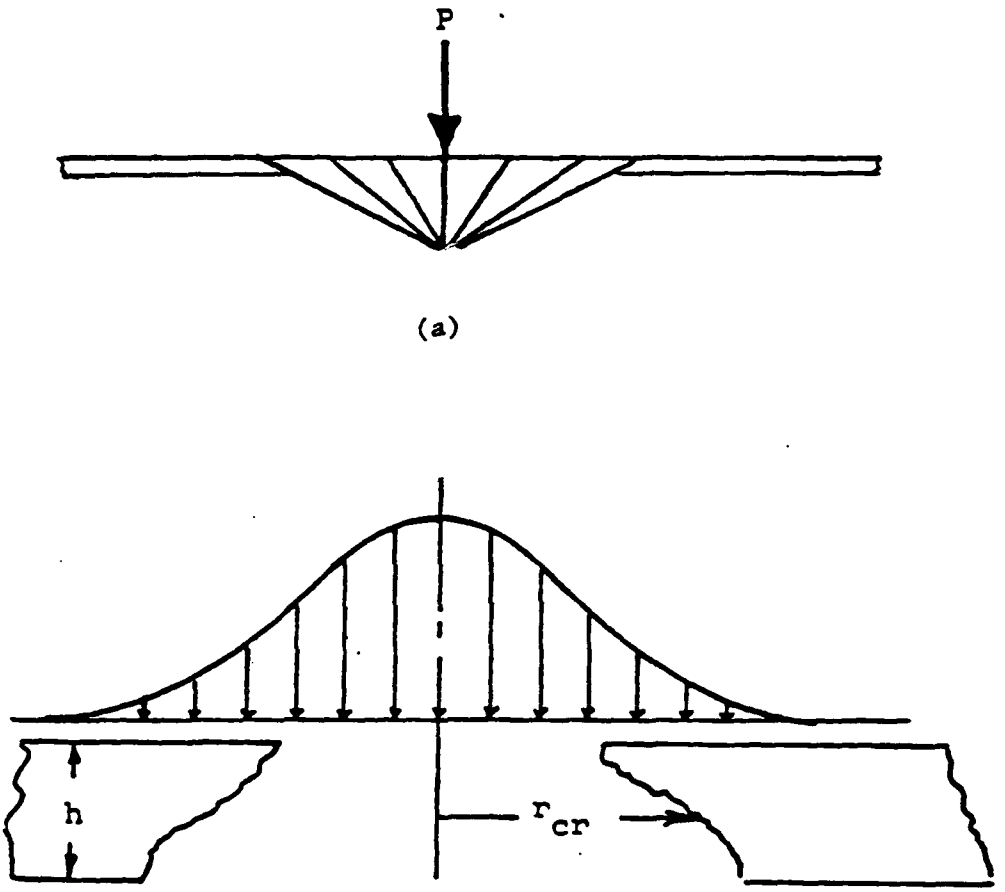

Figure 49. Localized Shear Failure Mechanism (a) Static Domain, (b) Dynamic Domain. (Reference 75)

In the present study, the critical shear breaching radius is conservatively assumed to be one-half of the effective depth of the beam or the slab, based on which the effective shear mass under the concentrated load is computed. This is consistent with the experimental observations on punching shear failure in reinforced concrete members under static conditions as reported in Reference 22.

A direct localized dynamic shear failure in reinforced concrete is not a well-understood phenomenon and as Ross and Rosengren (Reference 22) point out, in addition to extensive experimental studies, many details on concrete strength, effectiveness of stirrups, and loading conditions are needed before analytical techniques can provide adequate results.

I. SOLUTION OF NONLINEAR EQUATION OF MOTION

In this study, the nonlinear Equation of motion was solved using the Newmark-Beta method. The iterative technique is summarized as follows.

1. Let at some time t, acceleration $\ddot{u}^{(s)}$, velocity $\dot{u}^{(s)}$, and displacement $u^{(s)}$ be known.

2. Assume at the next time step $t+\Delta t$, the acceleration is $\ddot{u}^{(s+1)}$.

3. Compute $\dot{u}^{(s+1)}$ and $u^{(s+1)}$ from the equation provided by Newmark (Reference 49):

$$\dot{u}^{(s+1)} = \dot{u}^{(s)} + \Delta t\ (\ddot{u}^{(s)} + \ddot{u}^{(s+1)}) \tag{147}$$

$$u^{(s+1)} = u^{(s)} + \dot{u}^{(s)}\,\Delta t + (\tfrac{1}{2} - \beta)\,\ddot{u}^{(s)}(\Delta t)^2 + \beta\,\ddot{u}^{(s+1)}(\Delta t)^2 \tag{148}$$

where β is assumed depending on the variation of the acceleration, and will affect the convergence speed and stability of the iterations.

4. Compute $\ddot{u}^{(s+1)}$ from the equation of motion rewritten as follows :

$$\ddot{u}^{(s+1)} = \frac{Q_e(t+\Delta t)}{M_e} - 2\,\xi\,\omega'_n\,\dot{u}^{(s+1)} - \frac{R_e}{M_e} \tag{149}$$

5. Repeat steps 3 and 4 until the variation in $\ddot{u}(s+1)$ between consecutive steps is small.

More details on the Newmark-Beta method can be found in References 44,49, and 76.

J. COMPUTER PROGRAM AND FLOW CHART FOR DYNAMIC ANALYSIS

Based on the formulations presented in this section, the computer program BSDOF for the dynamic flexural and direct shear analysis of structural elements was developed. This program is currently ready for use on IBM PC/AT as well as IBM 4341 computers. The program was employed to analyze a number of experimental cases in which reinforced concrete elements were subjected to localized impact or blast loads. The analyses for these cases are provided in Section IV. The contents of the program BSDOF are illustrated by a general flow diagram in Figure 50.

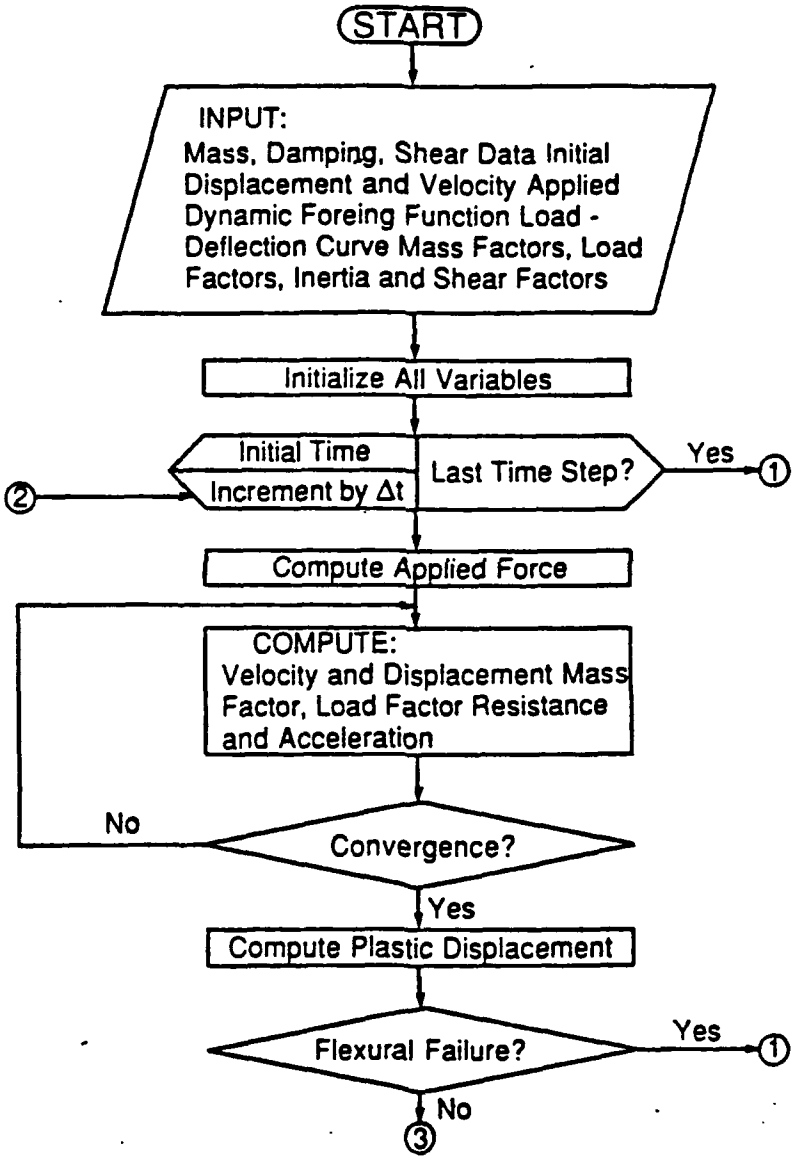

Figure 50. Flow Diagram for Program BSDOF

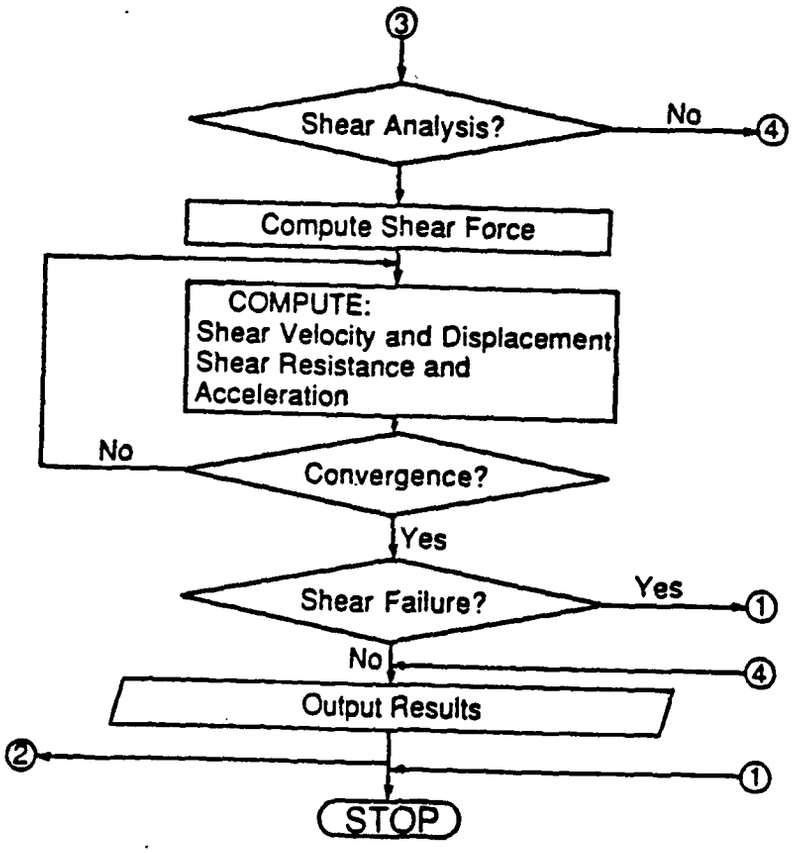

Figure 50. Flow Diagram For Program BSDOF

(concluded)

(The reverse of this page is blank.)

SECTION IV
ANALYSIS AND RESULTS

A. INTRODUCTION

For demonstrating the application of the present model and the accuracy of the numerical results, the analytical/computational procedure developed herein is employed for analyzing several cases. All structural elements analyzed herein were studied experimentally by other investigators and the results obtained from the present approach are compared with the previous findings.

The present section contains analyses of reinforced concrete structural elements in the static and the dynamic domain of behavior. In the static domain three groups of tests are considered, two groups of reinforced concrete members without axial forces (beams) and one group of reinforced concrete beams with axial forces (beam-columns). In the dynamic domain the analysis is performed for two groups: (1) reinforced concrete specimens subjected to localized impact loads, and (2) analyses of reinforced concrete walls subjected to localized blast loads, caused by detonation of conventional explosive devices.

B. ANALYSIS IN THE STATIC DOMAIN

The analytical procedure employed for the analysis of beams under static conditions consists of the following two steps;

1. Analysis for obtaining the complete moment-curvature relationship for the cross section subjected to the combined effects of flexure, shear and axial compressive force. Here, the computer program ZCON is employed.

2. Analysis for deriving the load-deformation (resistance function) of the reinforced concrete structural element from the moment-curvature behavior. In this step the computer program LOADDEF is employed.

The numerical results for each member are illustrated by a moment-curvature diagram for the cross section and a load-deflection curve for the structural element.

1. Analysis of Reinforced Concrete Beams

The two groups of beams analyzed in this section were obtained from two different sources and comprise nine beams tested by Burns and Siess in Reference 1 (Group 1), and nine beams from an experimental study by Bresler and Scordelis in Reference 36 (Group 2). All 18 cases considered in this section were simply-supported reinforced concrete members loaded laterally at their midspan by a single concentrated force. For beams of Reference 1, this load was applied through a rigid short (column-like) stub and therefore, a plastic hinge would be assumed to form on each side of the rigid column.

The beams tested by Burns and Siess (Reference 1) were moderately reinforced (0.67 percent $\leq \rho \leq$ 2.63 percent , 0.61 percent $\leq \rho' \leq$ 2.63 percent) with moderate-strength tension (45.1 $\leq f_y \leq$ 48.5 ksi) and compression (45.5 $\leq \rho \leq$ 50 ksi) reinforcement. The ratio of the shear span to effective depth for this group ranged from 4 to 7.2. Figure B-1 in the Appendix B represents the schematic arrangements of these beams and the details of geometrical and material properties of these group of beams are provided in Tables B-1 and B-2 and B-3 in Appendix B. The input material properties and the numerical results for the moment-curvature and the load-deflection analyses are illustrated in detail for one case, namely beam J8, and for the remaining beams in this group the results are summarized and presented by plots of moment-curvature and load-deflection, respectively.

A graphical illustration of the moment-curvature behavior of beam J-8 is shown in Figure 51. The ultimate computed moment for this beam, 889 kip-inches, compares very well with the ultimate experimental moment, 878 kip-inches. Similarly, the load-deflection behavior of beam J-8 from the onset of loading to the ultimate (collapse) condition is shown along with the measured experimental data in Figure 51. The computed ultimate load (27.2 kips) is only 1 percent larger than the measured load at the ultimate condition (27.1 kips), and the computed deflection at the collapse condition (16.6 inches) is only 2.5 percent larger that its experimental counterpart (16.2 inches). In addition, it can be observed in Figure 51 that the computed load-deflection diagram simulates the experimental observations quit accurately. Table B-4 in Appendix B demonstrates a typical output file for the moment-curvature and the load-deflection analysis of this beam.

The numerical results at the ultimate condition for the remaining beams from Reference 1, namely beams J17, J18, J13, J14, J20, J5, J6, and J22 are presented in Table 1. These results indicate that the present analytical/computational procedure is effective in that the ultimate mean computed load for the nine beams in this group at failure is within 1 percent from the mean experimental failure load, with a standard deviation of 0.04. Moreover, the ratio of the average computed midspan deflection to the measured deflection just before collapse is 0.97 with a standard deviation of only 0.11, indicating that the present approach for the computation of the deflection at the ultimate curvature provides good results. But, as it can be observed, the degree of variability for the computed deflections is larger than that for the ultimate loads. Results illustrated by Figures B-4 through B-11 in Appendix B show the complete moment-curvature and load-deflection behavior for beams in this group. The present behavioral model for the effect of shear in reducing the ultimate flexural capacity of the beams has improved the result, particularly for beams J20, J6, and J22. The experimental points which are marked on the load-deflection diagrams are the actual measured readings during the tests. The present procedure provides the means for predicting the resistance of the member at all stages of loading with a fairly good accuracy.

TABLE 1. RESULTS FOR SLENDER RECTANGULAR BEAMS OF REFERENCE 1

Beam	a/d	Collapse Load, Q (Kips)		Collapse Deflections (Inches)		$\frac{Q_{Comp}}{Q_{Meas}}$	$\frac{\Delta_{Comp}}{\Delta_{Meas}}$	Failure Mode[a]	
		Q_{Meas}	Q_{Comp}	Δ_{Meas}	Δ_{Comp}			Exp.	Ana.
J8	7.20	27.1	27.2	16.2	16.6	1.00	1.02	C	C
J17	7.20	27.2	27.7	18.1	14.3	1.02	0.80	C	C
J18	7.20	27.0	27.3	15.5	16.4	1.04	1.06	C	C
J13	5.14	42.5	39.6	13.7	12.3	0.93	0.90	C/S	T/S
J14	5.14	39.0	36.9	11.5	10.4	0.95	0.90	C/S	C/S
J20	5.14	37.7	36.9	10.2	9.4	0.98	0.92	C/S	C/S
J5	4.00	54.0	51.3	12.8	11.9	0.95	0.93	T/S	T/S
J6	4.00	52.3	53.4	10.0	10.4	1.02	1.04	C/S	T/S
J22	4.00	51.0	50.7	7.3	8.7	0.99	1.19	C/S	C/S
					Avg :	0.99	0.97		
					STD :	0.04	0.11		

[a] C : Compression Flexural Failure
S : Shear Failure
T : Tension Flexural Failure
C/S : Combination of C & S
T/S : Combination of T & S
1 Kip = 4.448 KN
1 In. = 25.4 mm

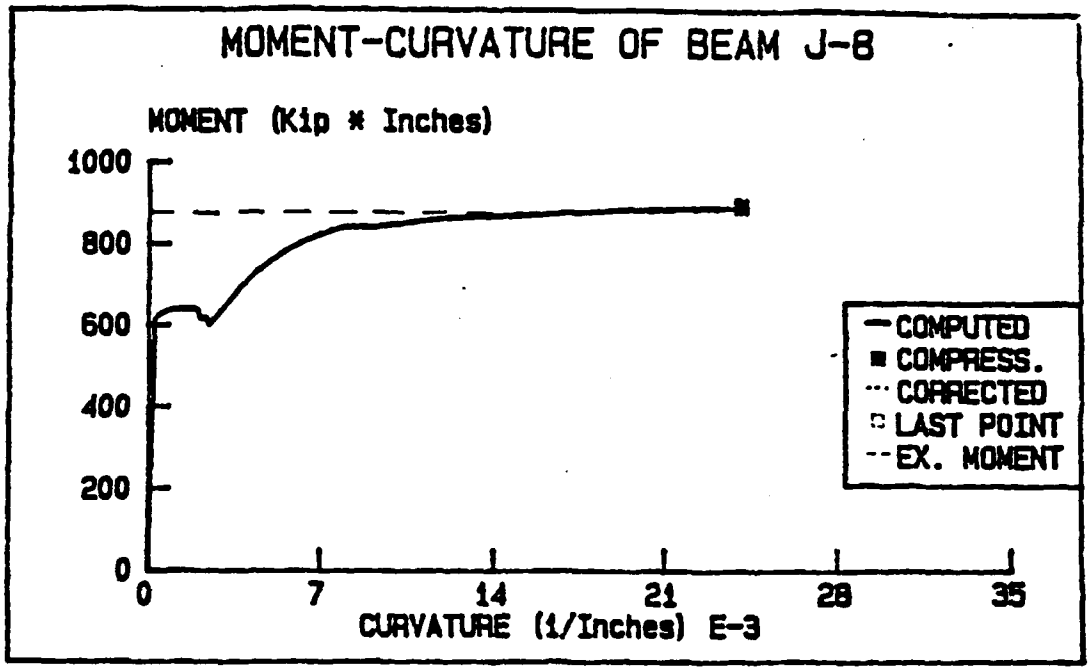

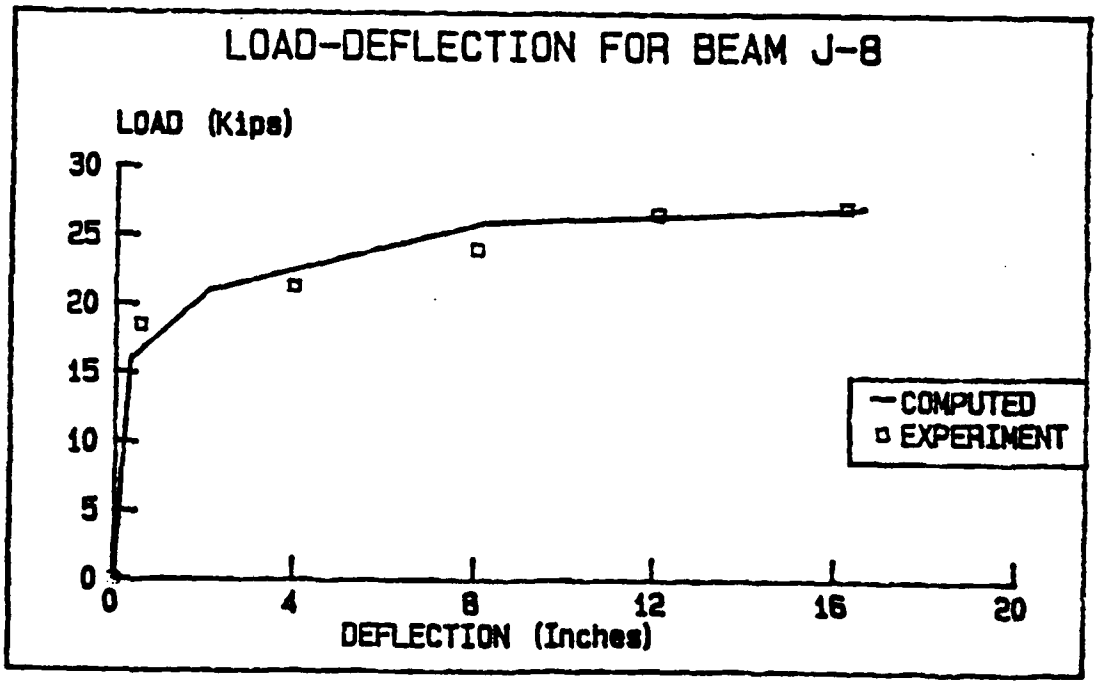

Figure 51. Moment-Curvature and Load-Deflection Relationships Beam J8

The beams tested by Bresler and Scordelis (Reference 36) were reinforced heavily (1.80 percent $\leq \rho \leq$ 3.66 percent) with high strength longitudinal tensile reinforcement ($f_y \approx$ 80 ksi), and a very small percentage of compression reinforcement (0.18 percent $\leq \rho' \leq$0.37 percent). In fact, a number of these beams were over-reinforced. In addition, these beams were deliberately designed with very low amounts of transverse reinforcement. The ratio of the shear span to the effective depth for this group ranged form 3.97 to 6.94. Figure B-2 in Appendix B shows the detail of the cross sections and Tables B-1, B-2, and B-3 provide the material and geometric properties for the nine beams in this group.

The numerical results for these nine beams at the ultimate condition is presented in Table 2. The proposed behavioral model for the effect of shear in reducing the ultimate flexural capacity, and the proposed model for the behavior of over-reinforced beams at failure has been proven effective. The mean ratio of the computed ultimate load to the measured failure load for this group is 0.94 with a standard deviation of 0.07, and the average computed deflection for the nine beams at collapse is only 1 percent less than the average of the experimental deflection values, with a standard deviation of 0.09. The analytical moment-curvature and load-deflection curves for these nine cases (beams A1,A2,A3,B1,B2,B3,C1,C2, and C3) are presented in Figures B-12 through B-20 in Appendix B. From these figures it can be observed that all these beams exhibited a brittle compression failure with very little ductility at the ultimate condition. For all nine cases examined here, the peak flexural moment decreased significantly before the development of ductile behavior. This sort of response was observed during the experiment and it can be primarily attributed to the fact that these beams had high ratios of high strength tensile reinforcement, and relatively small amounts of compression and confining reinforcement.

From Figures B-12 to B-20 it can be seen that although the computed load-deflection curves for these nine cases are reasonably close to the experimental data, they do not seem to follow the data as well as the beams in the first group discussed earlier in this section. In a few cases, particularly beams A1, B1, and C1, measured deflections are generally smaller than computed values. Such disagreement is primarily because the present model assumes a fully cracked section along the span of the beam (i.e., additional stiffness of the beam at low levels of load, due to the tension carried by the concrete between the flexural cracks, is not included in the analysis) and therefore, it is reasonable to expect the computed deflections to be higher than the actual deflections. But, this phenomenon has very little effect on the analysis of ductile members (first group of beams), because these additional inelastic deformations are small compared to the inelastic deflections. For the second group, the beams do not exhibit inelastic ductility and the assumption that the beam is fully cracked along the span could result in predicting larger deflections at early loading stages. Even though as the load approaches the ultimate value, these beams are more extensively cracked and as a result, the difference between the computed and the measured deflections become smaller.

TABLE 2. RESULTS FOR SLENDER RECTANGULAR BEAMS (REFERENCE 36)

Beam	a/d	Collapse Load, Q (Kips)		Collapse Deflections (Inches)		$\frac{Q_{Comp}}{Q_{Meas}}$	$\frac{\Delta_{Comp}}{\Delta_{Meas}}$	Failure Mode[b]	
		Q_{Meas}	Q_{Comp}	Δ_{Meas}	Δ_{Comp}			Exp.	Ana.
A1	3.97	105.	97.	0.56	0.62	0.92	1.11	C/S	C/S
A2[a]	4.90	110.	101.	0.90	0.86	0.92	0.96	C/S	C/S
A3	6.94	105.	105.	1.35	1.50	1.00	1.11	C	C
B1[a]	3.92	100.	93.	0.54	0.54	0.93	1.00	C/S	C/S
B2[a]	4.93	90.	79.	0.82	0.81	0.88	0.99	C/S	C/S
B3	6.91	80.	87.	1.39	1.51	1.09	1.09	C	C
C1	3.95	70.	57.	0.70	0.63	0.87	0.90	C/S	C/S
C2[a]	4.91	73.	65.	0.79	0.68	0.90	0.86	C/S	C/S
C3[a]	6.95	61.	56.	1.45	1.27	0.97	0.88	C	C
					Avg :	0.94	0.99		
					STD :	0.07	0.09		

[a] Overreinforced beams.

[b] C : Compression Flexural Failure
S : Shear Failure
C/S : Combination of C & S

1 Kip = 4.448 KN
1 In. = 25.4 mm

2. Analysis of Reinforced Concrete Beam-Columns

In this section, two beams and nine beam-columns obtained from an experimental study by Yamashiro and Siess (Reference 17) are analyzed. All 11 specimen were symmetrically reinforced with moderate grade steel in tension ($45.9 \leq f_y \leq 50.$ ksi) and in compression ($44.7 \leq f_y \leq 50.3$ ksi). The flexural reinforcement ratio, ρ, ranged between 0.67 to 3.33 percent. The axial compressive force, P_{axial}, was applied without eccentricity and its magnitude for each case was smaller than one-half of the axial load at the balanced conditions, P_b. Figure B-3 in Appendix B illustrates the schematic arrangement of the specimens and Tables B-1, B-2, and B-3 contain all material and geometric properties for the 11 test specimen in this group. The numerical results for each member are illustrated by a moment-curvature diagram for the cross section and a moment-deformation curve for the element, in which the computed results are compared with the experimental measurements.

Figure 52 represents the moment-curvature and the moment-deflection plots of beam J-29. This ratio of compression and tension reinforcement for this beam-column was 3.33 percent and a constant axial force of 25 kips was continuously applied during the experiment. The result obtained from the present procedure agree well with the experimental measurements. The computed failure moment for this member was 1261 kip-inches which is only 10 percent larger than the measured ultimate moment (1150 kip-inches). The computed deflection at collapse was 11.3 inches, within 1 percent of the measured data (11.2 inches). In addition, it can be observed in Figure 52 that the computed values on the moment-deflection curve are close to experimental data for all levels of loading.

The computed moments and deflections at ultimate (just before collapse) for the beams and the beam-columns in this group are presented in Table 3. It is observed that on the average, the ratio of the computed to the measured values for moments and deflections at collapse are 1.04 and 0.91, respectively, and the standard deviation for these two average quantities are 0.05 and 0.14, respectively. Comparing the analytical results of members in this group with the nine beams of Reference 1 (analyzed earlier in this section), shows that the accuracy of the present approach in predicting the response of the elements at the ultimate condition to be slightly reduced when axial compressive force is present. The fact that the average ratio of the computed deflections to the measured deflections is 0.91 is probably due to an increase in the length of the plastic hinge in the presence of axial force. Presently, no analytical or empirical formulations are available to account for the influence of axial force on the development of the plastic zones. Nevertheless, the present numerical technique is still effective in that it can provide adequate results at the ultimate condition for all practical purposes.

Figures B-21 through B-30 in Appendix B depict the moment-curvature and the moment-deflection diagrams for these beams. One

TABLE 3. RESULTS FOR SLENDER RECTANGULAR BEAM–COLUMNS OF REFERENCE 17

Beam[b]	P_{axial}[a] (Kips)	Collapse moment (Kip-In.)		Collapse Deflections (Inches)		$\frac{M_{Comp}}{M_{Meas}}$	$\frac{\Delta_{Comp}}{\Delta_{Meas}}$	Failure Mode[c]	
		M_{Meas}	M_{Comp}	Δ_{Meas}	Δ_{Comp}			Exp.	Ana.
J24	0.	248	251	15.5	18.6	1.01	1.20	T	T
J25	25.0	302	338	12.8	10.2	1.12	0.80	C	C
J26	50.0	415	412	0.94	0.86	0.99	0.92	C	C
J27	75.0	490	506	0.85	0.79	1.03	0.93	C	C
J34	75.0	475	491	0.72	0.59	1.03	0.83	C	C
J15	50.0	1000	963	10.8	7.9	0.96	0.73	C	C
J16	25.0	931	932	13.5	9.7	1.00	0.72	C	C
J28	0.	1090	1205	13.5	14.9	1.11	1.10	C	C
J29	25.0	1150	1261	11.2	11.3	1.10	1.01	C	C
J30	50.0	1180	1241	12.9	10.7	1.05	0.83	C	C
J31	75.0	1100	1160	7.3	6.7	1.05	0.92	C	C
					Avg :	1.04	0.91		
					STD :	0.05	0.14		

[a] Axial force acted at the plastic centroid for all beams.
[b] For all beams a/d= 7.2.
[c] C : Compression Flexural Failure
T : Tension Flexural Failure
1 Kip-In. = 0.113 KN-m
1 In. = 25.4 mm

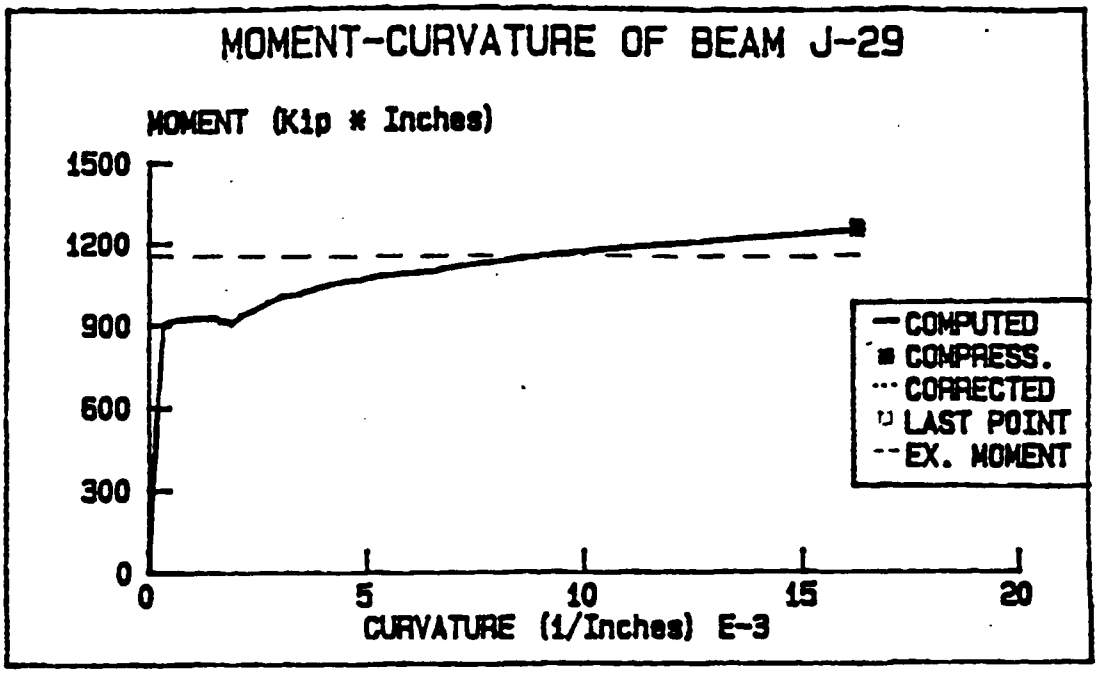

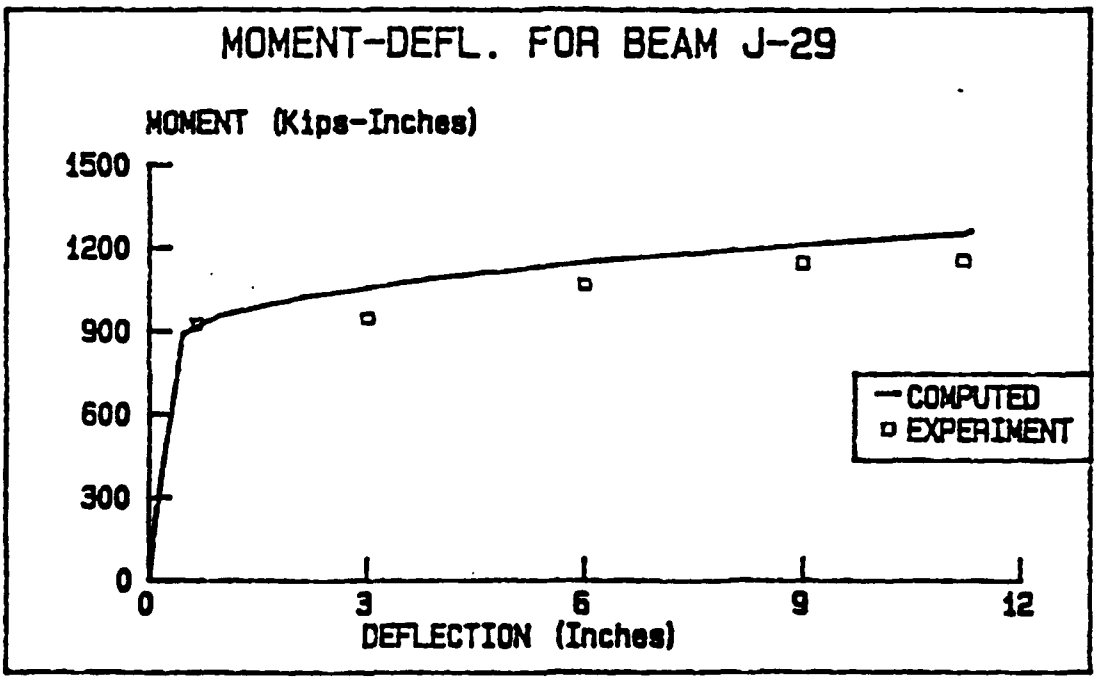

Figure 52. Moment-Curvature and Load-Deflection Relationships Beam J29

significant observation can be made in regards to the effect of axial load on the ductility of beam-columns. Members J24, J25, J26, and J27 have similar material and geometric properties, and vary only by the magnitude of the axial force. The computed results indicate that increasing the magnitude of the axial force reduces the ductility of the element. Similar observation can be made when the result of beams J15 and J16 are compared to one another. The computed moment-deflection curves and the experimental measurements are reasonably close for all cases.

C. ANALYSIS IN THE DYNAMIC DOMAIN

The analytical procedure for analysis of reinforced concrete structural elements subjected to dynamic excitations consists of the following steps:

1. Analysis for computing the complete moment-curvature of the cross section based on the input material and geometric properties.

2. Analysis for deriving the resistance function and the deformed shape function of the reinforced concrete element, based on the moment-curvature data and the boundary conditions. Here, all necessary parameters of the equivalent dynamic system i.e., mass factor, load factor, inertia and support shear factors are computed and stored at every load step.

3. Dynamic analysis of the structural element subjected to time dependent forcing function using an equivalent SDOF system. The information obtained in step two is utilized here for evaluating the time dependent (and perhaps nonlinear) flexural and the shearing response of the element.

The analytical procedure for analysis of reinforced concrete beams subjected to localized impact loads is based on the experimental result reported by Feldman and Siess in Reference 77. In that study five simply supported reinforced concrete beam specimens, namely C-1, H-1, J-1,G-1, and I-1 were subjected to suddenly applied dynamic loads. Adequate data were not collected in two cases.

Due to partial failure of the laboratory instruments, the dynamic loading data for beam C-1 was not recorded during the experiment. Instead, the authors estimated the step pulse based on the data collected from the chamber pressures and trigger settings in Reference 77. Also, during the preparation for testing, beam I-1 was accidentally loaded statically to almost 7.5 kips, enough to cause extensive flexural cracks. In addition, during the dynamic testing of beam I-1, the dynamic mid-span deflection exceeded the range of the laboratory equipment and it was limited by a wooden block placed

beneath the midspan point of the beam. Therefore, the validity of the recorded data after the contact time is highly questionable, since the beam was resisted by the wooden compression block.

Nevertheless, all five cases are analyzed here and the analytic results, as obtained from the present approach, are compared to the measured data for the magnitude and the time of occurrence of peak midspan deflections, permanent (residual) deflection, and peak dynamic support shear force. In addition, the experimental deflection-time plots and reaction-time plots are compared with the analytic curves. Additional analytic result, including the moment-curvature, load-deflection, velocity and acceleration-time history plots are presented for each case as well.

The material and geometric properties of these four specimen are given in Tables C-1, C-2 and C-3 in Appendix C and are described briefly here. The beams had overall dimensions of 6 inches by 12 inches by 106 inches and were loaded by a concentrated dynamic load at the midspan. These beams were reinforced with two Number 7 bars for tension (bottom), two Number 6 bars for compression (ρ =2 percent ,ρ'=1.46 percent), and Number 3 stirrups were placed at 7 inches intervals. The concrete compressive strength of each specimen (Table C-1) is computed by averaging the two batches for each case, as reported in Reference 77. With the exception of beam H-1, it can be seen in Tables C-2 and C-3 that in many instances complete and sufficient data for the specific properties of flexural reinforcement was not provided in Reference 77. In that case, the average value of the same property in the other beams is used in the computation. This approximation is not expected to introduce any significant error in the analysis, because all these specimen were built from the same shipment of materials and cast at about the same time. In addition, no data for the ultimate strength and strain of flexural reinforcement was given in Reference 77. For the type of steel that was used in that study ($46.08 \leq f_y \leq 48.30$ and $(0.0014 \leq \varepsilon_y \leq 0.0016)$, the ultimate strength and strain values of steel is taken to be 72 ksi and 0.15 inches/inch, respectively.

The range of maximum initial measured strain rate was approximately between 0.24 to 0.42 inches/inch/sec. for the tensile reinforcement and between 0.21 to 0.43 inches/inch/sec. For the concrete in compression. Using the minimum of these values and the information provided earlier in Section III on the enhancement of materials under dynamic conditions, a 25 percent enhancement on the compressive strength of concrete, yield strength and the ultimate strength of flexural reinforcement is used in the analysis of these beams.

The applied load was measured continuously during the experiment by a a calibrated dynamometer. In the present analysis, that information is closely approximated by a piecewise multilinear curve. The mass of a typical beam was computed using the average normal weight for reinforced concrete (150 pcf). Lastly, 2 percent external damping ratio was used in the analysis of five beams as presented next.

a. Analysis of Beam C-1

Since it was not possible to input the exact experimental loadings, the multilinear loading function shown in Figure 53 is used in the analysis which closely approximates the experimental dynamic load applied to beam C-1 (Figure C-1 in Appendix C). Figure 54 depicts the computed displacement-time history at the midspan of this beam. The peak experimental displacement response of the beam, measured as 3.0 inches, was reached at 50 milliseconds (Figure C-2 in Appendix C). These observations agree very closely with the analytical results, where the peak displacement is computed as 3.1 inches at 45 milliseconds. In addition, The permanent deflection of this beam, 2.2 inches, compares very well with the analytical residual deflection of 2.4 inches. The computed resistance-displacement diagram for beam C-1 is shown in Figure 55.

There is also a reasonably good agreement between the measured values for the dynamic reaction (support shear force) and the analytical dynamic reaction using the procedure proposed in this study. The peak dynamic force was measured as 19 kips at 15 milliseconds (Figure C-1 in Appendix C). The peak computed support reaction is 17.4 kips and at 13.8 milliseconds (Figure 56). Furthermore, the analytical reaction-time history shown in Figure 56 is not considerably different from the measured response (Figure C-1 in Appendix C), indicating for the effectiveness of the formulation proposed in this study.

Plots of moment-curvature, load-deflection, velocity and acceleration time histories for the midspan point of beam C-1 are presented in Figures C-3 through C-6 in Appendix C.

b. Analysis of Beam H-1

The analytical load-time history and the experimental impact loading for beam H-1 are shown in Figures 57 and C-7, respectively. The analytical midspan displacement response is shown in Figure 58. Again the agreement between the peak measured displacement and the peak computed displacement is very good. The maximum measured displacement was 8.9 inches and recorded at 58 milliseconds (Figure C-8 in Appendix C). In the analysis, the peak displacement of 8.5 inches is reached at 62 milliseconds. The agreement between the experimental and the analytical values for the residual deformation is also good. The experimental value for the permanent deformation was reported to be 7.5 inches which compared well with the analytic result of 6.8 inches, as illustrated by the resistance-displacement plot shown in Figure 59.

The measured and the computed results for the dynamic support reaction of beam H-1 were also in agreement. The maximum measured dynamic reaction was 19 kips and recorded at 16.7 milliseconds (Figure C-7 in Appendix C). From Figure 60, it can be seen that the peak

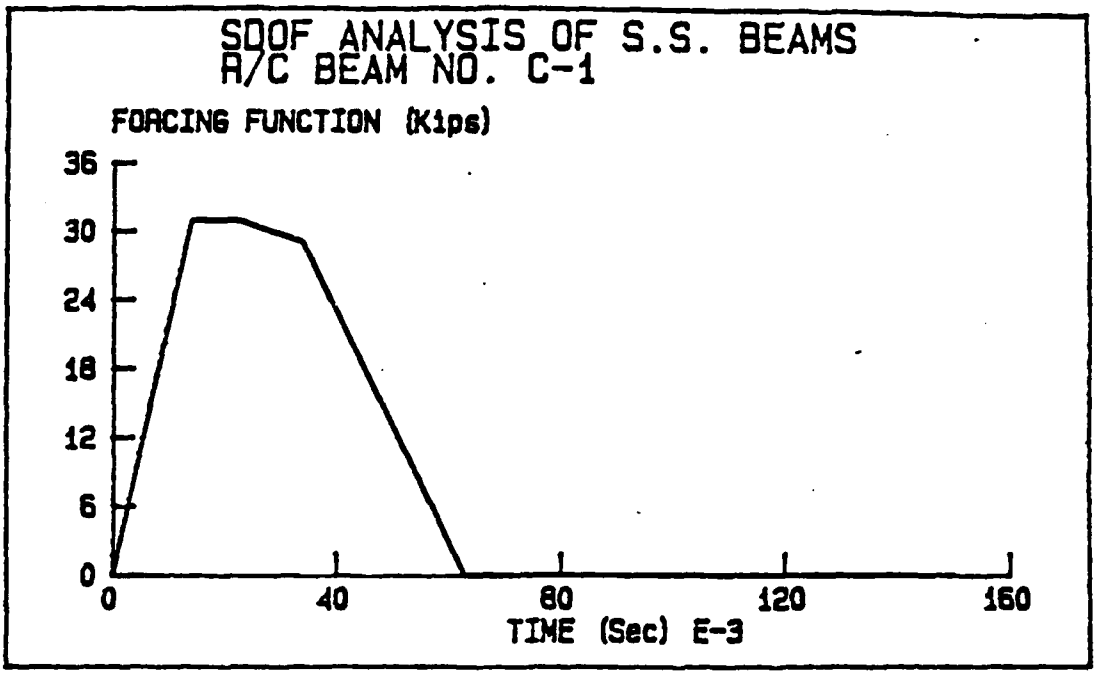

Figure 53. Applied Load Versus Time for Beam C-1

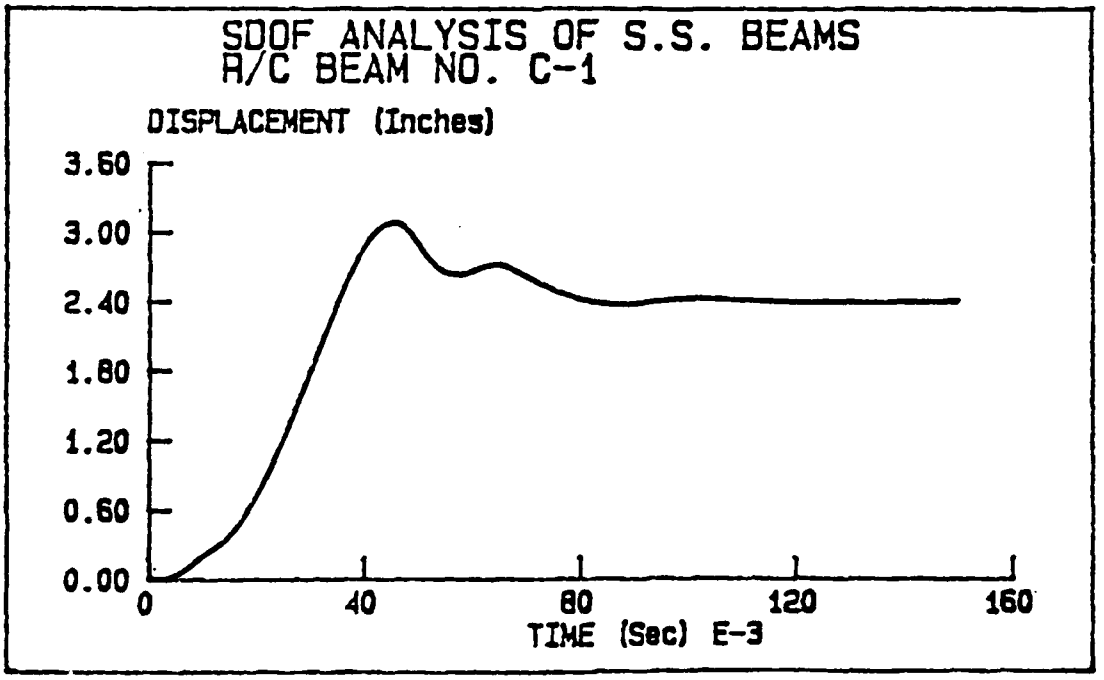

Figure 54. Midspan Displacement Versus Time for Beam C-1

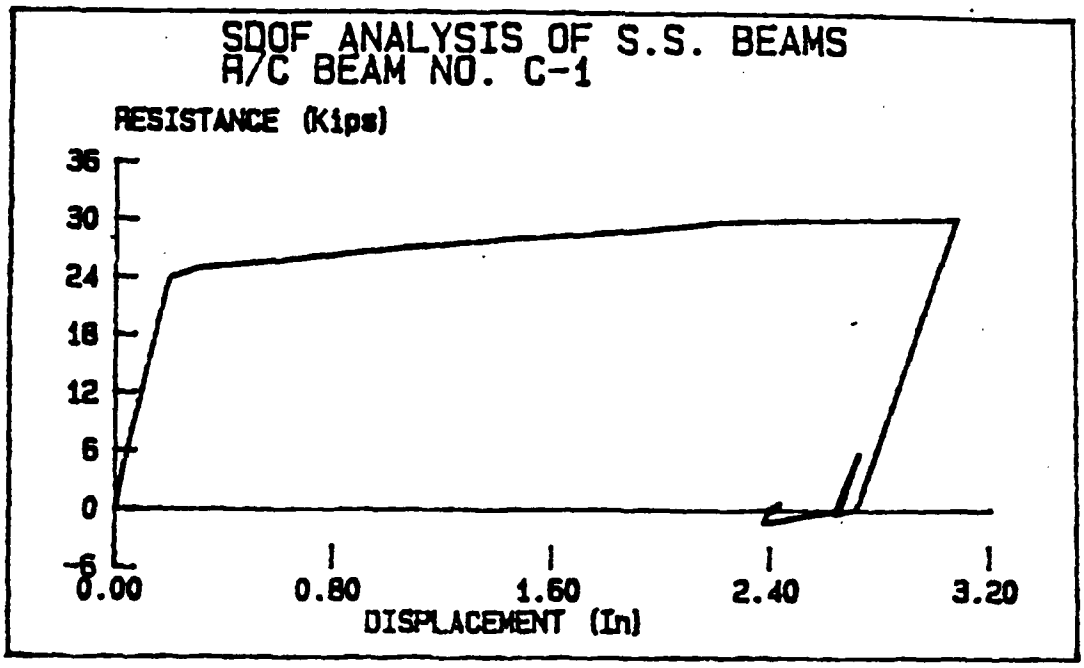

Figure 55. Resistance Versus Displacement for Beam C-1

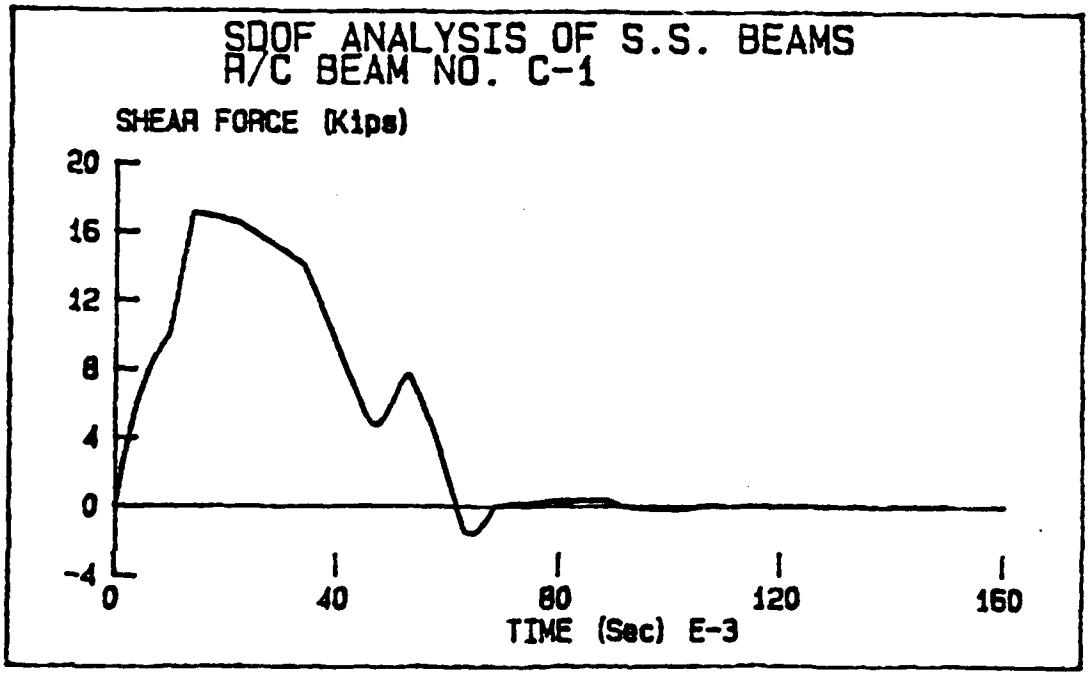

Figure 56. Support Reaction Versus Time for Beam C-1

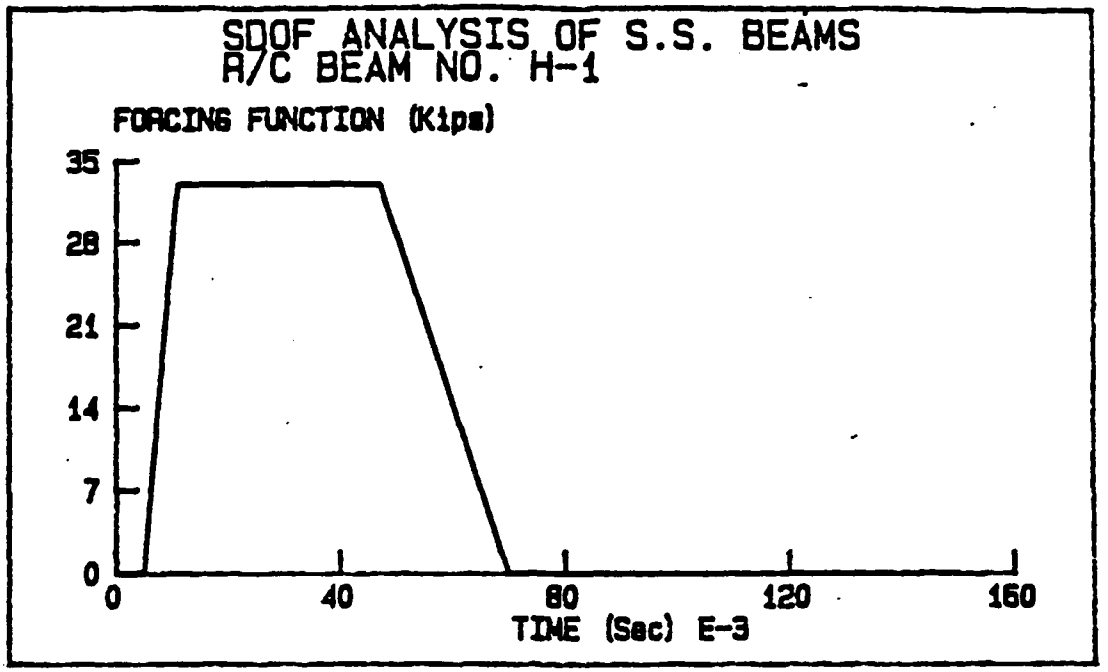

Figure 57. Applied Load Versus Time for Beam H-1

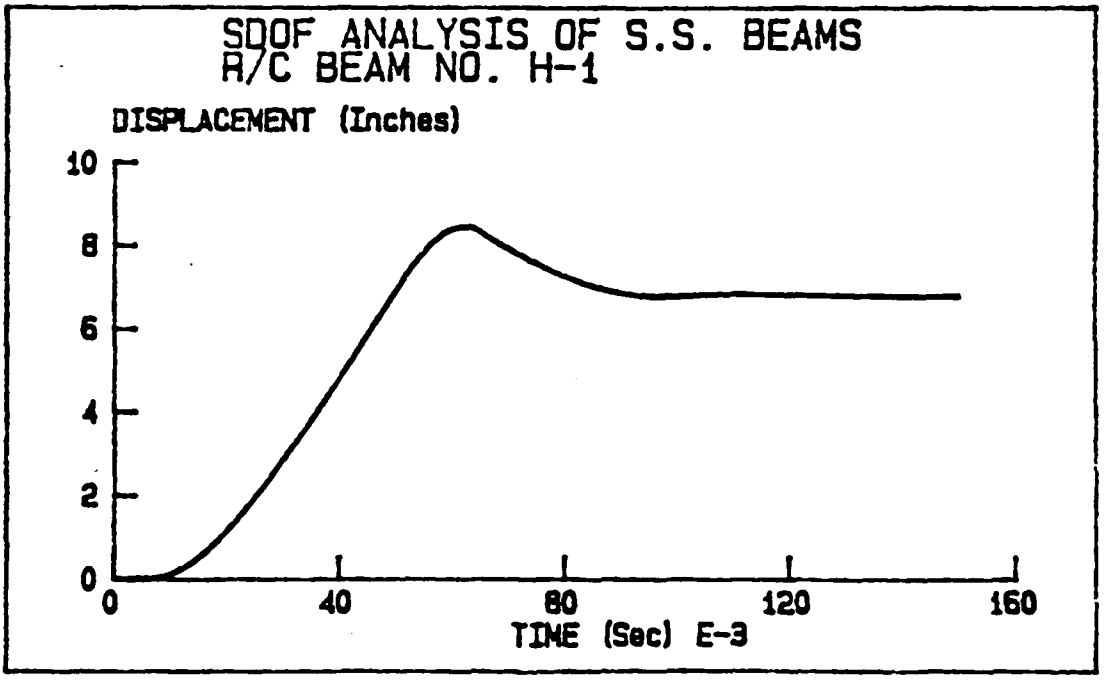

Figure 58. Midspan Displacement Versus Time for Beam H-1

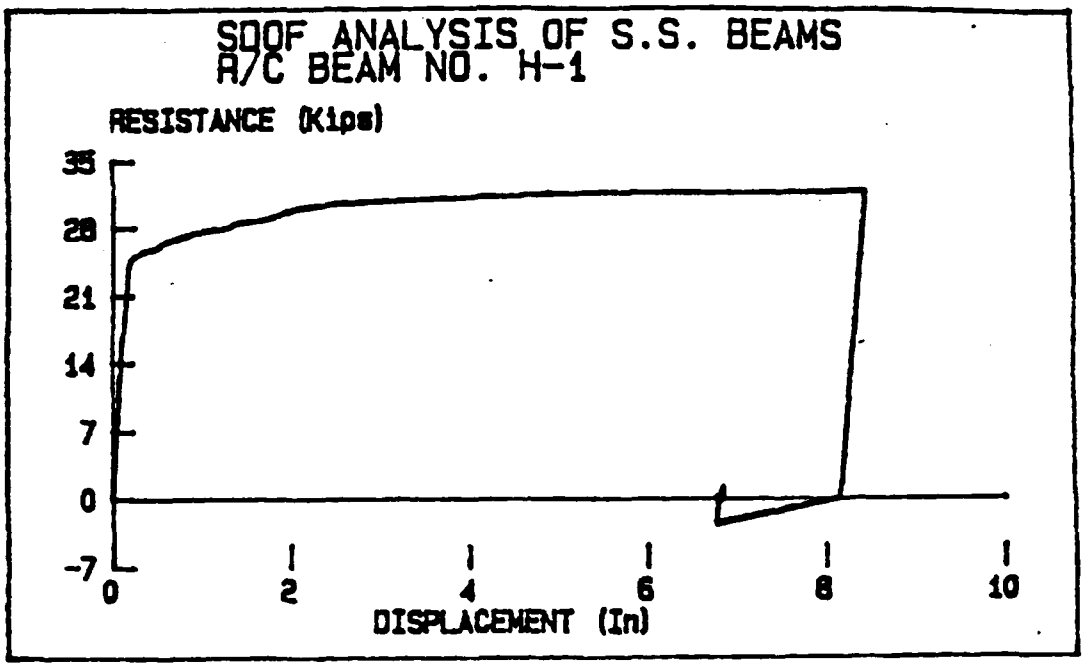

Figure 59. Resistance Versus Displacement for Beam H-1

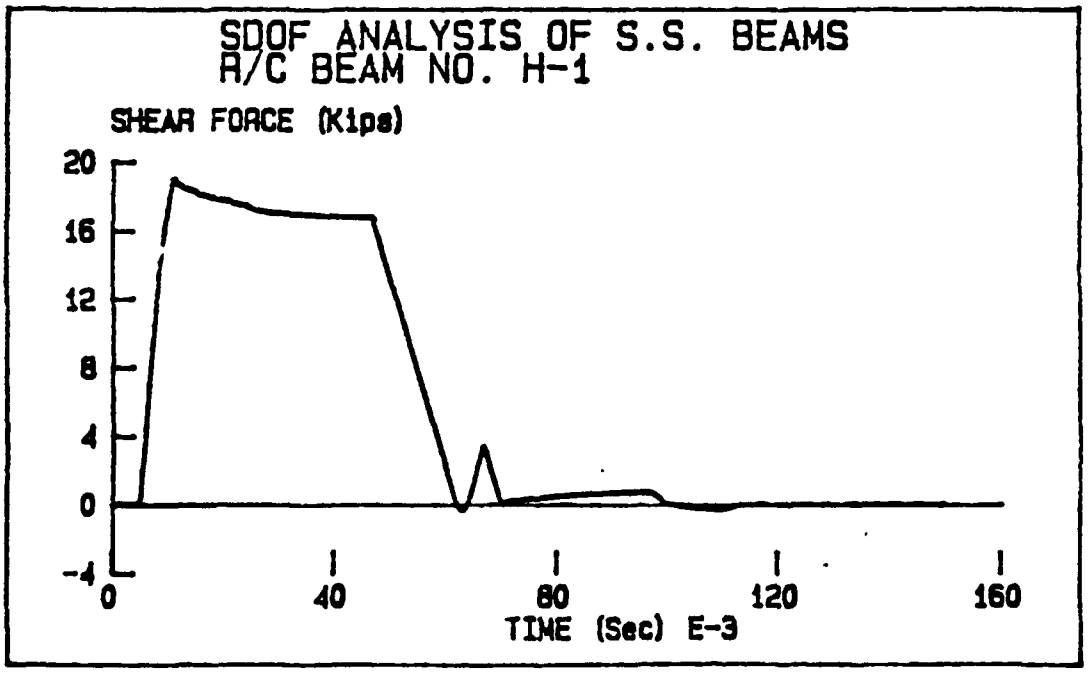

Figure 60. Support Reaction Versus Time for Beam H-1

dynamic reaction of 19 kips is reached at approximately 11 milliseconds. By comparing the results in Figures 60 and Figure C-7, equally good agreements between the computed and the measured reaction-time curves is also noticed for this beam.

The analytic results for the moment-curvature, load-deflection, velocity and acceleration time histories for beam H-1 can be found in Figures C-9 through C-12 in Appendix C.

c. Analysis of Beam J-1

Figures 61 and C-13 show the analytical and the experimental loading functions for beam J-1. The experimental and the computed midspan deflections-time diagrams are given in Figures 62 and C-14, respectively. The peak deflection obtained from the analytic model is 0.63 inches at 40 milliseconds. These values agree with the measured data, 0.76 inches at at a time of 32 milliseconds, as shown in Figure C-14. The computed permanent deflection for this beam is 0.32 inches (Figure 63) which is very close to the measured residual displacement of 0.3 inches.

Figures 64 and C-13 show the analytic and the experimental result for the dynamic shear force at the support. The maximum shear force at the support was computed as 13.2 kips (Figure 64). This value does not agree well with the peak measured shear force of 19 kips (Figure C-13). But, the computed time to the maximum shear force is 21 milliseconds, which is nearly the same as the experimental time of 22 milliseconds. Figures C-15 through C-18 illustrate the results for this case.

d. Analysis of Beam G-1 and I-1

Unforunately, because of an instrumentation failure, the experimental load function for Beam G-1 was not recorded in Reference 77. Instead, the load pulse for this beam was estimated by the authors in Reference 77 from chamber pressures and trigger settings data, as shown in Figure C-19. The analysis for this beam was performed using the estimated step pulse (Figure 65) and the computed midspan displacement-time results are shown in Figure 66. Unlike the previous cases, the analytic results for this case do not agree with the measured data. The computed peak displacement of 1.9 inches (Figure 66) is considerably different from the measured peak deflection of 4.2 inches (Figure C-20). Similarly, the computed residual deflection of 0.71 inch disagreed with the measured value of 3.0 inches.

From the experimental loading data of the previous three cases, i.e., beams C-1, H-1, and J-1, it seems that assuming a perfect rectangular step pulse for beam G-1 was really not well-justified. Moreover, because there is no reason to believe that the estimated magnitude of the applied load for beam G-1 is the same as the actual dynamic load applied to this beam, gross disagreement between the analytic result and the measured data is not surprising. This example shows that regardless of the analytic technique, inadequate

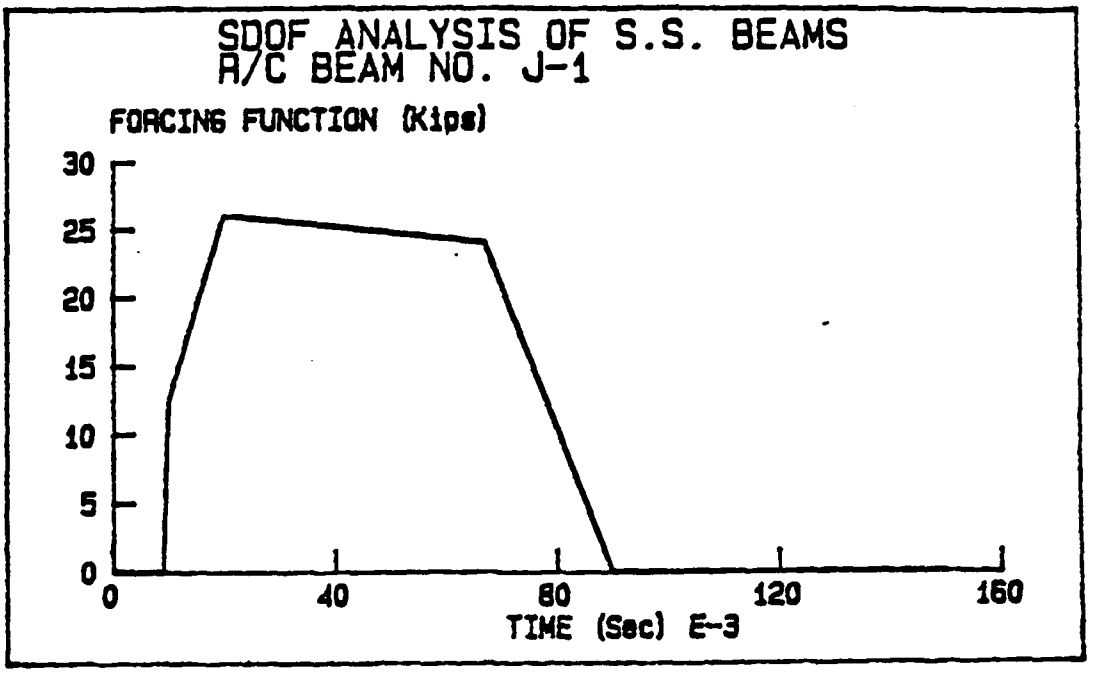

Figure 61. Applied Load Versus Time for Beam J-1

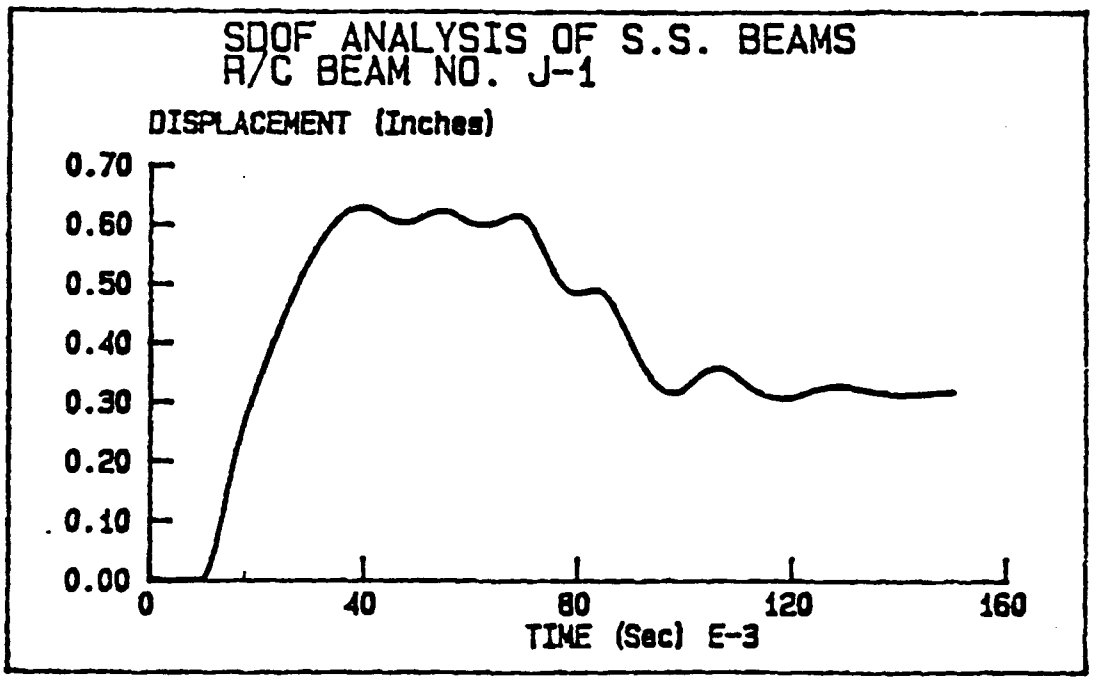

Figure 62. Midspan Displacement Versus Time for Beam J-1

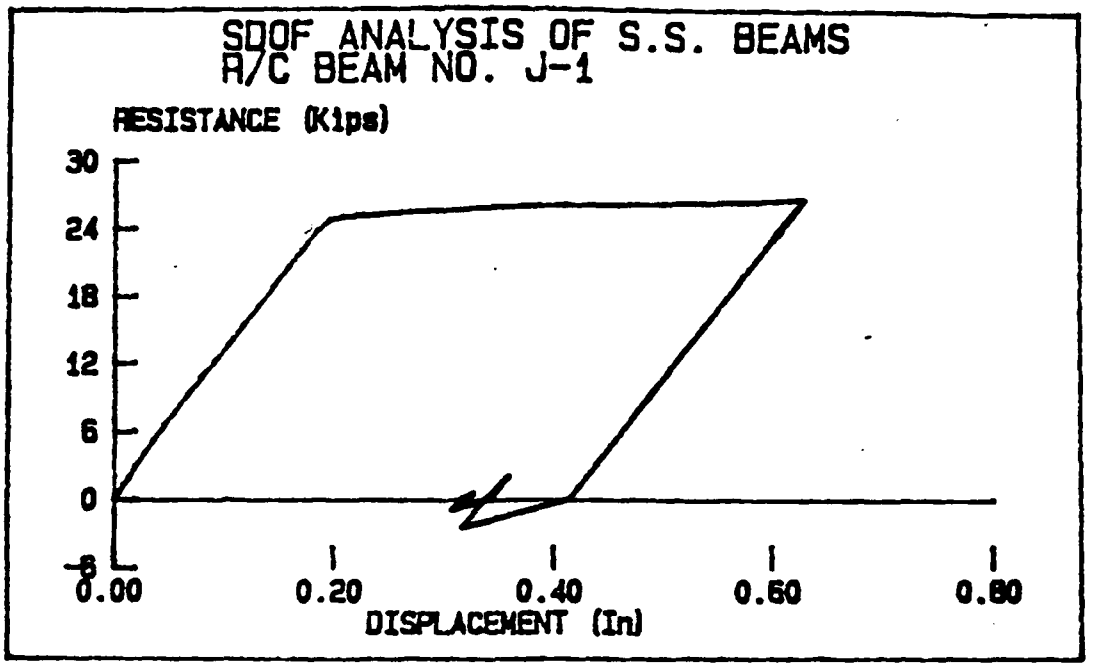

Figure 63. Resistance Versus Displacement for Beam J-1

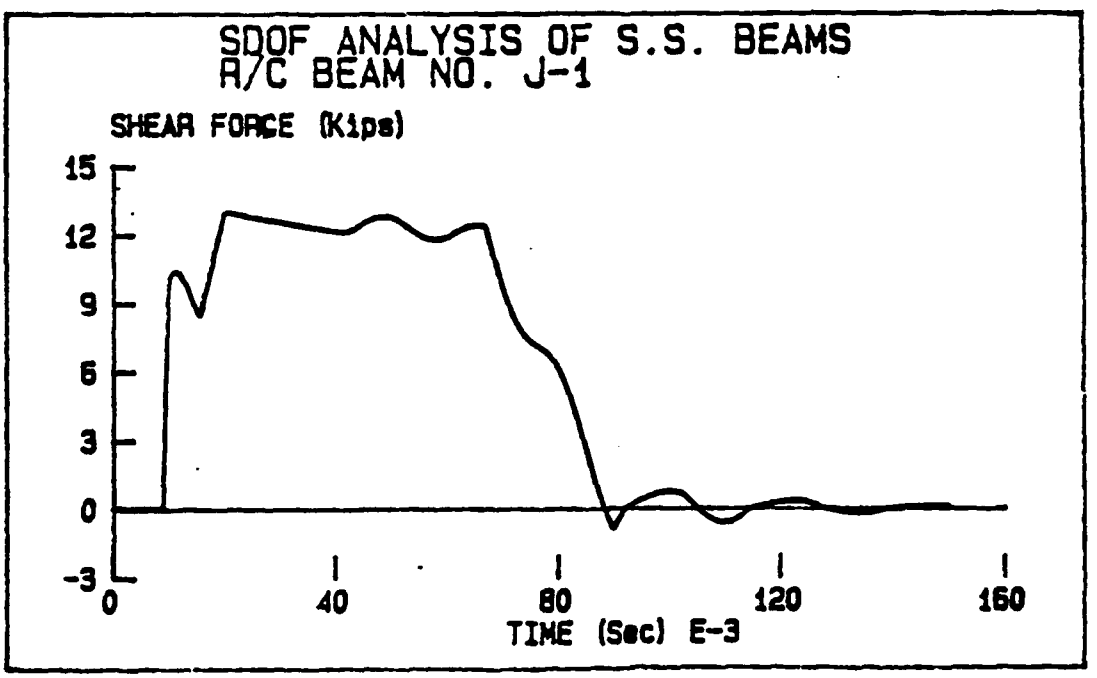

Figure 64. Support Reaction Versus Time for Beam J-1

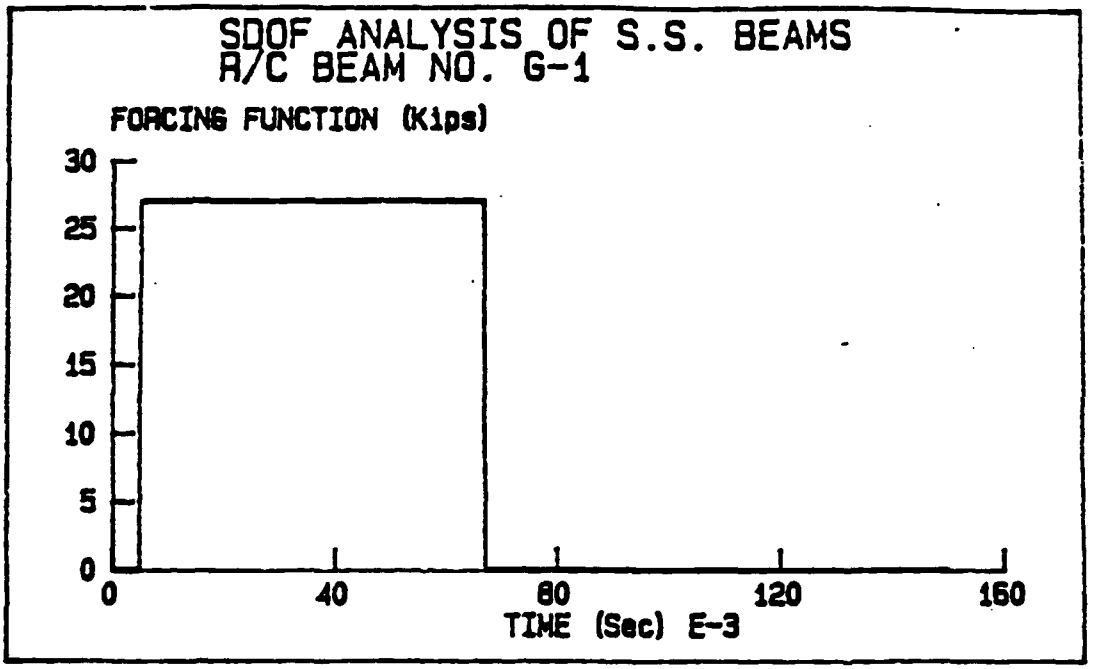

Figure 65. Applied Load Versus Time for Beam G-1

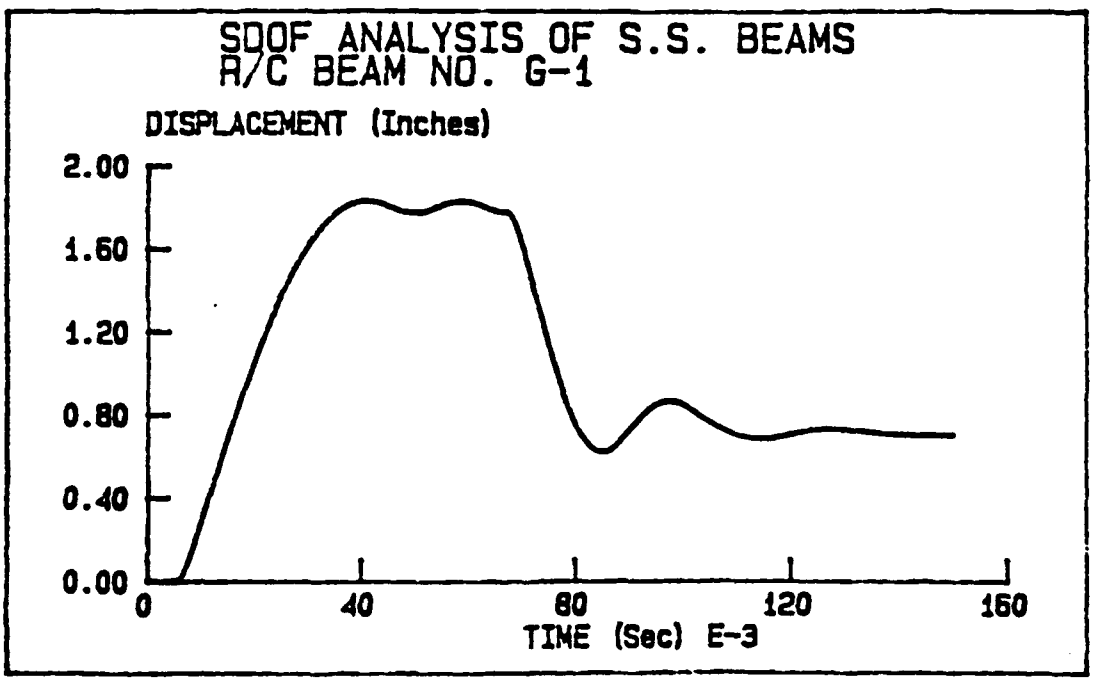

Figure 66. Midspan Displacement Versus Time for Beam G-1

description of the applied load can effectively induce gross errors in the results. A correct knowledge of the applied load is a prerequisite for successful analysis of structures.

Figure 67 shows the analytic load for beam I-1, as obtained from the experimental data given in Figure C-21. As mentioned earlier, the experiment on beam I-1 was disrupted (to protect the equipment from damage) by limiting the midspan deflection of the beam by a wooden block placed directly below the midspan point. Therefore, the experimental data recorded beyond that point (see beam hit stop in Figure C-21), including the measured peak and the permanent displacement, could not be considered valid. The result of the analysis for this beam indicates the occurrence of a flexural failure as a result of extensive crushing of concrete at a displacement of approximately 9.5 inches at 65 milliseconds, as shown in Figure 68. Interestingly enough, these values agree closely with the measured deflection of 10 inches at a time of 72 milliseconds, when the beam came in contact with the wooden block (Figure C-22). Therefore, it would be reasonable to conclude that if the wooden block was not present, the beam would have failed during the experiment.

Measured and analytical results for the peak displacement, maximum response time, and the permanent deflections of the above five beams are summarized in Table 4. It can be seen that there is good agreement between the experimental data and the computed values for all specimen of this test series with the exception of beam C-1, for which an accurate description of the impact load was not available. Considering the wide range of uncertain variables involved, the agreement between the measured data and the computed values is a convincing demonstration of the effectiveness of the present procedure. Measured and computed results for the peak magnitude and the response time of the dynamic reactions are listed in Table 5. In view of the inherent limitations of an equivalent SDOF system, and the uncertainties involved in the analysis, the results seem quite satisfactory for all practical purposes.

2. Analysis of Reinforced Concrete Walls Subjected to Localized Blast Loads

This analysis is based on the experiments conducted at the U.S. Army Waterways Experiment Station, sponsored by the U.S. Air Force Engineering and Services Center (Reference 78). In that study, a number of one-half scale model tests were conducted against simulated reinforced-concrete wall sections using cylindrical charges. These tests were performed in two series. In the first series, six walls were tested, two of which were transversely reinforced with dowels and in one case, Test I-5, the experimental results were not provided in Reference 78. Therefore, only structures I-1, I-2, and I-6 are analyzed here. In the second series, the tests were mostly aimed towards investigating methods to control concrete spalling. Therefore, three of the walls used spall plates, two walls had berms of silty sand placed against the exterior face, and the remaining of the walls in this series had very deep cross sections, and thus, would not fall within the assumptions and capabilities of the present approach.

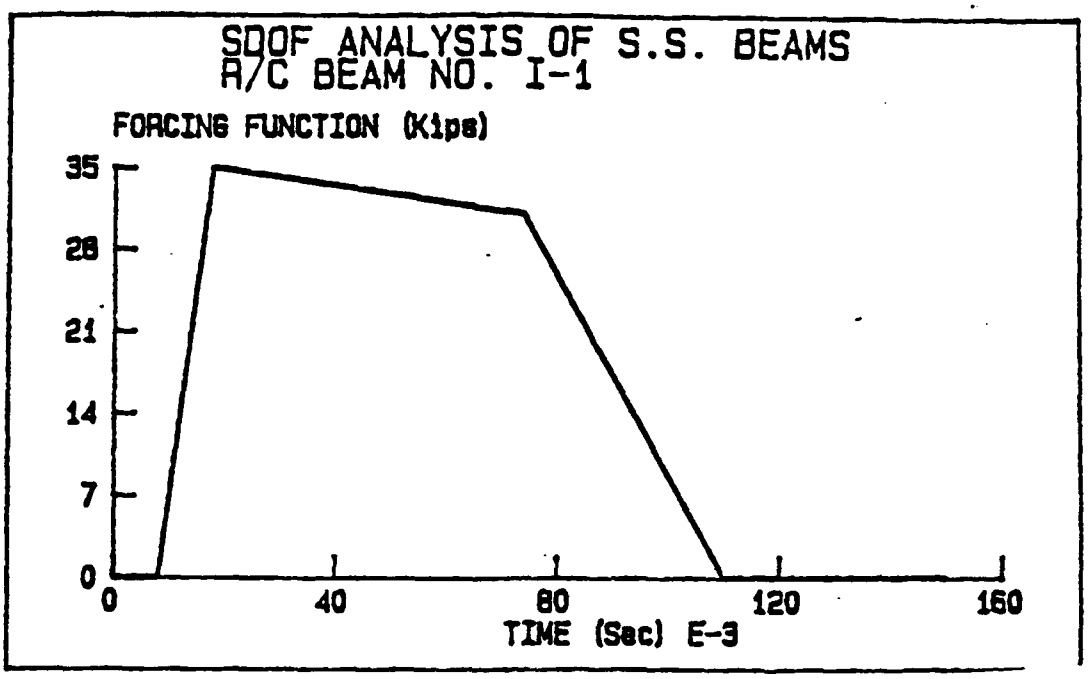

Figure 67. Applied Load Versus Time for Beam I-1

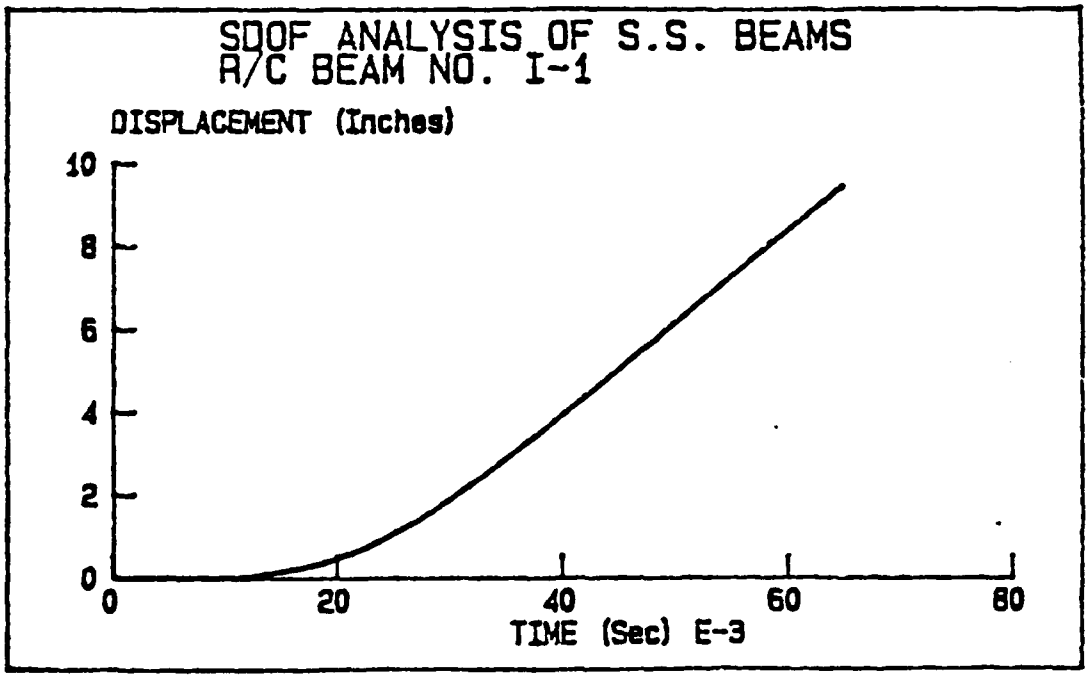

Figure 68. Midspan Displacement Versus Time for Beam I-1

TABLE 4. RESULTS OF DYNAMIC ANALYSIS FOR BEAMS OF REFERENCE 77

Beam	Peak Deflection (Inches)		Peak Response Time (Milliseconds)		Permanent Deflection (Inches)	
	Measured	Computed	Measured	Computed	Measured	Computed
C-1	3.0	3.1	50	45	2.2	2.4
H-1	8.9	8.5	58	62	7.5	6.8
J-1	.76	.63	32	40	.3	.32
G-1[a]	4.2	1.9	67	40	3.0	.71
I-1[b]	10.	9.5	72	65	—	—

TABLE 5. RESULTS OF DYNAMIC ANALYSIS FOR BEAMS OF REFERENCE 77

Beam	Peak Dynamic Reaction (Kips)		Peak Response Time (Milliseconds)	
	Measured	Computed	Measured	Computed
C-1	19.	17.4	15.	13.8
H-1	19.	19.	16.5	11.1
J-1	19.	13.2	22.	22.
G-1[a]	21.5	22.1	12.	6.3
I-1[b]	20.	20.5	17.6	18.

[a] Computed results based on estimated load pulse
[b] Beam deflection stopped by wooden block in experiment.

Tables D-1 and D-2 in the Appendix provide the material and geometric properties of the three walls, and Figures D-1 and D-2 show the reinforcement detail of the three test structures analyzed here. The wall slabs were reinforced symmetrically and had dimensions of 65 inches (165 cm) in length, 158 inches (400 cm) in width, and 12.6 inches (32 cm) in height. The reinforcement ratio was 0.01, 0.005, and 0.0025 for slabs I-1, I-2, and I-6, respectively. Unfortunately, sufficient data for some of the specific properties of flexural reinforcement (i.e., strain at the initiation of work hardening and at the ultimate) was not given in Reference 78. Based on the yield data for the reinforcement, these values are estimated as 0.025 and 0.25, respectively. In addition, the ultimate stress, f_u, for the longitudinal reinforcement of beam I-1 was not provided and here it was assumed equal to the corresponding values in the other two slabs (115 ksi). It must be noted that data given in Reference 78 was in metric (SI) units and therefore, it had to be converted to the U.S. customary units for the purpose of the computations.

In order to reduce the rigid body motion of the box-type test structures, they were fastened to a reaction structures before testing. The reaction structure consisted of an L shaped reinforced concrete structure in which the test structure was placed, and six large concrete filled blocks, as shown in Figure D-3 in Appendix D. The explosive device used was the same for each test, and it was placed vertically on the ground surface at some unspecified distance from the test wall. Each test was instrumented to record the blast pressure loading on the slab and structural motion data, including the deflection of the wall slab at the midheight.

Although the same charge was used in all tests, there was a considerable scatter in the recorded pressure data, particularly at the high-pressure region on the lower half of the wall. The localized peak pressure occurs almost at the midheight of the bottom half of the wall, and it varies significantly from one test to another as shown in Figure D-4. There was also a tremendous amount of variability in the distribution of the recorded pressure data at other times. Figure D-5 shows the distribution of the pressures along the height of the wall at various times, and Figure D-6 shows the spatial distribution of the pressure at 0.6 millisecond (almost the average arrival time for these cases) after the detonation. Due to the uncertainties with regard to the magnitude and distribution of the applied load, the use of advanced techniques for the computation of the total applied force is really not justified. Instead, it was decided to compute the magnitude and the duration of the applied force based on the average recorded data, and simple assumptions with respect to the spatial distribution of the applied pressures, as presented next.

Since the peak pressures along the height of the wall do not occur at the same time, the peak force can be obtained by approximately evaluating the volume of the "pressure solid". The "pressure solid" consists of one half of an elliptic cone (upper

portion), and a wedge with a rectangular base (lower portion) as shown in Figure D-6. The intensity of the applied pressure at the peak point of the solid and at the base of the wall are taken from the average recorded data as 58 and 50 Mpa, respectively (Figure D-4 in Appendix D). Therefore, the average magnitude of the peak applied force can be computed as follows:

1. Compute Volume 1 : The "pressure solid" is assumed as one half of a cone with an elliptic base for which the lengths of the major and minor axis are 1200 mm and 500 mm, respectively (Figure D-6).

$$\forall_1 = (0.5)(0.333)(58)(\pi)(1200\ \text{mm})(500) = 18221\ \text{KN} \quad (150)$$

2. Compute Volume 2 : The pressure solid is a wedge with a rectangular base area. The dimensions of the base are approximately 2400 and 200 mm along the major and minor axis, respectively (Figure D-6).

$$\forall_2 = (0.5)(0.5)(58+50)(200\ \text{mm})(2400\ \text{mm}) = 12960\ \text{KN} \quad (151)$$

3. Compute total applied force :

$$F = \forall_1 + \forall_2 = 18221 + 12960 = 31181\ \text{KN} \approx 7000\ \text{kips} \quad (152)$$

The centroid of the applied force is computed to be approximately 250 mm (10 inches) from the base of the wall.

The duration of the applied load is again taken from the same average pressure data recorded on the walls. Referring to Figures D-7 and D-8 in Appendix D, the average duration of loading is approximately the sum of the average duration of positive pressure (approximately 1.5 milliseconds in Figure D-7) and the time difference between the average time of measured arrival at the top and the bottom of the wall (approximately 0.5 milliseconds). Thus, the average loading duration of approximately 2 millisecond is assumed in the analysis with a triangular variation of force with time, as shown in Figure 69.

Clearly, the preceding computations is only an approximation of the actual applied load function. But, considering the uncertainties associated with the magnitude and the distribution of the applied load, employing any other complex technique does not necessarily seem to present a more accurate formulation. Nevertheless, in the future one could consider employing a reliable spatial pressure-time function.

The procedure for the analysis of these walls followed along the same line as before. The boundary conditions at both ends of the wall were assumed to by fully restrained against rotation and translation. Because of the high rate of loading, a 30 percent enhancement on the stress properties of the reinforcing steel and concrete was assumed. The mass of a typical wall was computed using the average normal

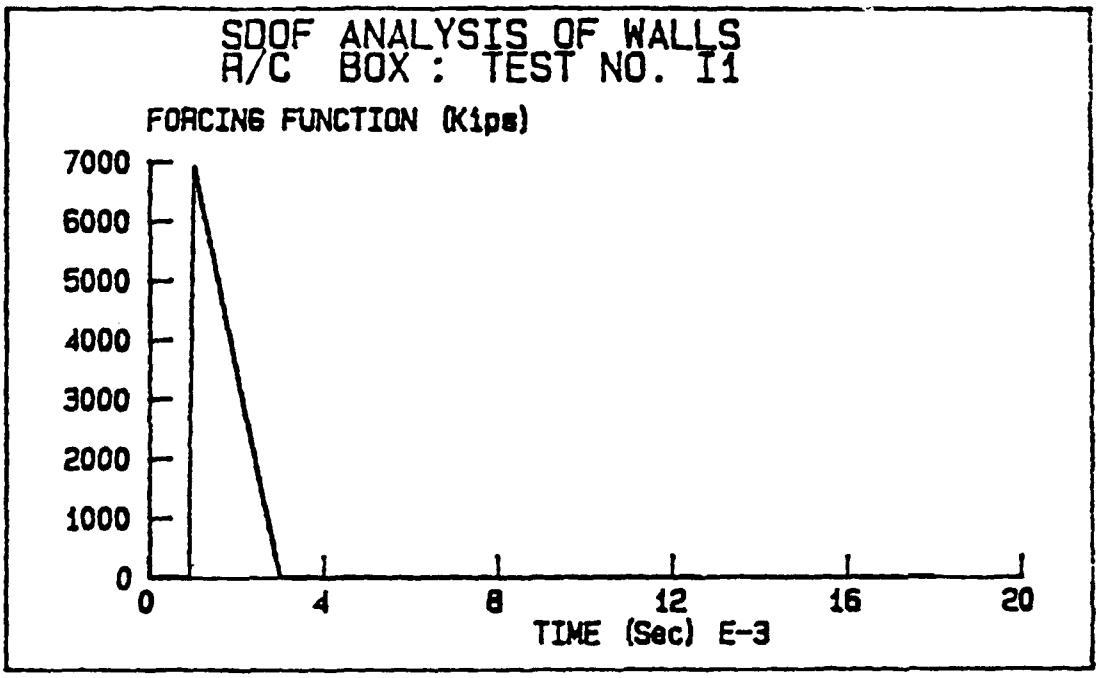

Figure 69. Load-Time History for Walls I1, I2, and I6

weight for reinforced concrete (150 pcf). And, 2 percent external damping ratio was used in the analysis of the three walls, as presented next.

The analytic results for each wall are presented by midspan deflection-time and velocity-time histories for which the critical values are compared with the available experimental data. Additional analytic results including moment-curvature relationship, load-deflection diagram, resistance-displacement curve, acceleration-time history, support shear forcing function, and support shear resistance-displacement diagram are provided in Appendix D for each case.

1. Analysis of Wall I-1

Figures 70 and 71 show the results for the analytical deflection and velocity-time histories at themidspan of wall I-1. The peak deflection obtained from the analytic model is 0.34 inches at 3.2 milliseconds. These values are in fair agreement with the measured data, 0.5 inch at a time of 3.2 milliseconds, as shown in Figure D-9. The computed permanent deflection for this beam is 0.13 inches which agrees closely with the measured residual displacement of 0.13 inches. The peak computed velocity for this beam is 237 inches/sec. which is also in good agreement with the experimental value of 256 inches/sec.

2. Analysis of Wall I-2

Figures 72 and 73 present the analytic result of displacement- and velocity-time histories at the midspan of Wall I-2. The measured and the computed results for the peak displacement are in good agreement. The maximum measured displacement was 0.85 inches and recorded at 6 milliseconds (Figure D-10 in Appendix D). From Figure 72, it can be seen that the computed peak deflection of 0.72 inch was reached at approximately 4.2 milliseconds. The computed permanent deformation of 0.38 inch was also in good agreement with the experimental data of 0.33 inch. The peak velocity of this beam was measured as 315 inches which compared well with the computed value of 358 inches/sec (Figure 73).

3. Analysis of Wall I-6

The computed deflection and velocity responses of wall I-6 are given in Figures 74 and 75, respectively. The agreement between the peak measured and computed midspan deflection is very good in this case. The maximum measured displacement was 1.52 inches and recorded at 12.4 milliseconds (Figure D-11 in Appendix D). In the analysis, the computed peak displacement was 1.52 inches, but it was reached at 6.7 milliseconds. The agreement between the experimental and the analytic values for the residual deformation is also good. The experimental value for the permanent deformation was reported to be approximately 0.66 inch which compared well with the analytic result of 0.68 inch. The maximum computed velocity of 394 inches/sec. also compared well with the measured value of 479 inches/sec.

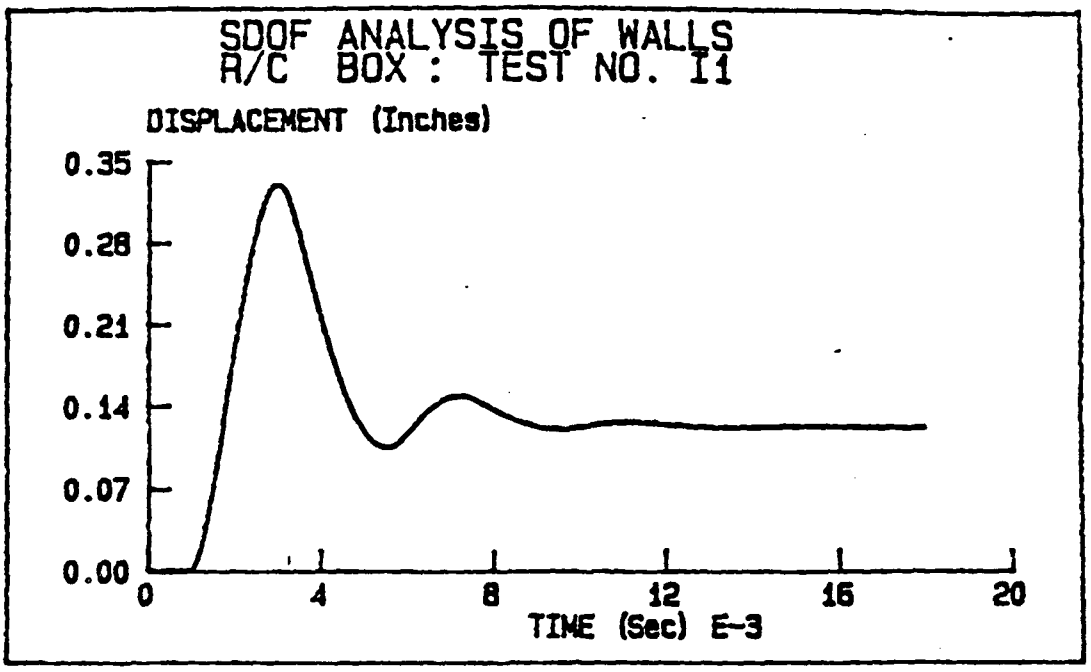

Figure 70. Midspan Displacement Versus Time for Wall I-1

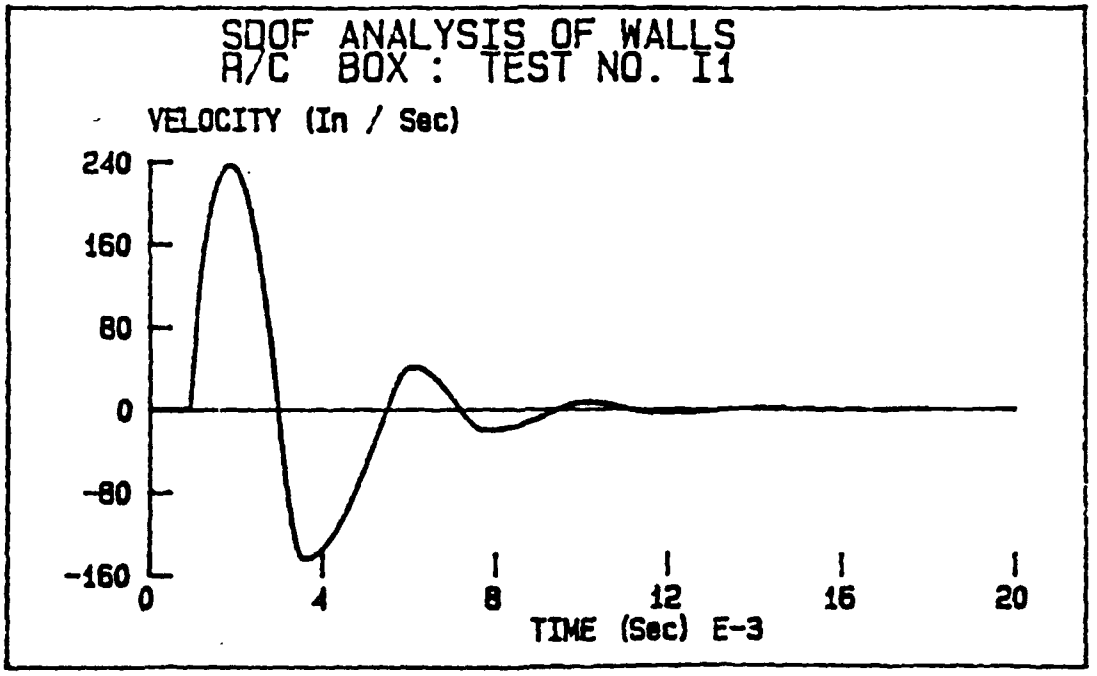

Figure 71. Midspan Velocity Versus Time for Wall I-1

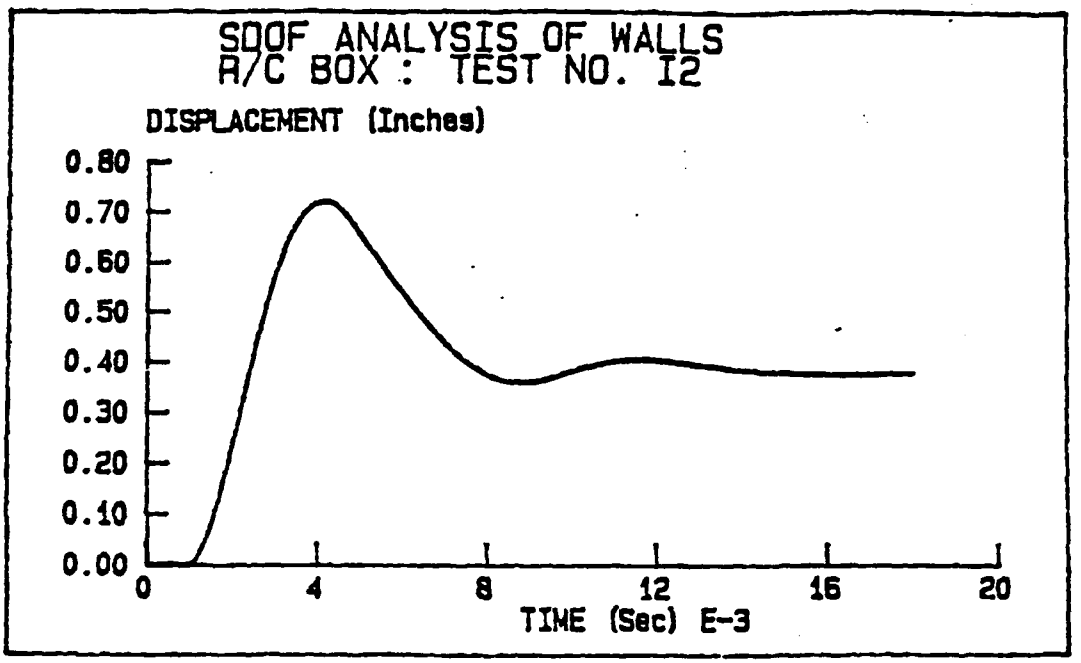

Figure 72. Midspan Displacement Versus Time for Wall I-2

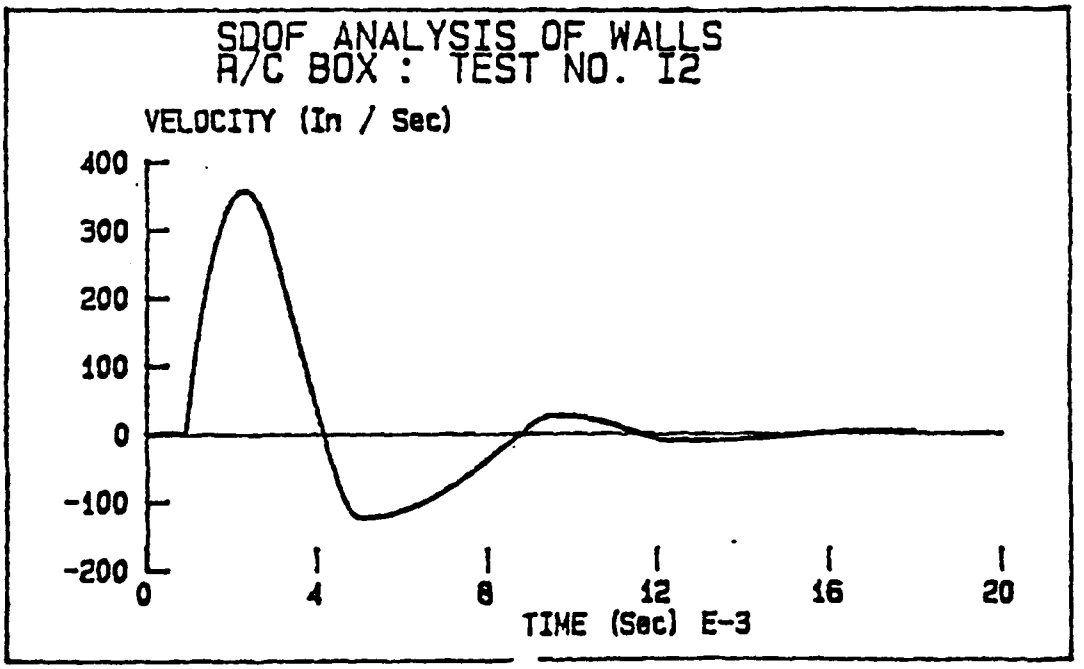

Figure 73. Midspan Velocity Versus Time for Wall I-2

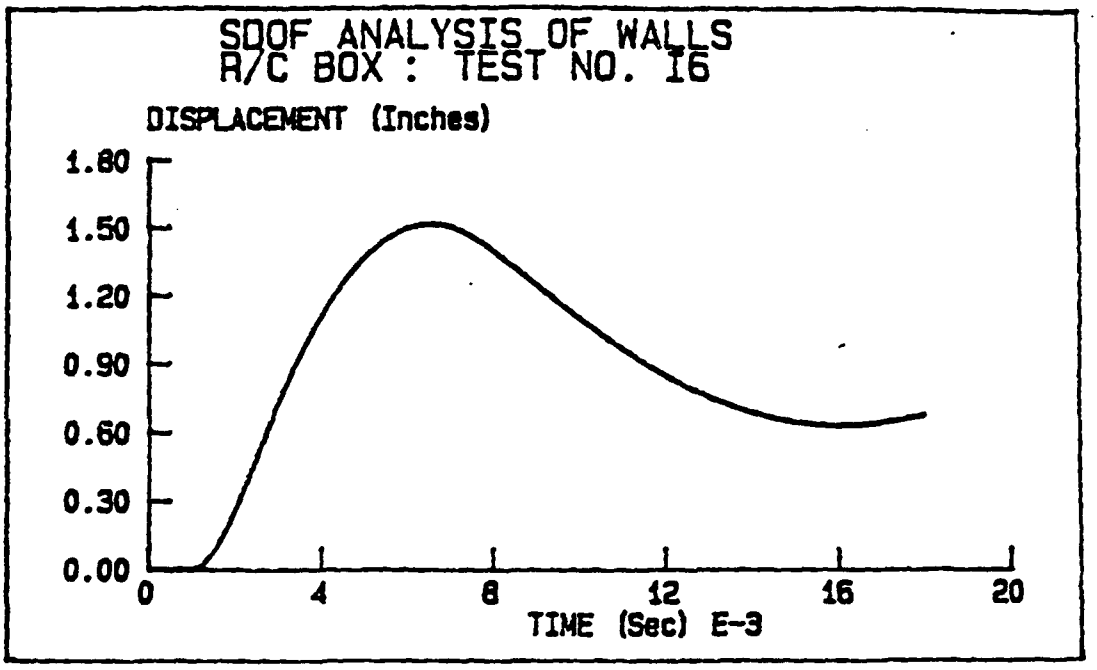

Figure 74. Midspan Displacement Versus Time for Wall I-6

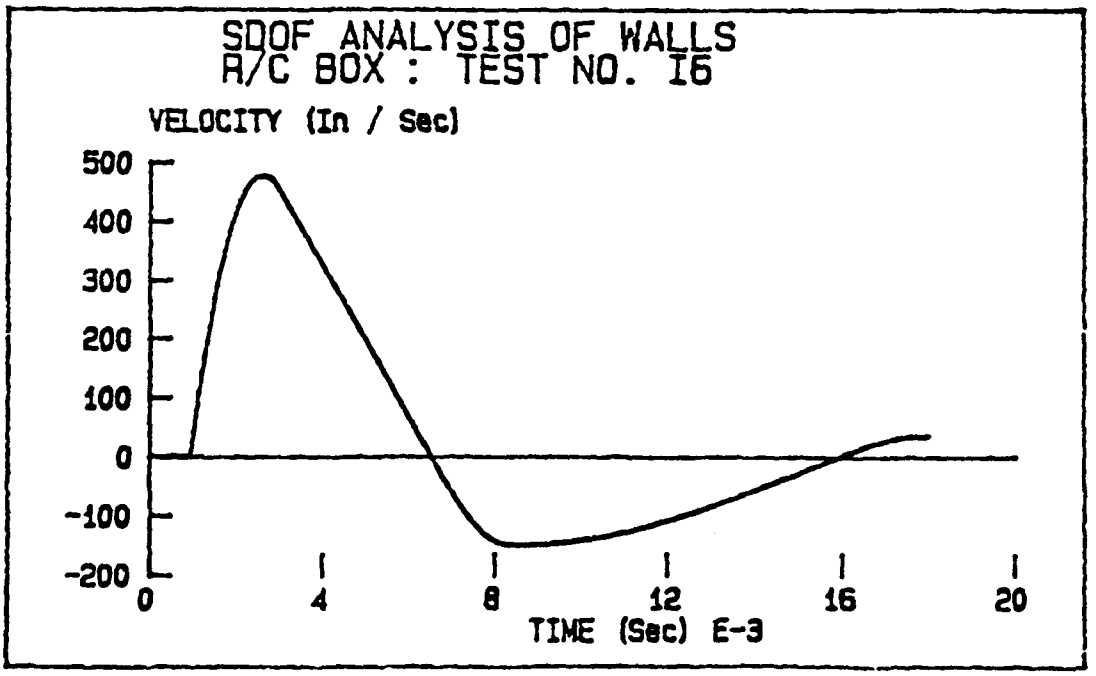

Figure 75. Midspan Velocity Versus Time for Wall I-6

Table 6 presents the summary of the analysis for the three walls examined here. Considering all the uncertainties involved with the input information data and all assumptions employed in the present approach, the analytic results are generally within reasonable agreement of the experimental values. It can be seen that the peak deflection response values are close for all three walls. Permanent structural deflection is a good measure of the structural damage, and in all three cases the computed and the measures residual deflections compare well with one another. Furthermore, the fact that the computed peak response time is always less that the measured value is an indication that the assumed approximation for the time and spatial distribution of forcing function is not quite consistent with the actual loading data. In general, the experimental and the analytic values for the peak velocity response are also in good agreements.

Unfortunately, because of stress wave transmission through the concrete, adequate data on the measured structural accelerations were not recorded during the tests. However, the computed mid-span acceleration for walls I-1, I-2, and I-6 are provided in Figures D-15, D-21, and D-27. In addition, experimental observations in Reference 78 indicated that in all cases structural shearing response was highly localized and mostly confined to the lower region of the wall, near the floor connection. The analytic results for the support shearing deformation, based on Hawkins direct shear resistance mechanism as discussed in Section III, suggest a similar conclusion as reflected in Figures D-16 and D-17 for I-1, Figures D-22 and D-23 for I-2, and Figures D-28, D-29 for I-6 in Appendix D. But, since no experimental data on the shear deflections were collected, quantitative comparisons between test values and the computed results are not possible.

TABLE 6. RESULTS OF DYNAMIC ANALYSIS FOR WALLS OF REFERENCE 78

Wall	Peak Deflection (Inches)		Peak Response Time (Milliseconds)		Permanent Deflection (Inches)	
	Measured	Computed	Measured	Computed	Measured	Computed
I-1	0.50	0.34	4.5	3.2	0.13	0.13
I-2	0.85	0.72	6.0	4.2	0.33	0.38
I-6	1.52	1.52	12.4	6.7	0.66	0.68

TABLE 6 (Continued)

Beam	Peak Mid-Span Velocity (In./ Sec.)	
	Measured	Computed
I-1	256	235
I-2	315	358
I-6	394	479.

(The reverse of this page is blank)

SECTION V
SUMMARY, CONCLUSIONS, AND RECOMMENDATIONS

A. SUMMARY

The analytical procedure developed herein is aimed at a better understanding of reinforced concrete structural elements and complete systems under severe localized loads in the static and dynamic domains. Furthermore, the goal was to develop a reliable and efficient computational approach for the analysis of such systems.

1. Static Domain

In the static domain, modified analytical/empirical methods are developed for studying the behavior of reinforced concrete beams and beam-columns under the combined influence of flexure, shear, and axial compressive forces. The computational procedure employs explicit relationships between these mechanisms for evaluating structural element behavior at any stage of its existence. The numerical procedure consists of two parts. In the first part, the moment-curvature diagram of the cross section is computed, based on the assumption of linear strain distribution in the cross section, and accurate description of stress-strain relationships for the materials. The moment-curvature relationship was modified to represent the influence of shear and axial forces on the flexural response. The formation of plastic hinges, and the implementation of rational failure criteria for defining the behavior of the structural element at the ultimate condition were also considered. In the second part, the load-deflection relationship and the deformed shape of the structural element are computed from the modified moment-curvature formulation by numerical integration. Here, the development of the analytical technique was aimed towards obtaining a quantitative description of the behavior of the structure from the onset of loading to the ultimate failure condition. The proposed step-by-step computational procedure accounts for the nonlinear distribution of curvatures on the span as well as the possibility of nonlinearities associated with the support conditions.

The theoretical/empirical model created for the influence of transverse reinforcement on the flexural behavior of the element considers the behavior of deep and slender beams. The present shear model is primarily based on the truss mechanism analogy, and extensive test results, as reported in the literature.

A central issue addressed herein was the adoption of rational failure criteria for defining the transition of each structural member into the ultimate capacity stage. For ductile (under-reinforced) members, these criteria were characterized by the ultimate strains of reinforcement, unconfined, and confined concrete. For brittle cases, the peak flexural moment was employed for defining the transition into failure. Attention was given to a careful definition of the boundary conditions (linear, or nonlinear) which represented the effects of the adjoining structural elements on the response of the individual

member. Also, the formation of plastic hinges was monitored closely in order to capture the behavioral variations through the nonlinear domain.

2. Dynamic Domain

The concept of an equivalent SDOF system was adopted for the dynamic analysis of reinforced concrete elements subjected to short impulsive excitations. The approach for computing load-deflection relationships was modified for the dynamic analysis to include rate effects on material properties, and to incorporate mechanisms for energy dissipation and stiffness deterioration of the reinforced concrete element. In addition, the study treated the derivation of the SDOF parameters, such as mass factor, load factor, and the inertia factor by computing them from the deflected shape at every step for any combination of transverse and rotational boundary conditions. This approach allows one to overcome the computational difficulties encountered with material nonlinearities in dynamic analysis.

Another important topic treated herein was the influence of direct shear on the behavior of the element when subjected to high intensity dynamic excitations. For this purpose, an approximate procedure has been developed for computing the dynamic transverse forces at critical locations. These forces were combined with an existing direct shear resistance function, and implemented into the second SDOF system for the evaluation of the shearing response at critical locations. Here too, failure criteria were employed for capturing the ultimate response.

3. Results

The analytical/numerical model was employed for analyzing 29 beams and beam-columns under static conditions. These cases were examined experimentally be other investigators and consisted of nine beams that were tested by Burns and Siess (Reference 1), nine beams from the experimental investigation by Bresler and Scordelis (Reference 36), and 11 beam-columns from an experimental study by Yamashiro and Siess (Reference 17). All 29 structural elements considered in this study were simply supported rectangular reinforced concrete members loaded laterally at their midspan by a single concentrated force. Numerical results at collapse for the 29 beams indicated that the mean ratio of the computed to the measured collapse load is 0.99 with a deviation of about 5 percent. The mean ratio of the computed deflection to the measured deflection at collapse was 0.95 with a deviation of 12 percent. The predicted moment-curvature and load-deflection relationships for these structural elements illustrate that the present approach seems to simulate the experimental observations accurately.

To demonstrate the effectiveness of the analytical model for the dynamic problems, two groups of experimental dynamic cases were also analyzed. The first group consisted of five reinforced concrete beams subjected to localized impact loads that were tested by Feldman

and Siess (Reference 77). In general, the results for these beams were in good agreement with the measured experimental data. In nearly all cases, the predicted peak midspan dynamic displacement and the residual (permanent) deflection agreed closely with the available reported data. In addition, the computed and measured results for dynamic reactions, particularly the peak magnitude of the support shear force, were adequately close. This is an apparent indication of the effectiveness of the approximate procedure developed for computing the dynamic transverse force at the supports.

The second group of elements consisted of three reinforced concrete walls that were subjected to nearby cylindrical explosive charges (Reference 78). Because of the uncertain nature of loading as such, the agreement between the computed values with the measured responses were not as close as the beams of the first group. In two cases, the analytical peak midspan deflection compared well with the measured data, and the measured and computed values for the permanent mid-span deflections and velocities compared reasonably well with the measured values in all cases.

B. CONCLUSIONS

The following conclusions are drawn as a result of the present study.

1. The analytical/numerical method presented here can be used successfully for predicting the complete load-deflection behavior of rectangular reinforced concrete structural elements under the combined action of bending, shear and axial force. The analytical results indicated that the incorporation of the combined effects of bending, shear and axial compressive force into such simple and yet accurate model can provide results that are in good agreement with the available experimental data at all stages of loading up to failure. The overall adequacy of results confirms the assumptions regarding the stress-strain relationships for concrete and steel employed in the present analysis. The present approach can be employed with similar success for the analysis of two-way reinforced concrete slabs, as demonstrated in other studies (References 54 through 57).

2. The proposed behavioral model for the effect of shear in reducing the ultimate flexural capacity of the beams improved the results significantly. It was noticed that the influence of shear reinforcement on the flexural capacity of slender rectangular and T reinforced concrete beams was represented more accurately as a function of $\sqrt{a/d}$, while for deep rectangular beams it seem to depend on a/d. This could be an important fact which further illustrates the difference in behavior between slender and deep beams. Results were in good agreement with experimental findings and reconfirmed that the lack of an adequate amount of web reinforcement would reduce the ultimate strength of the member.

3. The method seems to simulate accurately experimental load-deflection data for reinforced concrete beams and beam-columns. The adequacy of the results for the 29 cases examined here is a convincing indication of the assumptions about the failure criteria and the formation and propagation of plastic hinges employed in the present model. In addition, inclusion of the second order nonlinear effect caused by the axial compressive force enhanced the accuracy of the numerical results for the beam-columns.

4. The application of the method developed in this study to analyzed reinforced concrete elements under impulsive dynamic excitation has also been proven effective. The equivalent SDOF is a simple, inexpensive, and accurate tool for evaluation of the structural response, if accurate behavioral models are employed. In nearly all cases examined here, the predicted structural damage, as reflected by the permanent deformations, agreed closely with the experimental observations. Thus, demonstrating the validity of the proposed dynamic resistance function. In general, the agreement between the measured and the predicted peak displacements was also good, indicating that the proposed approximate procedure for computing the parameters of the nonlinear SDOF system is indeed effective.

5. Considering the inherent limitations in employing a SDOF system, the proposed approximate model for predicting the dynamic support shear forces at the supports is effective. The agreement between the peak magnitude of the measured and predicted shear forces shows that the approximate approach can provide satisfactory results for all practical purposes.

6. The procedure developed here for computing the response of reinforced concrete structural elements can be used with great confidence, so long as the magnitude and the time variation of the applied dynamic load is known with reasonable certainty. Whenever experimentally applied loads were known, agreements between the measured and computed response were very close. On the other hand, for cases with less reliable loading information, the computed results deviated from the measures values.

C. RECOMMENDATIONS FOR FUTURE STUDIES

In order to develop more reliable analysis and design method, the following recommendation are suggested as ways that the analytical model could be improved.

1. Experiments should be conducted to obtain a more accurate description of the localized blast loads. Presently, the available information on the pressures generated from the detonation of cylindrical charges reflect considerable scatter in the data.

2. Controlled test series should be performed for studying the mechanics of failure under localized loads. The issues to be addressed should include the effect of concrete strength, transverse reinforcement, bond slip of the reinforcement, rate of straining, and the loading condition on the local shear resistance of the structural elements.

3. The development of reliable structural models for predicting the response of connections when the structural element is subjected to high intensity dynamic excitation is very important. That information can subsequently be combined with the present formulation in order to obtain a more realistic assessment of the complete structural system response.

4. The development of similar approximate techniques for analysis of other types of structural elements, such as arches, cylinders, closures, etc., is also important. In addition, the present approach could be adopted for studying the equipment-structure interaction under high intensity dynamic pressures.

(The reverse of this page is blank)

REFERENCES

1. Burns, N. H., and Siess, C. P., Load Deformation Characteristic of Beam-Columns Connections in Reinforced Concrete, SRS Report No. 234, University of Illinois, Urbana-Champaign, January 1962.

2. Park, R., and Paulay, T., Reinforced Concrete Structures, John Wiley and Sons Inc., New York, 1975, pp. 195-269.

3. Krauthammer, T., and Hall, W. J., Resistance of Reinforced Concrete Structures under High Intensity Loads, SRS Report No. 463, University of Illinois, Urbana-Champaign, May 1979.

4. Hognestad, D., A Study of Combined Bending and Axial Load in Reinforced Concrete Members, University of Illinois Engineering Experimental Station, Bulletin Series No. 399, November 1951.

5. Baker, A. L. L., and Amarakone, A. M. N., "Inelastic Hyperstatic Frame Analysis," Proceedings of the International Symposium on the Flexural Mechanics of Reinforced Concrete, ASCE-ACI, Miami, Nov. 1964, pp. 85-142.

6. Blume, J. A., Newmark, N. M., and Corning, L. H., Design of Multi-Story Buildings for Earthquake Motion, Portland Cement Association, Chicago, 1961.

7. Building Code Requirements for Reinforced Concrete, (ACI 318-83), American Concrete Institute, Detroit, Michigan, 1983.

8. Richart, F. E., Brandtzaeg, A., and Brown R. L., The Failure of Plain and Spirally Reinforced Concrete in Compression, University of Illinois Engineering Experimental Station, Bulletin No. 190, 1929.

9. Balmer, G. G., Shearing Strength of Concrete Under High Triaxial Stress-Computation of Mohr's Envelope as a Curve, Structural Research Laboratory Report No. SP-23, U.S. Bureau of Reclamation, 1949.

10. Kent, D. C., and Park, R., "Flexural Members with Confined Concrete," ASCE Journal of the Structural Division, Vol. 97, ST 7, July 1971, pp. 1969-1990.

11. Chan, W. W. L., "The Ultimate Strength and Deformation of Plastic Hinges in Reinforced Concrete Frameworks," Magazine of Concrete Research, Vol. 7, No. 21, Nov. 1955.

12. Sargin, M., Ghosh, S. K., and Handa, V. K., "Effect of Lateral Reinforcement upon the Strength and Deformation Properties of Concrete." Magazine of Concrete Research, Vol. 23, No. 75-76, June-Sept. 1971, pp. 99-110.

13. Corley, W.G., "Rotational Capacity of Reinforced Concrete Beams,"

ASCE Journal of the Structural Division, Vol. 92, ST5, October 1966, pp. 121-146.

14. Vallenas, J., Bertero, V. V., and Popov, E. R., Concrete Confined by Rectangular Hoops and Subjected to Axial Loads, Report No. UCB/EERC-77/13, University of California, College of Engineering, Berkeley, Calif. Aug., 1977.

15. Park, R., and Sampson, R. A., "Ductility of Reinforced Concrete Column Sections in Seismic Design," ACI Journal, Vol. 69, No. 9, Sept. 1972, pp. 543-551.

16. Ghosh, S. K., and Cohn, M. Z., Ductility of Reinforced Concrete Sections in Combined Bending and Axial Load, Inelasticity and Non-Linearity in Structural Concrete, Study No. 8, University of Waterloo Press, 1972, pp. 147-180.

17. Yamashiro, R., and Siess, C. P., Moment Rotation Characteristics of Reinforced Concrete Members Subject to Bending, Shear, and Axial load, SRS Report No. 260, University of Illinois, Urbana-Champaign, December 1962.

18. Litton, R. W., and Gidwani, J. M., Failure Criteria of Reinforced Concrete Structures, Report No. AFWL-TR-77-239, Vols. I & II, Air Force Weapons Laboratory, Kirtland Air Force Base, NM, May 1979.

19. Lane, E. G., Behavior of Reinforced Concrete Beams under Combined Axial and Lateral Loading, Report No. AFWL-TR-76-130, Air Force Weapons Laboratory, Kirtland Air Force Base, NM, May 1977.

20. Lane, E. G., Reinforced Concrete Beams under Combined Axial and Lateral Loading, Report No. AFWL-TR-81-99, Air Force Weapons Laboratory, Kirtland Air Force Base, NM, Jan. 1982.

21. Mattock, A. H., Discussion of "Rotational Capacity of Reinforced Concrete Beams," by W. G. Corley, ASCE Journal of the Structural Division, Vol. 93, ST2, April 1967, pp. 519-522.

22. Joint ASCE-ACI Task Committee 426, "The Shear Strength of Reinforced Concrete Members," ASCE Journal Of the Structural Division, Vol. 99, ST6, June 1973, pp. 1091-1187.

23. Kani, G. N. J., "Basic Facts Concerning Shear Failure," ACI Journal, Vol. 63, June 1966, pp. 675-692.

24. Leonhardt, F., and Walther, R., The Stuttgart Shear Tests, 1961", Translation No. 111, Cement and Concrete Association, London, England, 1964.

25. Kani, G. N. J., "A Rational Theory for the Function of Web Reinforcement," ACI Journal, Vol. 64, March 1969, pp. 185- 197.

26. Kani, G. N. J., "How Safe Are Our Large Reinforced Concrete Beam?," ACI Journal, Vol. 64, March 1967, pp. 128-141.

27. Zsutty, T. C., "Beam Shear Strength Prediction By Analysis of Existing Data," ACI Journal, Vol. 65, Nov. 1968, pp. 943-954.

28. Placas, A., and Regan, P. E., "Shear Failure of Reinforced Concrete Beams," ACI Journal, Vol. 68, October 1971, pp. 763-773.

29. Collins, M. P., "Towards a Rational Theory for Reinforced Concrete Members in Shear," ASCE Journal of the Structural Division, ST4, April 1978, pp. 649-666.

30. Fenwick, R. C., and Paulay, T., "Mechanism of Shear Resistance of Concrete Beams," ASCE Journal of the Structural Division, Vol. 94, ST10, Oct. 1968, pp. 2235-2350.

31. Thurlimann, B., Shear Strength of Reinforced and Prestressed Concrete Beams - CEB Approach, Tech. Report, ACI Symposium, 1976, Feb. 1977, Revised Copy.

32. Thurlimann, B., Torsional Strength of Reinforced and Prestressed Concrete Beams - CEB Approach, Bulletin 113, ACI Publication SP-59, Detroit, 1979.

33. Ramirez, J. A., "Reevaluation of AASHTO Design Procedures for Shear and Torsion in Reinforced and Prestressed Concrete Beams," Ph.D Thesis, University of Texas at Austin, 1983.

34. Chen, W. F., Plasticity in Reinforced Concrete, John Wiley and Sons Inc., New York, NY, 1972.

35. Clark, A. P., "Diagonal Tension in Reinforced Concrete Beams," ACI Journal, Vol. 48, No. 2, Oct. 1951, pp. 145-156.

36. Bresler, B., and Scordelis, A. C., Shear Strength of Reinforced Concrete Beams, Series 100, Issue 13, Structure and Material Research, Dept. of Civil Engineering, University of California, Berkeley, June 1961.

37. Mattock, A. H., and Wang, Z., "Shear Strength of Reinforced Concrete Members Subject to High Axial Compressive Stress," ACI Journal, Vol. 81, May-June 1984, pp. 287-298.

38. Mattock, A. H., Haddadin, M. J., and Hong, S. T., "Stirrup Effectiveness in Reinforced Concrete Beams with Axial Force," ASCE Journal of the Structural Division, Vol. 97, ST9, Sept. 1971, pp. 2277-2297.

39. Mattock, A. H., "Diagonal Tension Cracking in Concrete Beams with Axial Force," ASCE Journal of the Structural Division, Vol. 95, ST9, Sept. 1969, pp. 1887-1900.

40. Rosenblueth, E., and Diaz de Cossio, R., "Instability consideration in Limit Design of Concrete Frames, Proceedings of

the International Symposium on the Flexural Mechanics of Reinforced Concrete, ASCE-ACI, Miami, Nov. 1964, pp. 439-456.

41. Sawyer, H. A., "Design of Concrete Frames for Two Failure States," Proceedings of the International Symposium on the Flexural Mechanics of Reinforced Concrete, ASCE-ACI, Miami, Nov. 1964, pp. 405-431.

42. Biggs, J. M., Introduction to Structural Dynamics, McGraw-Hill, New York, NY, 1964.

43. Timoshenko, S. P., Young, D. H., and Weaver W., Vibration Problems in Engineering, 4th Ed., John Wiley and Sons Inc., New York, NY, 1974.

44. Clough, R. W., and Penzien, J., Dynamics of Structures, McGraw-Hill, New York, NY, 1975.

45. Design of Structures to Resist the Effects of Atomic Weapons, U.S. Army Corps of Engineering Manual EM 1110-345-415, March 1957.

46. Baker, W. E., Cox, P. A., Westine, P. S., Kulesz, J. J., and Strehlow, R. A., Explosion Hazards and Evaluation, Elsevier Scientific Publishing Company, New York, 1983.

47. Sozen, M. A., "Hysteresis in Structural Elements," Applied Mechanics in Earthquake Engineering, Applied Mechanics Division Vol. 8, ASME, 1974, New York, pp. 63-98.

48. Iwan, W. D., "On a Class of Models for the Yielding Behavior of Continuous and Composite Systems," Journal of the ASME, Vol. 34, No. 3, Sept. 1967, pp. 612-617.

49. Newmark, N., M., and Rosenbleuth, E., Fundamentals of Earthquake Engineering, Prentice-Hall, Englewood Cliffs, NJ, 1971.

50. Agrawal, G. L., Tulin, L. G., and Gerstle, K. A., "Response of Doubly Reinforced Beams to Cyclic Loading," ACI Journal, V. 62, No. 51, July 1965, pp. 823-835.

51. Brown R. H., and Jirsa, J. O., "Reinforced Concrete Beams Under Load Reversals," ACI Journal, Vol. 68, No. 5, May 1971, pp. 380-390.

52. Park R., Kent, D. C., and Sampson, R. A., "Reinforced Concrete Members With Cyclic Loading," ASCE Journal of the Structural Division, Vol. 98, No. ST7, July 1972, pp. 1341-1360.

53. Clough, R. W., and Johnston, S. B., "Effect of Stiffness Degradation on Earthquake Ductility Requirements," Proceeding, Japan Earthquake Engineering Symposium, Tokyo, Oct. 1966, pp. 227-232.

54. Krauthammer, T., and Parikh, M., "Structural Response Under Localized Dynamic Loads," Proceeding, 2nd Symposium on the Interaction of Non-Nuclear Munitions with Structures, Panama City Beach, FL, April 1985, pp. 52-55.

55. Krauthammer, T., "Shallow-Buried RC Box-Type structures," ASCE Journal of the Structural Division, Vol. 110, No. 2, March 1983, pp. 637-651.

56. Krauthammer, T., Bazeos, N., and Holmquist, T. J., "Modified SDOF Analysis of RC Box-Type Structures", ASCE Journal of the Structural Division, Vol. 112, No. 4, April 1986, pp. 726-744.

57. Kiger, S. A., and Painter, J. T., "A Computational Procedure for Response of Buried Structures to Conventional Weapons," Proceeding, 2nd Symposium on the Interaction of Non-Nuclear Munitions with Structures, Panama City Beach, FL, April 1985, pp. 41-44.

58. Watstein, D., "Effect of Strain Rate on the Compressive Strength and Elastic Properties of Concrete," ACI Journal, Vol. 24, No. 8, April 1953, pp. 729-742.

59. Bazant, Z., P., and Byung, H. O., "Strain Rate Effect in Rapid Triaxial Loading of Concrete," ASCE Journal of Engineering Mechanics Division, Vol. 108, No. EM5, Oct. 1982, pp. 764-787.

60. Soroushian, P., Choi, K. B., and Alhamad, A., "Dynamic Constitutive Behavior of Concrete," ACI Journal, Vol. 83, No. 2, March-April 1986, pp. 251-259.

61. Soroushian, P. and Choi, K. B., "Steel Mechanical Properties at Different Strain Rates," ASCE Journal of the Structural Division, Vol. 113, No. 4, April 1987, pp. 663-672.

62. Newmark, N. M., "Design of Structures for Dynamic Loads Including the Effects of Vibration and Ground Shock," Symposium on Scientific Problems of Protective Construction, Zurich, July 1963.

63. Criswell, M. E., Strength and Behavior of Reinforced Concrete Slab-Column Connections Subjected to Static and Dynamic Loadings, Technical Report N-70-1, U.S. Army Engineer Waterways Experimental Station, Vicksburg, Mississippi, Dec. 1970.

64. Furlong, R. W., Thompson, J. N., Burns, N. H., and Perry, E. S., Shear and Bond Strength of High-Strength Reinforced Concrete Beams under Impact Loads-First Phase, Technical Report AFWL-TR-67-113, Air Force Weapons Laboratory, May 1968.

65. Seabold, R. H., Dynamic Shear Strength of Reinforced Concrete Beams - Part III, Technical Report R695, Naval Civil Engineering Laboratory, Sept. 1970.

66. Soroushian, P., and Obaseki, K., "Strain Rate-Dependent Interaction Diagrams for Reinforced Concrete Section," ACI Journal, Vol. 83, No. 1, Jan.-Feb. 1986, pp. 102-110.

67. Ross, T. J., Direct Shear Failure in Reinforced Concrete Beams Under Impulsive Loading, Air Force Weapons Laboratory, Final Report No. AFWL-TR-83-84, Sept., 1983.

68. Kiger, S. A., Getchell, J. V., Slawson, T. R., and Hyde, D. W., Vulnerability of Shallow-Buried Flat Roof Structures, U.S. Army Engineer Waterways Experiment Station, Technical Report SL-80-7, Six Parts, Sept., 1980 - Sept., 1984.

69. Slawson, T. R., Dynamic Shear Failure of Shallow-Buried Flat-Roofed Reinforced Concrete Structures Subjected to Blast Loading, Final Report SL-84-7, U.S. Army Engineer Waterways Experimental Station, April 1984.

70. Keenan, W. A., "Shear Stresses in One-Way Slabs Subjected to Blast Load", Seventeenth Explosives Safety Seminar - Denver, Colorado, Sept. 1976.

71. Ross, T., J., "Characterizing Impulsive Failure in Buried Reinforced Concrete Elements," Proceeding, 2nd Symposium on the Interaction of Non-Nuclear Munitions with Structures, Panama City Beach, FL, April 1985, pp. 35-40.

72. Murtha, R. N., and Holland, T. J., Analysis of WES FY82 Dynamic Shear Test Structures, Naval Civil Engineering Laboratory, Technical Memorandum No. 51-83-02, Dec. 1982.

73. Walraven, J. C., and Reinhardt, H. W., "Theory and Experiment on the Mechanical Behavior of Cracks in Plain and Reinforced Concrete Subjected to Shear Loading," Heron, Vol.26, No. 1A. 1981.

74. Ross, C. A., and Rosengren, P. L., "Expedient Nonlinear Dynamic Analysis of Reinforced Concrete Structures," Proceeding, 2nd Symposium on the Interaction of Non-Nuclear Munitions with Structures, Panama City Beach, FL, April 1985, pp. 45-51.

75. Ross, C. A., Sierakowski, R. L., and Schauble, C. C., Concrete Breaching Analysis, Technical Report AFATL-TR-81-105, Air Force Armament Laboratory, December 1981.

76. Craig, R. R., Structural Dynamic: An Introduction to Computer Methods, John Wiley and Sons Inc., New York, NY, 1981.

77. Feldman, A., and Siess, C. P., Investigation of Resistance and Behavior of Reinforced Concrete Members Subjected to Dynamic Loading, Part III, SRS Report No. 165, University of Illinois, Urbana-Champaign, Sept. 1958.

78. Coltharp, D. R., Vitayaudom, K. P., Kiger, S. A., Semihardened Facility Design Criteria Improvement, Final Report ESL-TR-86-32, U.S. Army Engineer Waterways Experimental Station, Oct. 1981- Dec. 1984.

79. Wang, C. K., and Salmon, C. G., Reinforced Concrete Design, Third Edition, Harper & Row Publishers, New York, 1978.

(The reverse of this page is blank)

APPENDIX A

DIAGONAL TENSION FAILURE DATA

TABLE A-1. RECTANGULAR DEEP BEAM PROPERTIES AND THE INCLINATION OF THE CONCRETE COMPRESSION DIAGONALS AT ULTIMATE

Beam	f'_c (psi)	$\rho''f''$ (psi)	ρ^*	$\frac{a}{d}$	$\rho^*\frac{a}{d}$	α°
B11	3388	180	3.09	1.95	6.02	16.70
B12	3680	180	2.97	1.95	5.97	18.80
B13	3435	180	3.07	1.95	5.99	16.71
B14	3380	180	3.09	1.95	6.02	17.75
B15	3570	180	3.01	1.95	5.87	19.80
C11	3720	170	2.79	1.57	4.38	16.47
C12	3820	170	2.75	1.57	4.32	14.04
C13	3475	170	2.88	1.57	4.52	18.26
C21	3430	330	5.63	1.57	8.84	29.25
C22	3625	330	5.48	1.57	8.60	27.92
C24	3910	330	5.27	1.57	8.27	29.25
D16	4010	170	2.68	1.57	5.22	20.81
D17	4060	170	2.67	1.96	5.22	19.80
D18	4030	170	2.68	1.96	5.22	19.21
D26	4280	220	3.36	1.96	8.13	27.02
D27	4120	220	3.42	2.42	8.28	29.25
D28	3790	220	3.57	2.41	8.64	27.02
D41	3970	180	2.85	2.42	7.06	22.29
D42	3720	180	2.95	2.42	7.14	24.22
D43	3200	180	3.18	2.42	7.70	22.78
D51	4020	130	2.05	2.42	4.96	19.80
D52	4210	130	2.00	2.42	4.84	18.77
D53	3930	130	2.07	2.42	5.00	18.77
A11	3575	180	3.01	2.34	7.04	22.30
A12	3430	180	3.07	2.34	7.18	23.30
A13	3395	180	3.08	2.34	7.21	22.30
A14	3590	180	3.00	2.34	7.02	22.30

TABLE A-2. RECTANGULAR SLENDER BEAM PROPERTIES AND THE INCLINATION OF THE CONCRETE COMPRESSION DIAGONALS AT ULTIMATE

Beam	f'_c (psi)	$\rho'' f_y''$ (psi)	ρ^*	$\frac{a}{d}$	$\rho^* \sqrt{\frac{a}{d}}$	α°
A1	3490	47.2	0.80	3.92	1.58	11.17
A2	3520	47.6	0.80	4.93	1.78	10.76
A3	5080	47.2	0.66	6.91	1.73	11.17
B1	3590	69.2	1.15	3.95	2.28	12.84
B2	3360	70.0	1.21	4.91	2.59	14.37
B3	5620	70.0	0.93	6.95	2.45	16.08
C1	4290	93.9	1.43	3.95	2.84	16.33
C2	3450	95.2	1.62	4.93	3.60	15.89
C3	5080	93.9	1.32	6.98	3.49	18.58
R8	3870	83.5	1.34	3.36	2.46	15.63
R9	4290	167	2.55	3.36	4.67	23.09
R10	4295	83.5	1.27	3.36	2.33	16.50
R11	3800	83.5	1.35	3.36	2.48	14.00
R17	1850	83.5	1.94	3.36	3.56	17.70
R18	4540	83.5	1.24	3.36	2.27	14.77
R19	4390	167	2.52	3.36	4.62	20.42
R20	6230	83.5	1.06	3.36	1.94	13.92
R22	4280	83.5	1.28	3.36	2.35	15.63
C305-D0	3770	125.1	2.04	3.00	3.53	20.67
C310-D10	3520	250.2	4.22	3.00	7.30	31.56
C310-D20	3560	250.2	4.19	3.00	7.26	30.22
J13	4800	305.5	4.36	5.14	9.80	34.61
J14	4500	305.5	4.55	5.14	10.32	36.90
J20	4380	136.0	2.06	5.14	4.65	19.21
J5	5000	305.5	4.32	4.00	8.64	34.92
J6	5160	305.5	4.25	4.00	8.50	35.79
J22	4420	136.0	2.04	4.00	4.08	18.22

TABLE A-3. RECTANGULAR DEEP BEAM PROPERTIES AND THE INCLINATION OF THE CONCRETE COMPRESSION DIAGONALS AT ULTIMATE

Beam	f'_c (psi)	$\rho'' f''_y$ (psi)	ρ^*	$\frac{a}{d}$	$\rho^* \sqrt{\frac{a}{d}}$	α°
A2	4235	99	1.52	2.50	2.41	13.39
A3	4360	210	3.18	2.50	5.03	18.60
A4	4145	393	6.10	2.50	9.56	28.20
A5	3815	630	10.20	2.50	16.13	37.23
A6	3720	900	14.76	2.50	23.33	42.82
B3	4015	210	3.38	3.38	6.09	19.87
C2	4030	99	1.56	4.25	3.21	14.94
C3	3500	210	3.55	4.25	7.32	20.66
C4	3730	393	6.43	4.25	13.27	30.58
C5	4415	630	9.48	4.25	19.55	39.40
E2	2200	99	2.11	2.50	3.33	15.30
E3	1980	210	4.72	2.50	7.46	27.41
E4	1945	393	8.91	2.50	14.09	36.15
E5	2475	630	12.66	2.50	20.02	43.75
F3	6515	210	2.60	2.50	4.11	16.56
G3	3800	277	4.49	2.50	7.10	21.26
G4	3880	416	6.67	2.50	10.55	26.87
G5	3790	693	11.26	2.50	17.80	37.11
T1	4050	83.5	1.31	3.36	2.40	11.47
T3	3990	83.5	1.32	3.36	2.42	12.03
T4	4710	83.5	1.21	3.36	2.22	11.50
T5	4890	167	2.39	3.36	4.38	17.70
T10	4090	55.7	0.87	3.36	1.60	9.73
T13	1850	83.5	1.94	3.36	3.56	13.93
T22	4980	83.5	1.18	3.36	2.17	11.51
T25	7840	83.5	0.94	3.36	1.73	11.00
T31	4495	83.5	1.25	3.36	2.29	13.24
T33	5340	167	2.28	4.5	4.85	22.16
T7	3970	83.5	1.32	3.46	2.46	11.51

APPENDIX B

INPUT PROPERTIES AND RESULTS FOR ANALYSIS IN THE STATIC DOMAIN

TABLE B-1. PROPERTIES OF MEMBERS ANALYZED STATICALLY, GROUPS 1,2,3

Beam	f'_c	Width	Depth	Length	ρ	ρ'	P_{axial}	Stirrups
	psi	in.	in.	in.	%	%	Kips	
Group 1								
J5	5000	8.0	18.0	144	1.10	0.61	0	#3 @ 6.00"
J6	5160	8.0	18.0	144	1.10	1.10	0	#3 @ 6.00"
J8	4680	8.0	10.0	144	1.98	1.98	0	#3 @ 6.00"
J13	4800	8.0	14.0	144	1.41	1.41	0	#3 @ 6.00"
J14	4500	8.0	14.0	144	1.41	0.79	0	#3 @ 6.00"
J17	3900	8.0	10.0	144	1.98	1.98	0	#3 @ 6.00"
J18	4410	6.0	10.0	144	2.63	2.63	0	#3 @ 6.00"
J20	4380	8.0	14.0	144	1.41	1.41	0	#3 @ 6.00"
J22	4420	8.0	18.0	144	1.10	1.10	0	#3 @ 6.00"
Group 2								
A1	3490	12.1	18.0	144	1.81	0.180	0	#2 @ 8.25"
A2	3520	12.0	18.0	180	2.28	0.182	0	#2 @ 8.25"
A3	5080	12.1	18.0	252	2.73	0.182	0	#2 @ 8.25"
B1	3590	9.1	18.0	144	2.43	0.243	0	#2 @ 7.50"
B2	3360	9.0	18.0	180	2.43	0.243	0	#2 @ 7.50"
B3	5620	9.0	18.0	252	3.06	0.245	0	#2 @ 7.50"
C1	4290	6.1	18.0	144	1.80	0.361	0	#2 @ 8.25"
C2	3460	6.0	18.0	180	3.66	0.366	0	#2 @ 8.25"
C3	5080	6.1	18.0	252	3.63	0.363	0	#2 @ 8.25"
Group 3								
J15	4400	8.0	10.0	144	1.98	1.98	50	#3 @ 6.00"
J16	4550	8.0	10.0	144	1.98	1.98	25	#3 @ 6.00"
J24	5000	6.0	10.0	144	0.67	0.67	0	#3 @ 6.00"
J25	5050	6.0	10.0	144	0.67	0.67	25	#3 @ 6.00"
J26	4600	6.0	10.0	144	0.67	0.67	50	#3 @ 6.00"
J27	4920	6.0	10.0	144	0.67	0.67	75	#3 @ 6.00"
J28	5020	6.0	10.0	144	3.33	3.33	0	#3 @ 6.00"
J29	4410	6.0	10.0	144	3.33	3.33	25	#3 @ 6.00"
J30	4500	6.0	10.0	144	3.33	3.33	50	#3 @ 6.00"
J31	4280	6.0	10.0	144	3.33	3.33	75	#3 @ 6.00"
J34	4520	6.0	10.0	144	0.67	0.67	75	#3 @ 3.00"

TABLE B-2. PROPERTIES OF TENSION REINFORCEMENT, GROUPS 1,2,3

Beam	Size	f_y psi	ε_y %	ε_{sh} %	f_u psi	ε_u %	f_{fr} psi	ε_{fr} %
Group 1								
J5	2 #8	45.1	0.195	1.77	73.7	16.3	69.2	19.5
J6	2 #8	46.2	0.178	1.84	73.6	15.0	68.5	18.7
J8	2 #8	45.4	0.178	1.92	72.1	16.3	67.0	18.8
J13	2 #8	45.6	0.188	1.61	73.3	15.0	69.2	18.8
J14	2 #8	47.1	0.183	1.75	74.0	15.0	69.2	17.5
J17	2 #8	46.9	0.188	1.69	73.6	15.0	70.5	18.8
J18	2 #8	45.4	0.191	1.58	73.2	15.0	69.2	17.5
J20	2 #8	45.8	0.185	1.76	71.8	16.3	65.4	18.3
J22	2 #8	46.2	0.181	1.68	73.4	15.0	69.2	17.5
Group 2								
A1	4 #9	80.5	0.255	0.35	137.	8.33	110.	13.0
A2	5 #9	80.5	----------		same	----------		
A3	6 #9	80.1	----------		same	----------		
B1	4 #9	80.5	----------		same	----------		
B2	4 #9	80.5	----------		same	----------		
B3	5 #9	80.1	----------		same	----------		
C1	2 #9	80.5	----------		same	----------		
C2	4 #9	80.5	----------		same	----------		
C3	4 #9	80.5	----------		same	----------		
Group 3								
J15	2 #8	46.9	0.170	1.57	75.3	14.5	71.8	17.5
J16	2 #8	45.9	0.150	1.68	72.8	15.0	67.9	18.8
J24	2 #4	48.5	0.180	1.61	77.8	16.0	68.1	24.1
J25	2 #4	49.2	0.175	1.80	78.8	17.0	73.5	19.5
J26	2 #4	49.9	0.175	1.44	81.9	16.0	71.9	17.4
J27	2 #4	50.0	0.175	1.50	80.1	15.5	68.5	19.9
J28	2 #9	46.9	0.160	1.53	77.6	17.0	76.0	19.9
J29	2 #9	48.8	0.180	1.36	80.2	16.0	75.8	24.3
J30	2 #9	47.0	0.150	1.62	77.5	16.0	75.0	17.9
J31	2 #9	48.3	0.145	1.39	78.3	18.0	74.5	24.3
J34	2 #4	48.8	0.175	1.40	81.2	14.0	73.5	17.0

TABLE B-3. PROPERTIES OF COMPRESSION REINFORCEMENT, GROUPS 1,2,3

Beam	Size	f_y psi	ε_y %	ε_{sh} %	f_u psi	ε_u %	f_{fr} psi	ε_{fr} %
Group 1								
J5	2 #6	48.9	0.175	1.22	82.6	12.5	78.4	13.8
J6	2 #8	46.4	0.192	1.73	75.0	15.0	69.3	19.5
J8	2 #8	45.5	0.162	1.73	72.3	15.0	66.6	18.8
J13	2 #8	46.0	0.173	1.98	71.8	15.0	66.7	18.8
J14	2 #6	50.0	0.170	1.22	81.2	12.5	74.4	----
J17	2 #8	46.8	0.188	1.55	74.9	15.0	70.5	18.8
J18	2 #8	47.1	0.191	1.68	74.7	15.0	70.5	17.5
J20	2 #8	46.5	0.180	1.74	73.7	15.0	69.2	18.8
J22	2 #8	46.4	0.161	1.83	72.3	15.0	66.6	17.5
Group 2								
A1[a]	2 #4	51.0	0.184	1.38	83.8	16.9	75.0	18.5
Group 3								
J15	2 #8	47.3	0.160	1.57	75.3	15.0	71.8	18.1
J16	2 #8	44.7	0.150	1.69	71.4	15.0	67.9	18.8
J24	2 #4	47.8	0.175	1.55	76.9	17.5	65.2	22.8
J25	2 #4	49.2	0.175	1.77	78.0	15.5	68.0	22.3
J26	2 #4	49.0	0.170	1.42	80.3	16.0	69.0	20.6
J27	2 #4	50.1	0.175	1.48	81.3	18.0	69.7	21.4
J28	2 #9	46.7	0.170	1.62	77.6	17.5	75.0	23.4
J29	2 #9	48.6	0.160	1.50	80.4	15.6	76.2	25.0
J30	2 #9	47.2	0.145	1.00	80.2	15.8	75.0	24.1
J31	2 #9	47.9	0.160	1.44	80.2	18.7	75.5	24.5
J28	2 #4	50.3	0.175	1.40	81.9	16.0	74.0	20.4

[a] Same for Beams A1,A2,A3,B1,B2,B3,C1,C2,C3

TABLE B-4. MOMENT–CURVATURE AND LOAD–DEFLECTION OUTPUT FOR BEAM J8

```
MEMBER NAME                                : J-8
OUTPUT FILE FOR ORIGINAL M-C               : DUMP1
OUTPUT FILE FOR CORRECTED M-C (IF ANY)     : DUMP2
TENSION STEEL DATA
   YIELD STRESS          :    45400.00000000
   ULT. STRESS           :    72100.00000000
   ELASTIC STRAIN        :    1.78000005E-03
   STRN-HARD. STRAIN     :    1.92000009E-02
   ULT. STRAIN           :        0.16300000
   FRACTURE STRAIN       :        0.18799999
   NUMBER OF BARS        :             2
   BAR SIZE              : #           8
COMPRESSION STEEL DATA
   YIELD STRESS          :    45500.00000000
   ULT. STRESS           :    72300.00000000
   ELASTIC STRAIN        :    1.62000000E-03
   STRN-HARD. STRAIN     :    1.73000004E-02
   ULT. STRAIN           :        0.15000001
   NUMBER OF BARS        :             2
   BAR SIZE              : #           8
TRANSVERSE REINFORCEMENT DATA
   YIELD STRESS          :    50000.00000000
   SPACING OF TIES       :        6.00000000
   BAR SIZE              : #           3
   CLOSED RECT. TWO LEGGED TIES ASSUMED
CONCRETE DATA
   UNIAXIAL CYLINDER STRENGTH    :     4680.00000000
GEOMETRICAL DATA
   BEAM WIDTH                    :        8.00000000
   BEAM HEIGHT                   :       12.00000000
   BEAM EFFECTIVE DEPTH          :       10.00000000
   DEPTH OF COMPR. REINFORCEMENT :        2.00000000
   SIDE COVER(CLEAR TO STIRRUPS) :        1.50000000
GENERAL DATA
   AXIAL FORCE                   :    0.00000000E-01
   POINT OF APPL. OF AX. FORCE   :    0.00000000E-01
     (FROM TOP FIBERS)
   SHEAR SPAN (A)                :       72.00000000
   EXPERIMENTAL MOMENT           :      878.00000000
   EXPERIMENTAL CURVATURE        :    0.00000000E-01
   NUMBER OF DIV. IN ELAS. RANGE :             5
   NUMBER OF DIV. IN YIELD PLATEU:            20
   NUMBER OF DIV. IN STRN-HARD   :            30
   ENHANCEMENT FACTOR FOR DYNAMIC
      ANALYSIS (IF USE SDOF)     :        1.00000000

CODE KEY TABLE (3RD COLUMN IN M-C TABLE)
CODE = 1 : ANY POINT
     = 2 : EXPERIMENTAL MOMENT REACHED
```

- 3 : TENSION STEEL AT FRACTURE
- 4 : COMPRESSION STEEL AT ULTIMATE
- 5 : ULTIMATE CONCRETE STRAIN REACHED
- 7 : YIELD STRAIN IS REACHED
- 9 : STRAIN HARDENING STRAIN IS REACHED

M O M E N T - C U R V A T U R E T A B L E

CURVATURE	MOMENT	CODE	STL-STRAIN	TEN-FORCE	KD
MFEE					
0.000000	0.	1	0.0000	0.	0.0000
0.000054	124.	1	0.0004	14346.	3.4660
0.000109	248.	1	0.0007	28693.	3.4960
0.000165	371.	1	0.0011	43039.	3.5300
0.000221	493.	1	0.0014	57386.	3.5670
0.000278	614.	7	0.0018	71732.	3.6070
0.000386	622.	1	0.0027	71732.	3.1320
0.000492	627.	1	0.0035	71732.	2.8440
0.000598	631.	1	0.0044	71732.	2.6520
0.000703	634.	1	0.0053	71732.	2.5150
0.000811	637.	1	0.0061	71732.	2.4310
0.000918	639.	1	0.0070	71732.	2.3700
0.001026	639.	1	0.0079	71732.	2.3240
0.001134	640.	1	0.0087	71732.	2.2890
0.001243	641.	1	0.0096	71732.	2.2620
0.001352	641.	1	0.0105	71732.	2.2390
0.001460	641.	1	0.0114	71732.	2.2190
0.001569	640.	1	0.0122	71732.	2.2020
0.001677	640.	1	0.0131	71732.	2.1880
0.001786	639.	1	0.0140	71732.	2.1760
0.001895	639.	1	0.0148	71732.	2.1660
0.002004	638.	1	0.0157	71732.	2.1560
0.002133	617.	1	0.0166	71732.	2.2250
0.002242	617.	1	0.0175	71732.	2.2140
0.002351	617.	1	0.0183	71732.	2.2030
0.002482	599.	9	0.0192	71732.	2.2630
0.003119	647.	1	0.0240	79231.	2.3081
0.003734	693.	1	0.0288	84985.	2.2911
0.004347	730.	1	0.0336	89519.	2.2759
0.004960	759.	1	0.0384	93167.	2.2628
0.005570	783.	1	0.0432	96152.	2.2498
0.006178	803.	1	0.0480	98627.	2.2366
0.006784	819.	1	0.0528	100702.	2.2236
0.007390	834.	1	0.0575	102457.	2.2126
0.007994	845.	1	0.0623	103953.	2.2016
0.009262	842.	1	0.0671	105234.	2.7516
0.009978	850.	1	0.0719	106338.	2.7916
0.010688	856.	1	0.0767	107292.	2.8216
0.011403	861.	1	0.0815	108118.	2.8516
0.012124	866.	1	0.0863	108836.	2.8816

0.012999	868.	1	0.0911	109459.	2.9916
0.013781	870.	1	0.0959	110000.	3.0416
0.014596	871.	1	0.1007	110470.	3.1016
0.015380	873.	1	0.1055	110877.	3.1416
0.016055	875.	1	0.1103	111228.	3.1316
0.016741	878.	2	0.1151	111529.	3.1266
0.017413	880.	1	0.1199	111786.	3.1166
0.018083	882.	1	0.1247	112004.	3.1066
0.018765	884.	1	0.1294	112186.	3.1016
0.019431	885.	1	0.1342	112335.	3.0916
0.020096	886.	1	0.1390	112456.	3.0816
0.020774	888.	1	0.1438	112550.	3.0766
0.021435	888.	1	0.1486	112620.	3.0666
0.022095	889.	1	0.1534	112667.	3.0566
0.022772	889.	1	0.1582	112695.	3.0526
0.023428	889.	1	0.1630	112704.	3.0426
0.024083	898.	5	0.1678	112695.	3.0326

ECHO INPUT FILE FOR BEAM : J-8

MOM-CURV FILE (ORIGINAL) : DUMP1
MOM-CURV FILE (CORRECTED) : DUMP2
OUTPUT FILE NAME : DUMP3

LENGTH OF THE BEAM = 144.00000000
LOAD POINT FROM LEFT END = 72.00000000
NUMBER OF ELEMENTS = 60
INITIAL LOAD = 1.00000000
LOAD INCREMENT = 2.00000000
" " AFTER HINGE FORMATION = 0.50000000
CONVERGENCE FACTOR = 5.00000007E-02

BOUNDARY CONDITION AT END 1 = SS
BOUNDARY CONDITION AT END 2 = SS

L O A D - D E F L E C T I O N T A B L E

ISTEP	ITER	LOAD	DEFLECT AT CENT	ICODE	MAX DEFLECT VALUE	LOC	MASS FACTOR	INERTIA FACTOR	MOMENT AT LOAD
PDEL									
1	0	0.0	0.000	1	0.000	0.0	0.486	0.625	0.0
2	0	3.0	0.063	1	0.063	72.0	0.486	0.625	99.0
3	0	5.0	0.104	1	0.104	72.0	0.486	0.625	165.0
4	0	7.0	0.147	1	0.147	72.0	0.485	0.625	231.0
5	0	9.0	0.189	1	0.189	72.0	0.485	0.624	297.0
6	0	11.0	0.233	1	0.233	72.0	0.485	0.624	363.0
7	0	13.0	0.276	1	0.276	72.0	0.485	0.624	429.0
8	0	15.0	0.320	1	0.320	72.0	0.485	0.624	495.0
9	0	17.0	0.363	1	0.363	72.0	0.485	0.624	561.0
10	0	19.0	0.423	1	0.423	72.0	0.479	0.620	627.0
11	0	21.0	2.096	7	2.096	72.0	0.394	0.549	647.0
12	0	23.0	3.344	1	3.344	72.0	0.396	0.550	759.0
13	0	25.0	5.369	1	5.369	72.0	0.402	0.554	825.0
14	0	27.0	16.242	1	16.242	72.0	0.394	0.547	891.0
15	0	27.2	16.542	1	16.542	72.0	0.394	0.547	896.8
16	0	27.2	16.601	1	16.601	72.0	0.394	0.547	897.9

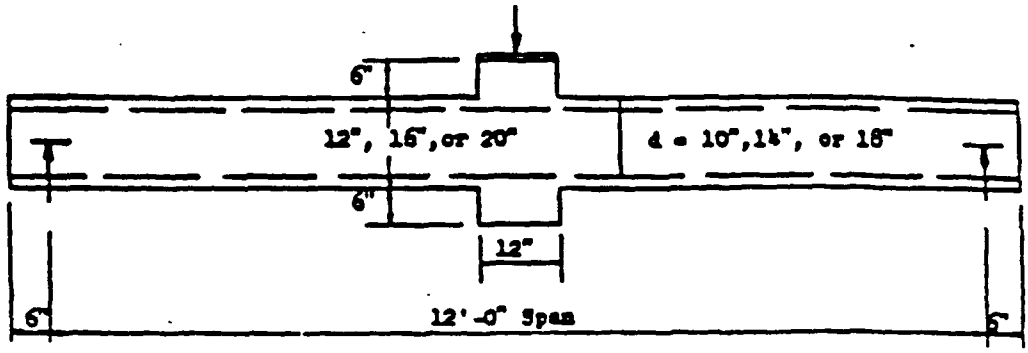

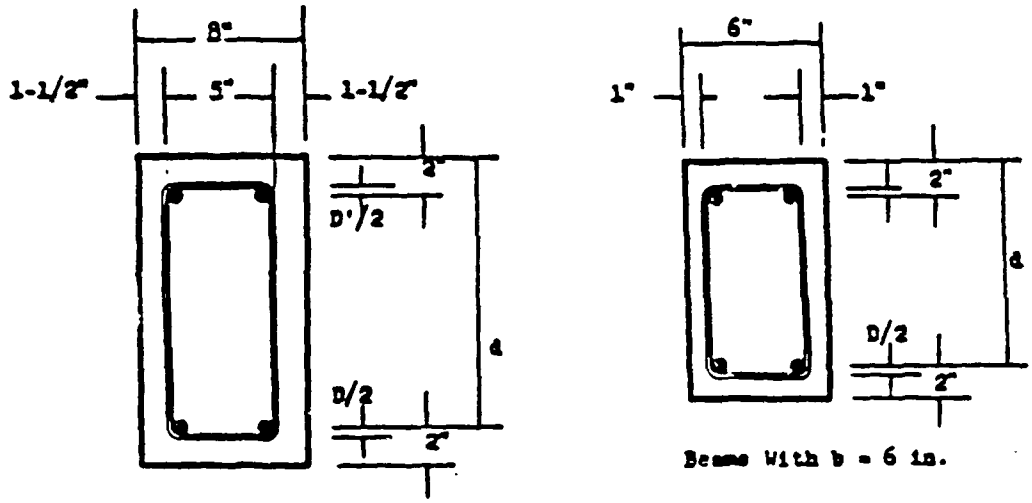

Figure B-1. Detailing of Beams: Group 1

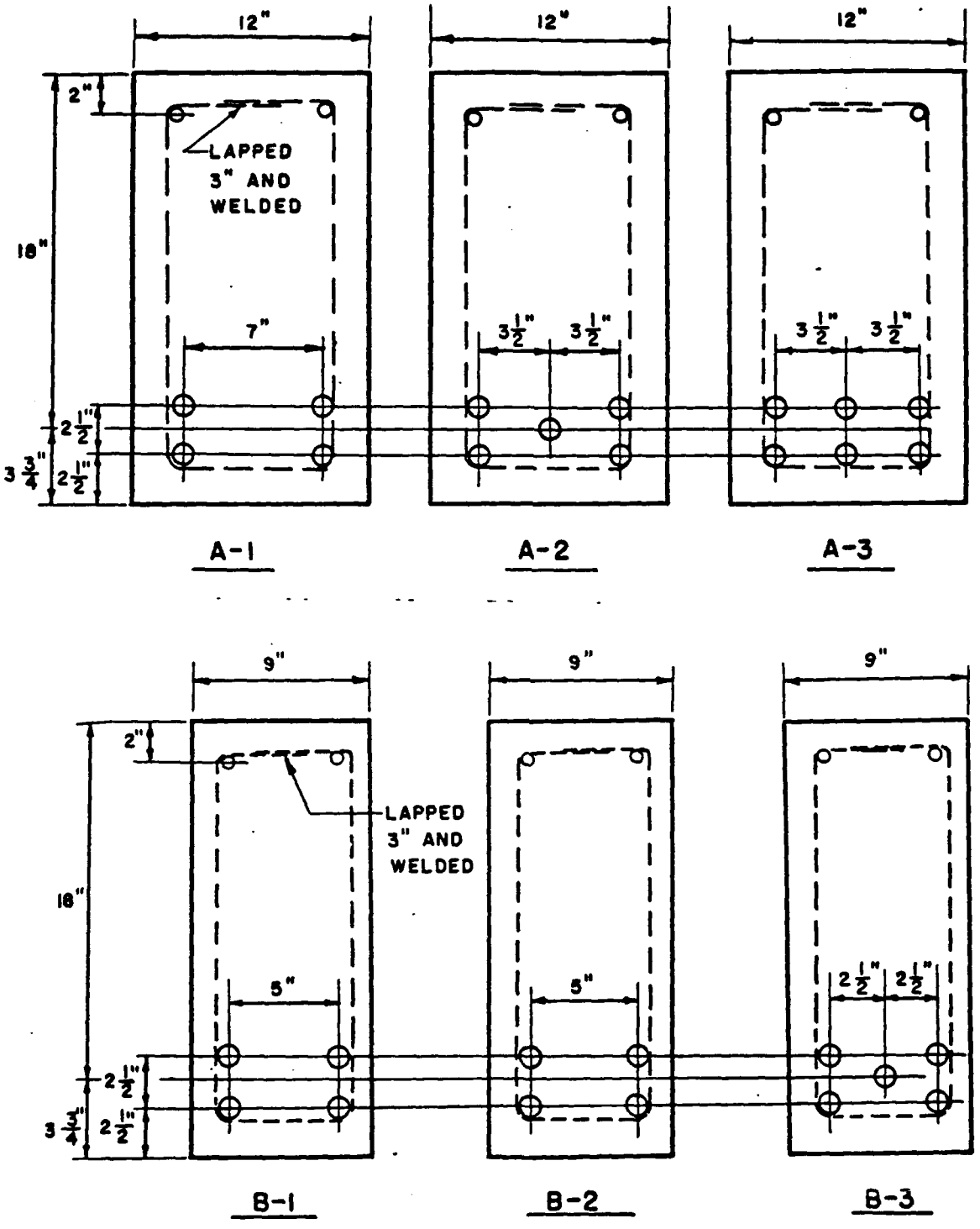

Figure B-2 Detailing of Beams: Group 2

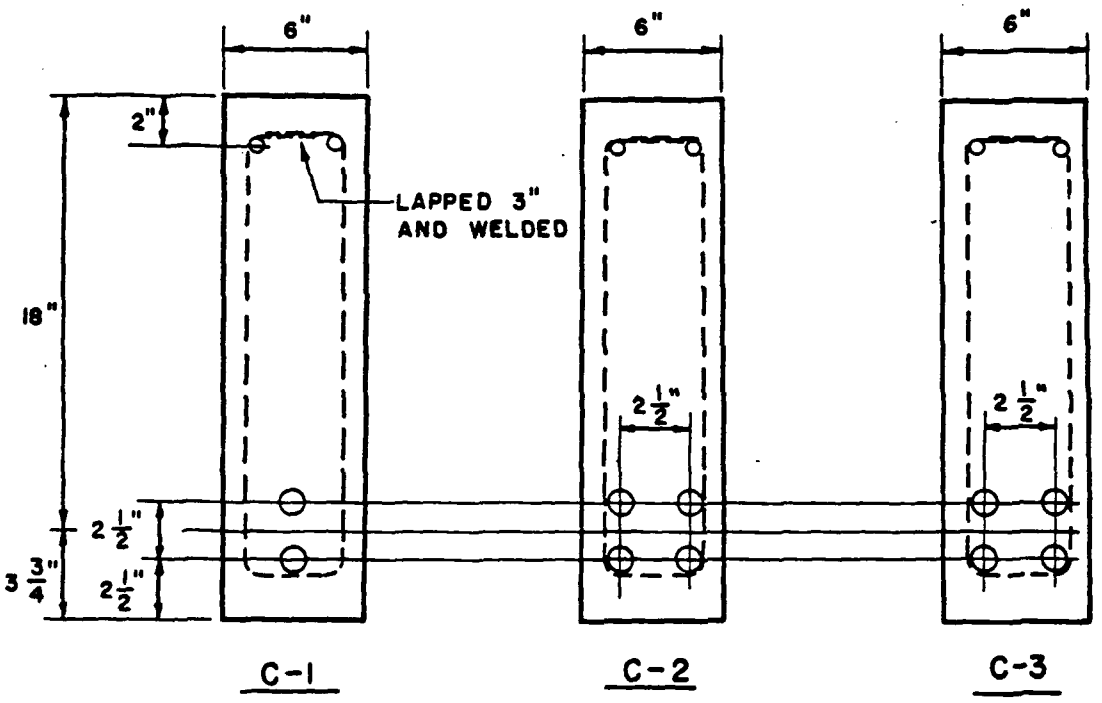

Figure B-2. Detailing of Beams: Group 2.

(concluded)

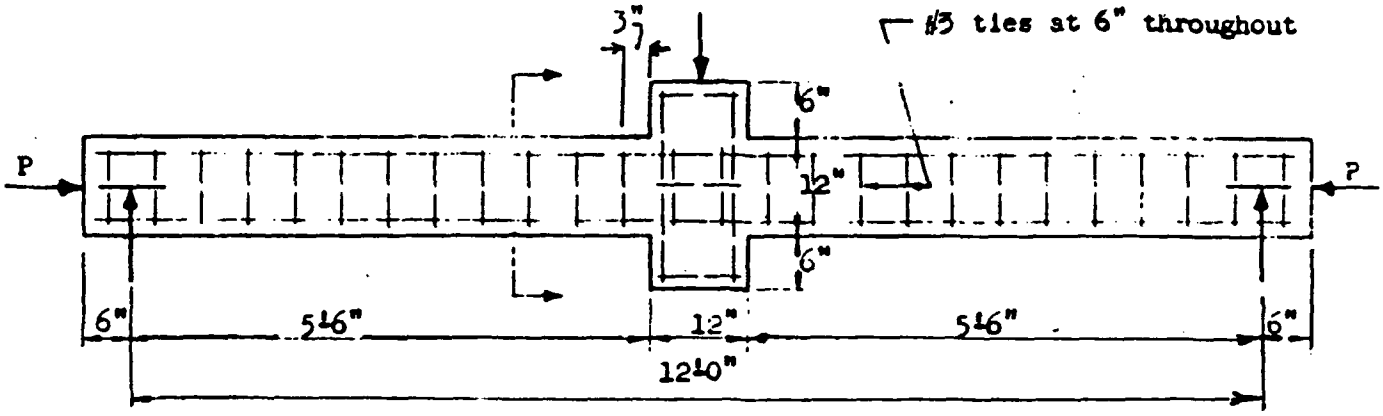

(a) Specimens J-15, J-16, J-24 through J-31

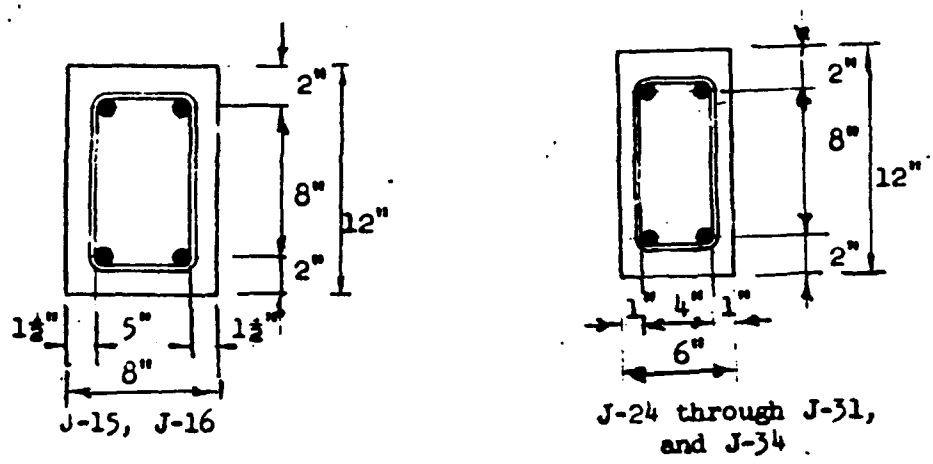

Figure B-3. Detailing of Beam-Columns: Group 3

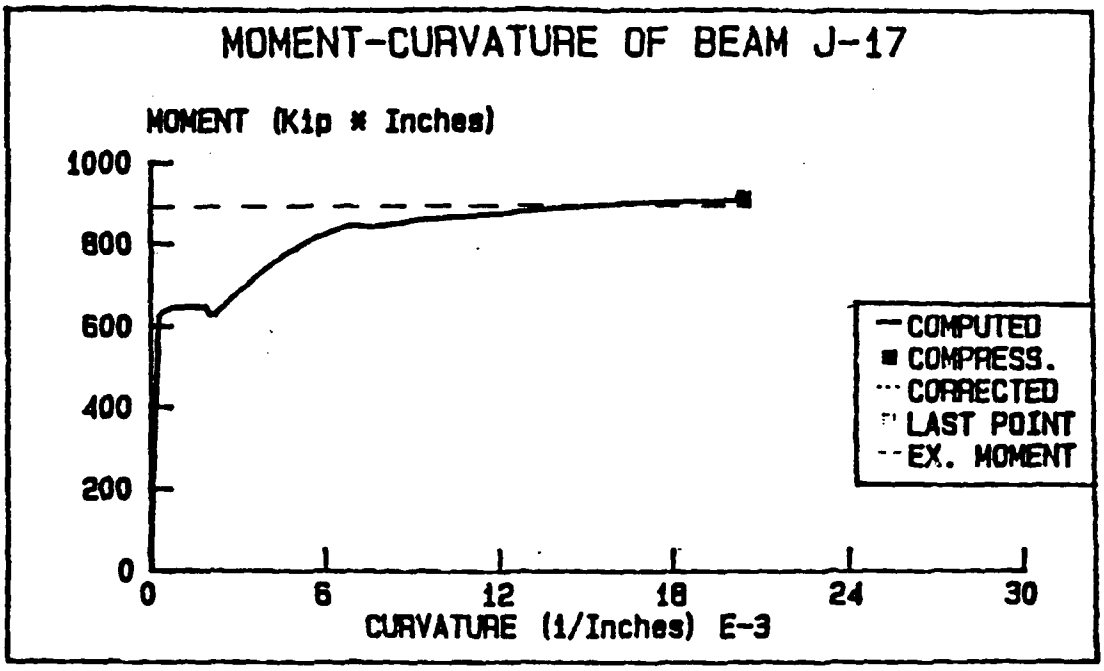

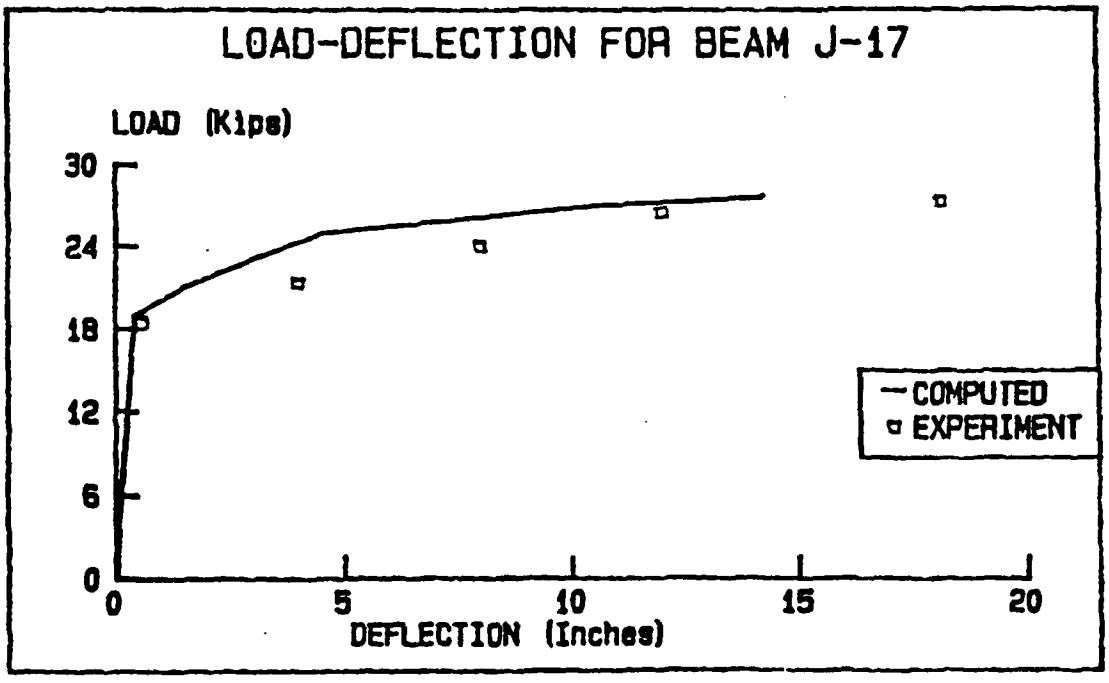

Figure B-4. Moment-Curvature and Load-Deflection Relationships Beam J17

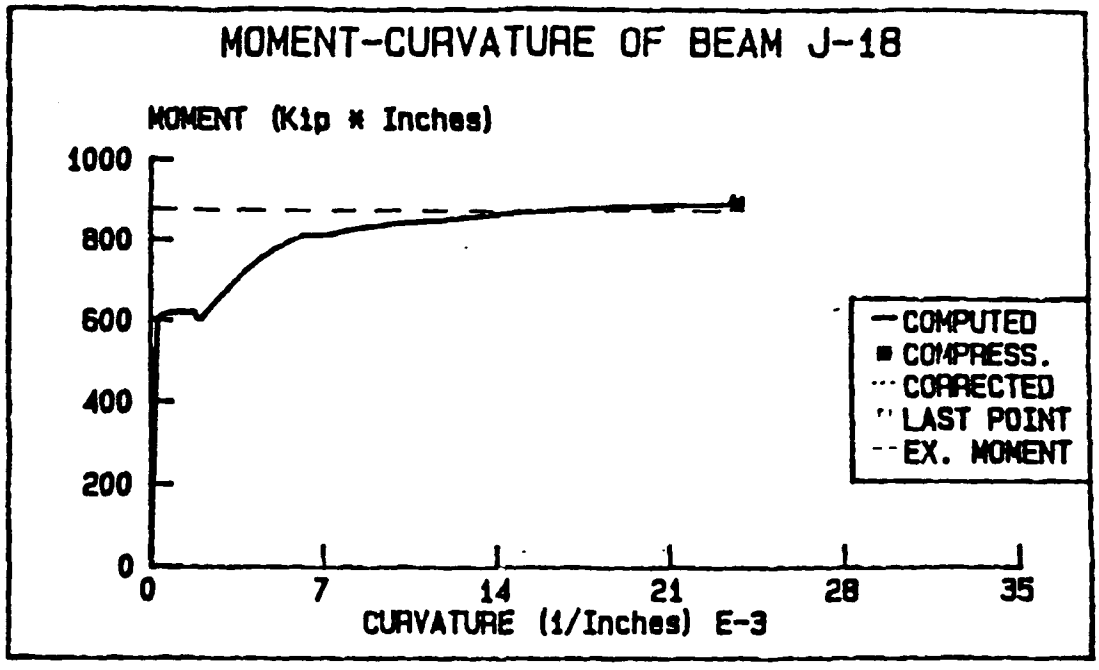

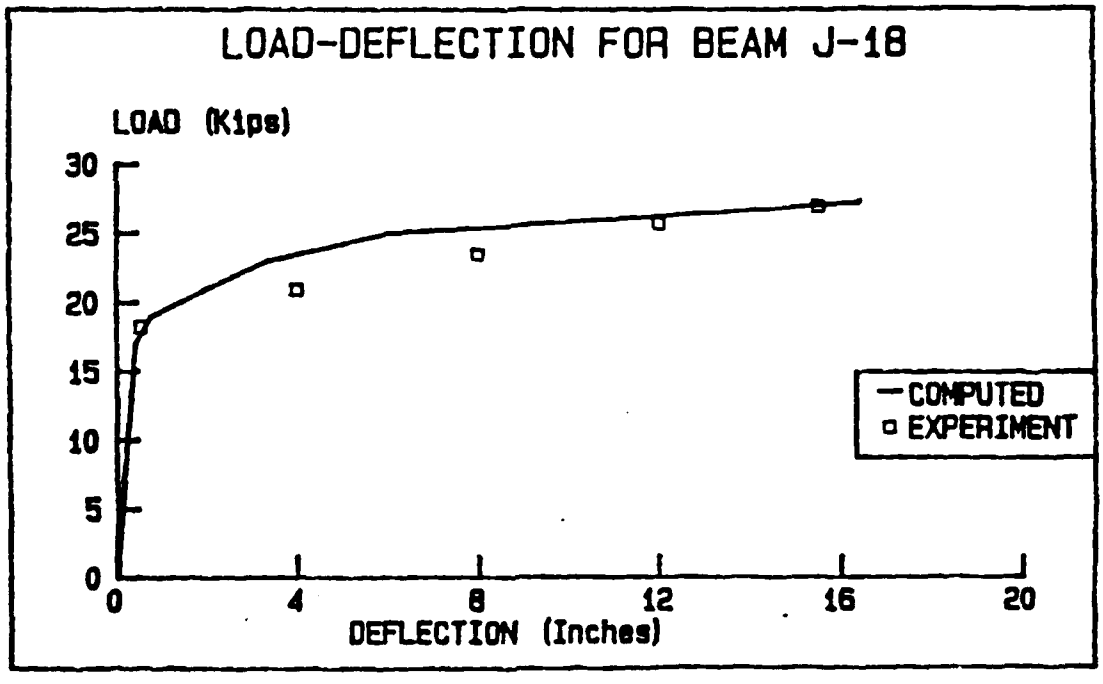

Figure B-5. Moment-Curvature and Load-Deflection Relationships Beam J18

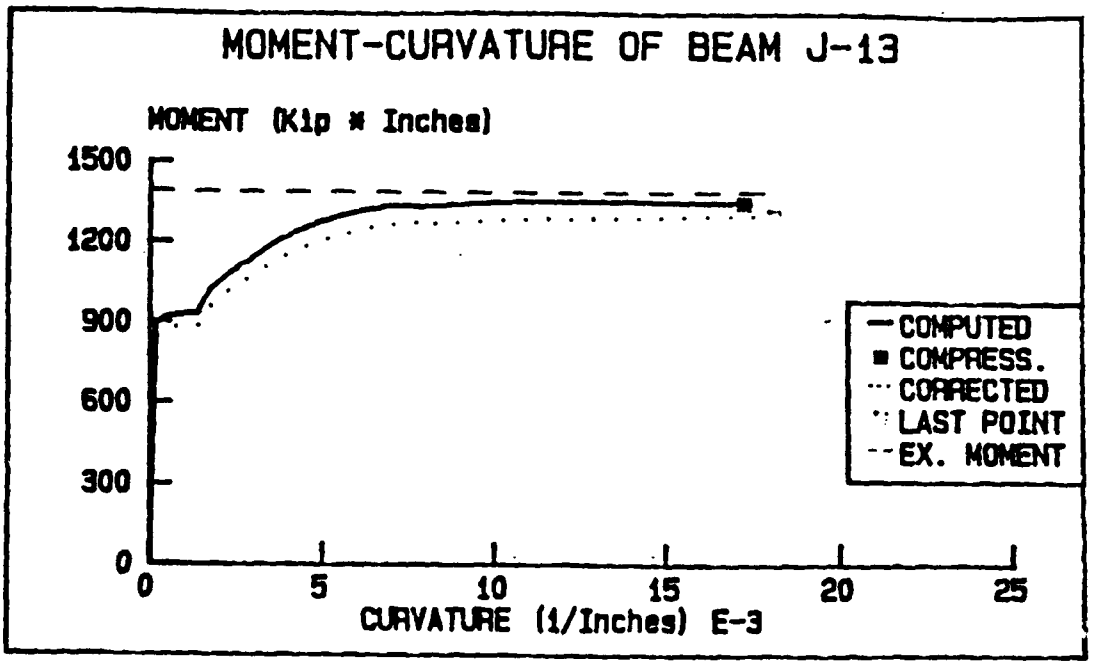

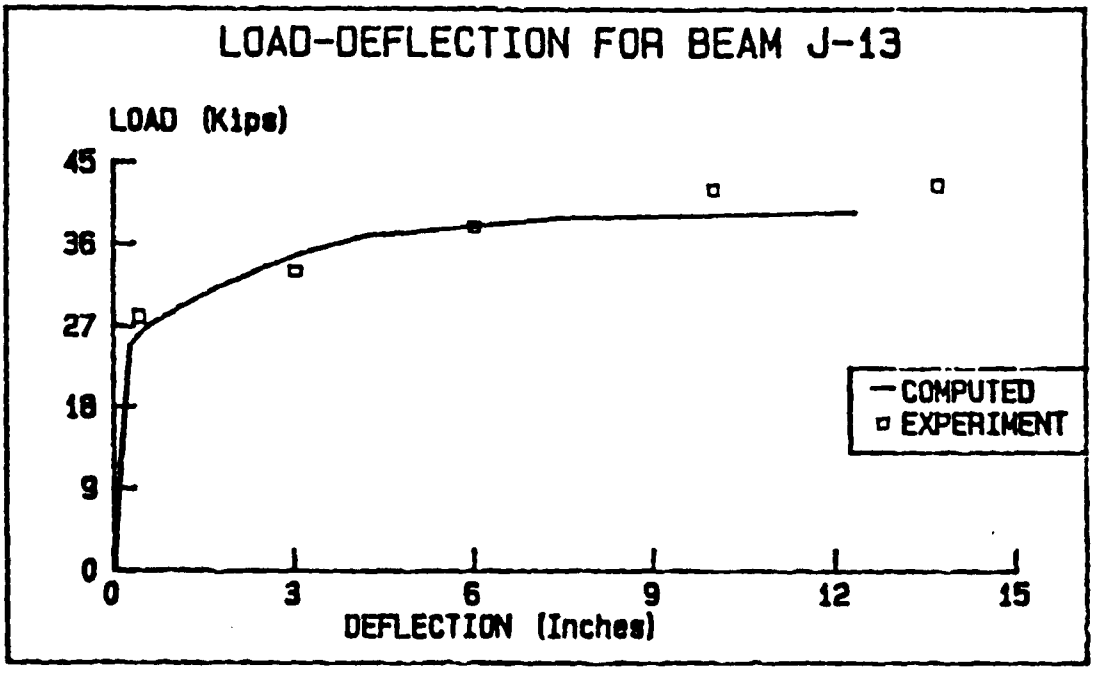

Figure B-6. Moment-Curvature and Load-Deflection Relationships Beam J13

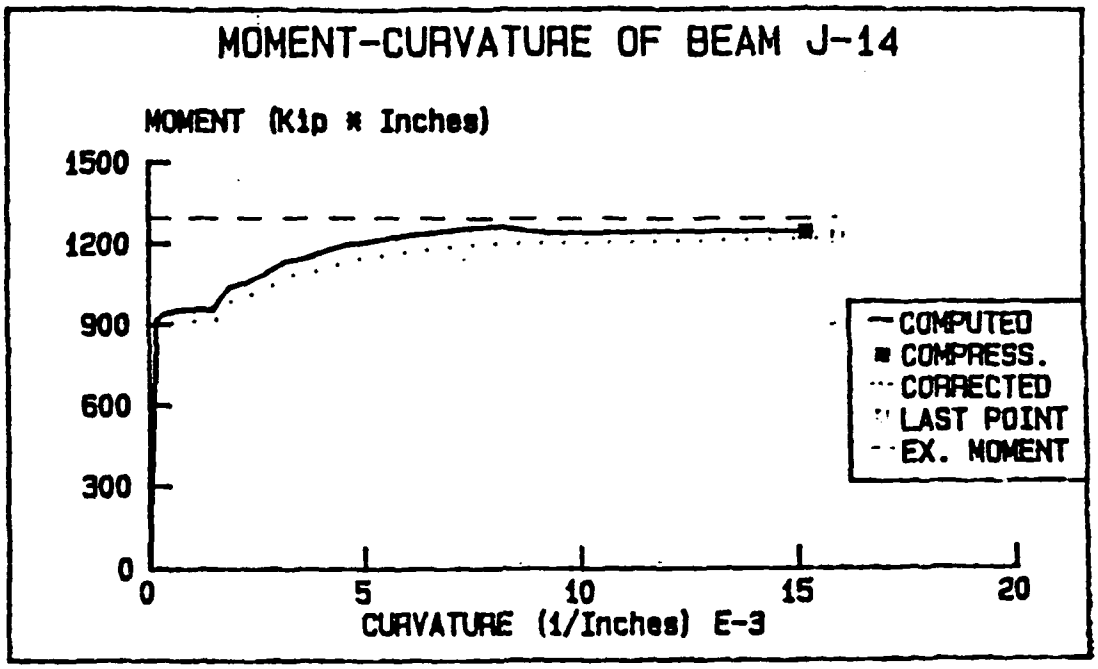

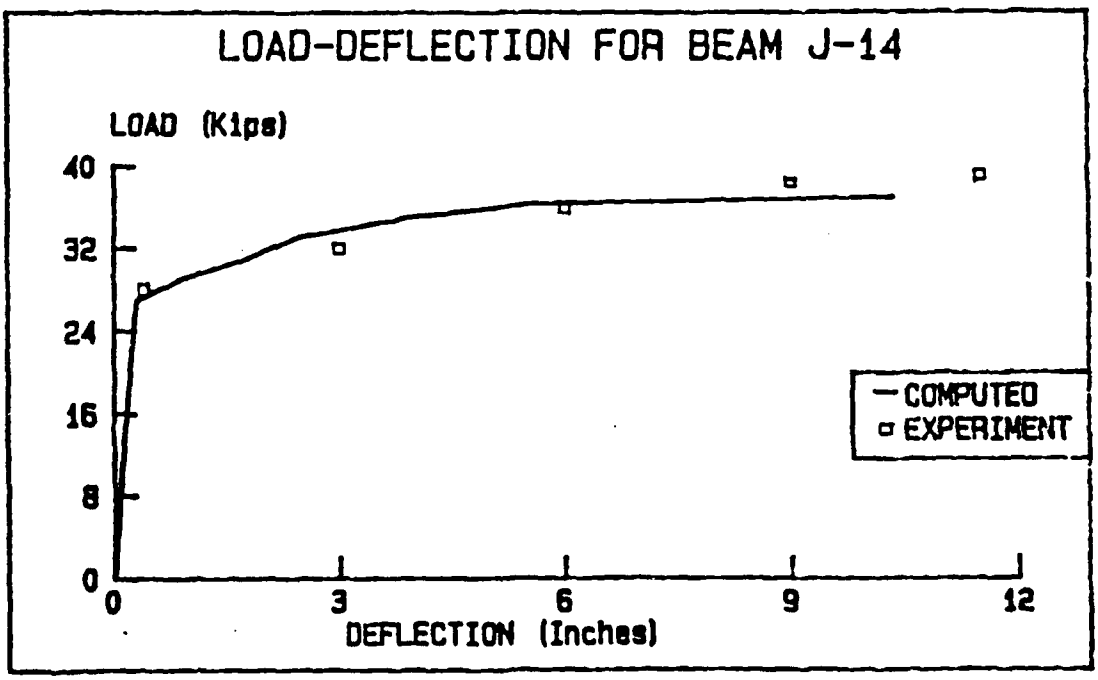

Figure B-7. Moment-Curvature and Load-Deflection Relationships Beam J14

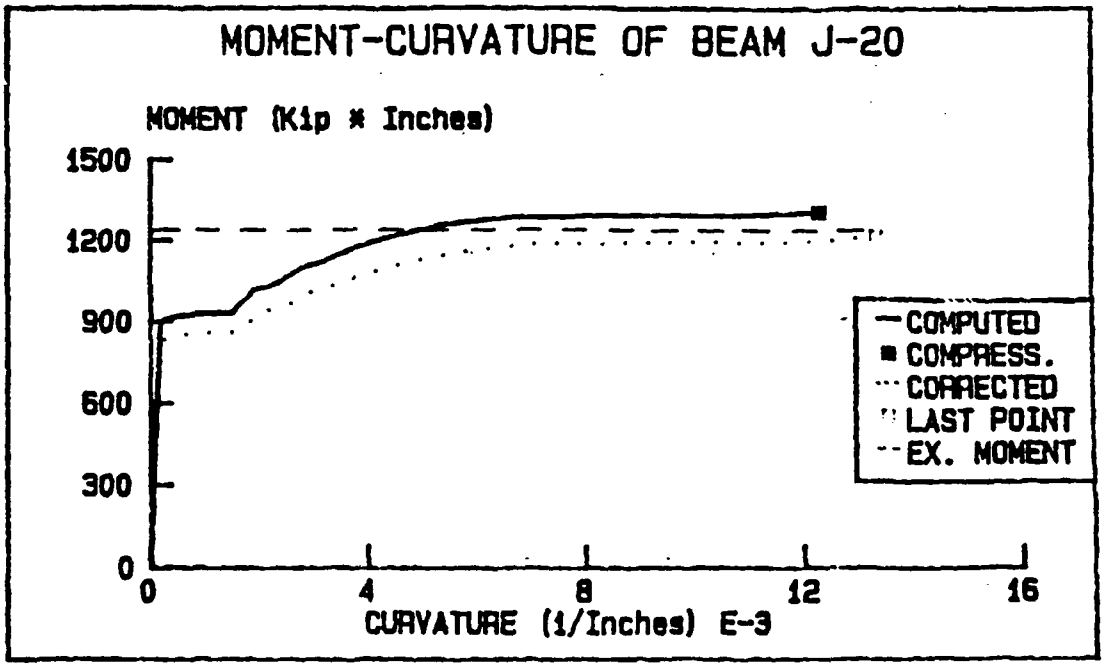

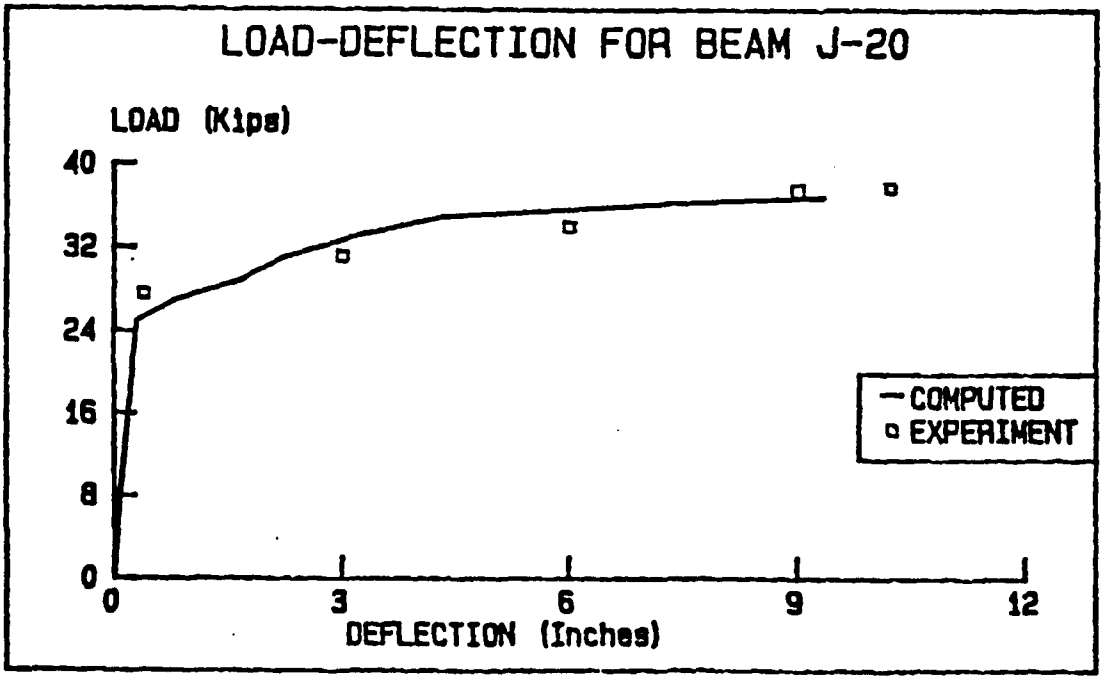

Figure B-8. Moment-Curvature and Load-Deflection Relationships Beam J20

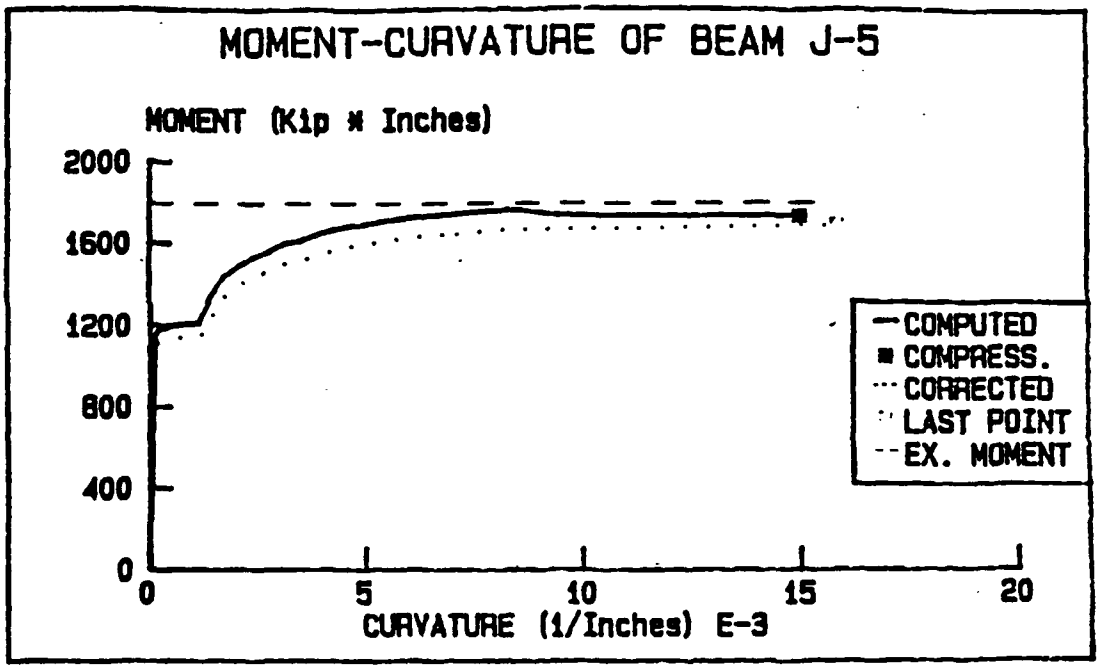

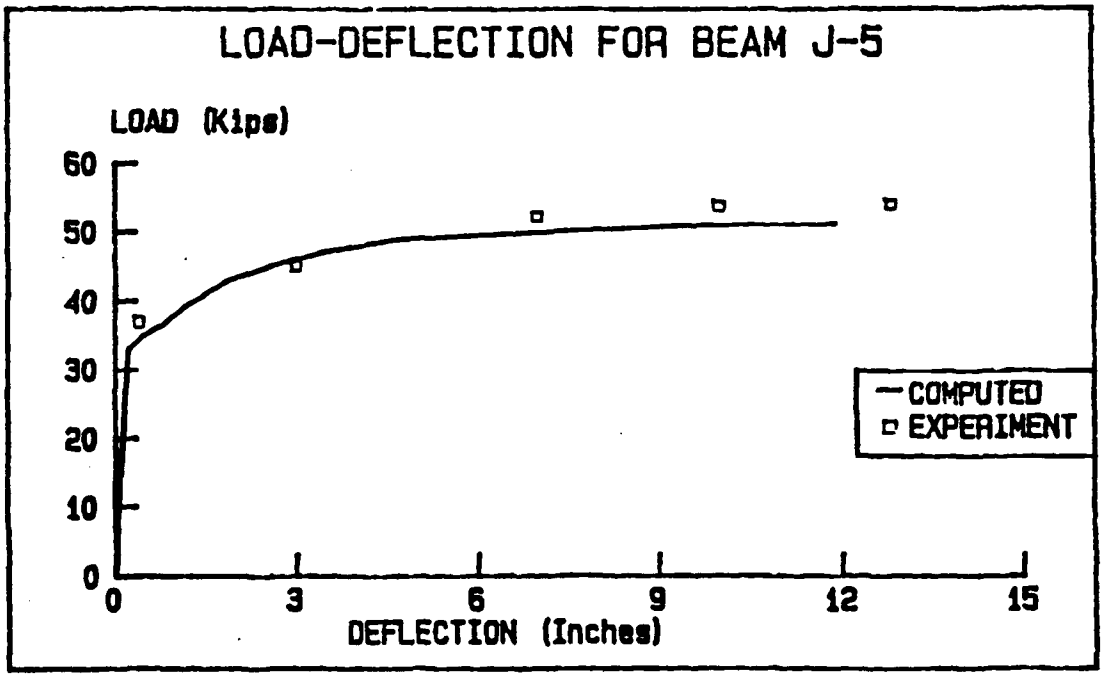

Figure B-9. Moment-Curvature and Load-Deflection Relationships Beam J5

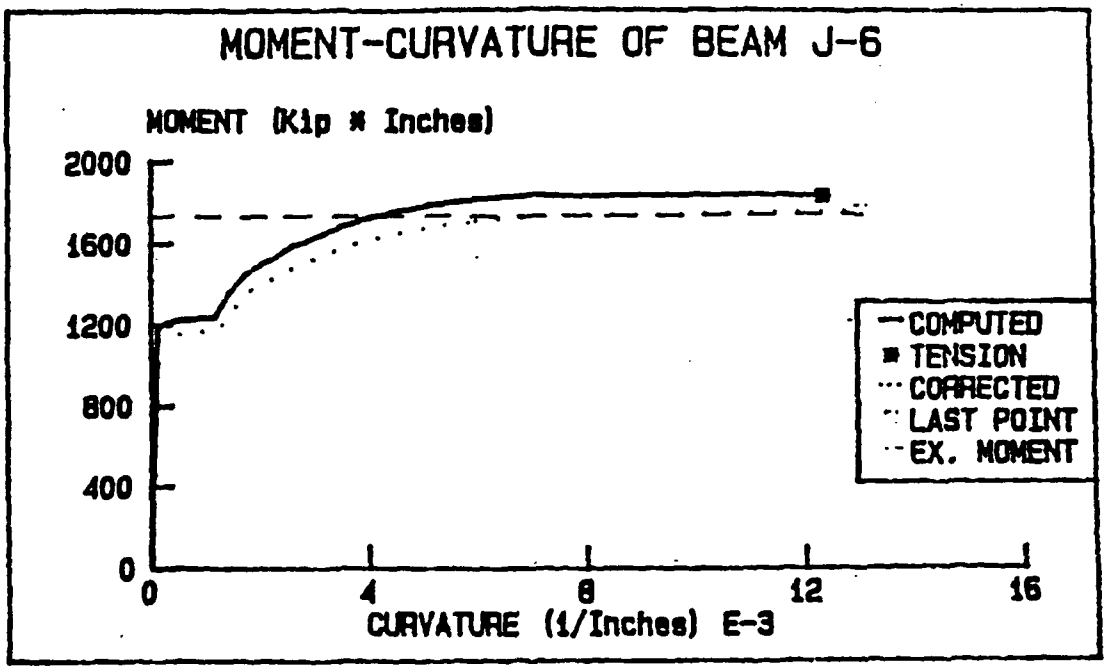

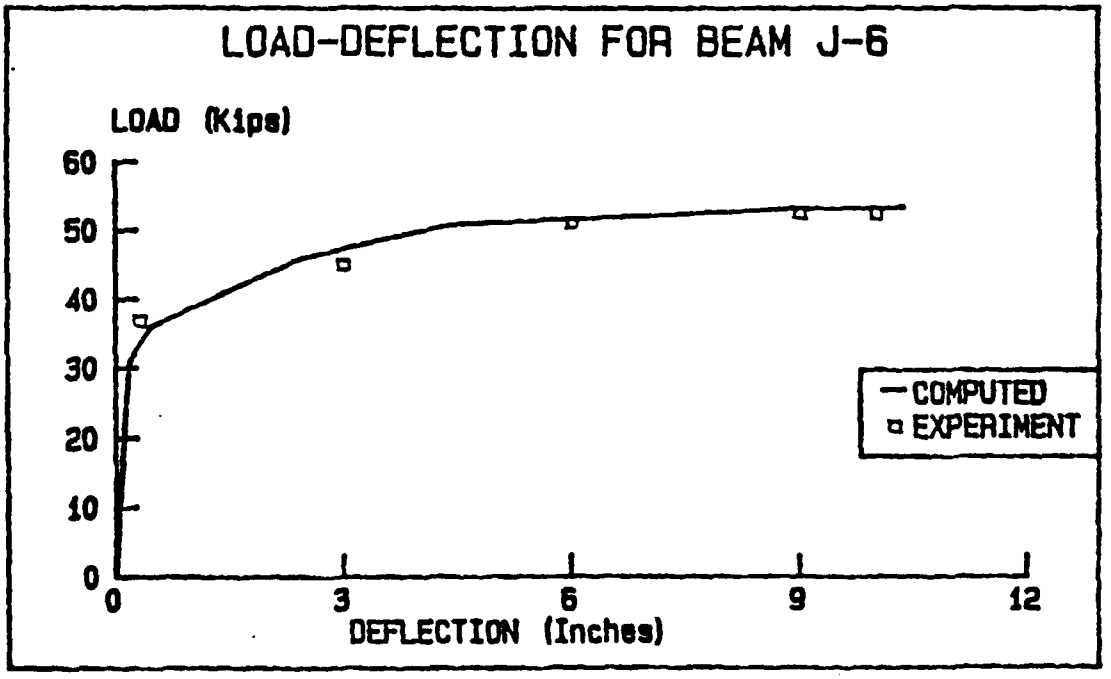

Figure B-10. Moment-Curvature and Load-Deflection Relationships Beam J6

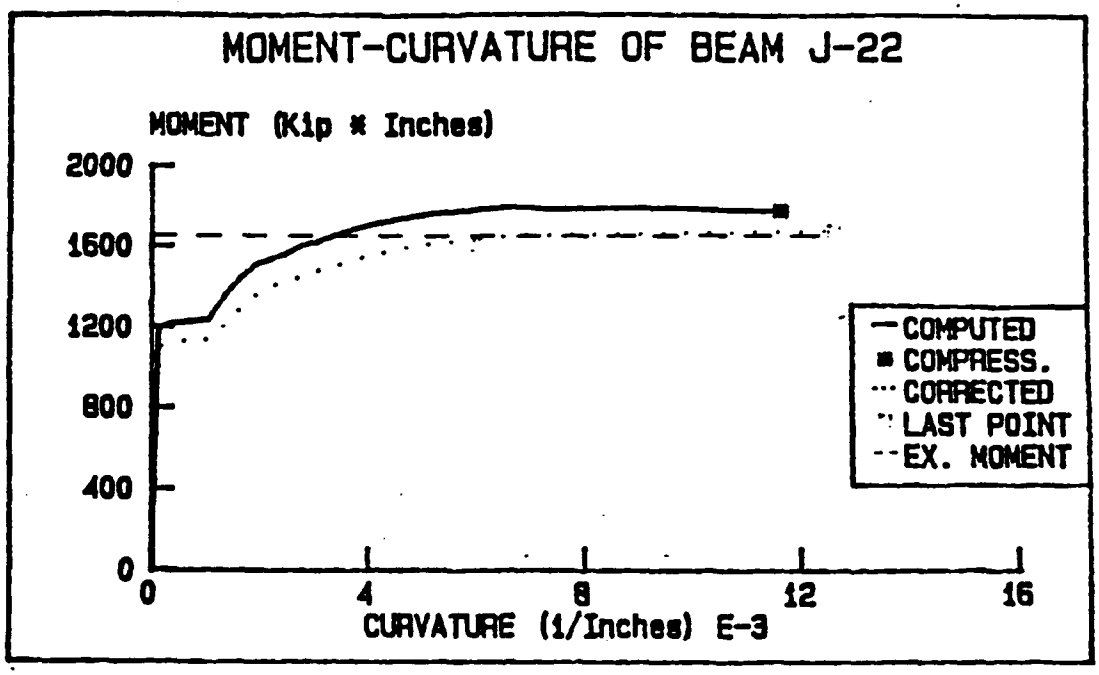

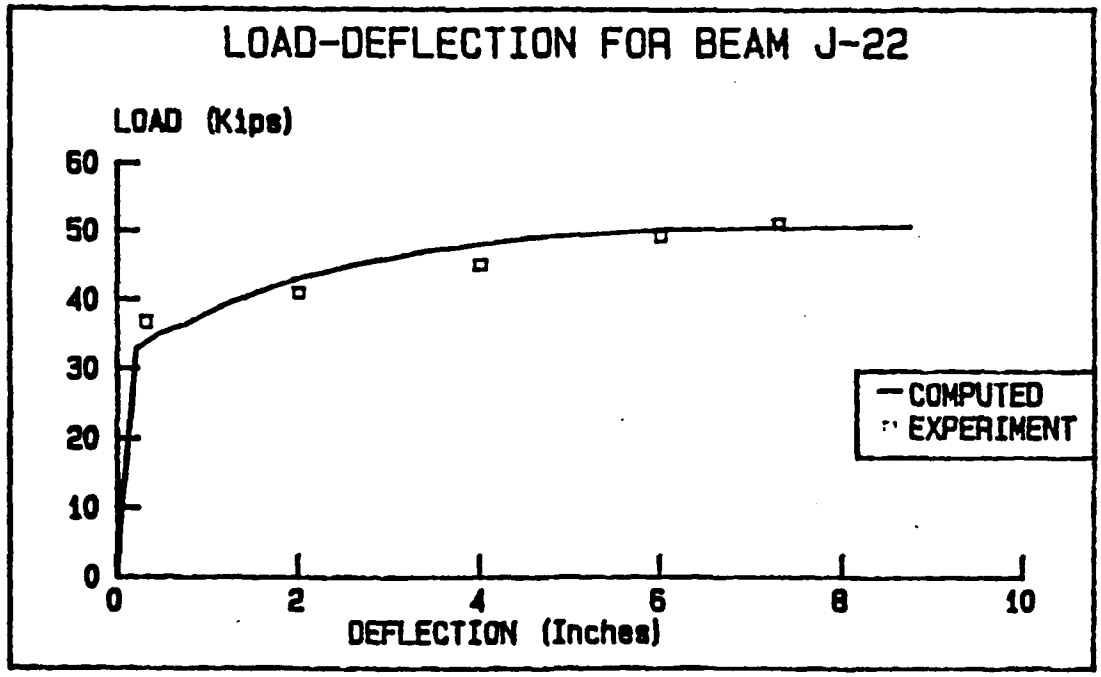

Figure B-11. Moment-Curvature and Load-Deflection Relationships Beam J22

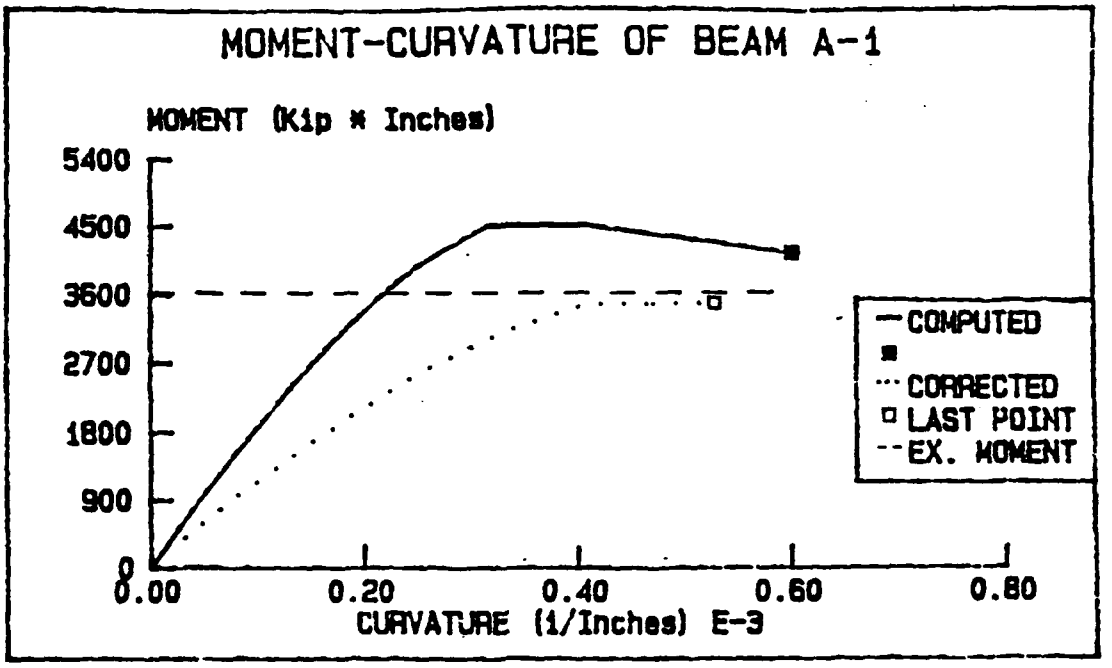

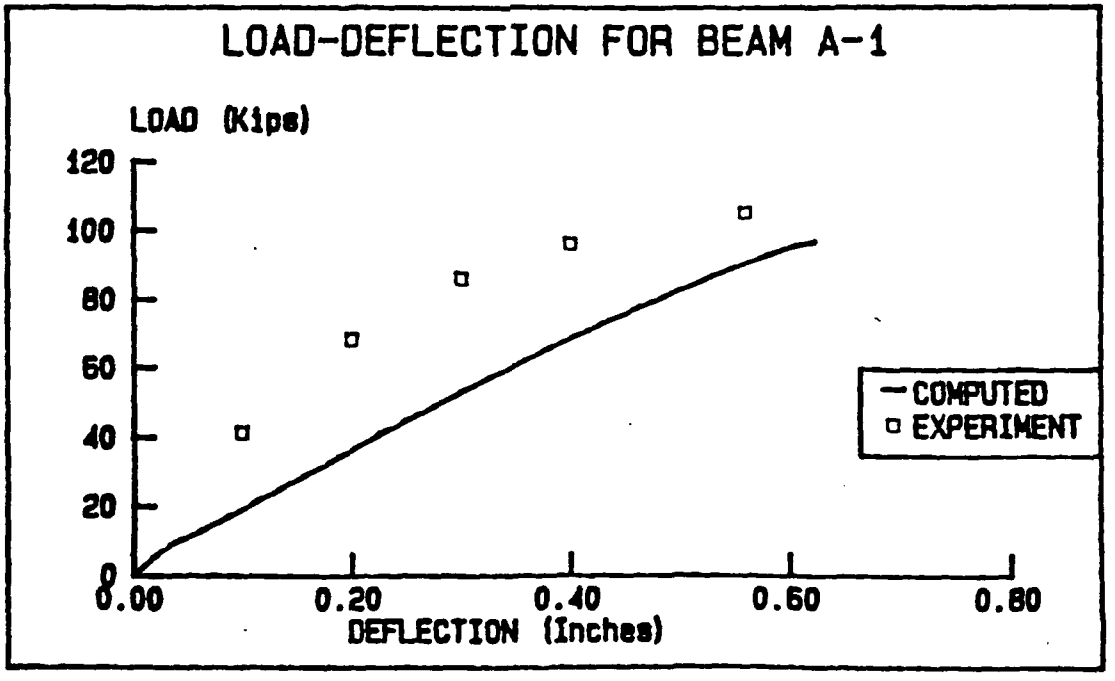

Figure B-12.Moment-Curvature and Load-Deflection Relationships Beam A1

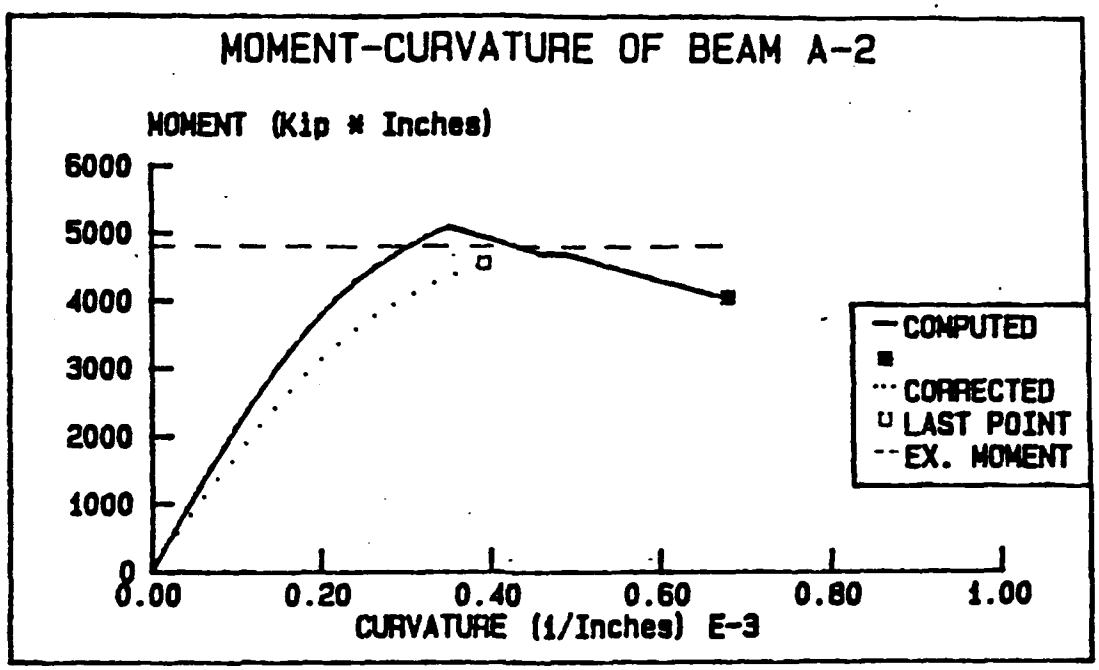

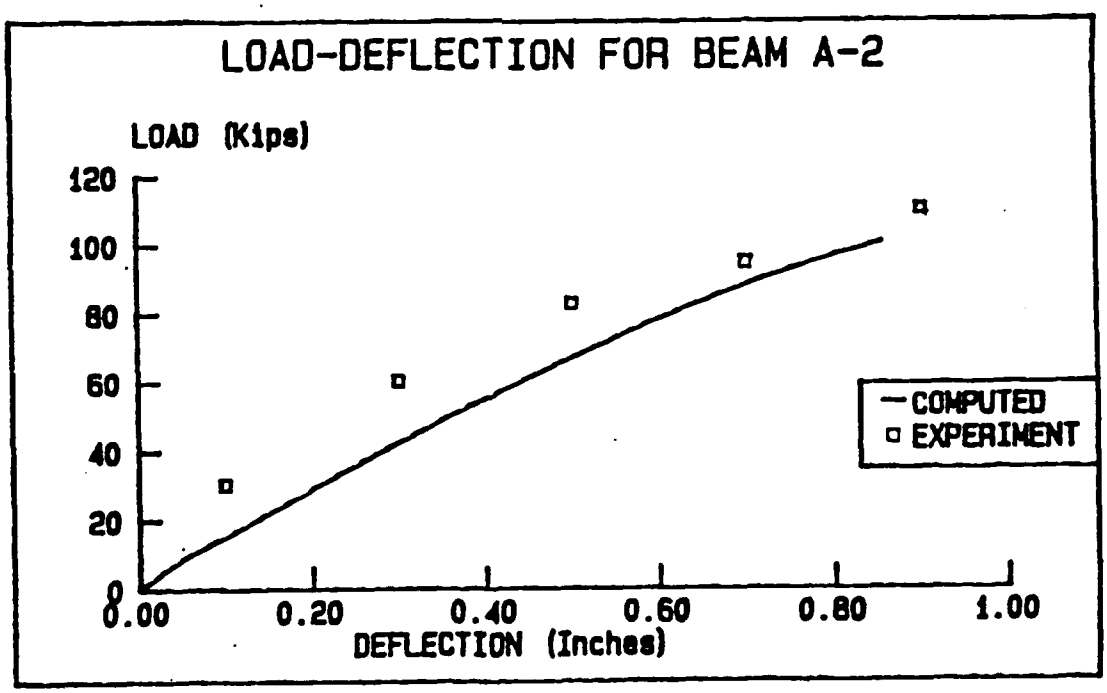

Figure B-13. Moment-Curvature and Load-Deflection Relationships Beam A2

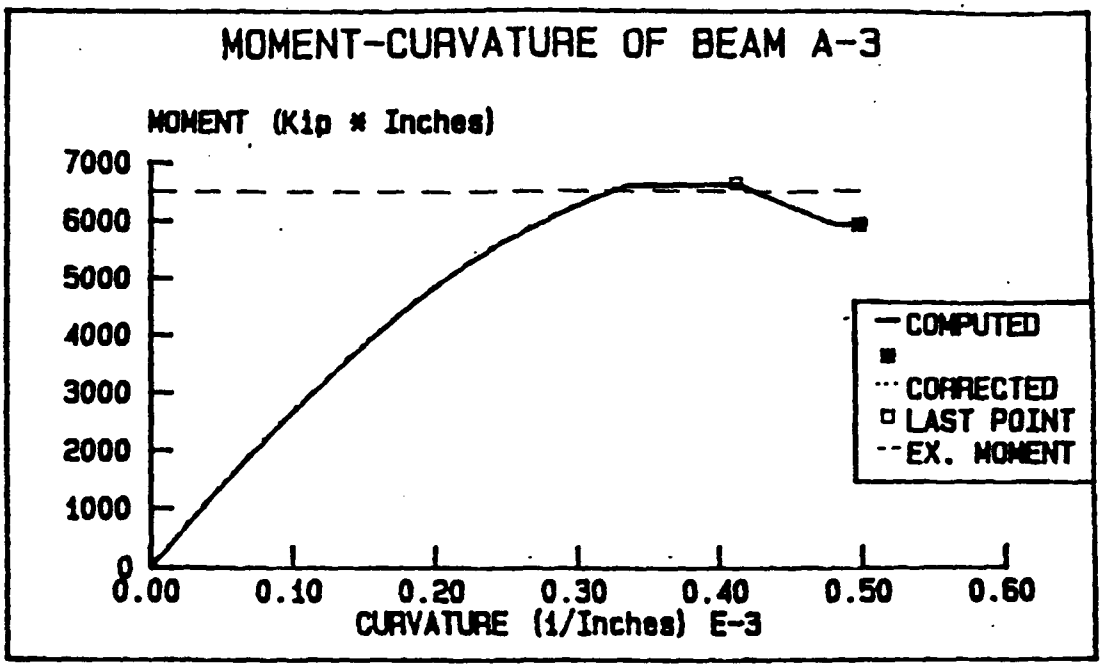

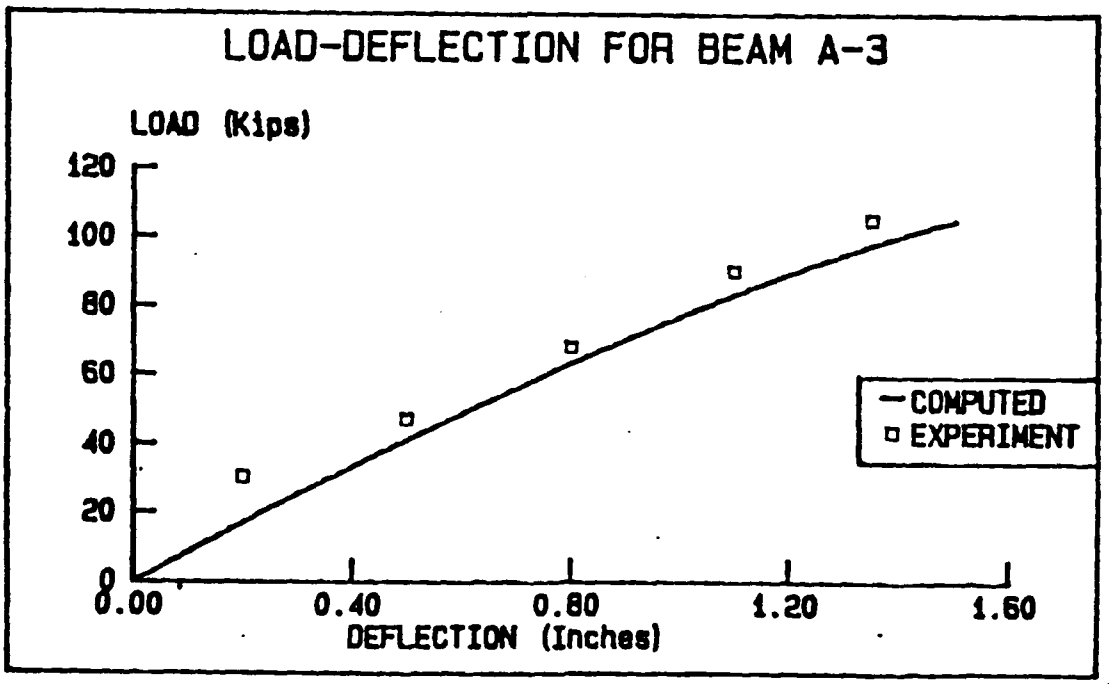

Figure B-14. Moment-Curvature and Load-Deflection Relationships Beam A3

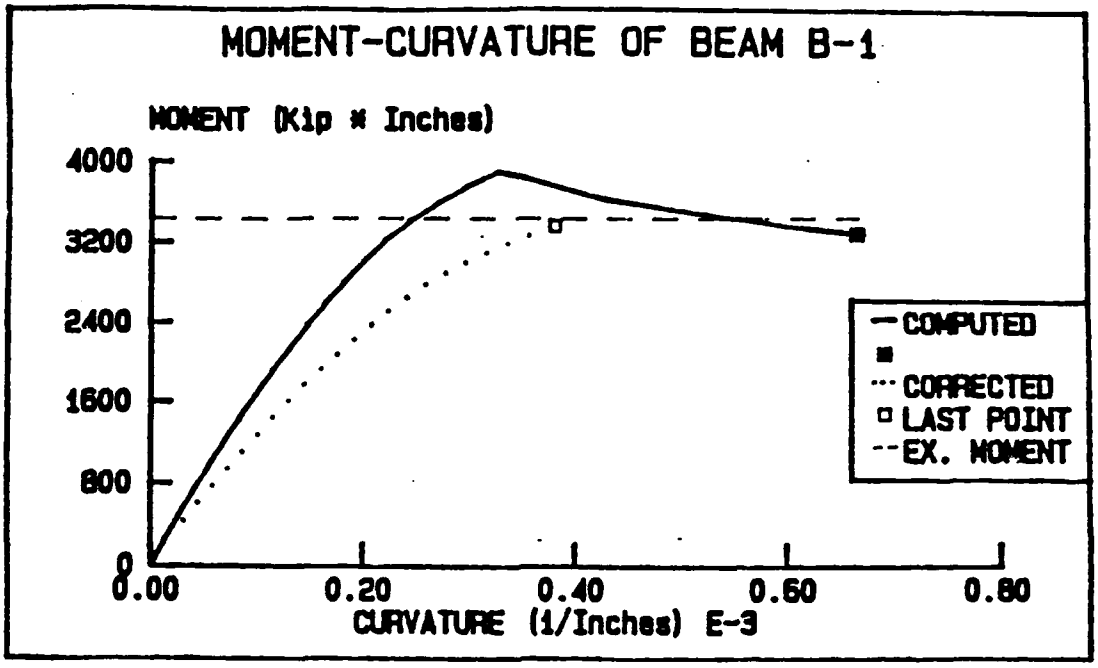

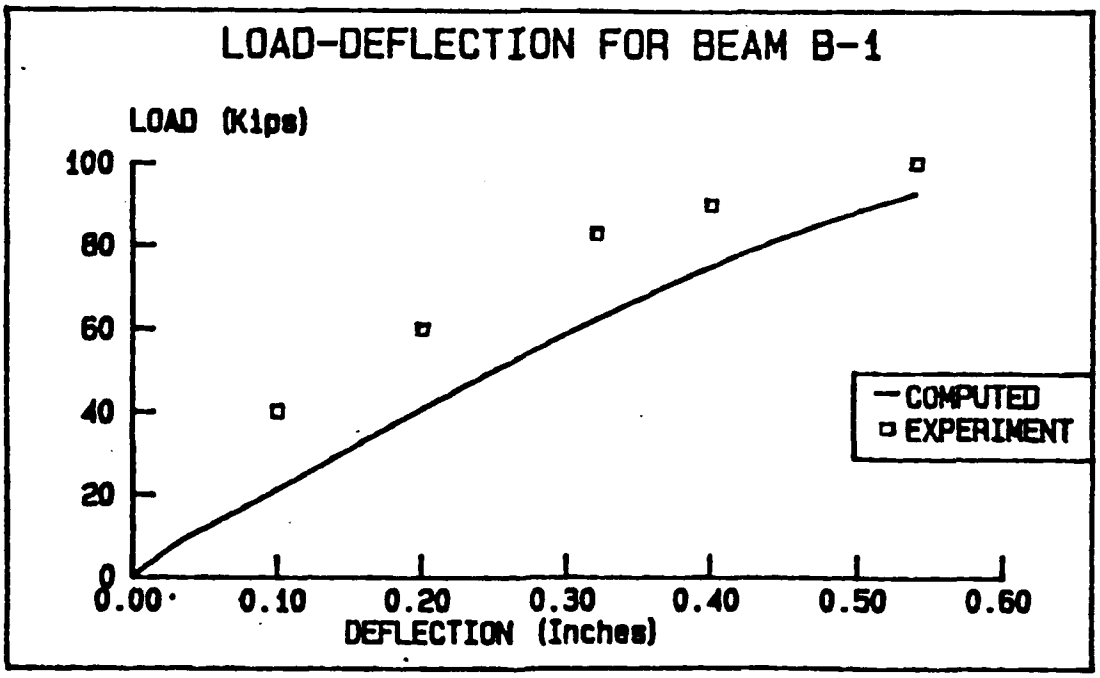

Figure B-15. Moment-Curvature and Load-Deflection Relationships Beam B1

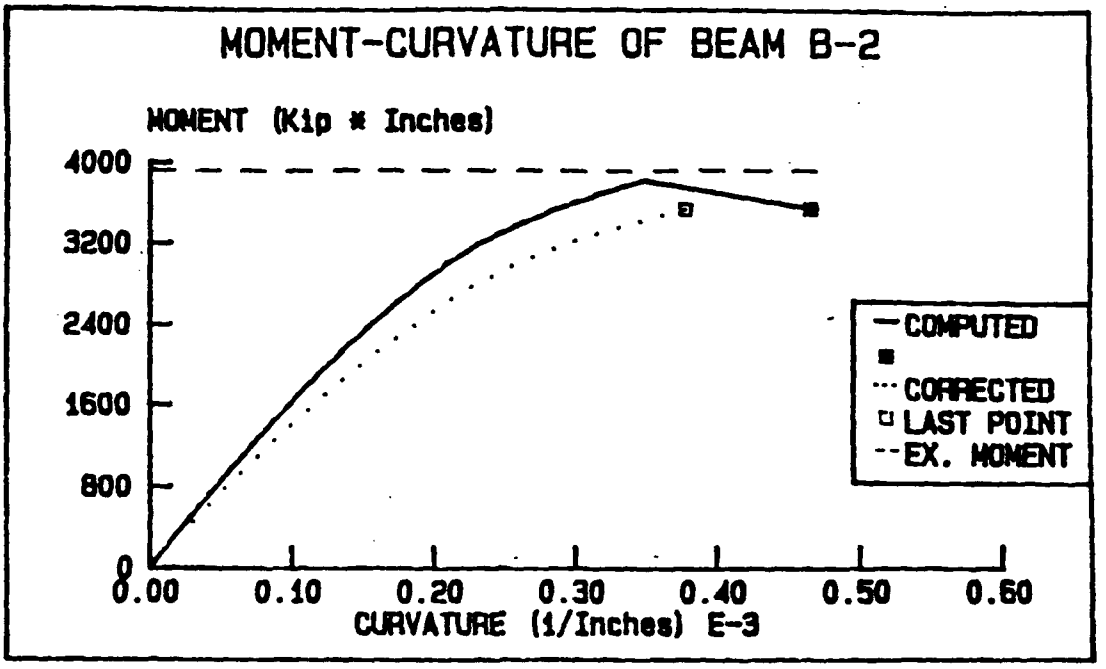

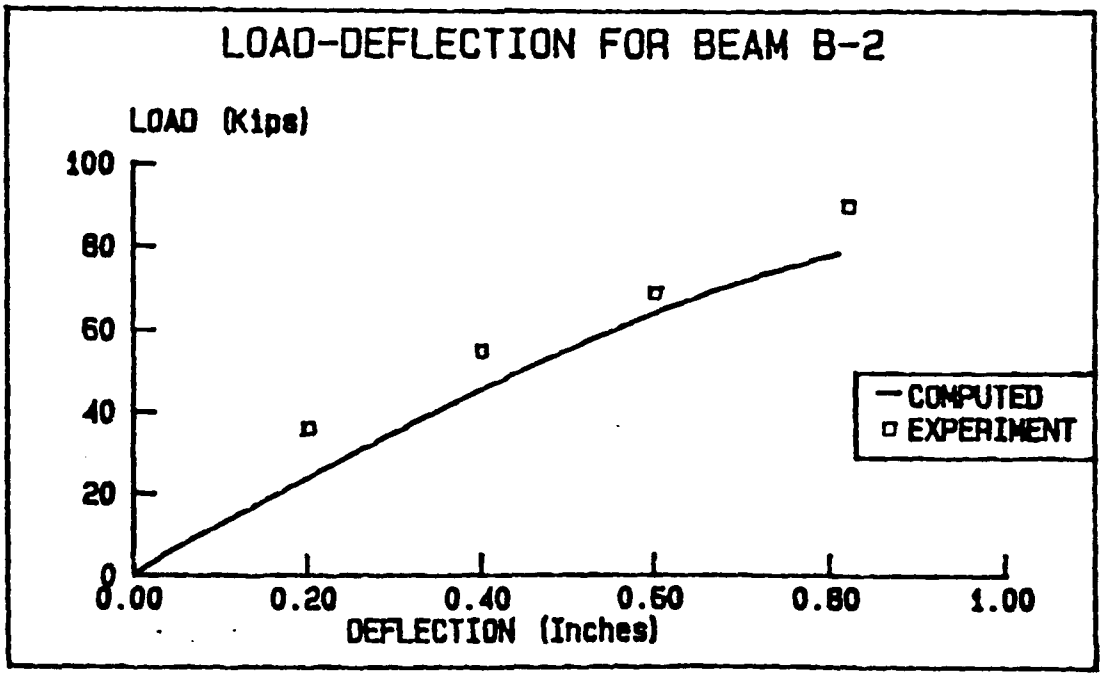

Figure B-16. Moment-Curvature and Load-Deflection Relationships Beam B2

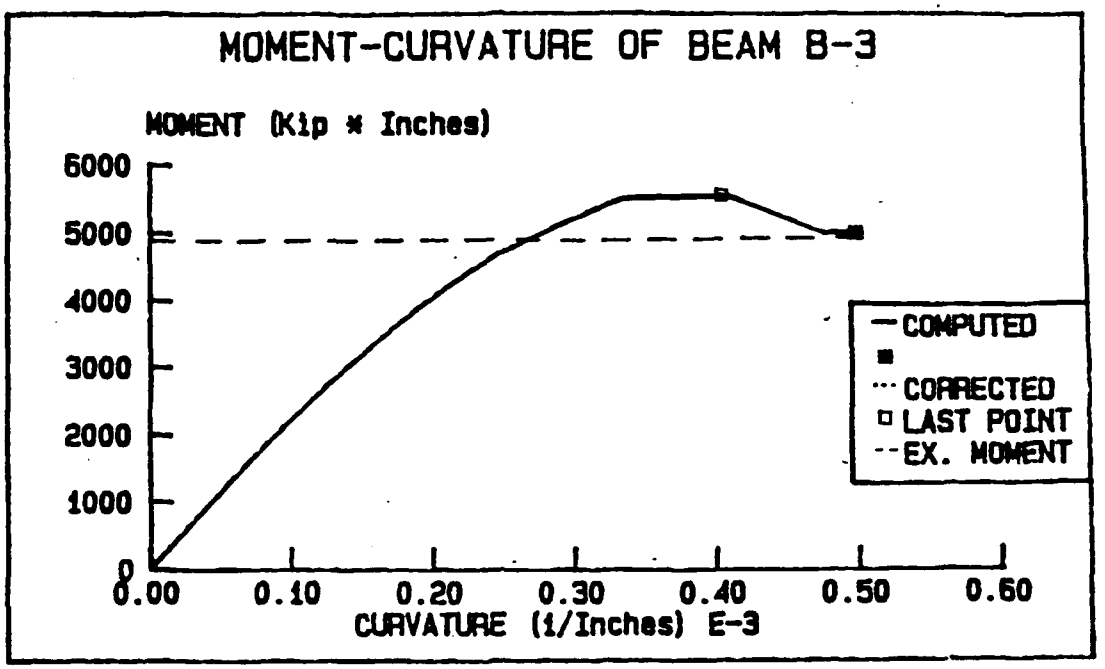

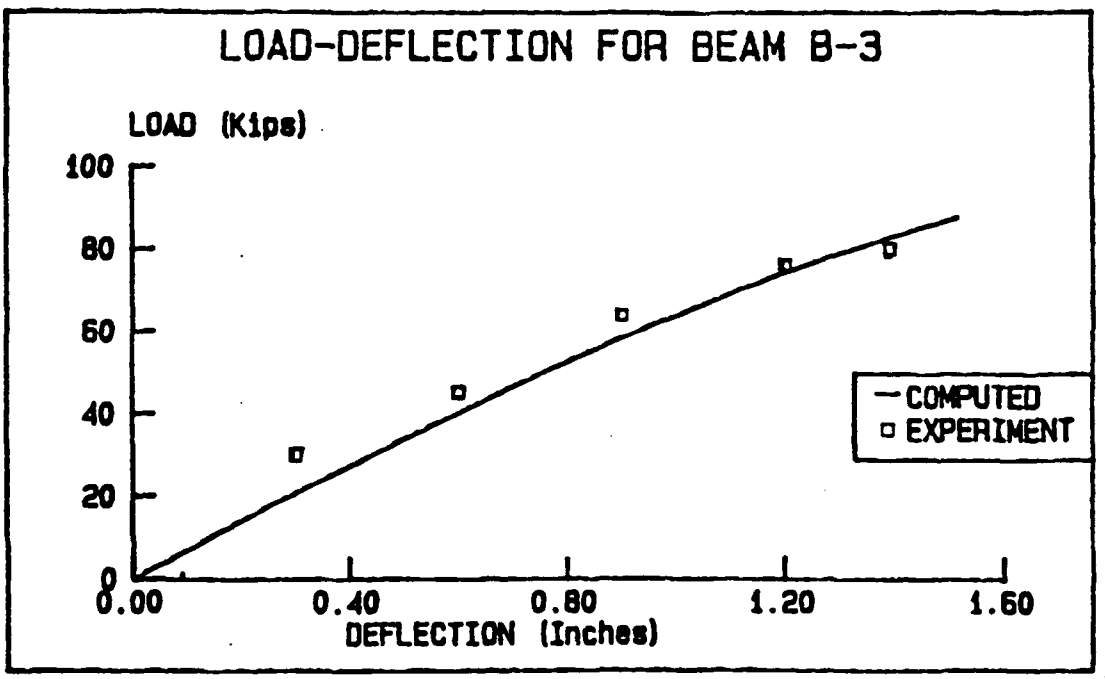

Figure B-17. Moment-Curvature and Load-Deflection Relationships Beam B3

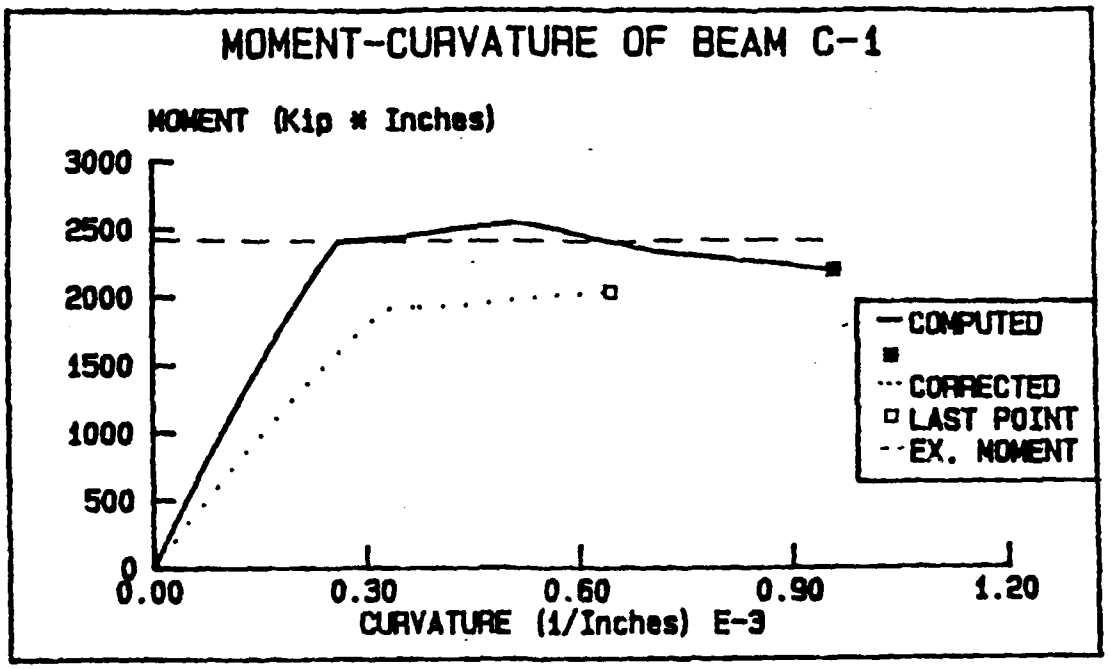

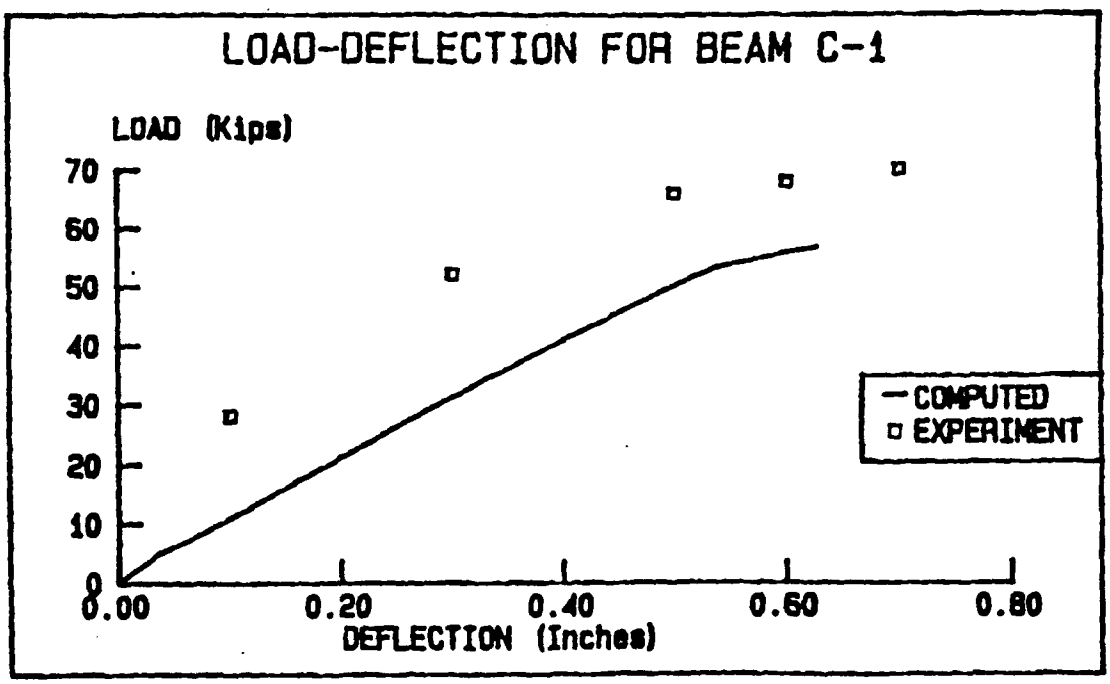

Figure B-18. Moment-Curvature and Load-Deflection Relationships Beam C1

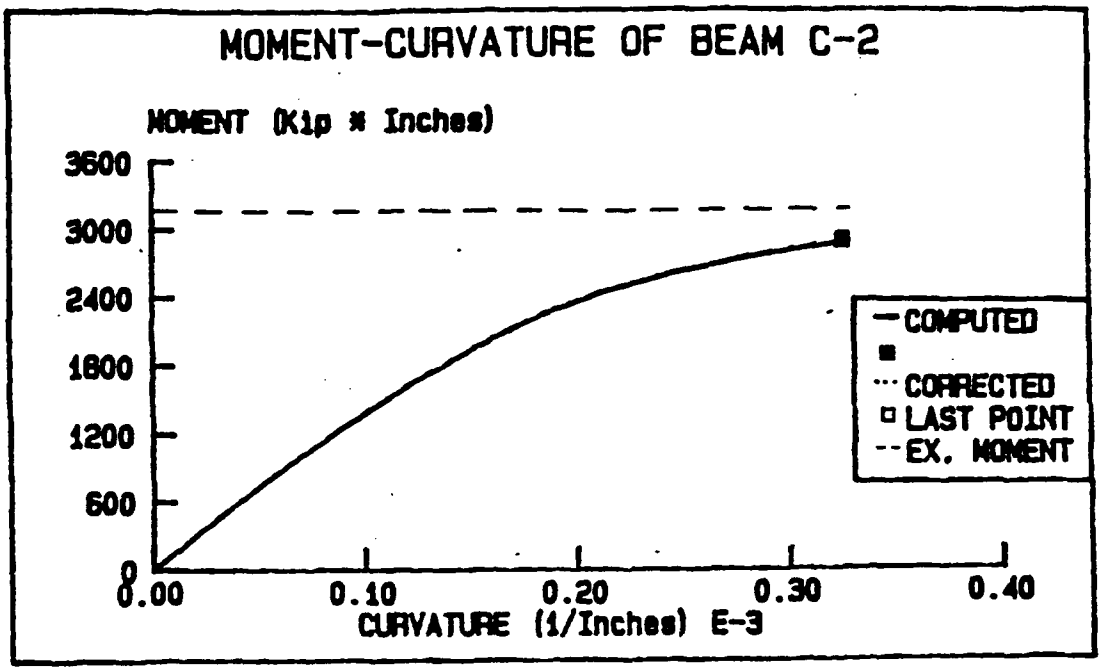

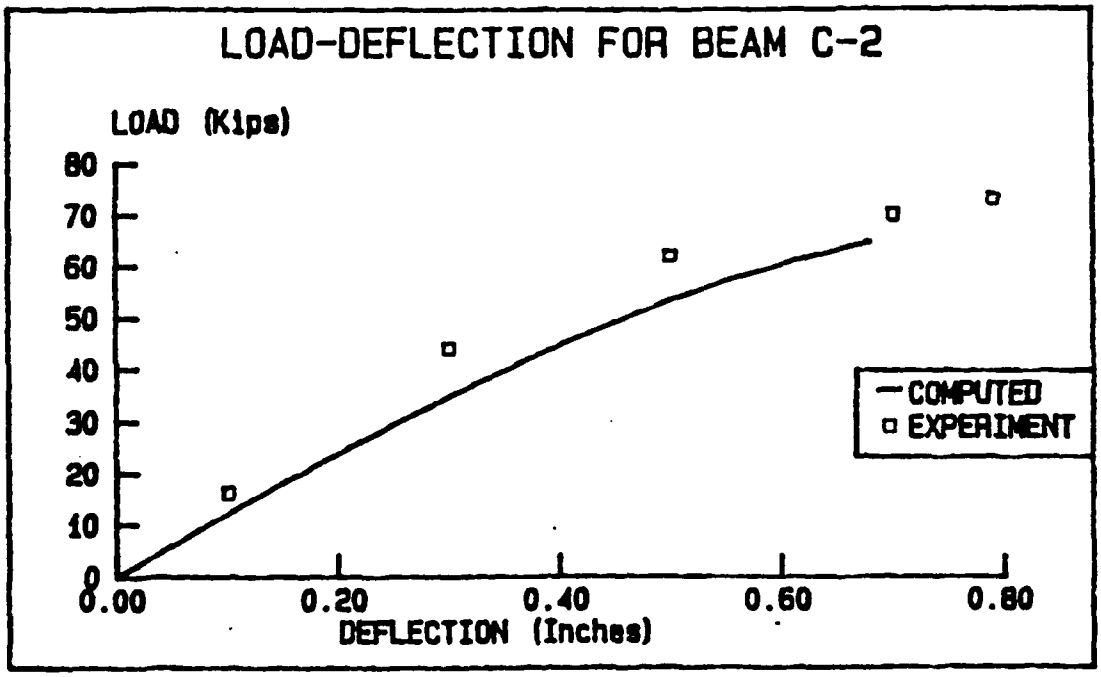

Figure B-19. Moment-Curvature and Load-Deflection Relationships Beam C2

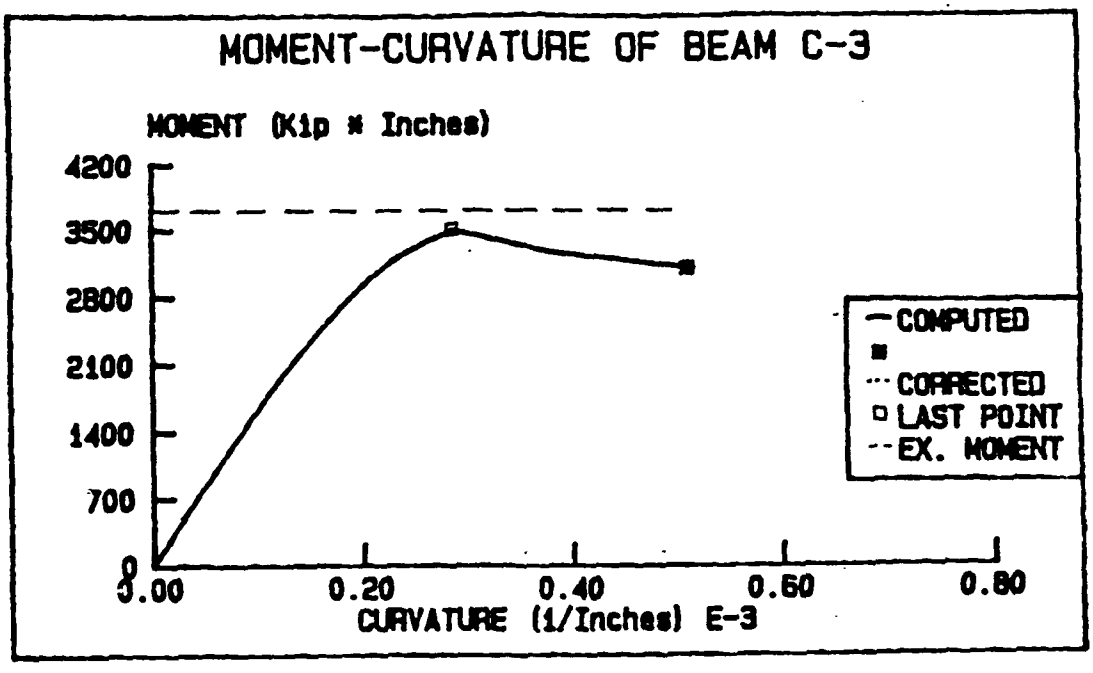

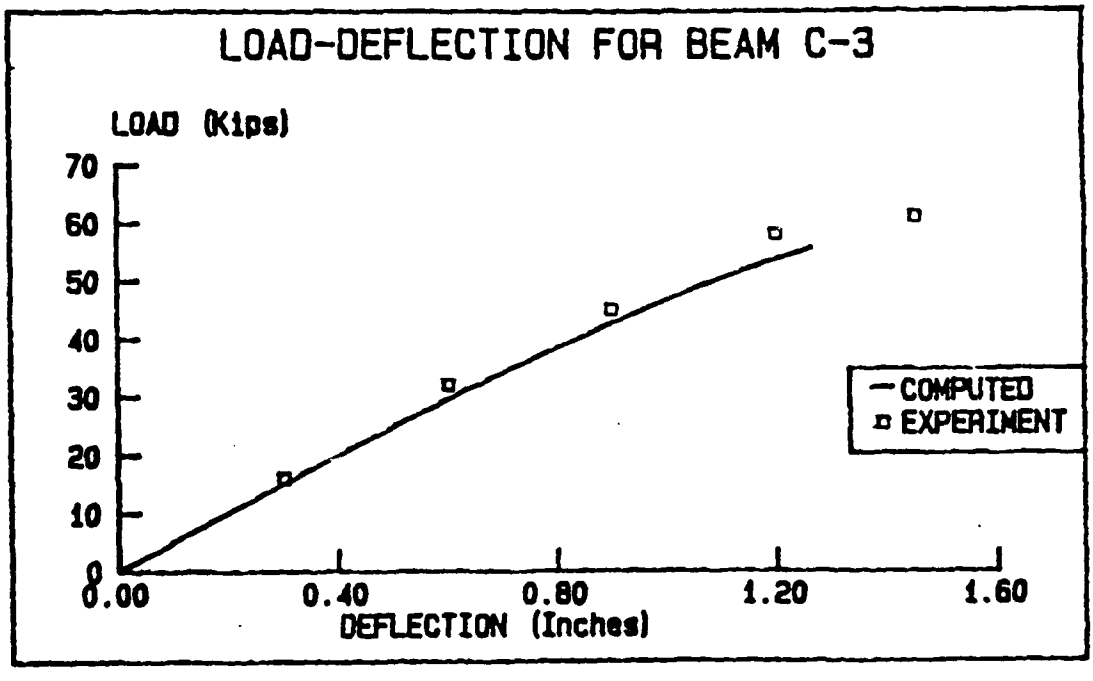

Figure B-20. Moment-Curvature and Load-Deflection Relationships Beam C3

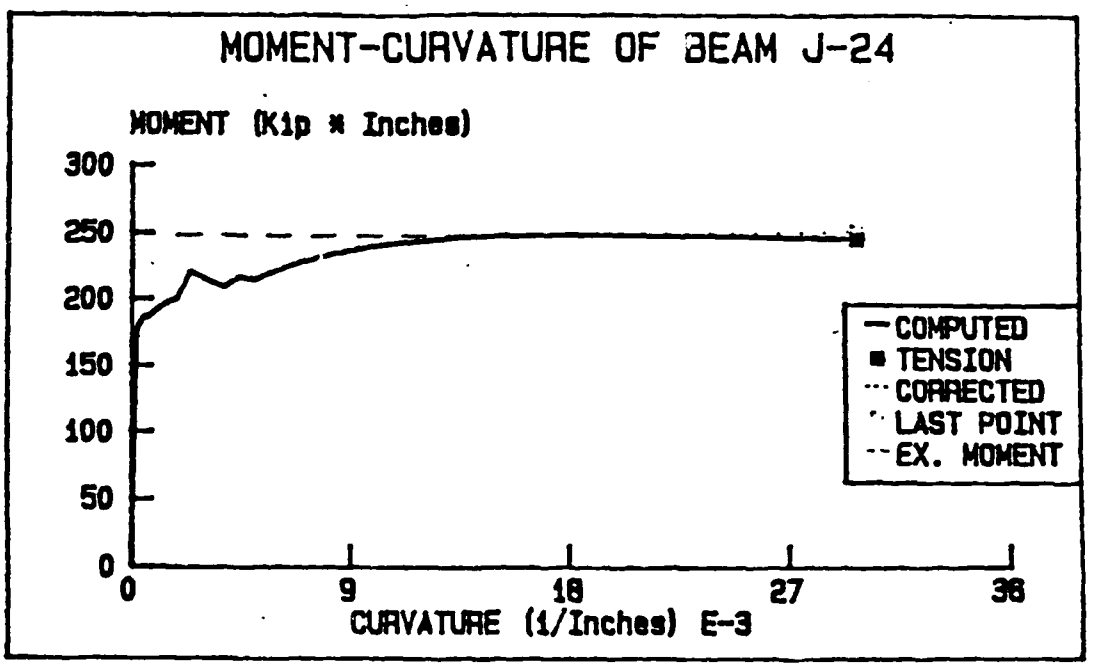

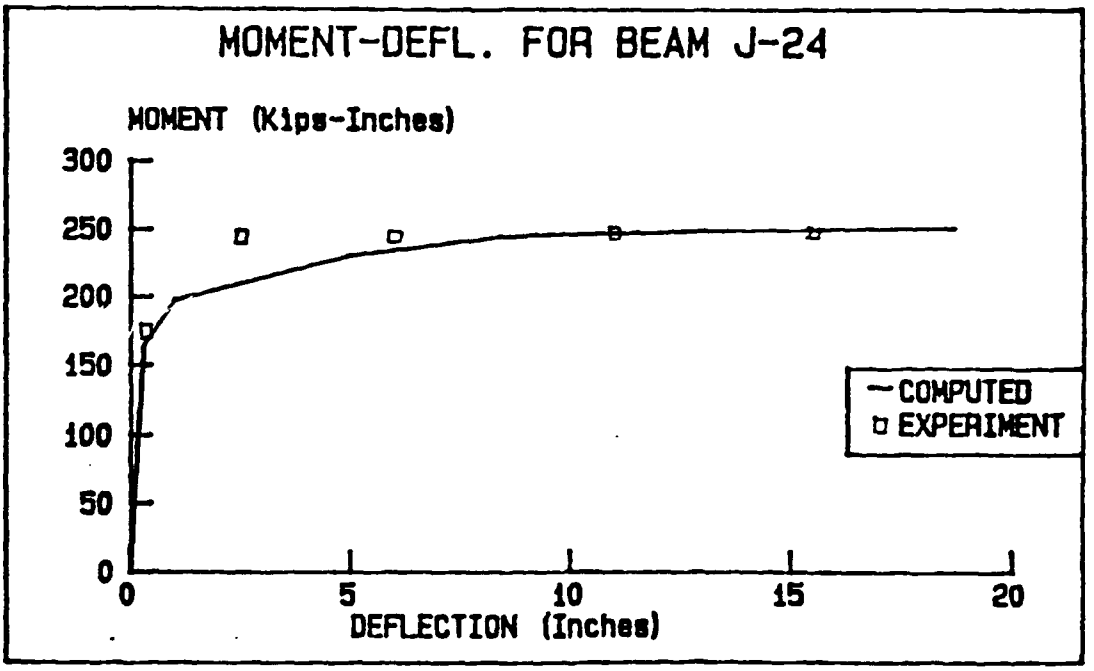

Figure B-21 Moment-Curvature and Load-Deflection Relationships Beam J24

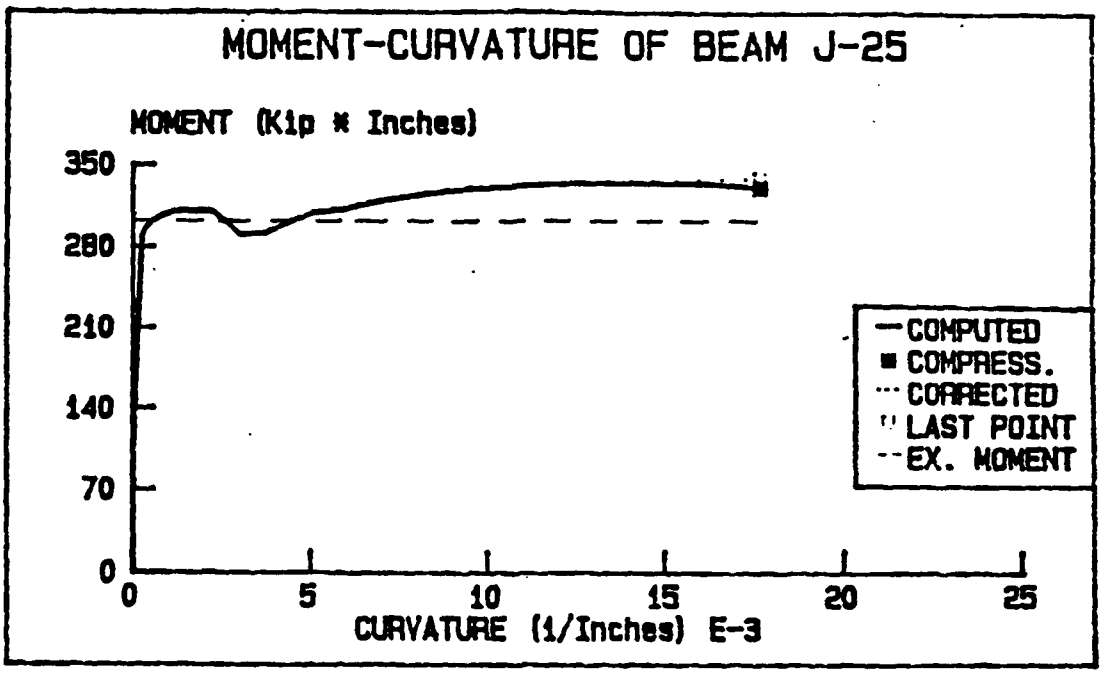

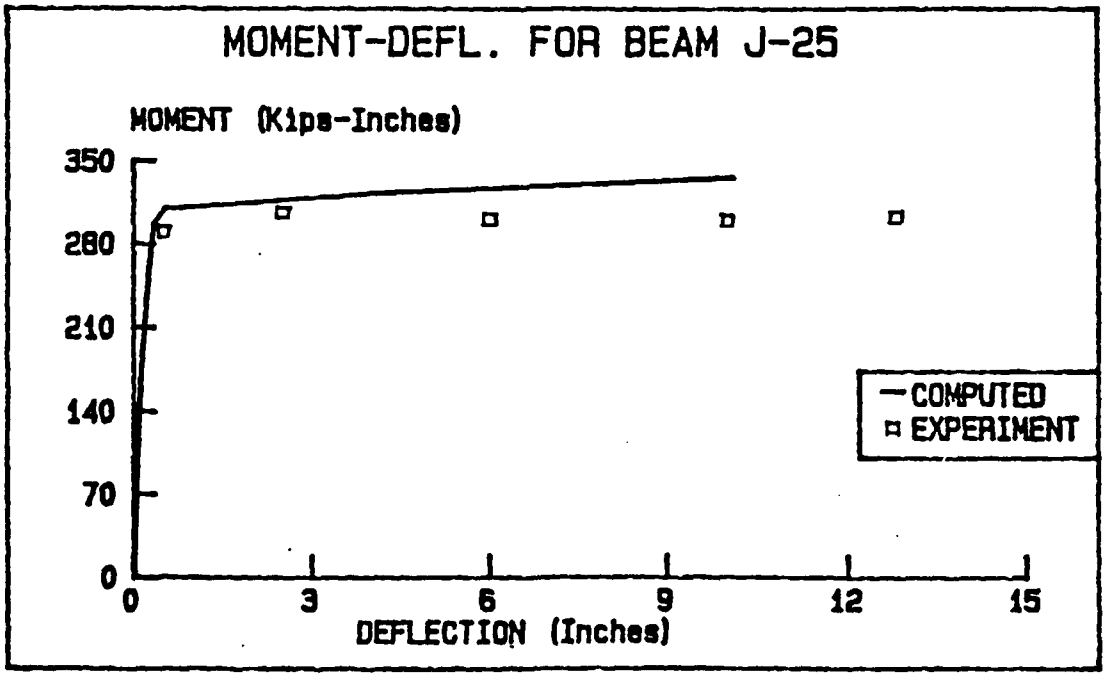

Figure B-22 Moment-Curvature and Load-Deflection Relationships Beam J25

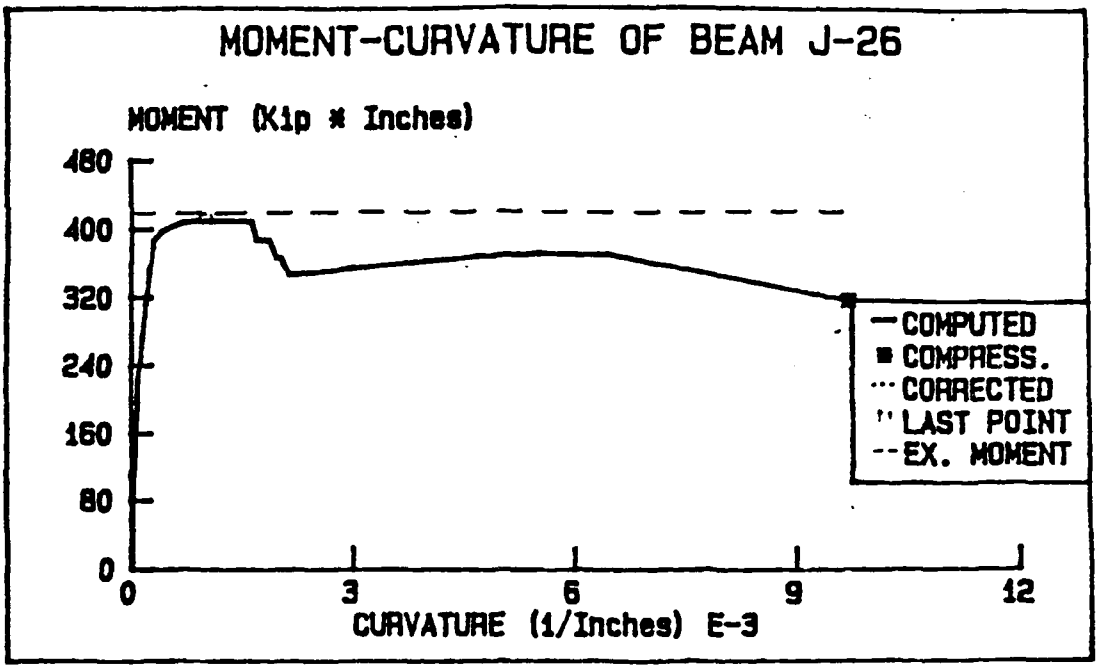

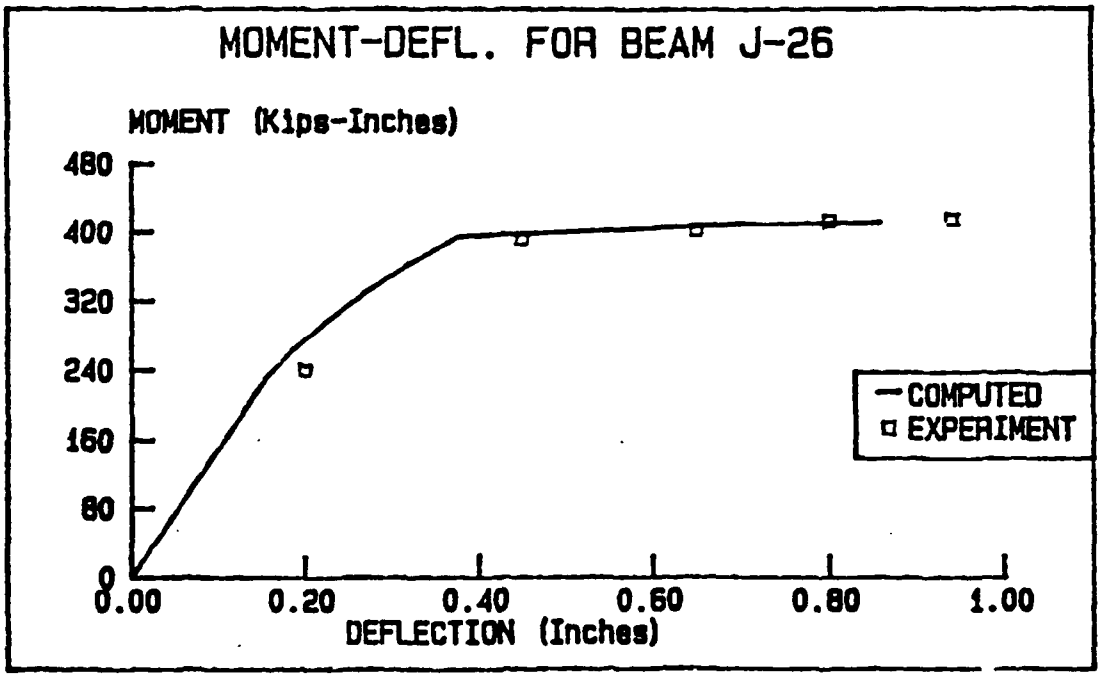

Figure B-23. Moment-Curvature and Load-Deflection Relationships Beam J26

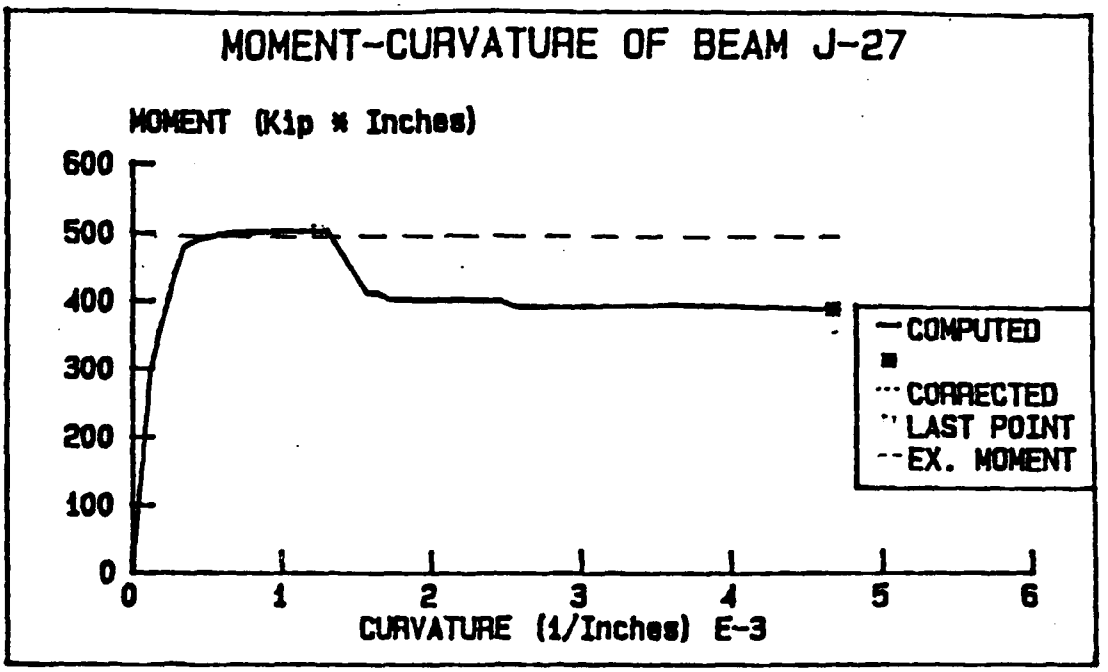

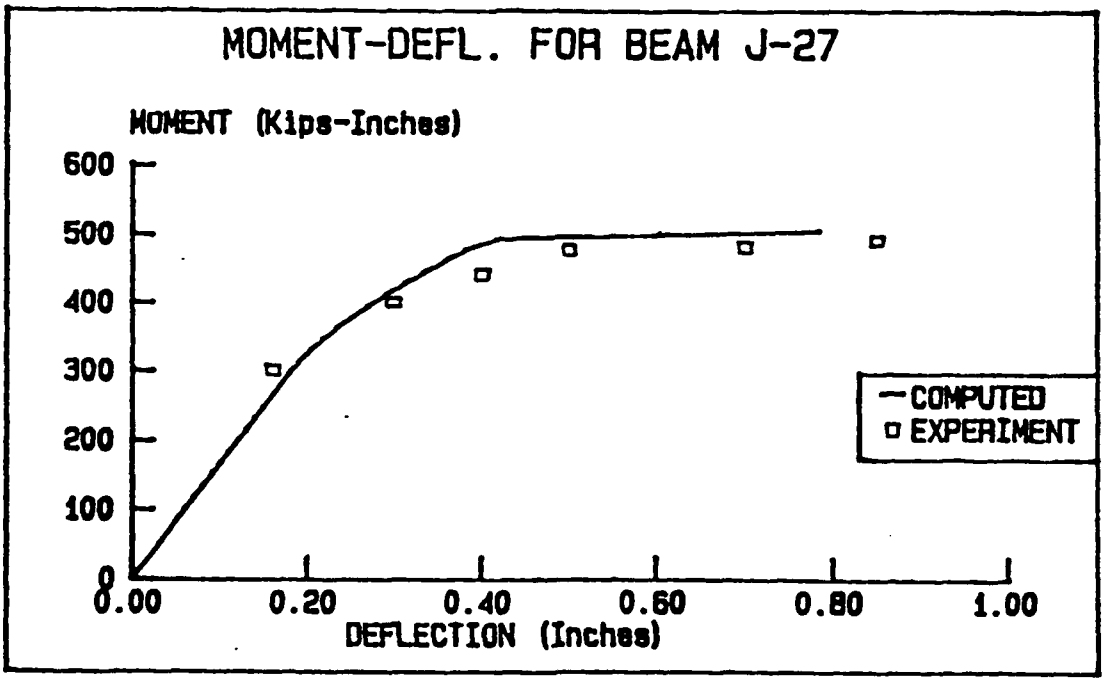

Figure B-24. Moment-Curvature and Load-Deflection Relationships Beam J27

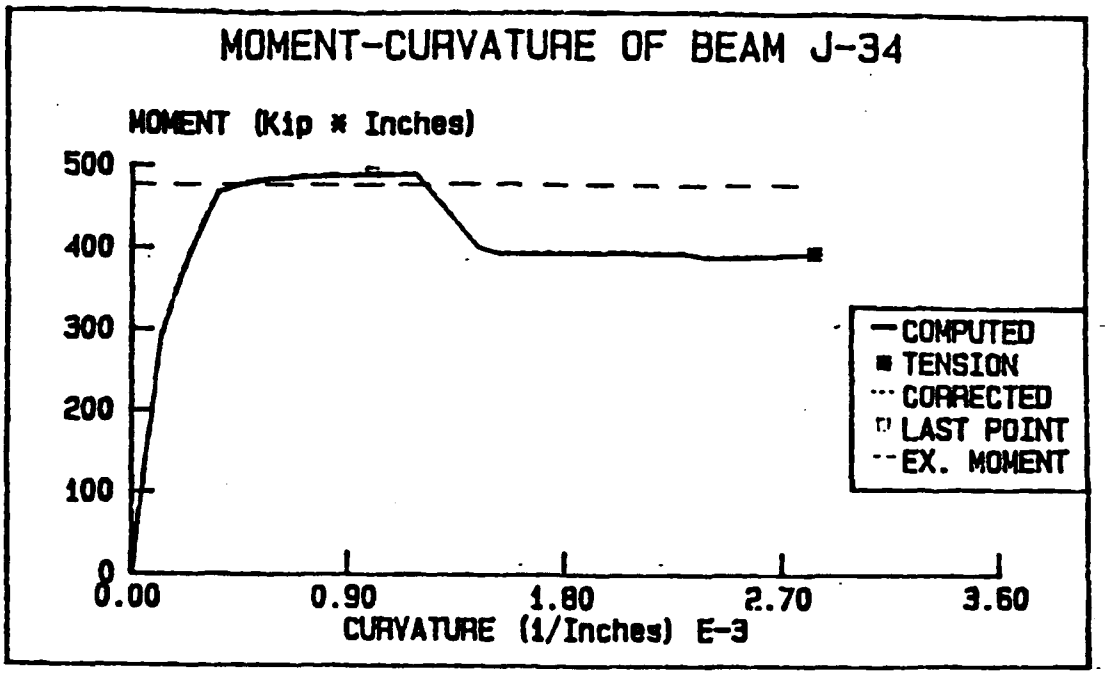

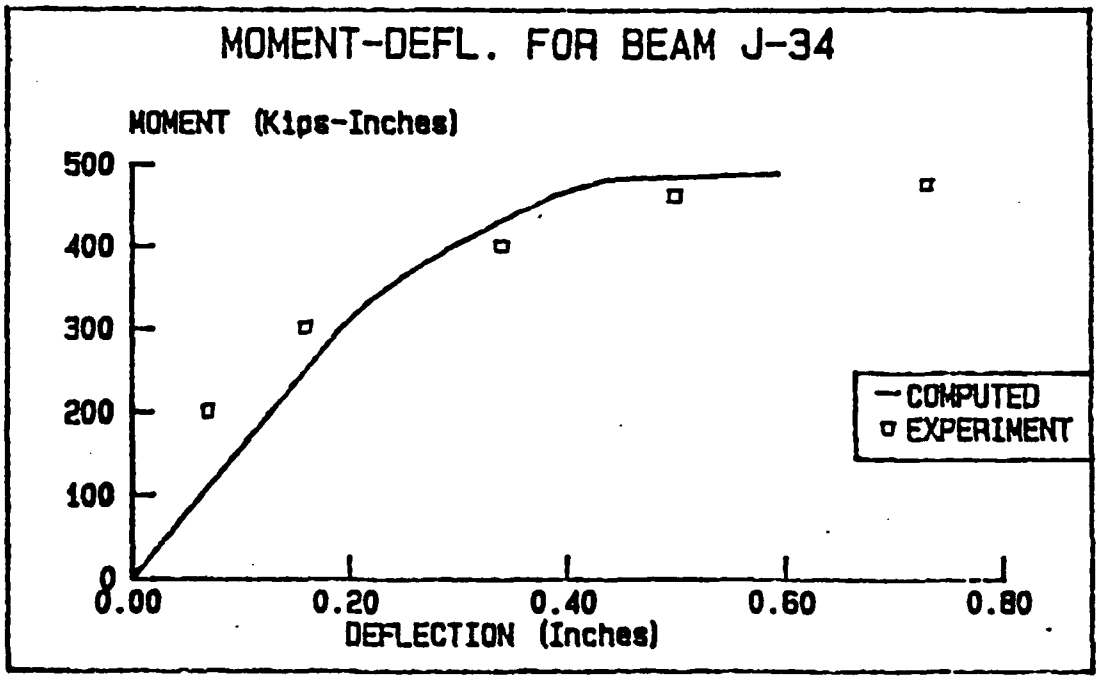

Figure B-25. Moment-Curvature and Load-Deflection Relationships Beam J34

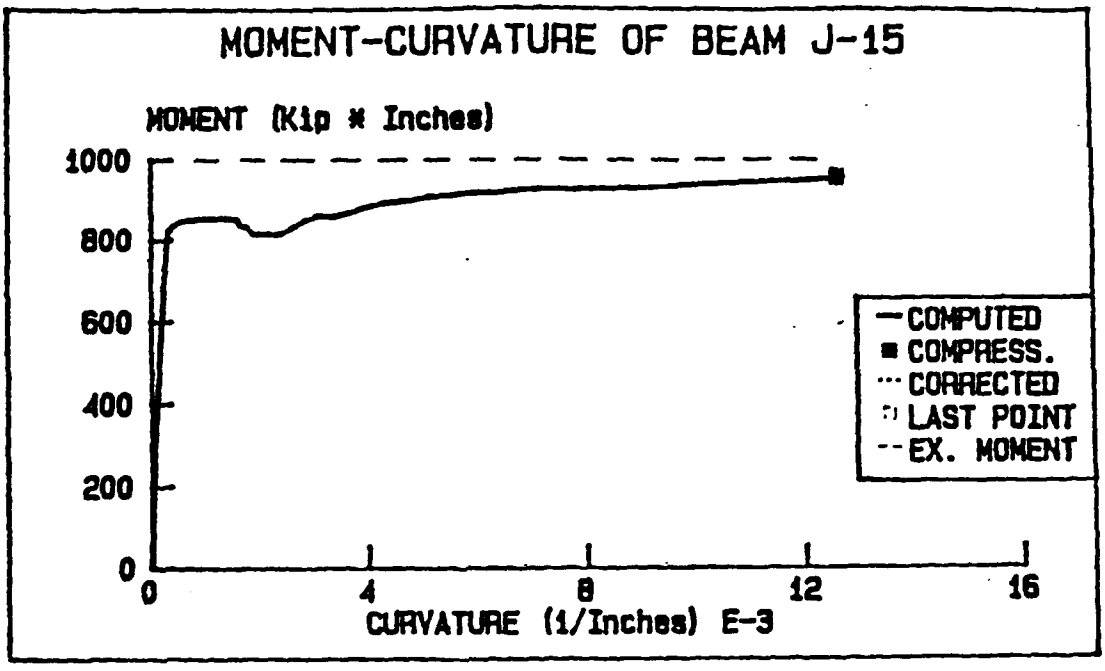

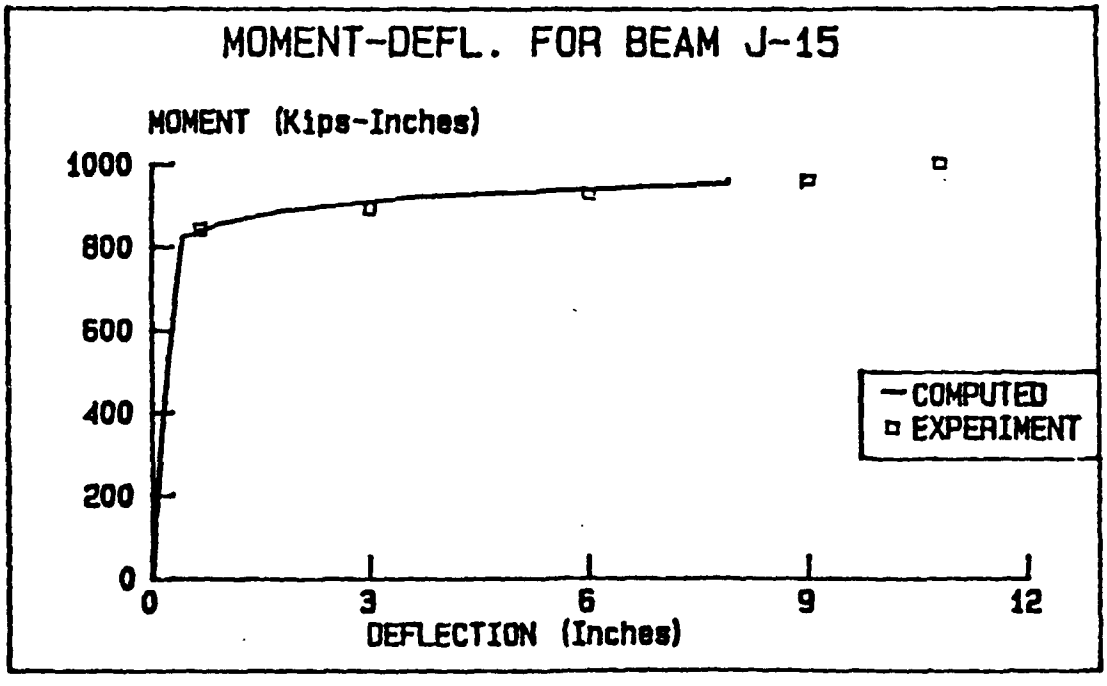

Figure B-26. Moment-Curvature and Load-Deflection Relationships Beam J15

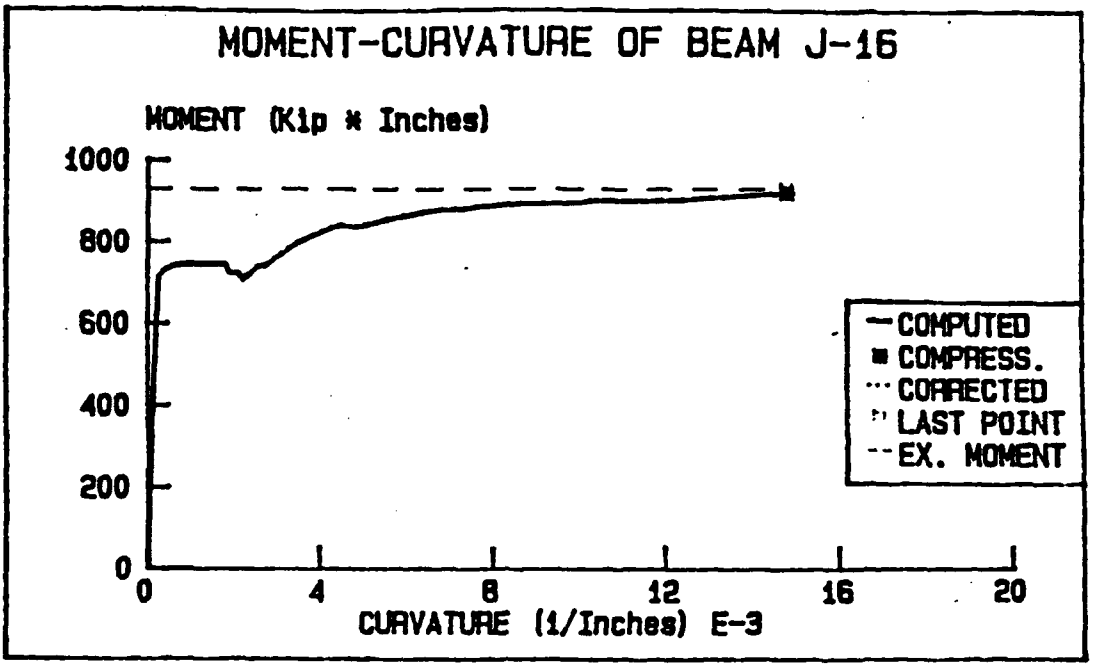

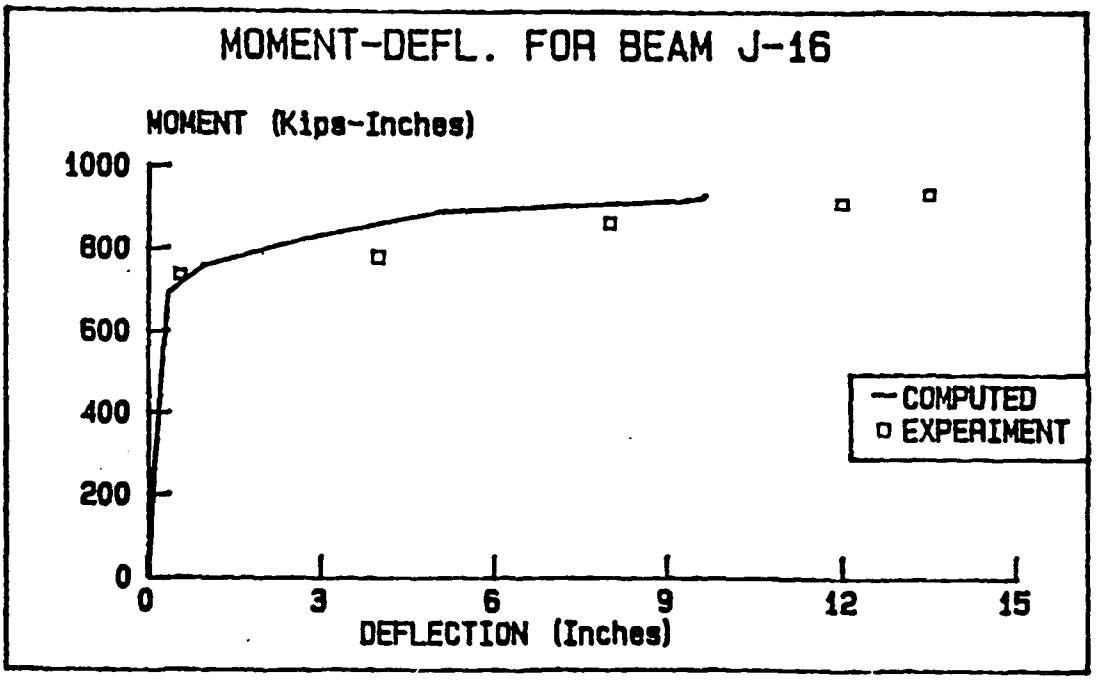

Figure B-27. Moment-Curvature and Load-Deflection Relationships Beam J16

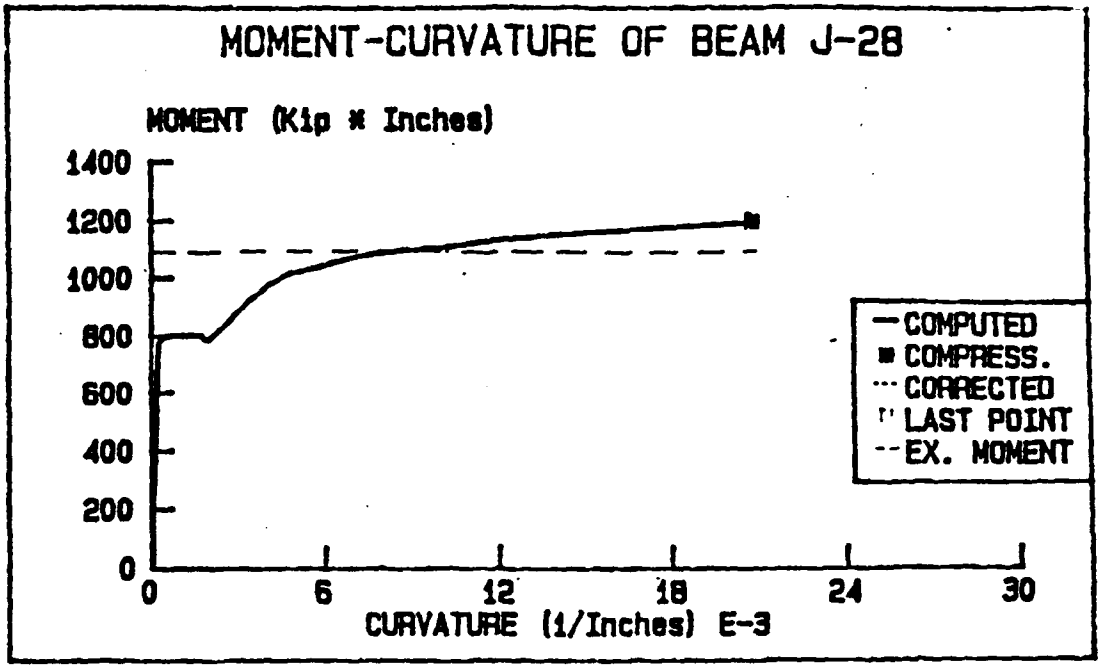

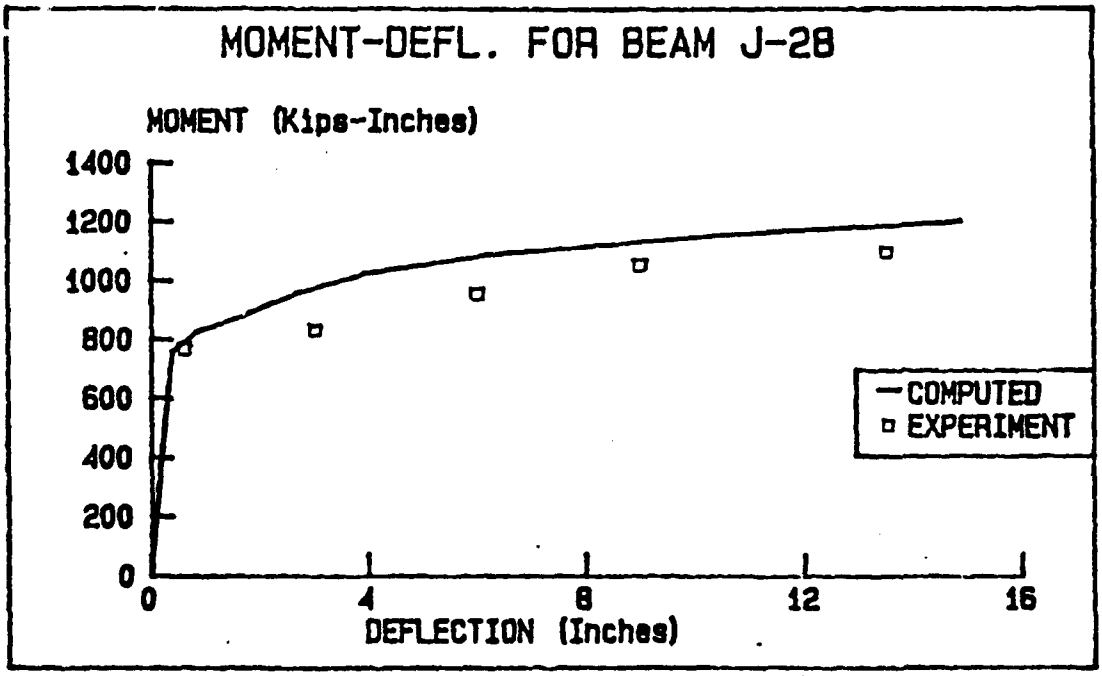

Figure B-28 Moment-Curvature and Load-Deflection Relationships Beam J28

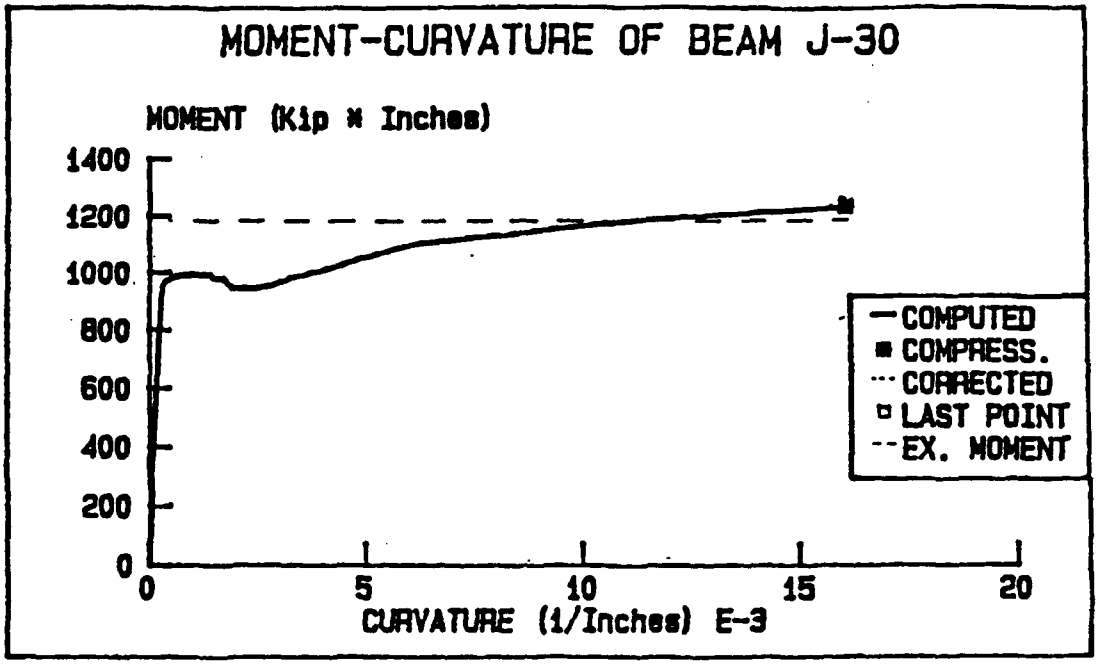

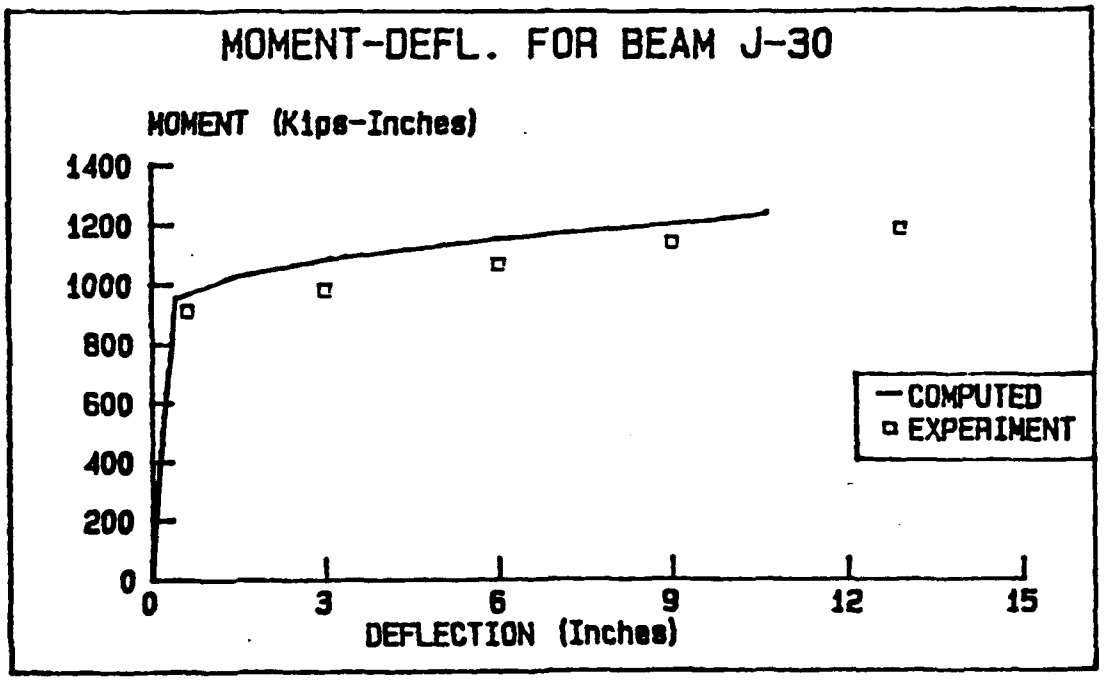

Figure B-29. Moment-Curvature and Load-Deflection Relationships Beam J30

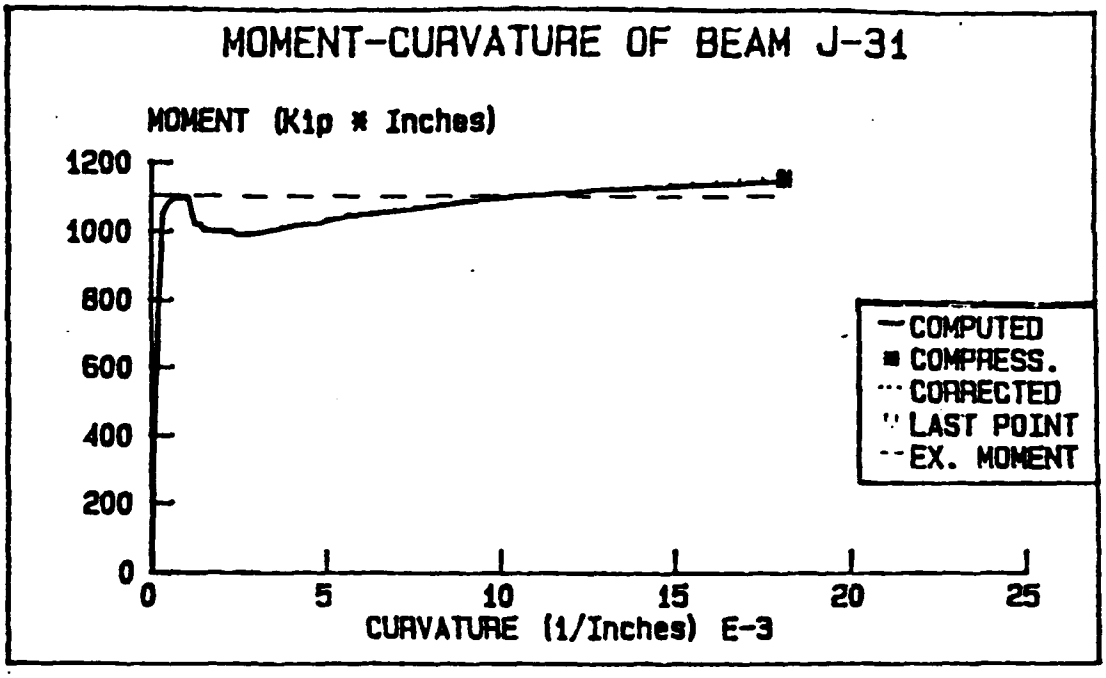

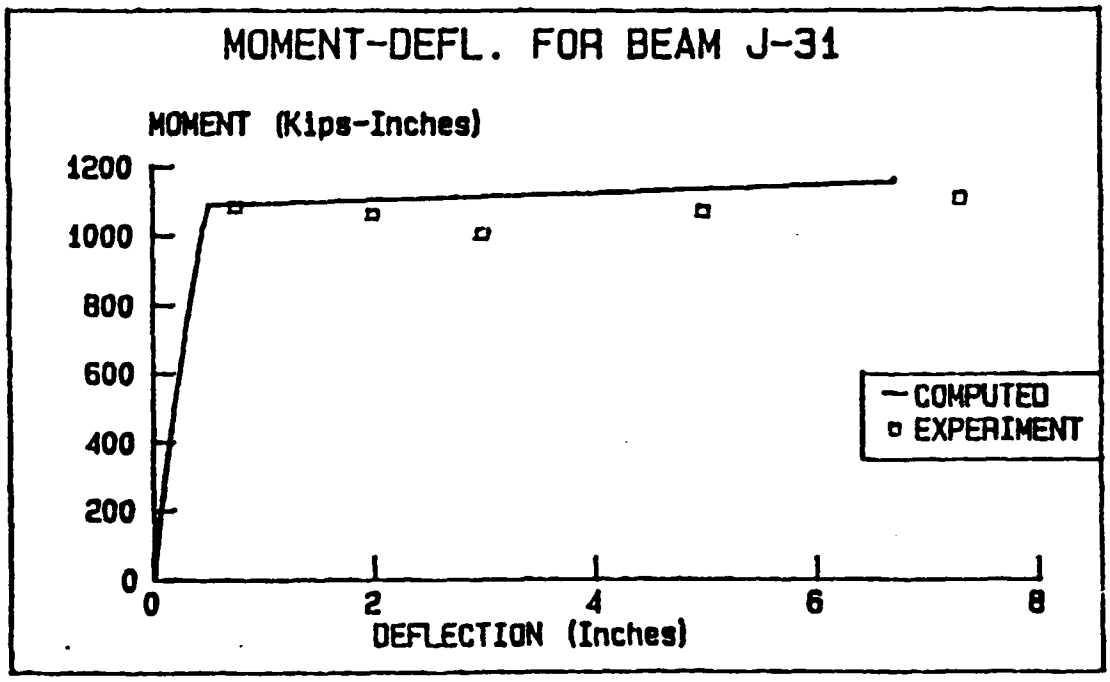

Figure B-30. Moment-Curvature and Load-Deflection Relationships Beam J31

(The reverse of this page is blank)

APPENDIX C

INPUT PROPERTIES AND RESULTS FOR ANALYSIS IN THE DYNAMIC DOMAIN - IMPACT

TABLE C-1 PROPERTIES OF BEAMS ANALYZED DYNAMICALLY

Beam[a]	f'_c psi	Width in.	Depth in.	Length in.	ρ %	ρ' %	Stirrups
C-1	5835	6.0	12.0	106	2.00	1.46	#3 @ 7.00"
H-1	5963	6.0	12.0	106	2.00	1.46	#3 @ 7.00"
J-1	6000	6.0	12.0	106	2.00	1.46	#3 @ 7.00"
G-1	6388	6.0	12.0	106	2.00	1.46	#3 @ 7.00"
I-1	6488	6.0	12.0	106.	2.00	1.46	#3 @ 7.00"

[a] All Beams: d=10 in., d'=8.5 in.

TABLE C-2. PROPERTIES OF TENSION REINFORCEMENT, DYNAMIC TESTS

Beam	Size	f_y psi	ε_y %	ε_{sh} %	f_u psi	ε_u %
C-1	2 #7	46.08	0.16	1.44	——	——
H-1	2 #7	47.17	0.14	1.25	——	——
J-1	2 #7	47.42	——	——	——	——
G-1	2 #7	47.75	——	——	——	——
I-1	2 #7	47.00	0.14	1.50	——	——

TABLE C-3. PROPERTIES OF COMPRESSION REINFORCEMENT, DYNAMIC TESTS

Beam	Size	f_y psi	ε_y %	ε_{sh} %	f_u psi	ε_u %
C-1	2 #6	46.70	——	——	——	——
H-1	2 #6	47.61	0.15	1.50	——	——
J-1	2 #6	48.86	0.16	1.20	——	——
G-1	2 #6	48.30	——	——	——	——
I-1	2 #6	47.95	——	——	——	——

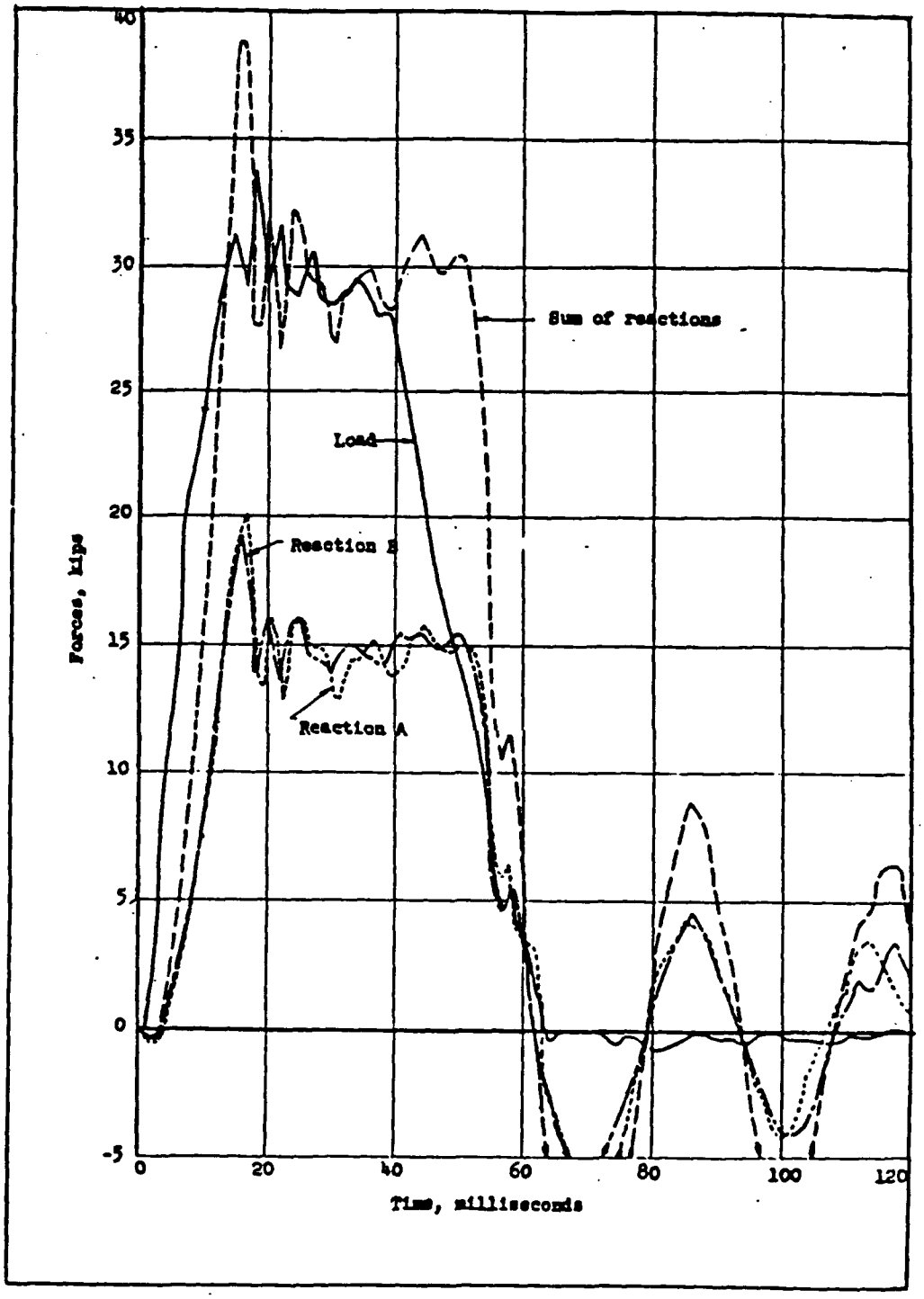

Figure C-1. Experimental Load and Reactions for Beam C-1. (Reference 77)

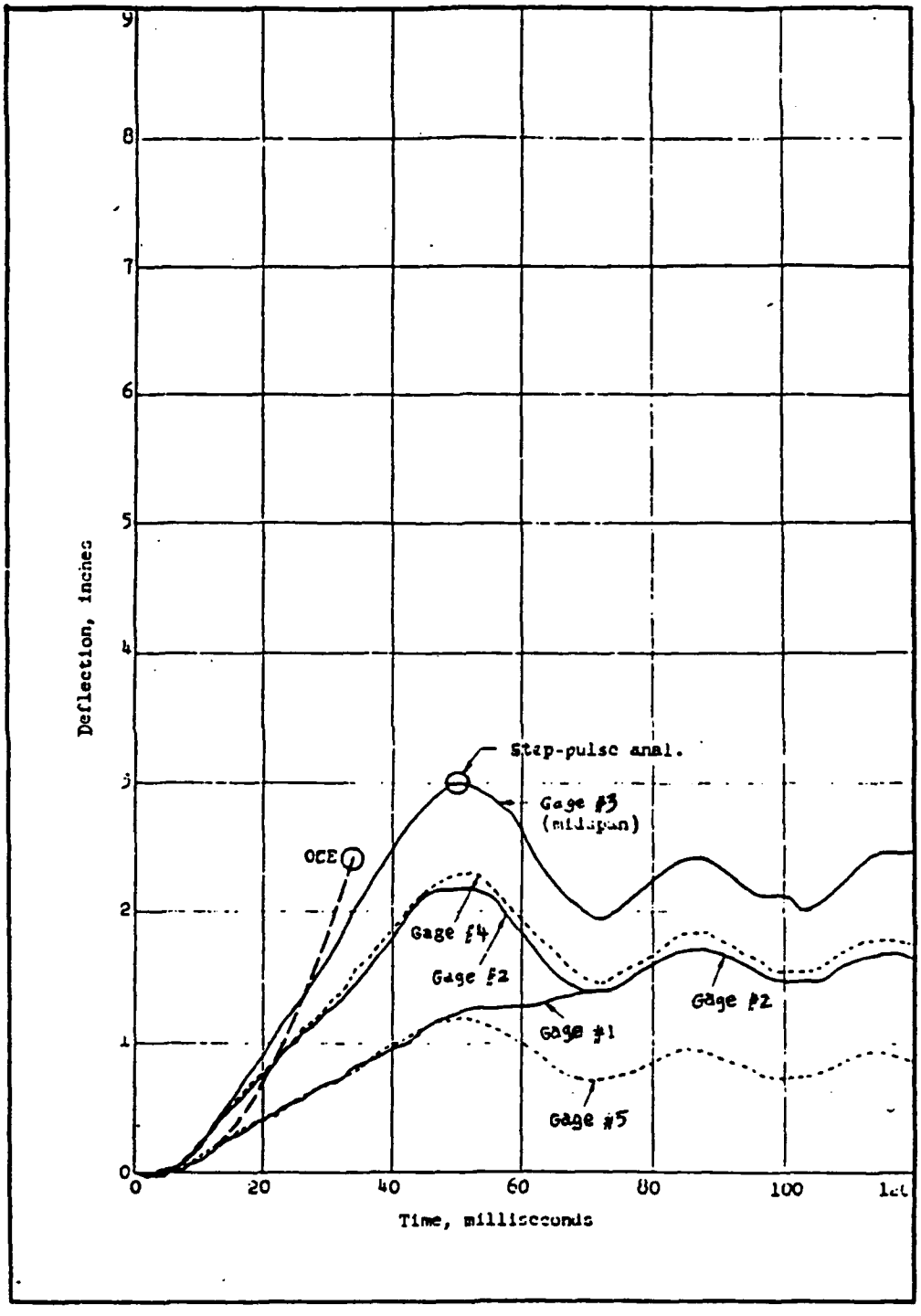

Figure C-2. Experimental Displacement Versus Time for Beam C-1. (Reference 77)

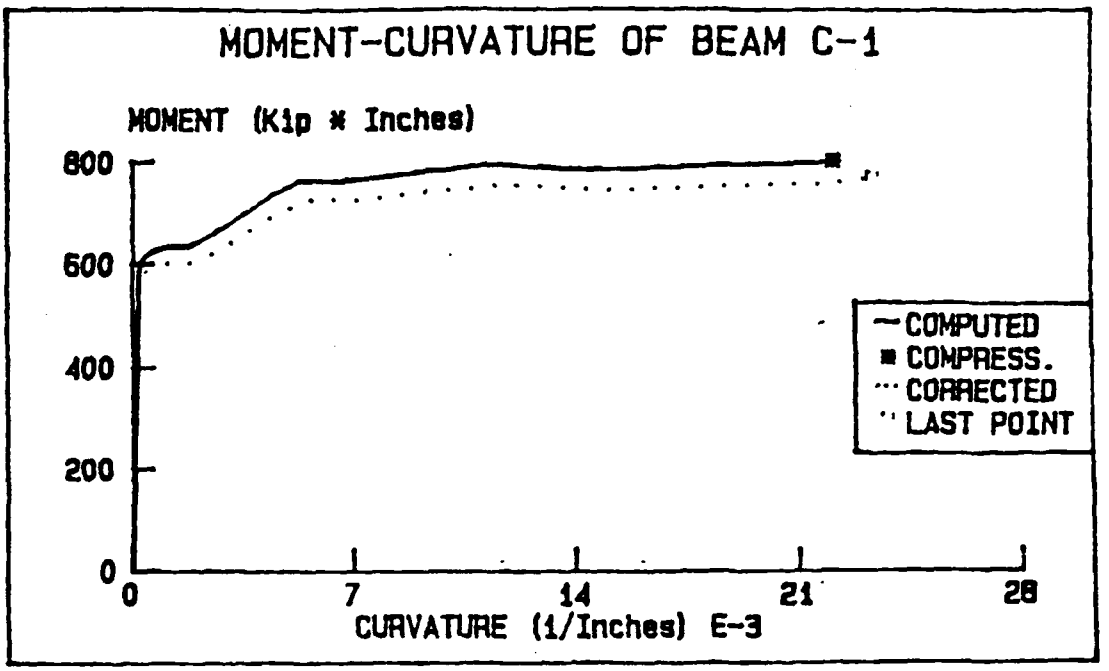

Figure C-3. Moment-Curvature Relationship for Beam C-1

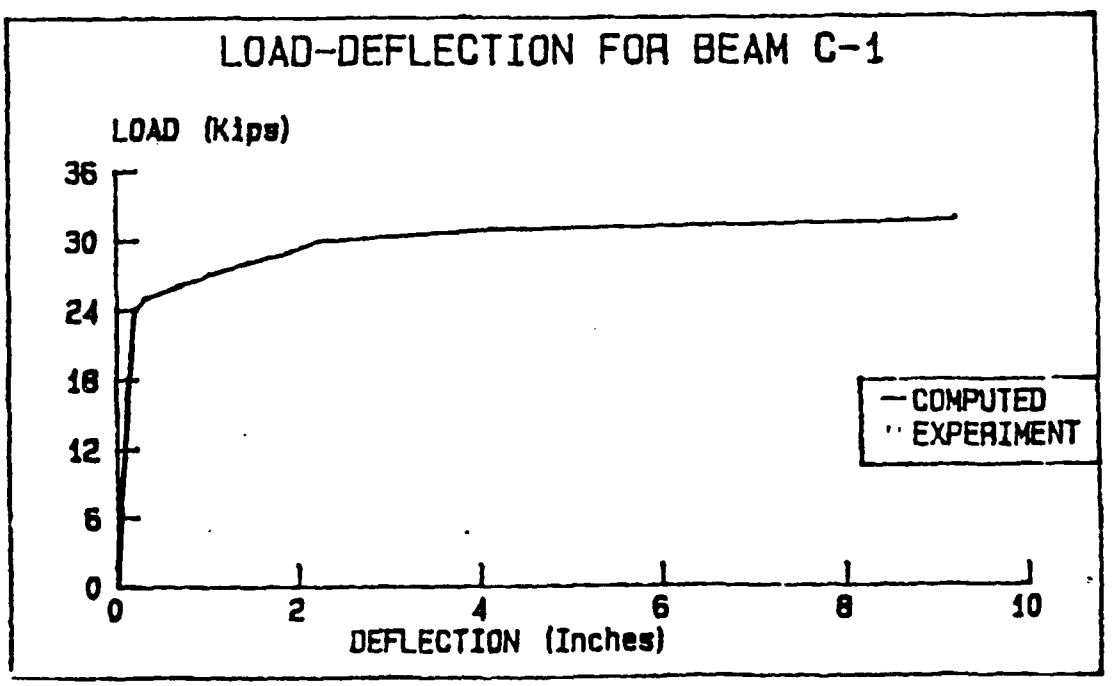

Figure C-4. Load-Deflection Relationship for Beam C-1

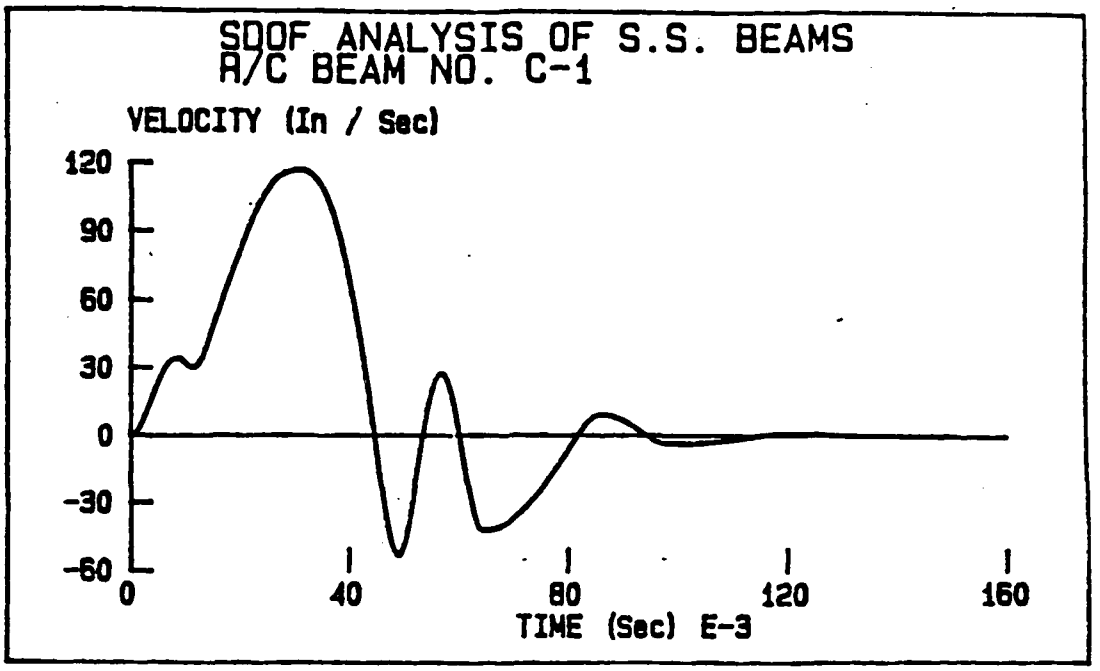

Figure C-5. Velocity Versus Time for Beam C-1

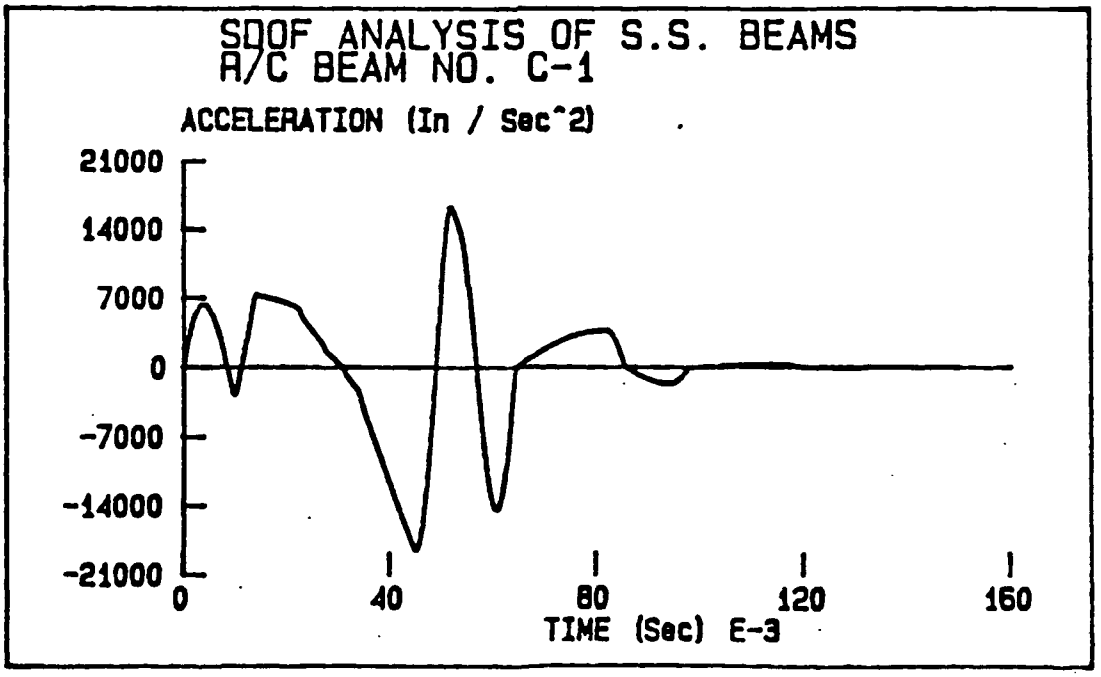

Figure C-6. Acceleration Versus Time for Beam C-1

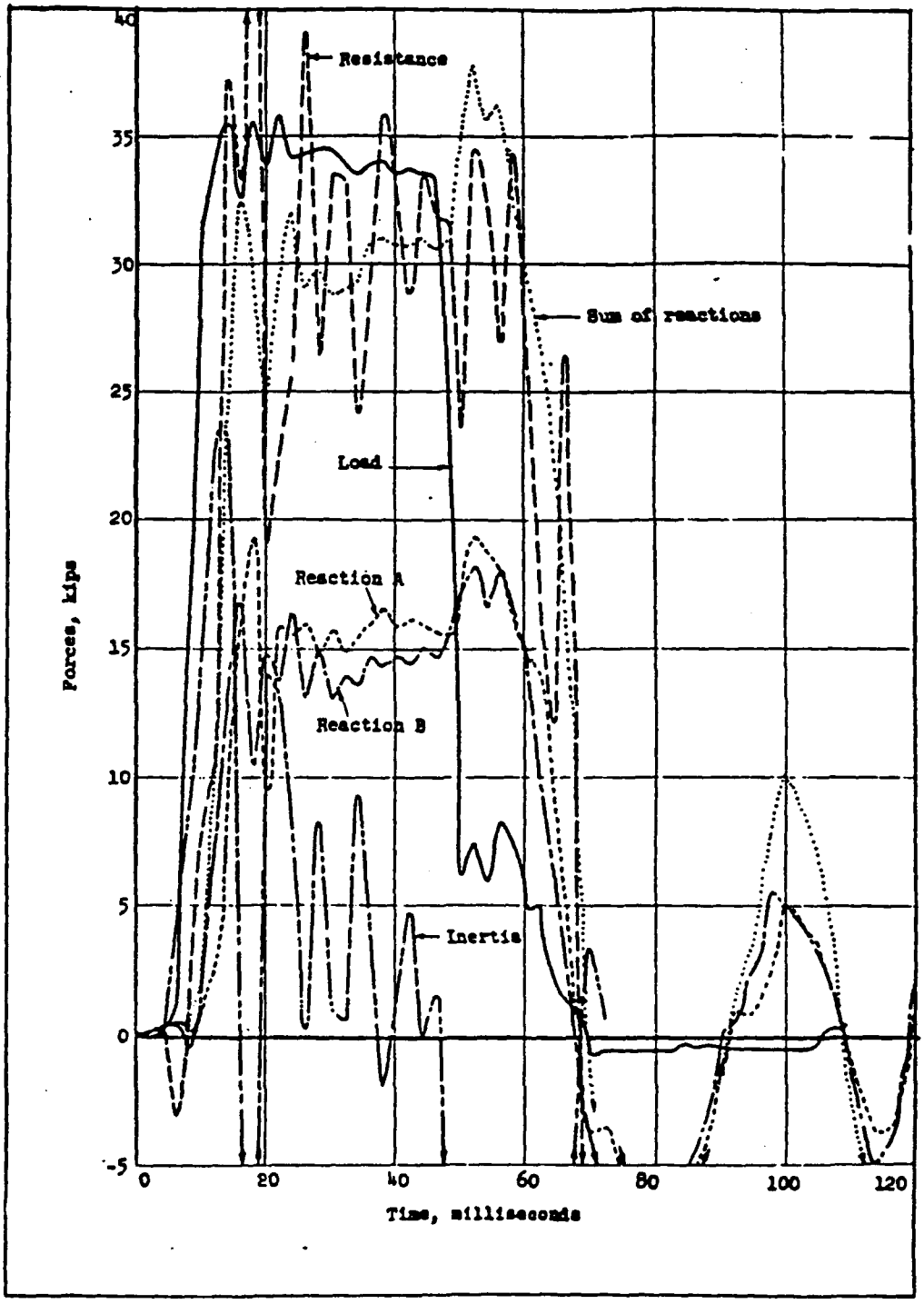

Figure C-7. Experimental Load and Reactions for Beam H-1. (Reference 77)

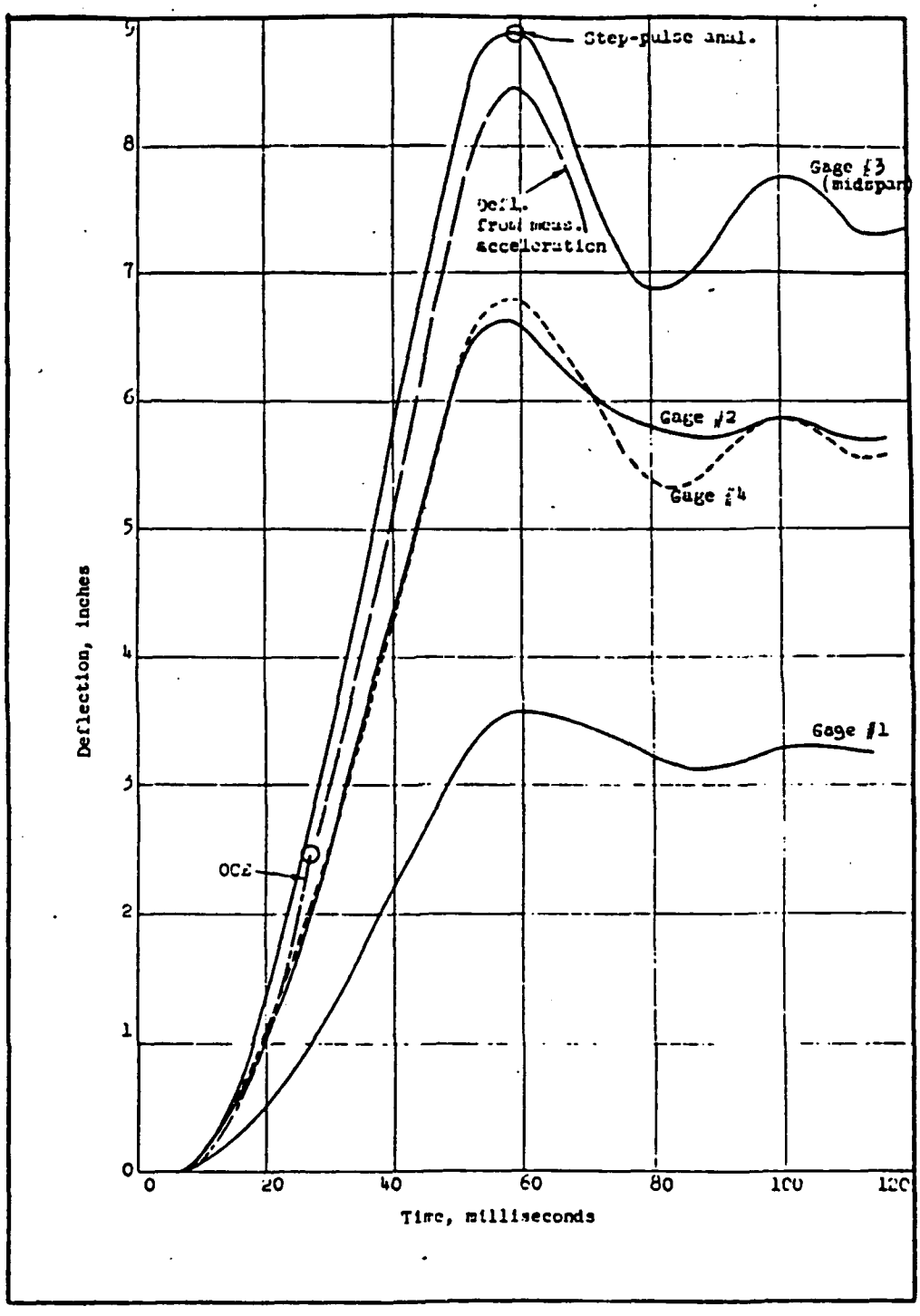

Figure C-8. Experimental Displacement Versus Time for Beam. H-1 (Reference 77)

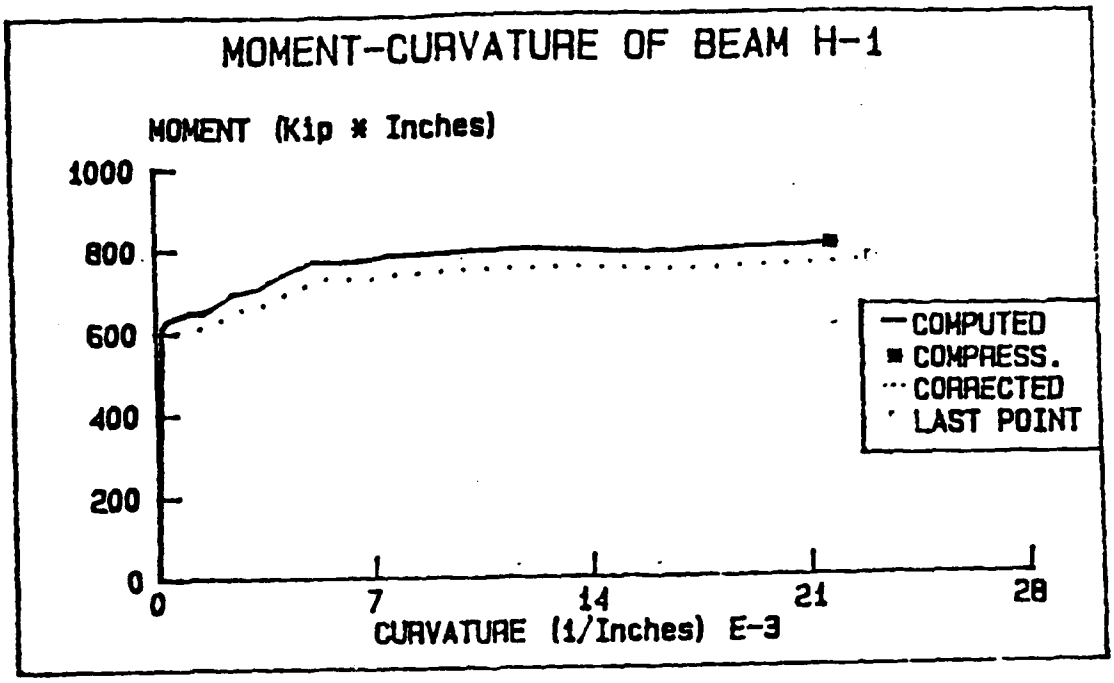

Figure C-9. Moment-Curvature Relationship for Beam H-1

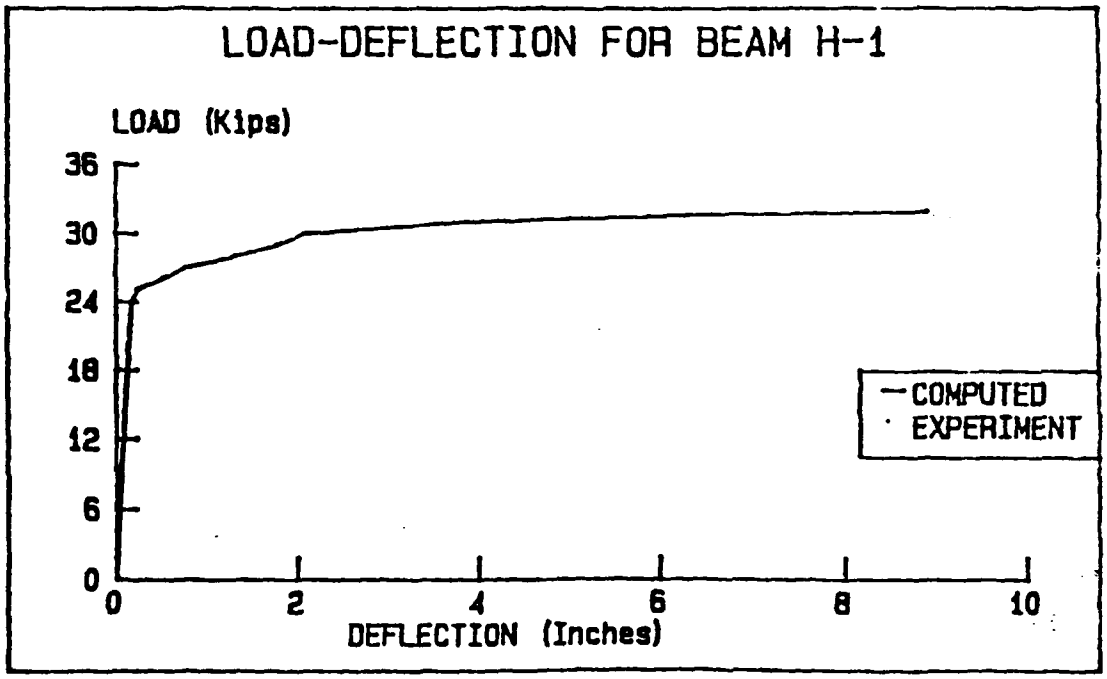

Figure C-10. Load-Deflection Relationship for Beam H-1

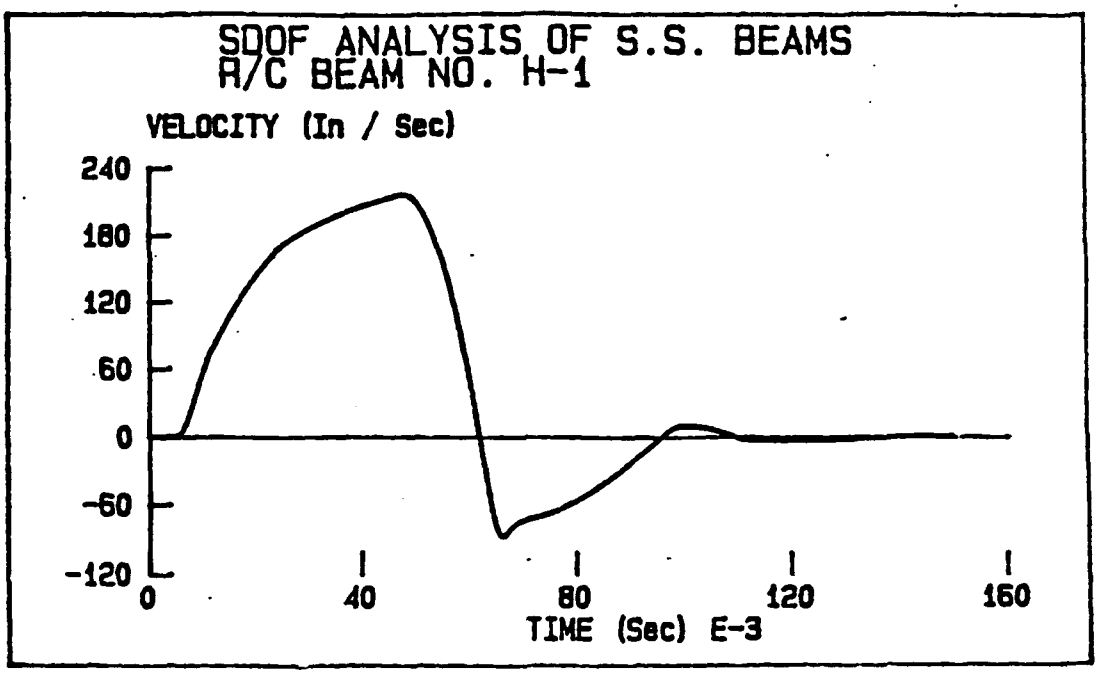

Figure C-11. Velocity Versus Time for Beam H-1

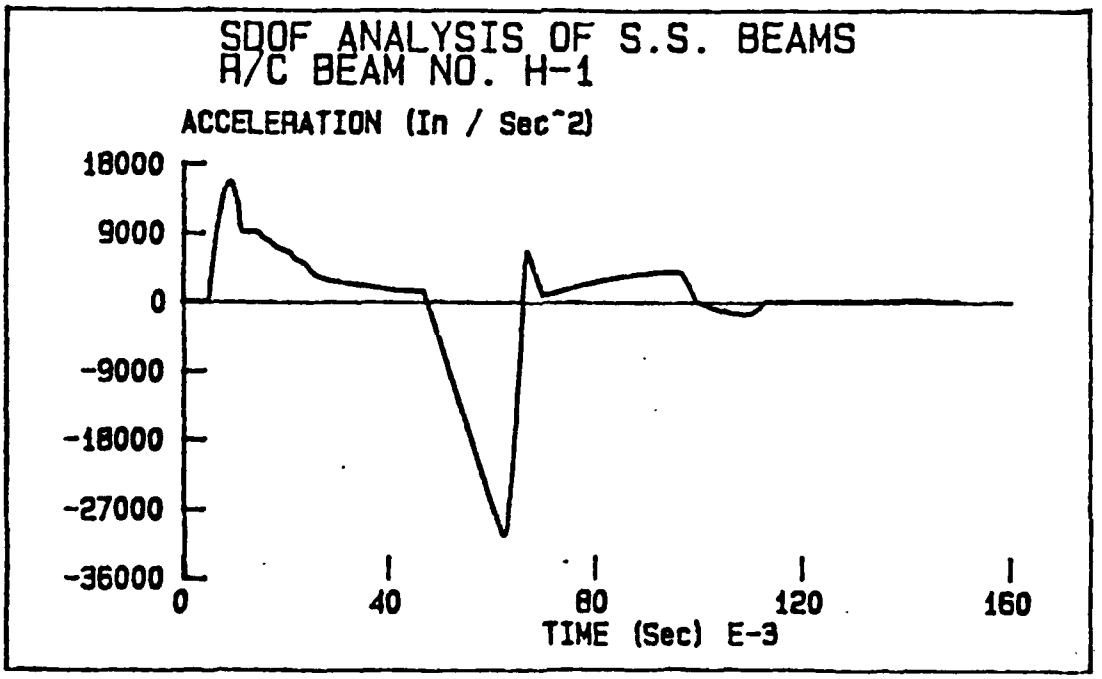

Figure C-12. Acceleration Versus Time for Beam H-1

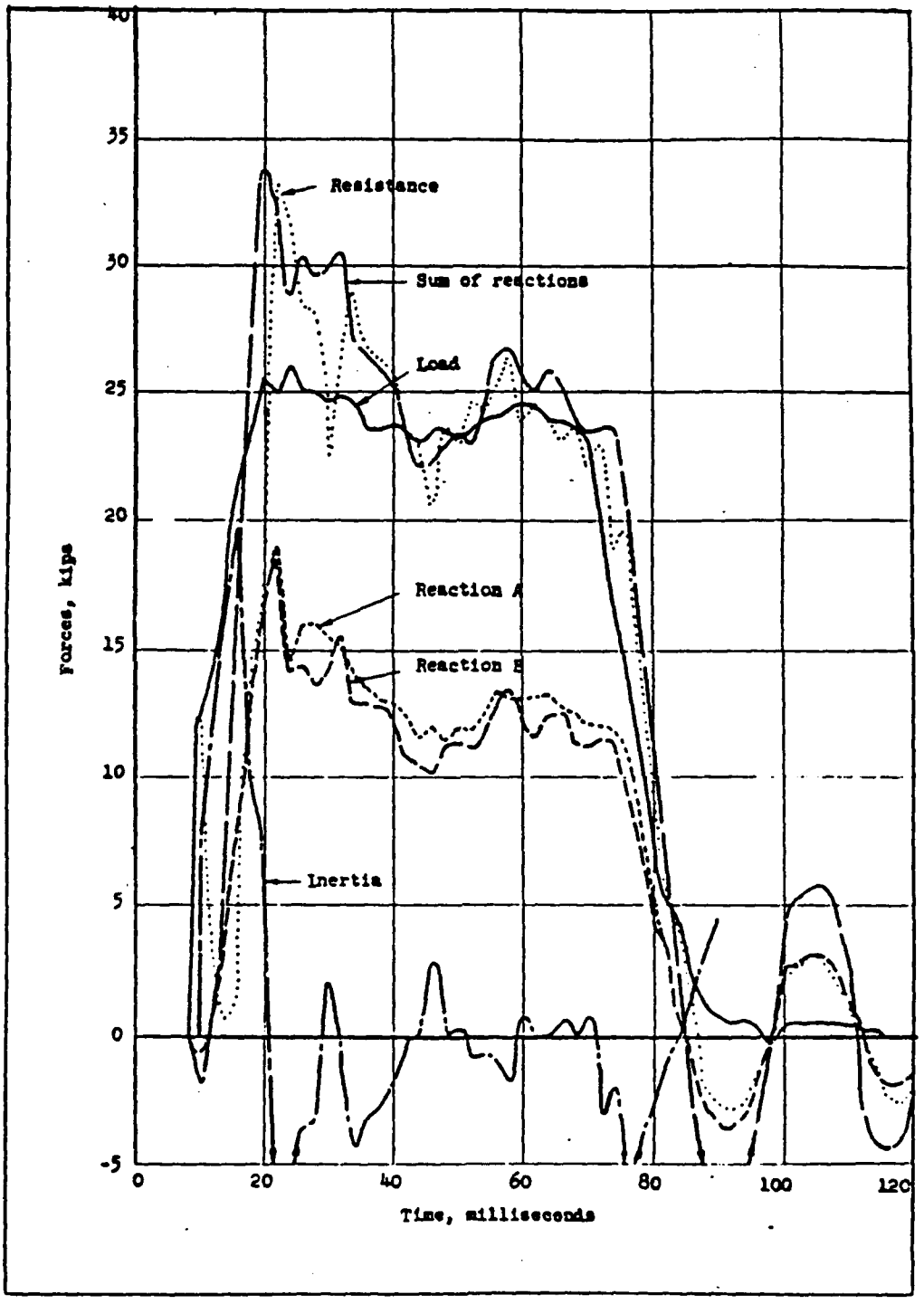

Figure C-13. Experimental Load and Reactions for Beam J-1. (Reference 77)

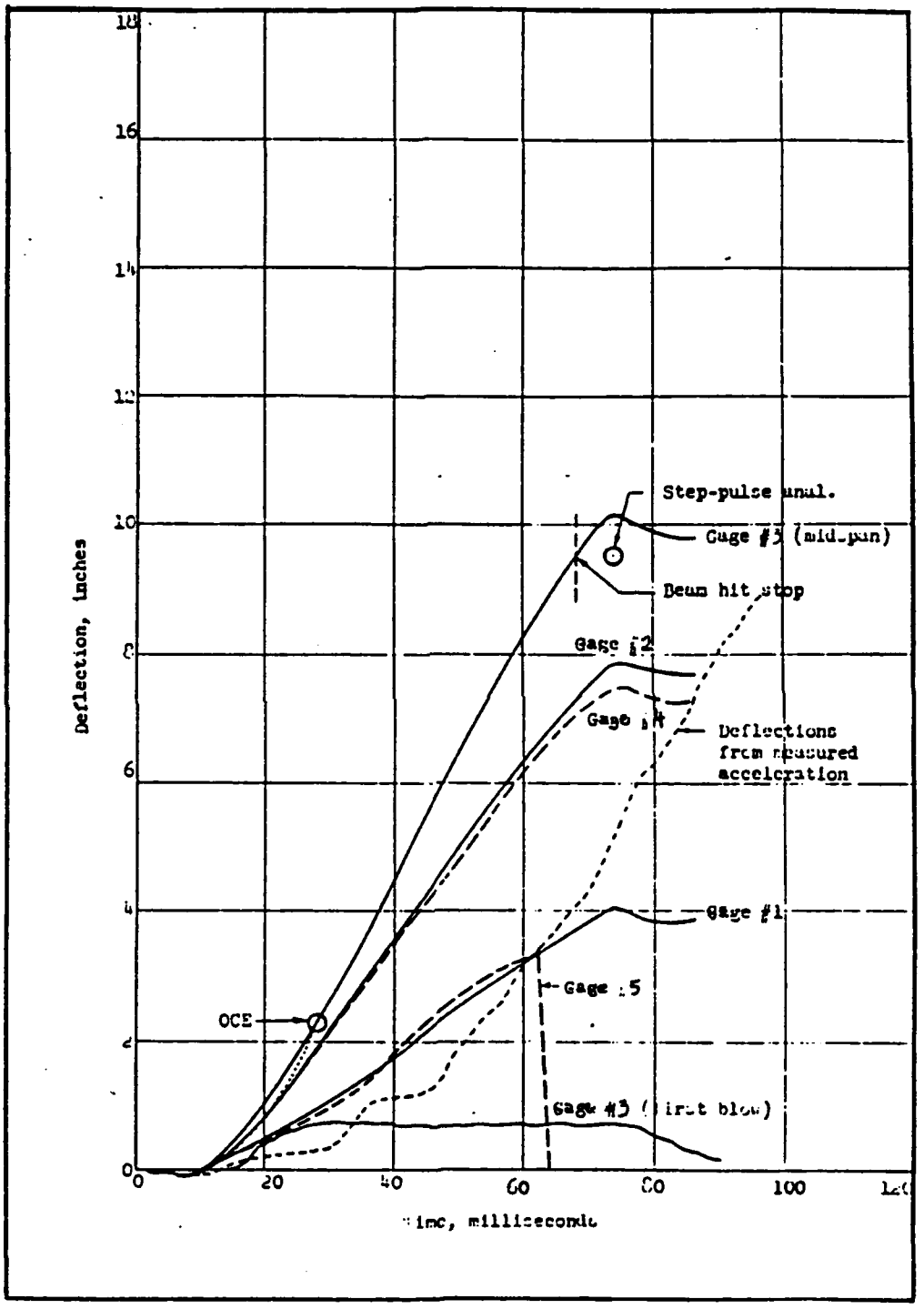

Figure C-14 Experimental Displacement Versus Time for Beam J-1. (Reference 77)

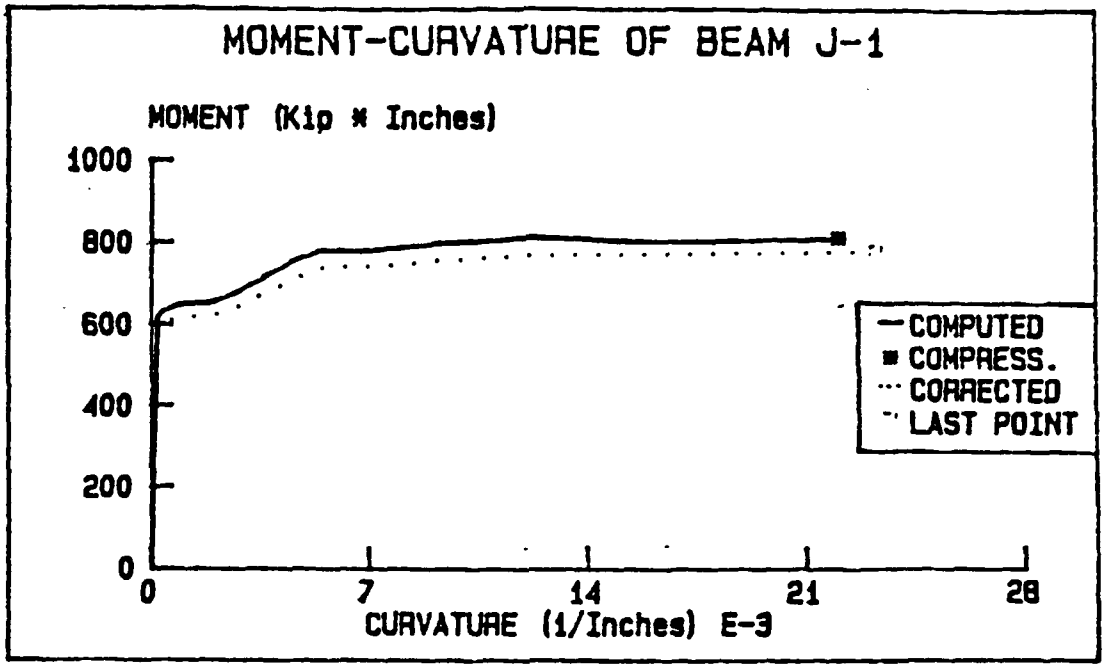

Figure C-15. Moment-Curvature Relationship for Beam J-1

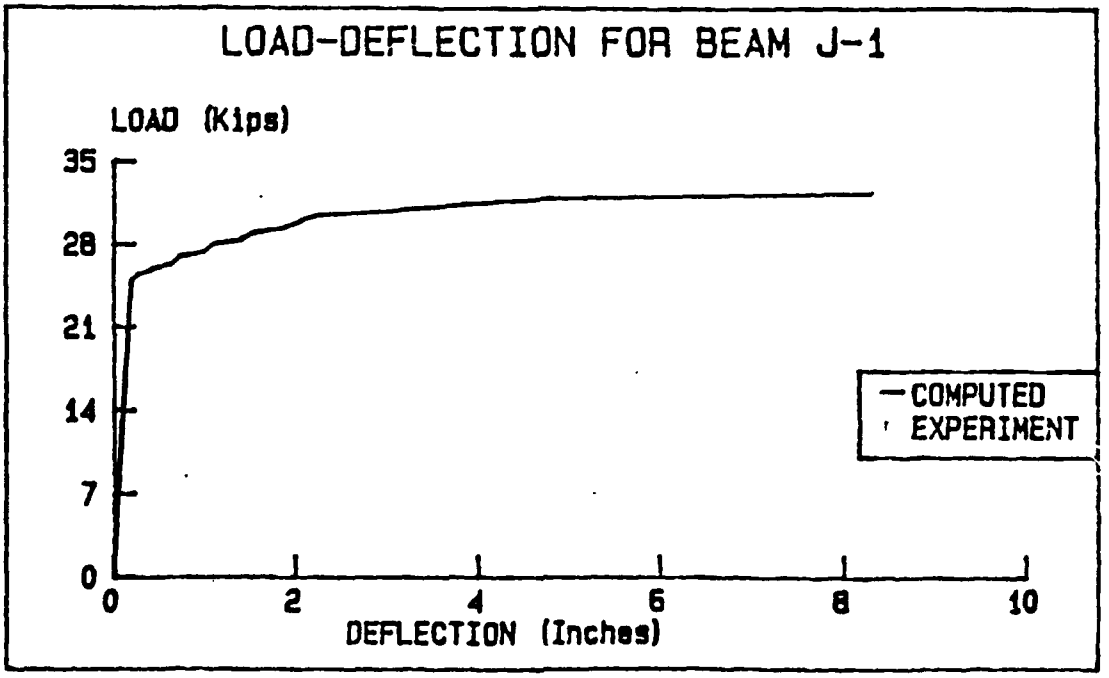

Figure C-16. Load-Deflection Relationship for Beam J-1

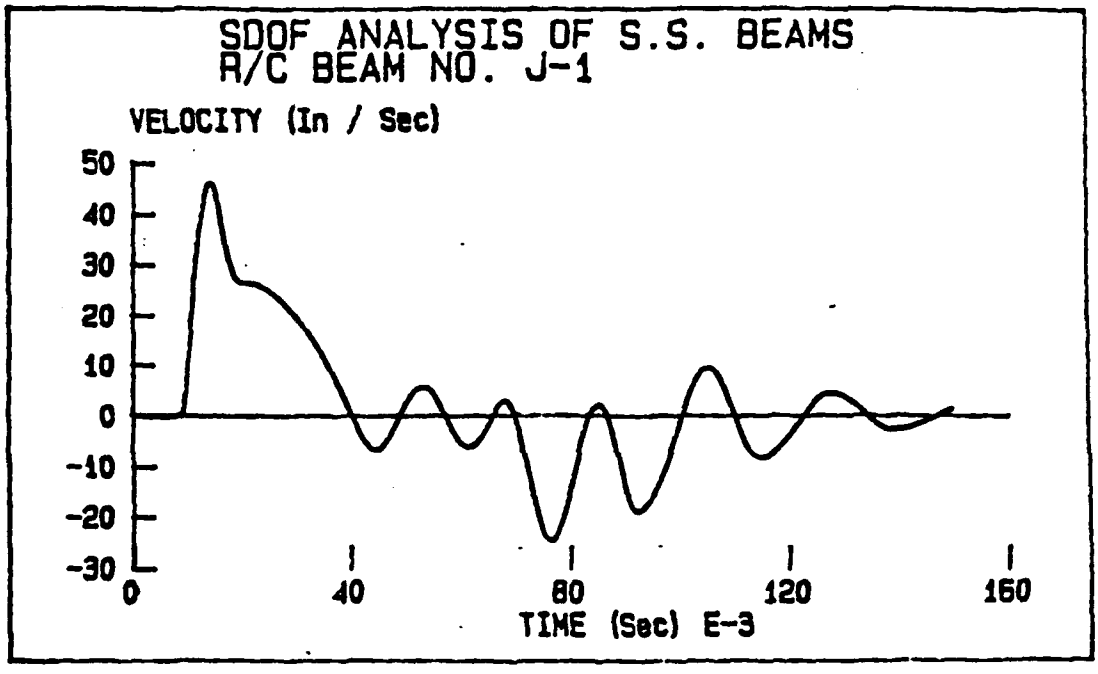

Figure C-17. Velocity Versus Time for Beam J-1

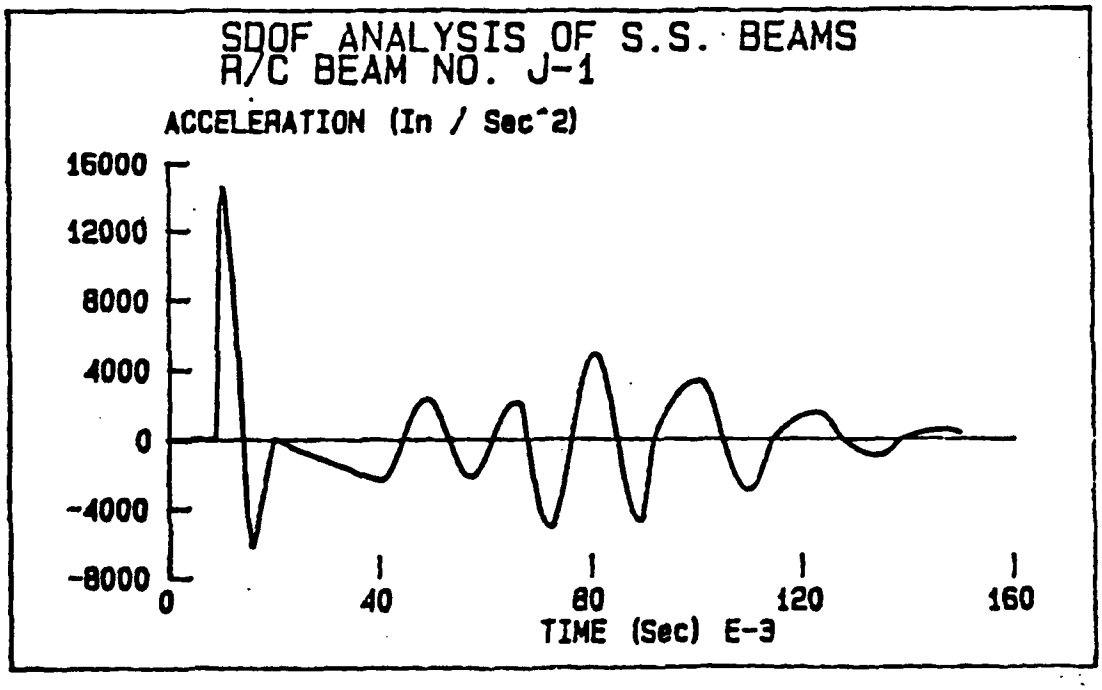

Figure C-18. Acceleration Versus Time for Beam J-1

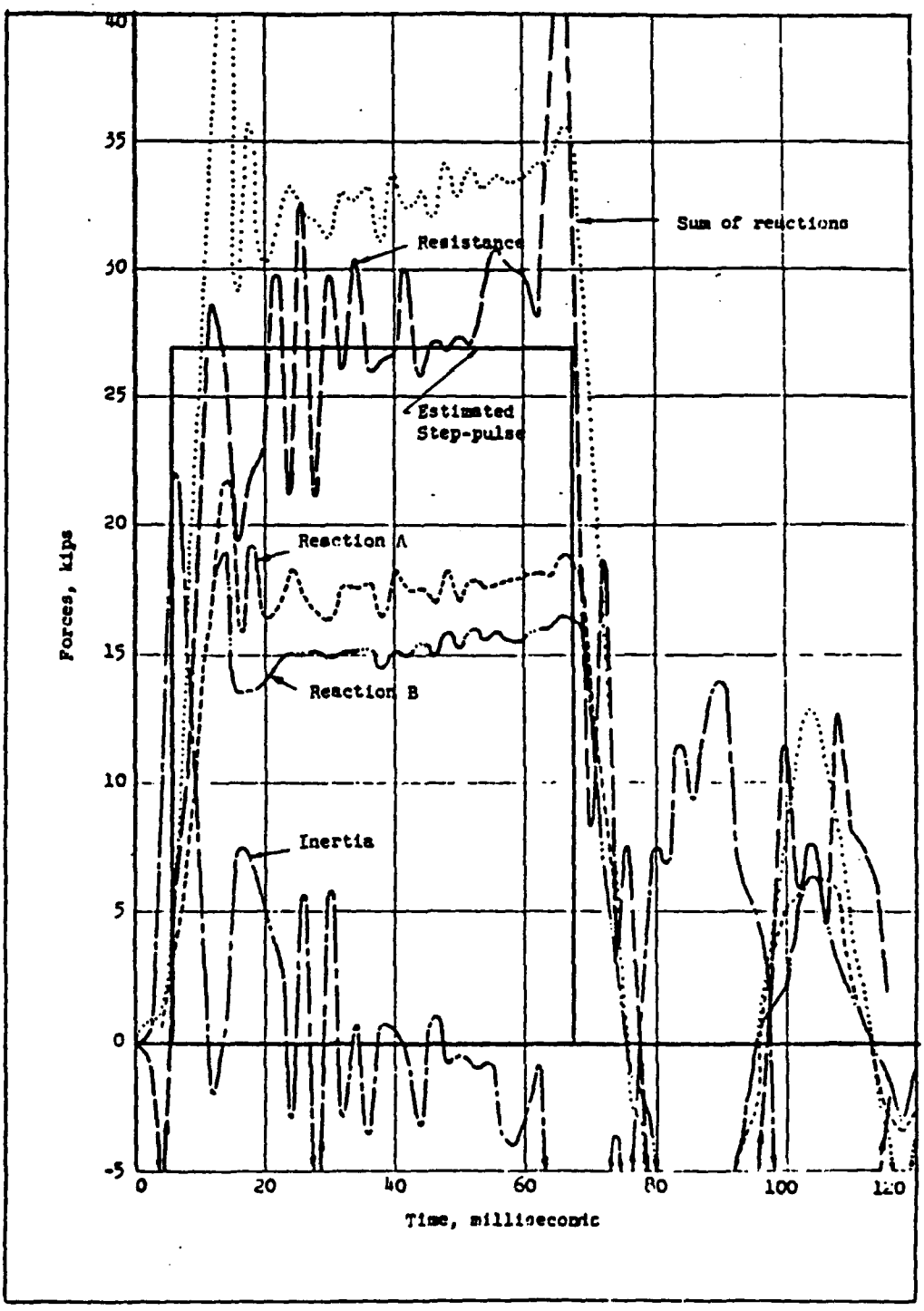

Figure C-19. Experimental Load and Reactions for Beam G-1. (Reference 77)

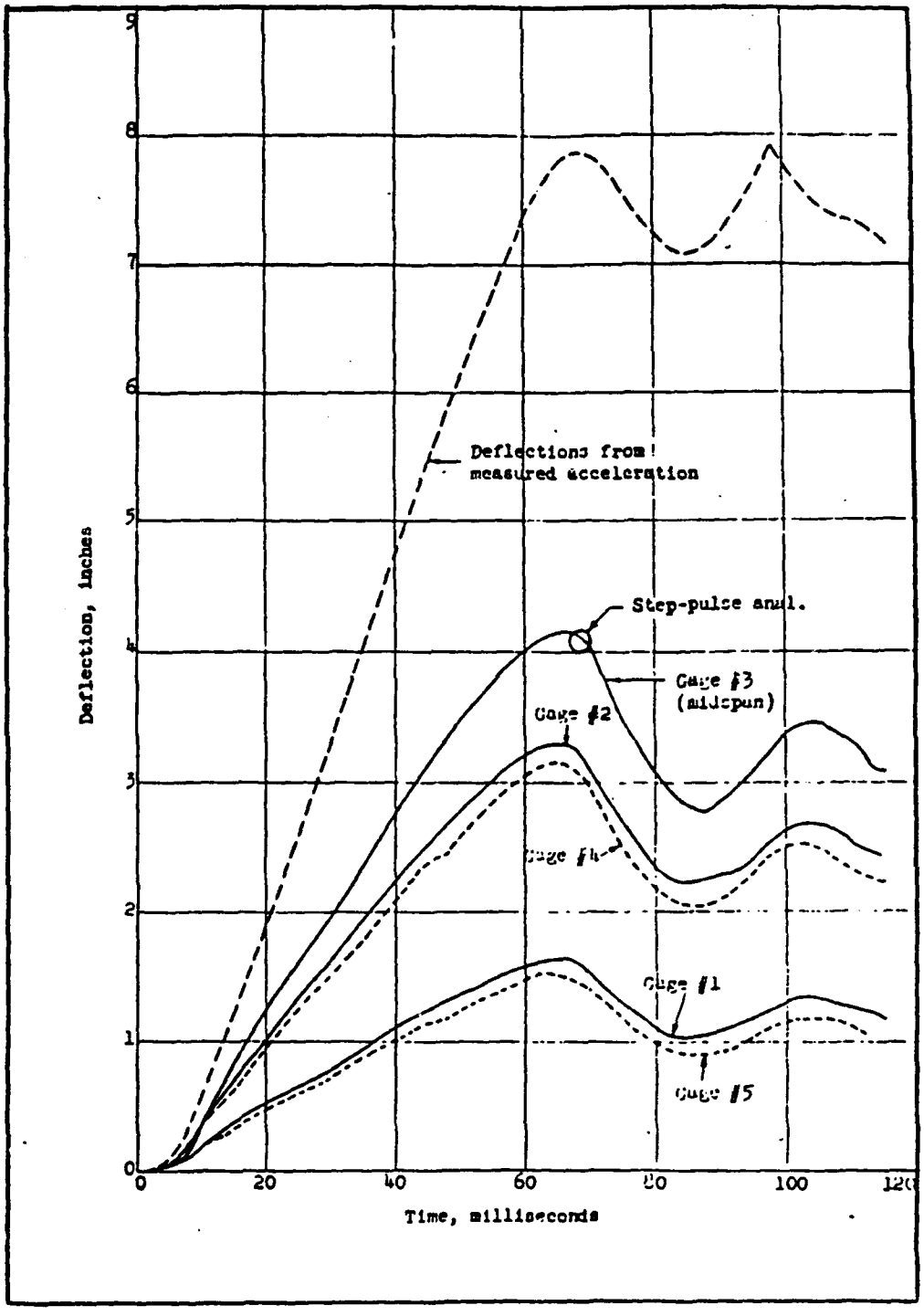

Figure C-20. Experimental Displacement Versus Time for Beam G-1. (Reference 77)

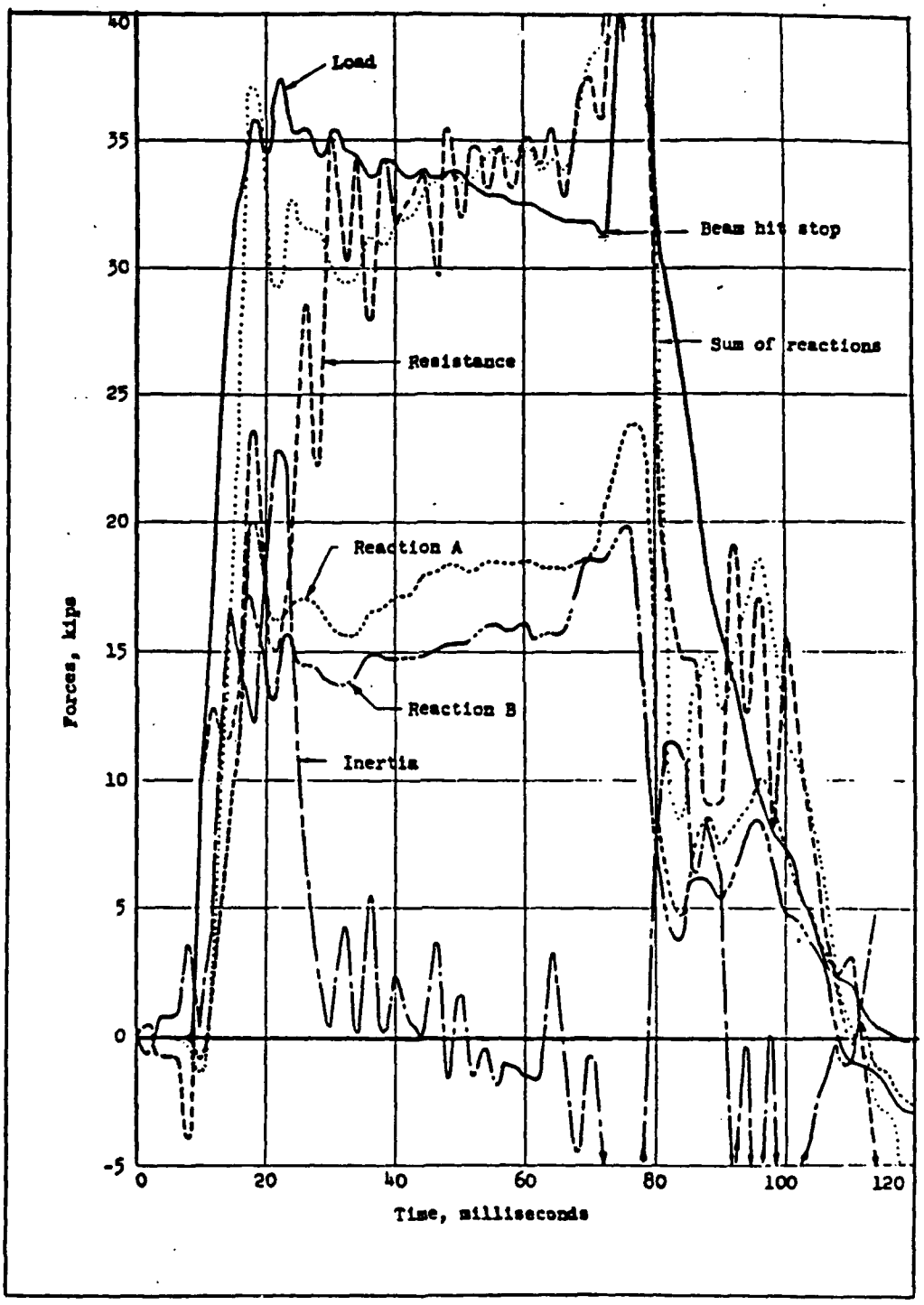

Figure C-21. Experimental Load and Reactions for Beam I-1. (Reference 77)

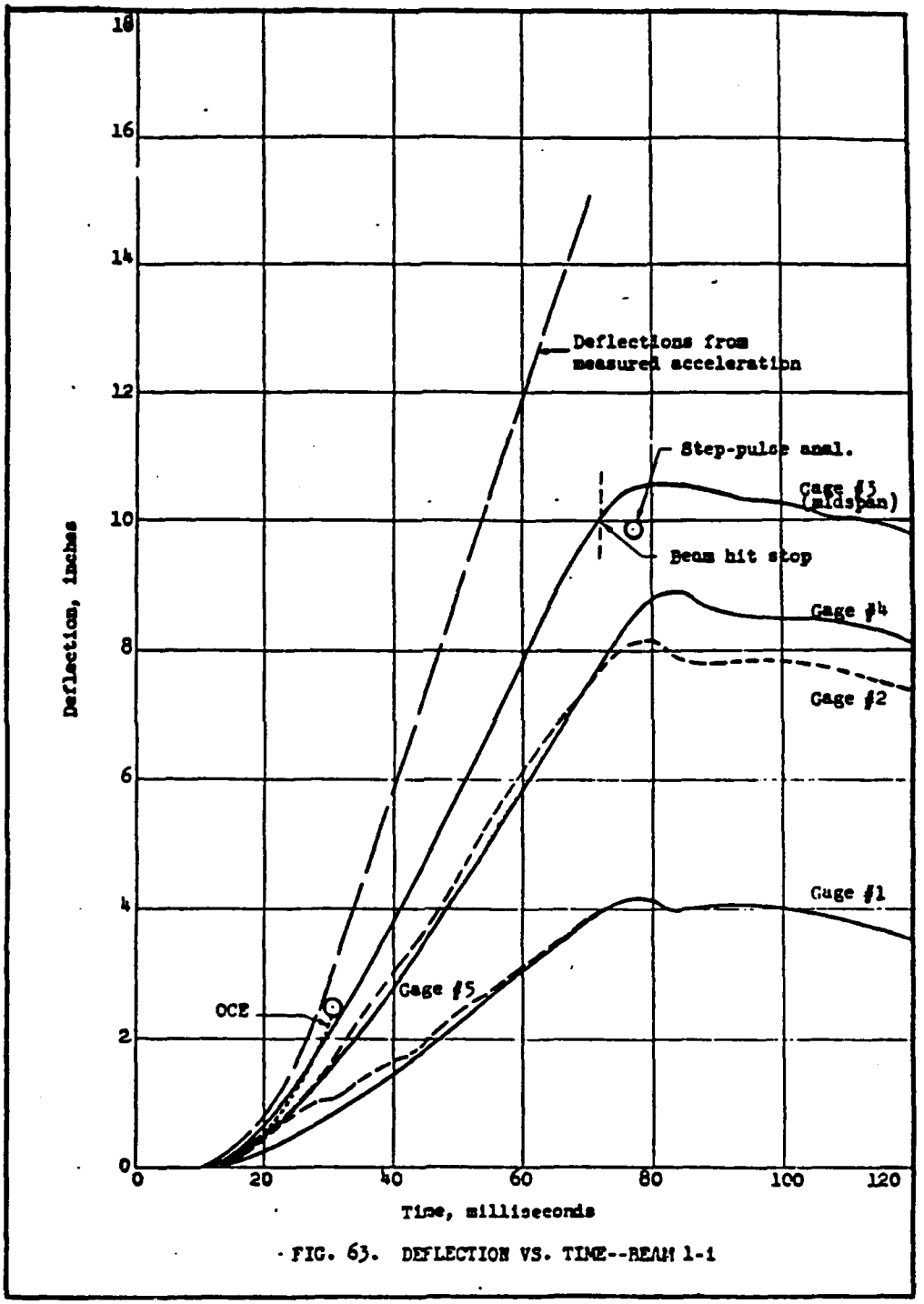

FIG. 63. DEFLECTION VS. TIME--BEAM I-1

Figure C-22. Experimental Displacement Versus Time for Beam I-1. (Reference 77)

APPENDIX D

INPUT PROPERTIES AND RESULTS FOR ANALYSIS IN THE DYNAMIC DOMAIN - BLAST

TABLE D-1. PROPERTIES OF WALLS ANALYZED DYNAMICALLY

Wall[a]	f'_c psi (Mpa)	ρ %	ρ' %
I-1	4951. (34.14)	1.00	1.00
I-2	4951. (34.14)	0.50	0.50
I-6	5547. (38.25)	0.25	0.25

[a] All Walls h = 12.6 in. (32 cm.), d = 11.6 in. (29.5 cm.)
L = 65. in. (165. cm), b = 158. in. (400. cm.)
Web Reinforcement : #3 @ 4 in. (ϕ10 @ 10 cm.)

TABLE D-2 PROPERTIES OF FLEXURAL REINFORCEMENT FOR WALLS

Wall	Size and Spacing	f_y ksi (Mpa)	ε_y %	ε_{sh} %	f_u ksi (Mpa)	ε_u %
I-1	30 #7 @ 5.25 (ϕ19 @ 10)	71.46 (492.7)	0.25	——	——— (———)	——
I-2	30 #5 @ 5.25 (ϕ13 @ 9)	73.29 (505.3)	0.26	——	115.0 (793.2)	——
I-6	15 #5 @ 5.25 (ϕ13 @ 18)	73.29 (505.3)	0.26	——	115.0 (793.2)	——

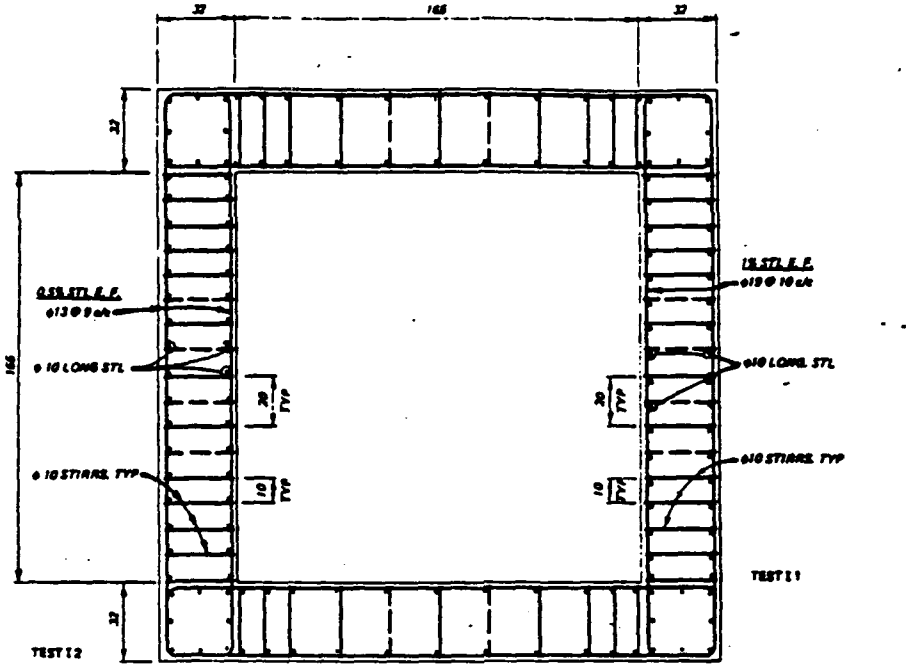

Figure D-1. Reinforcement Details for Walls I-1 and I-2. (Reference 78)

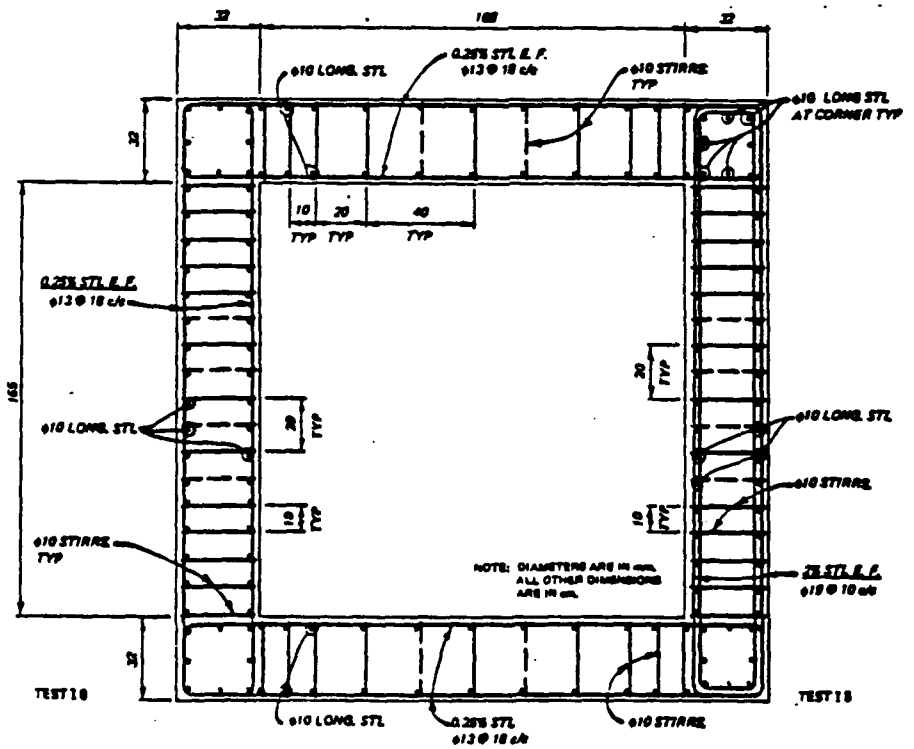

Figure D-2. Reinforcement Details for Wall I-6. (Reference 78)

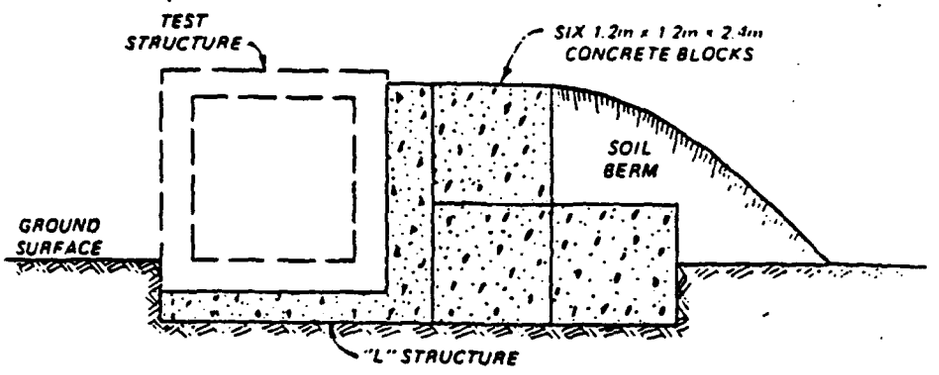

Figure D-3. Arrangement of the Reaction Structure. (Reference 78)

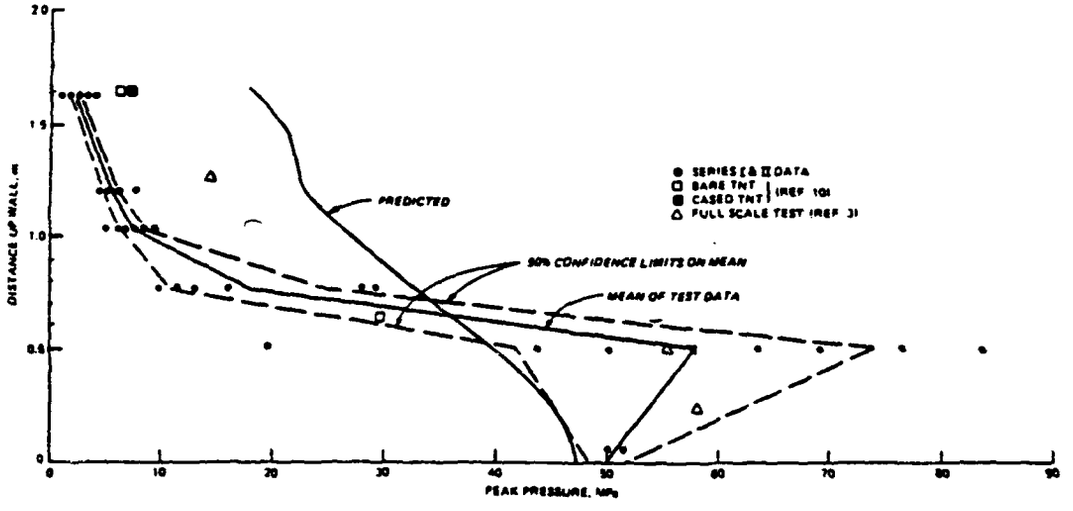

Figure D-4. Peak Pressure Along Wall Height. (Reference 78)

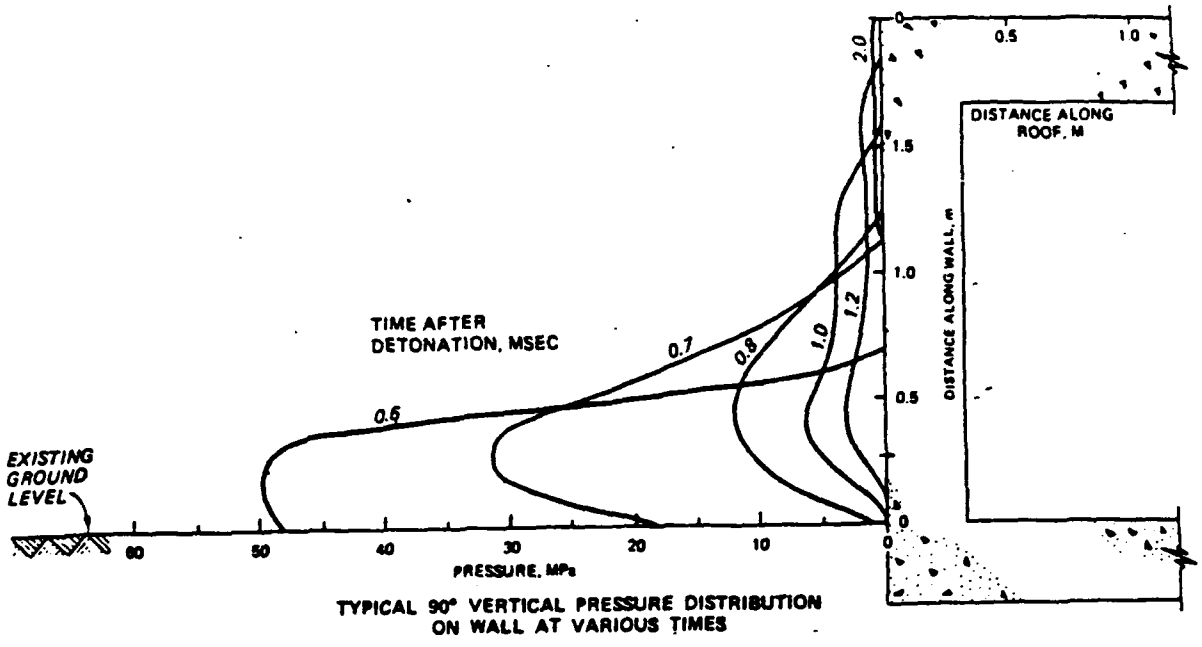

TYPICAL 90° VERTICAL PRESSURE DISTRIBUTION
ON WALL AT VARIOUS TIMES

Figure D-5. Pressure Distribution Along Wall Height at Various Times. (Reference 78)

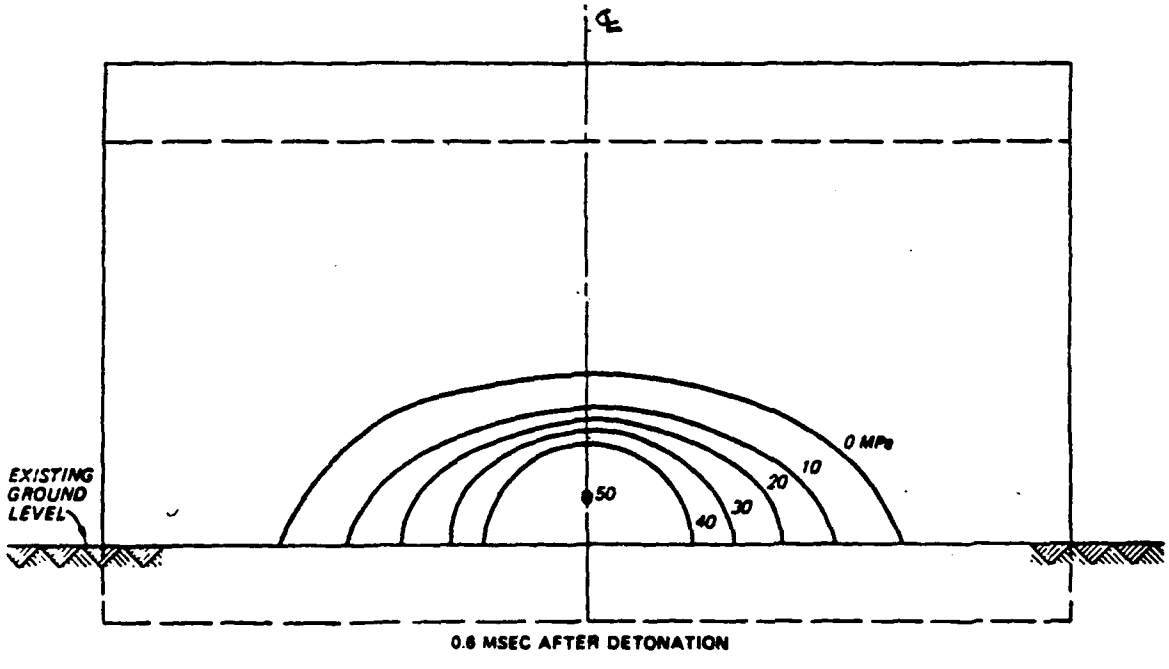

0.6 MSEC AFTER DETONATION

Figure D-6. Spatial Distribution of Pressure Early in Time. (Reference 78)

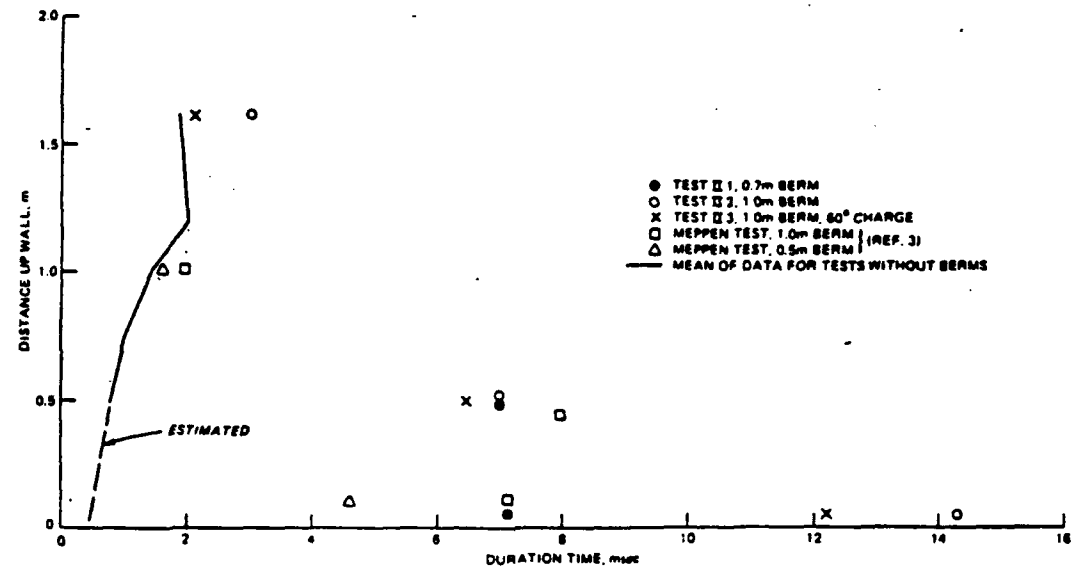

Figure D-7. Duration of Positive Pressure Along Wall Height. (Reference 78)

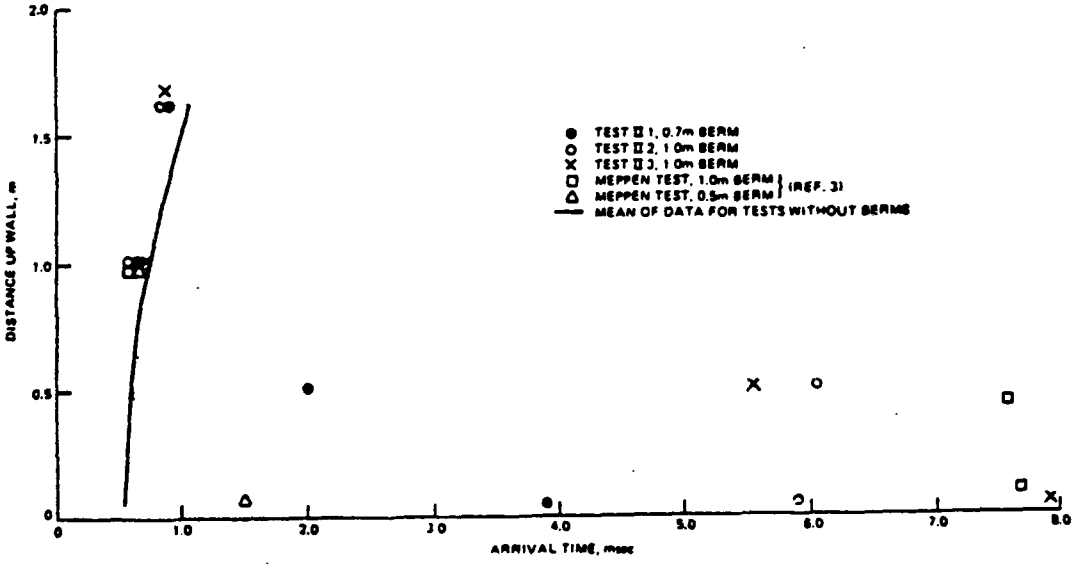

Figure D-8. Time of Arrival Along Wall Height. (Reference 78)

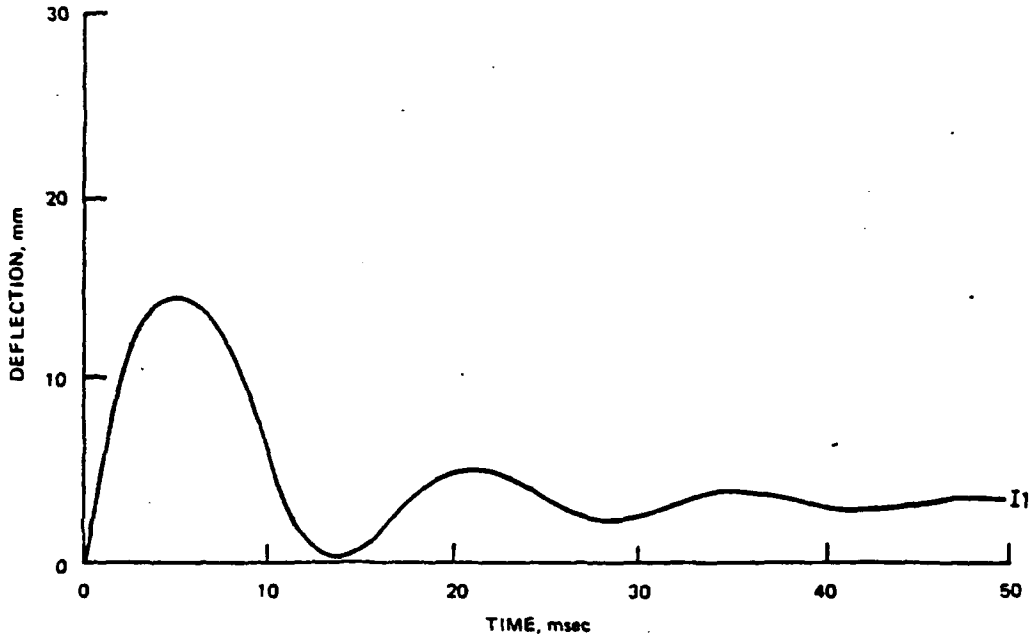

Figure D-9. Experimental Midspan Displacement for Wall I-1. (Reference 78)

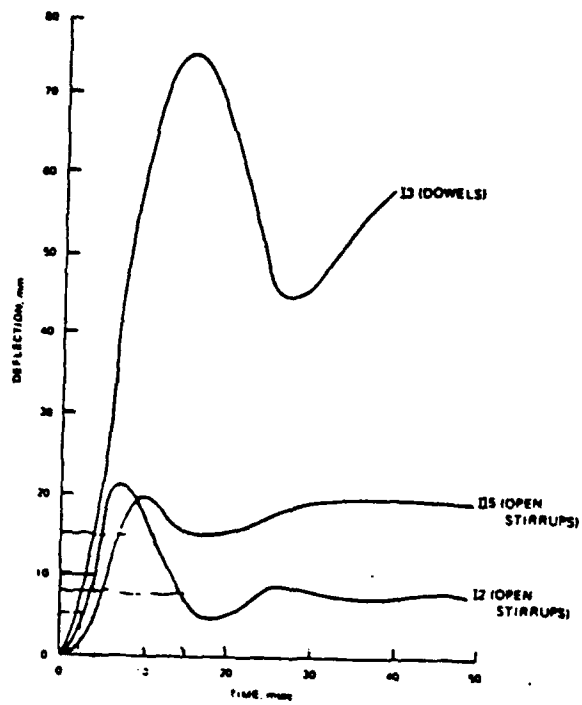

Figure D-10. Experimental Midspan Displacement for Wall I-2 (Reference 78)

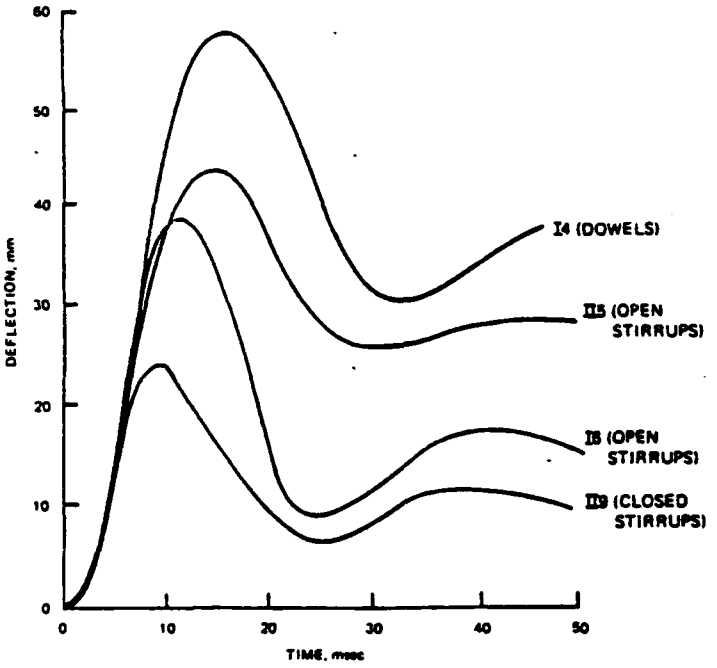

Figure D.11. Experimental Midspan Displacement for Wall I-6 (Reference 78)

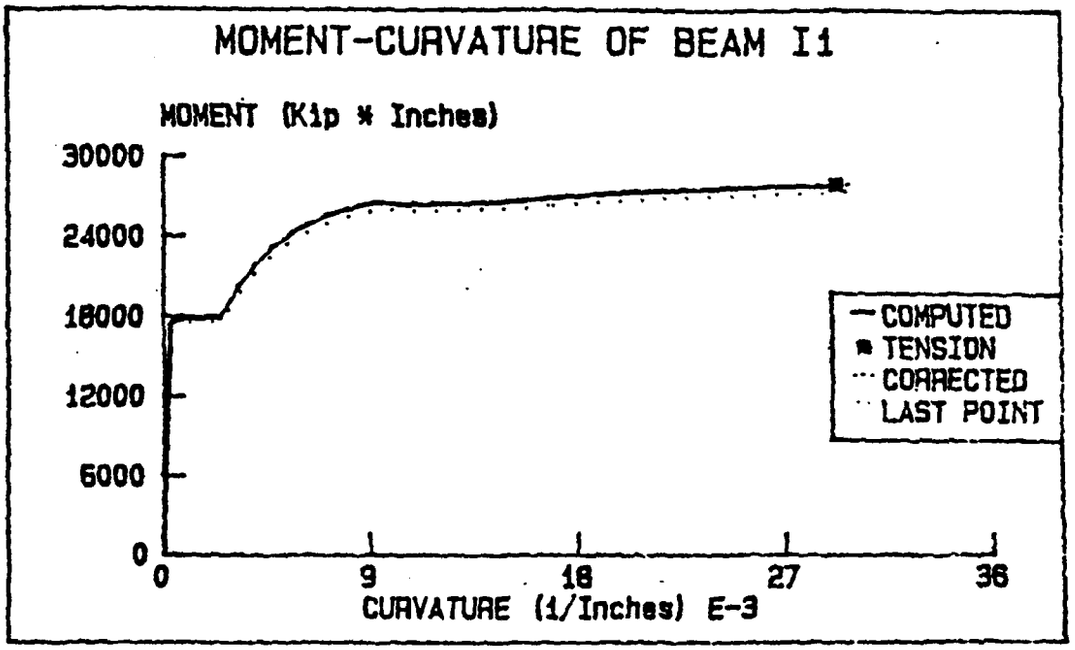

Figure D-12. Moment-Curvature Relationship for Wall I-1.

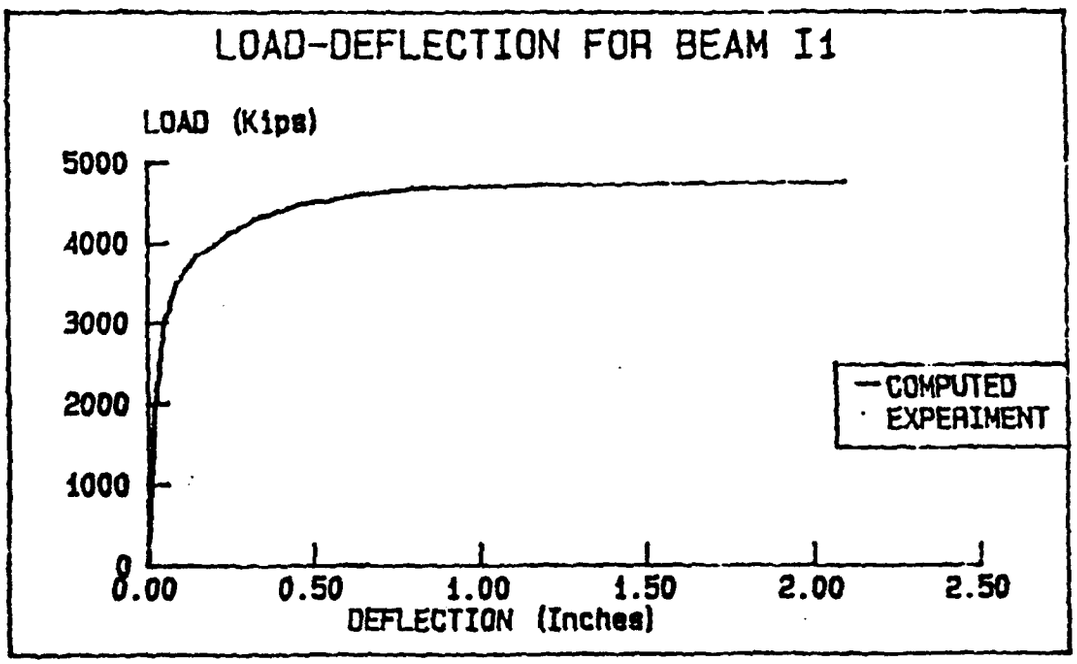

Figure D-13 Load-Deflection Relationship for Wall I-1.

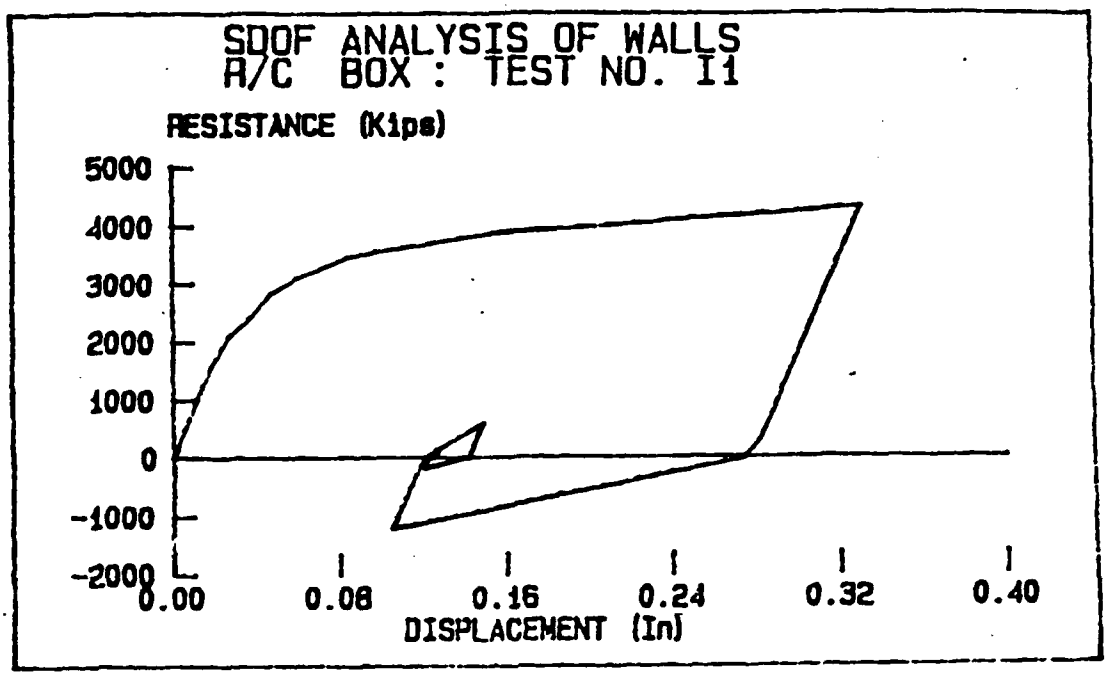

Figure D-14. Resistance-Displacement Relationship for Wall I-1.

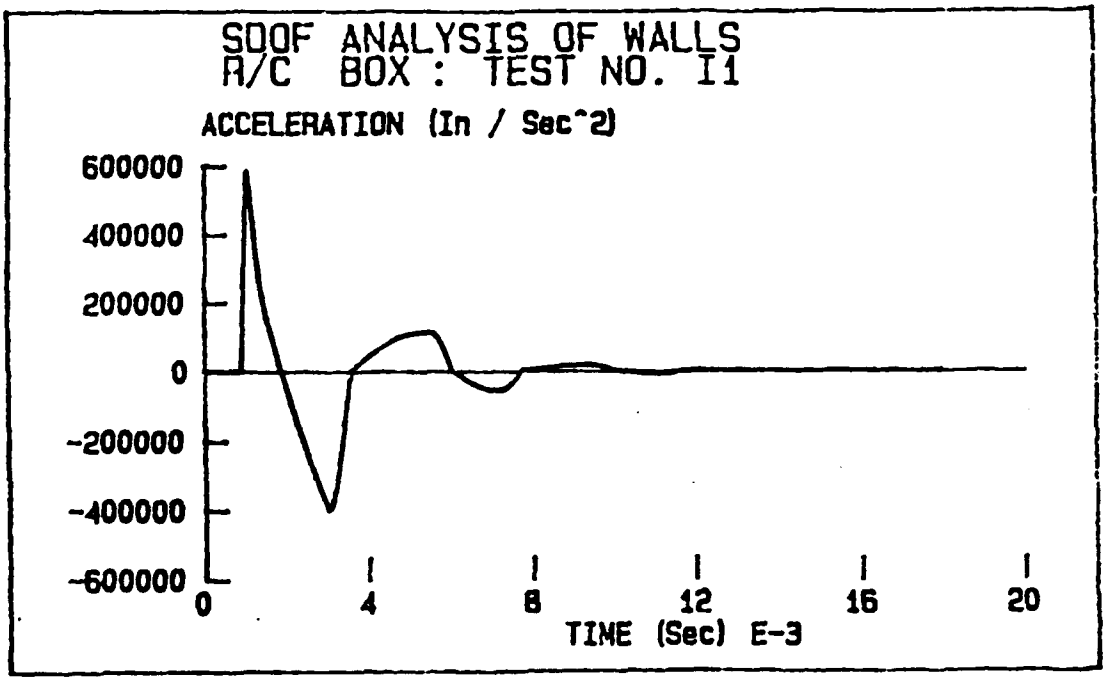

Figure D-15. Acceleration Versus Time for Wall I-1.

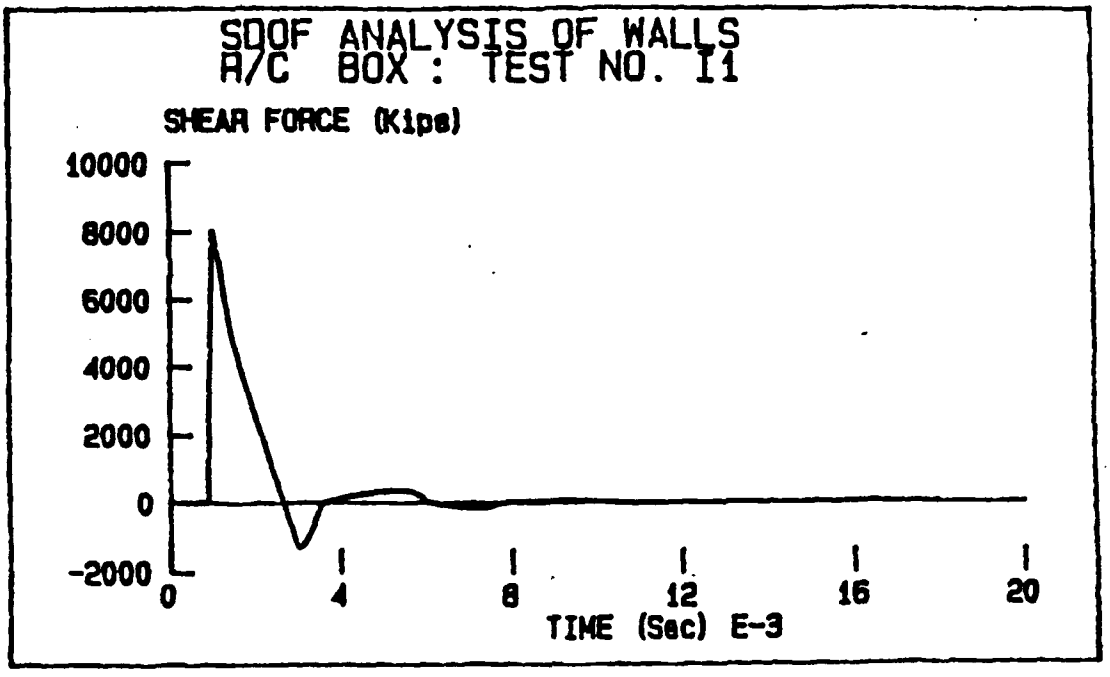

Figure D-16. Base Shear Force Versus Time for Wall I-1.

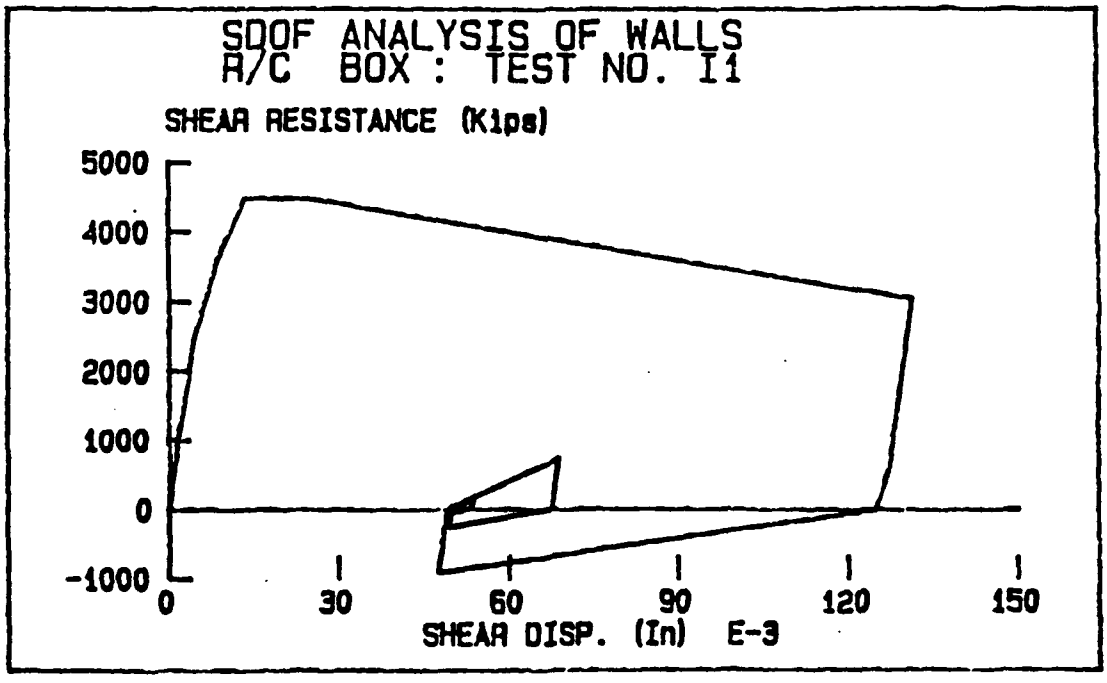

Figure D-17. Base Shear Resistance-Displacement for Wall I-1

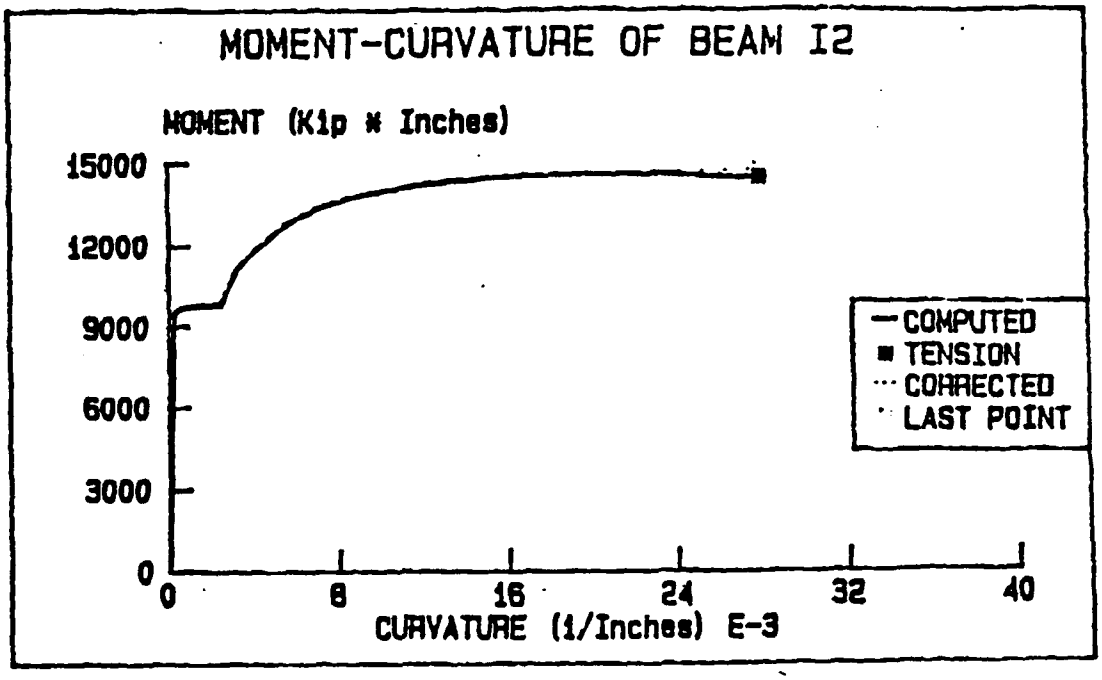

Figure D-18. Moment-Curvature Relationship for Wall I-2

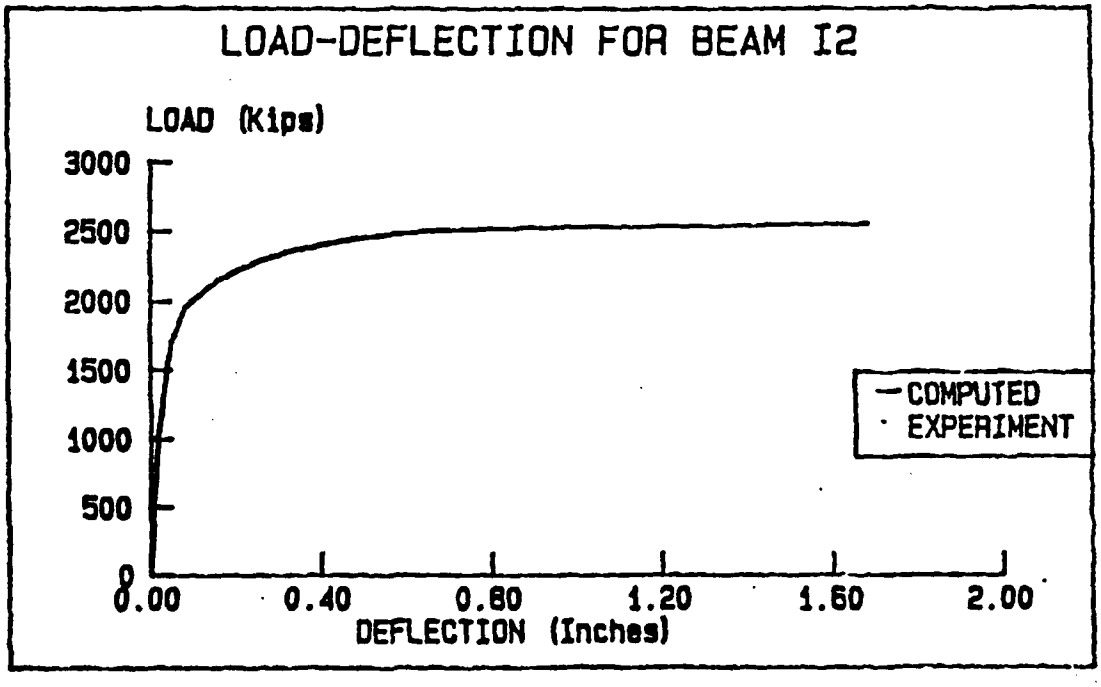

Figure D-19. Load-Deflection Relationship for Wall I-2.

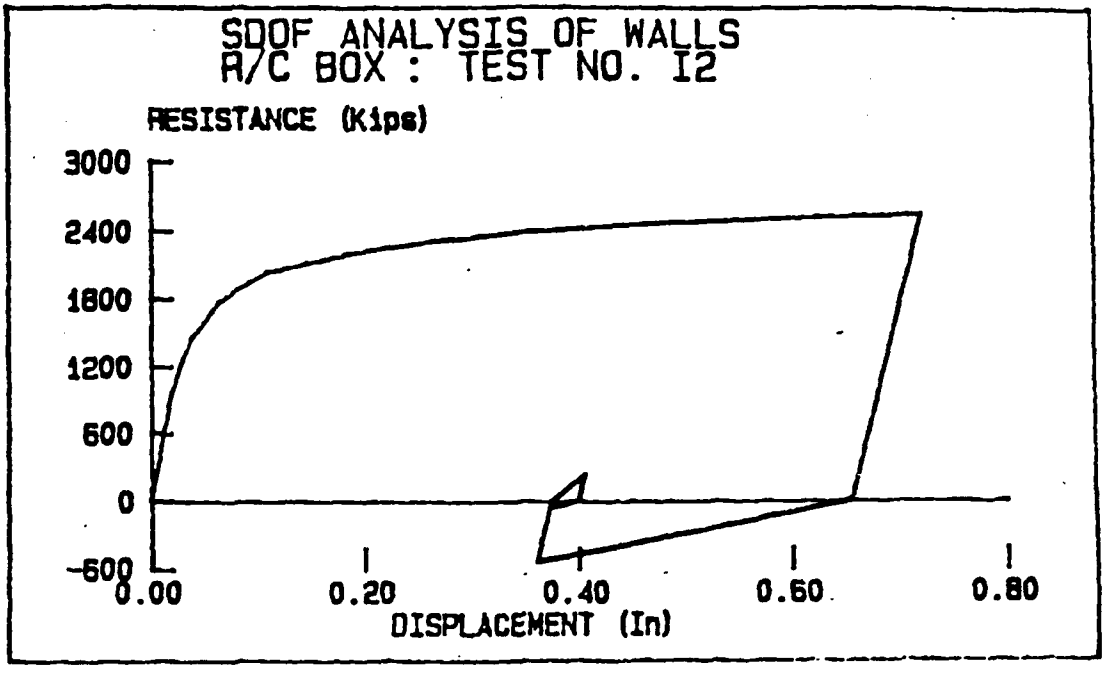

Figure D-20. Resistance-Displacement Relationship for Wall I-2.

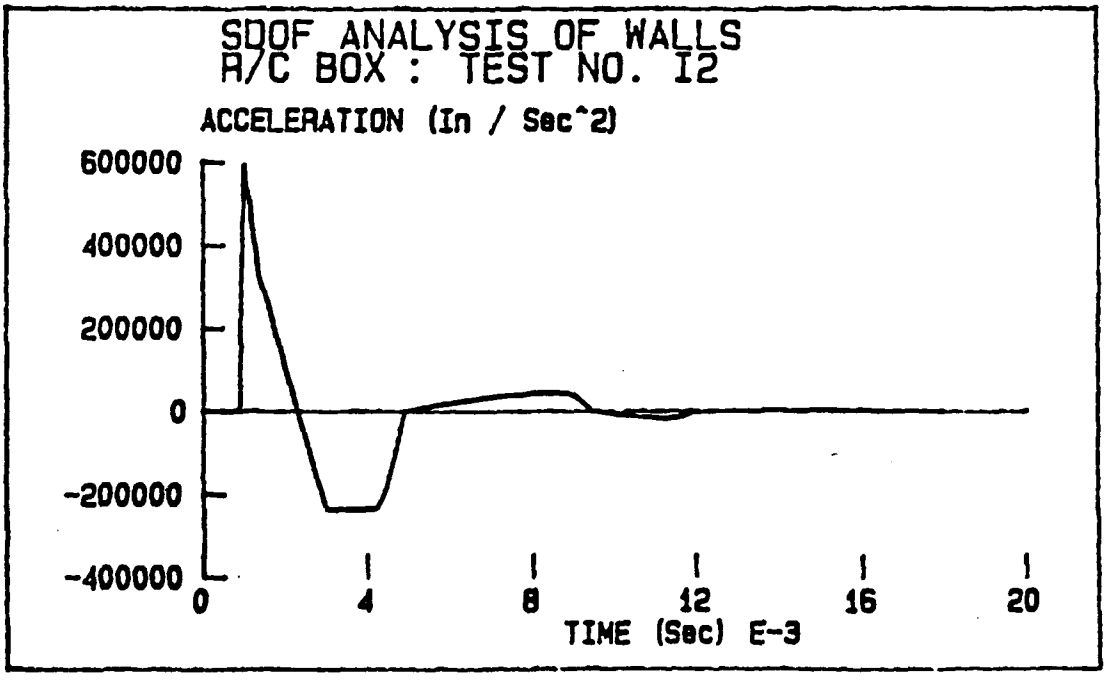

Figure D-21. Acceleration Versus Time for Wall I-2.

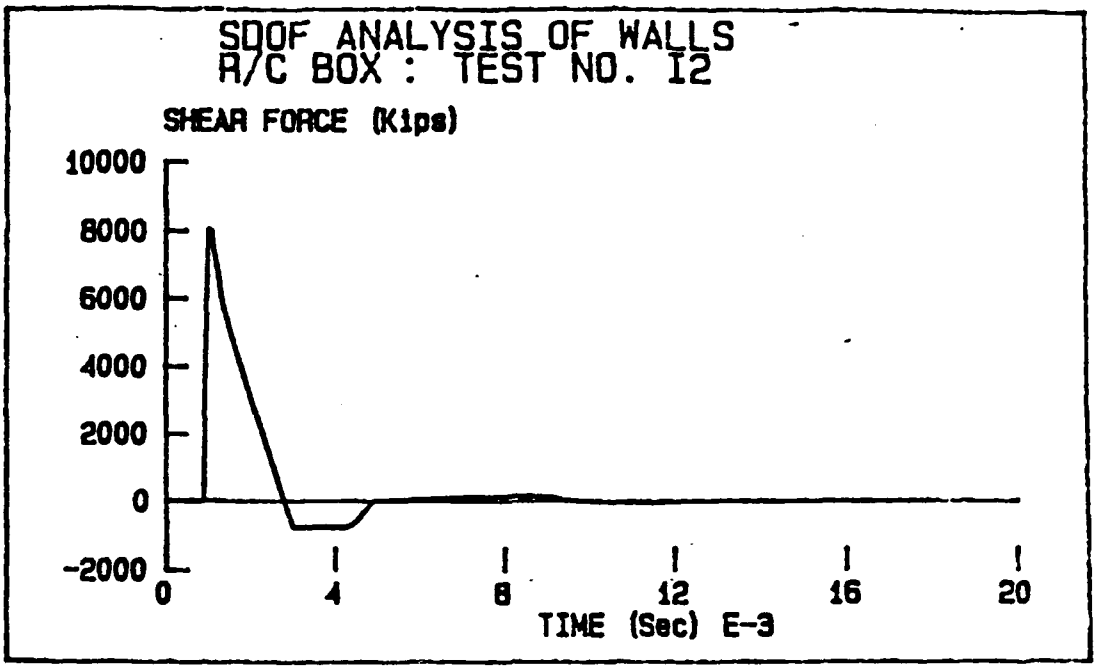

Figure D-22. Base Shear Force Versus Time for Wall I-2.

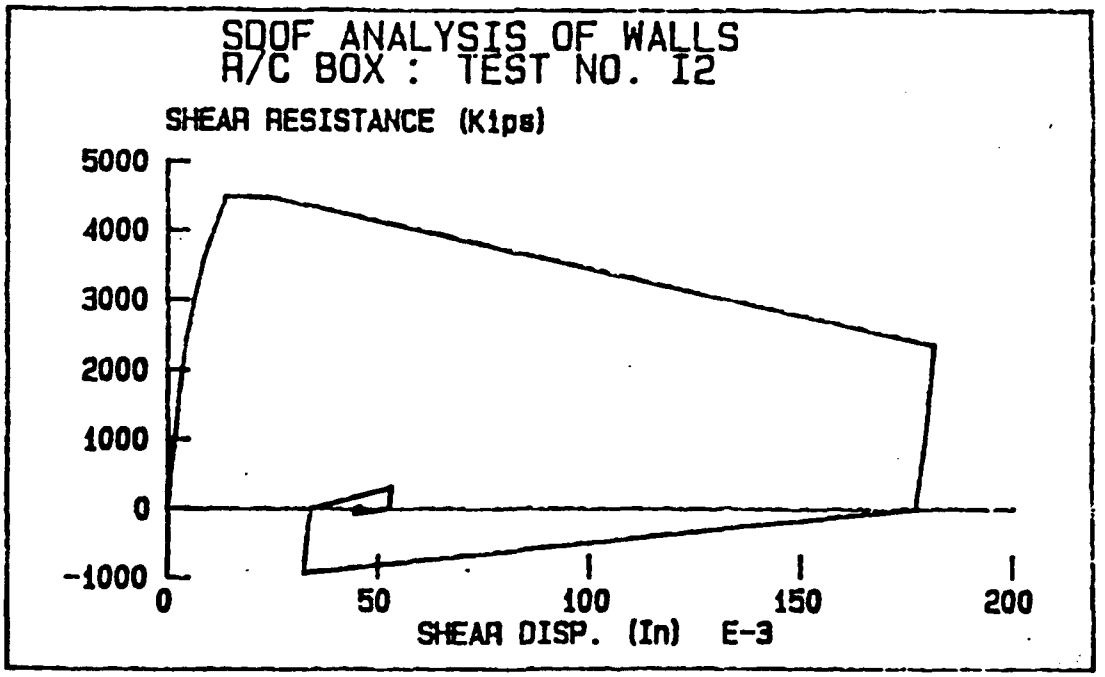

Figure D-23. Base Shear Resistance-Displacement for Wall I-2.

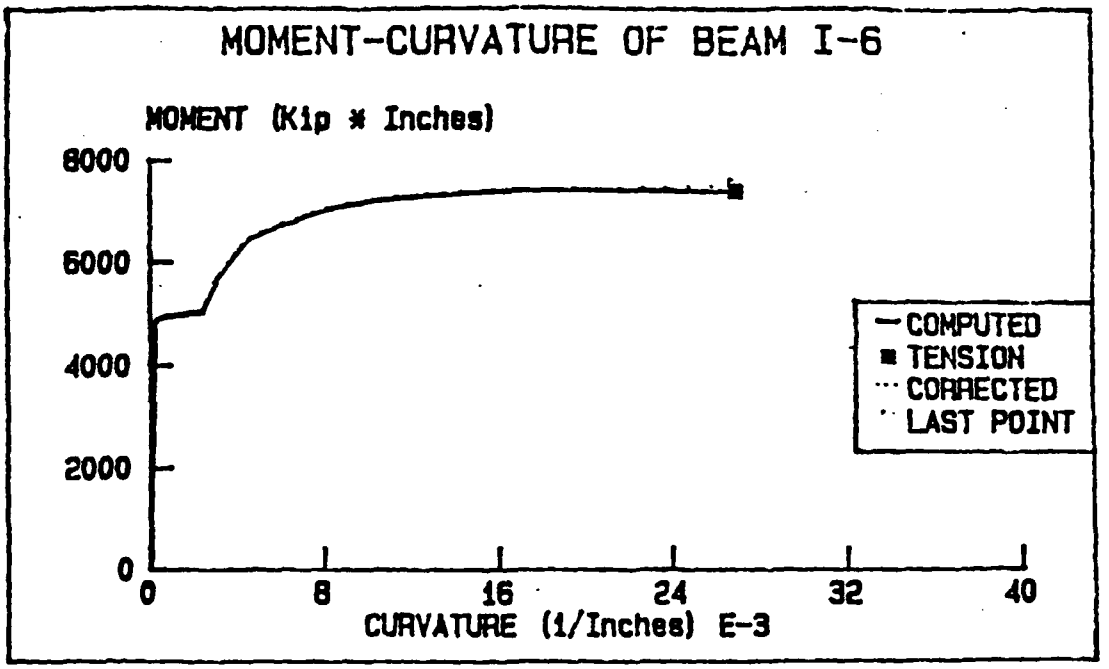

Figure D-24. Moment-Curvature Relationship for Wall I-6.

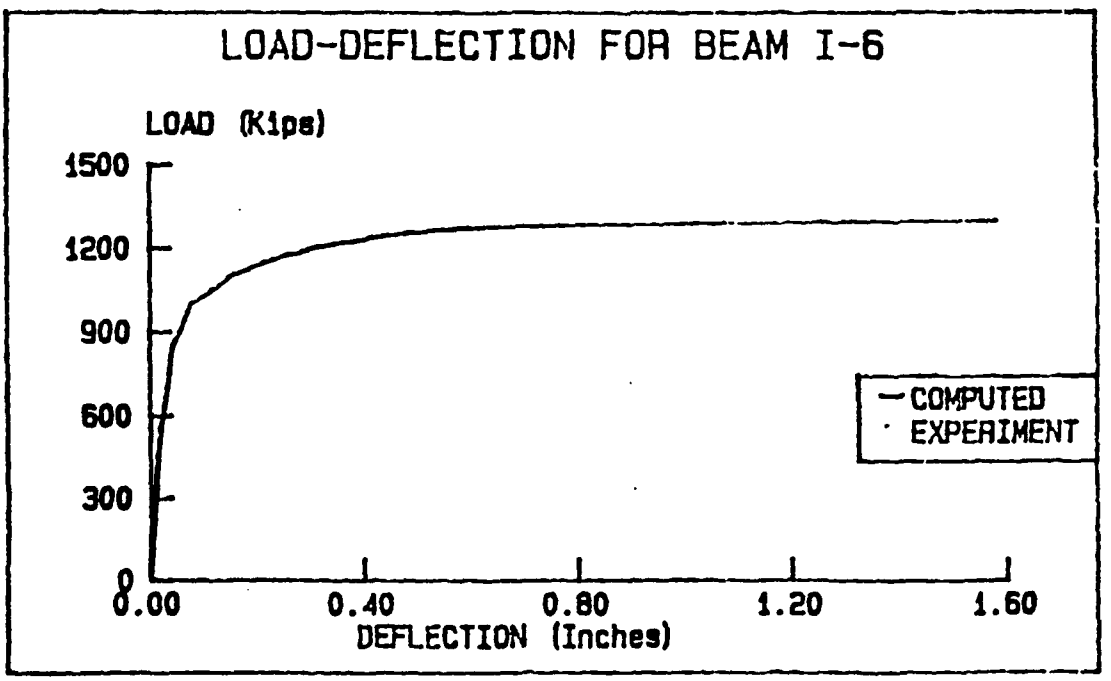

Figure D-25. Load-Deflection Relationship for Wall I-6.

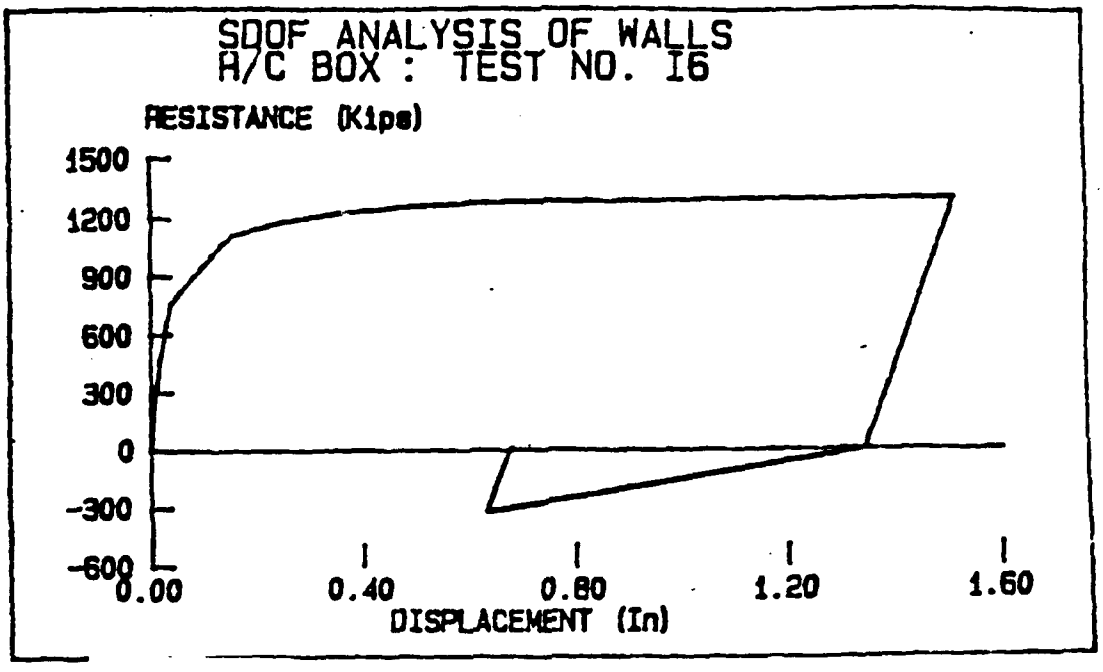

Figure D-26. Resistance-Displacement Relationship for Wall I-6.

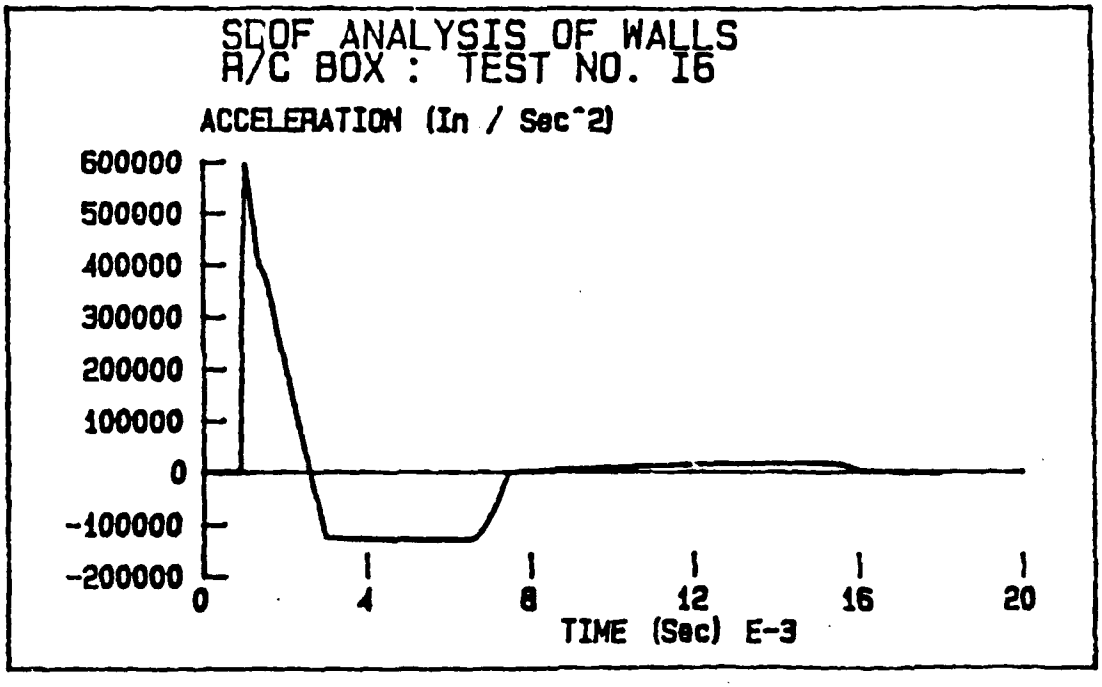

Figure D-27. Acceleration Versus Time for Wall I-6.

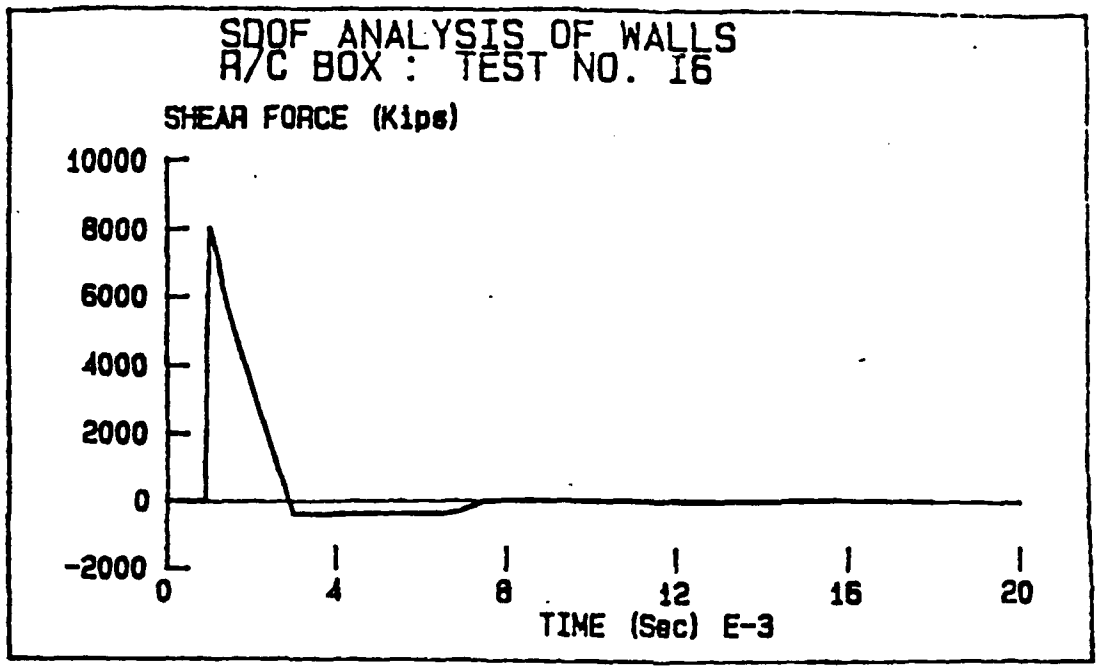

Figure D-28. Base Shear Force Versus Time for Wall I-6.

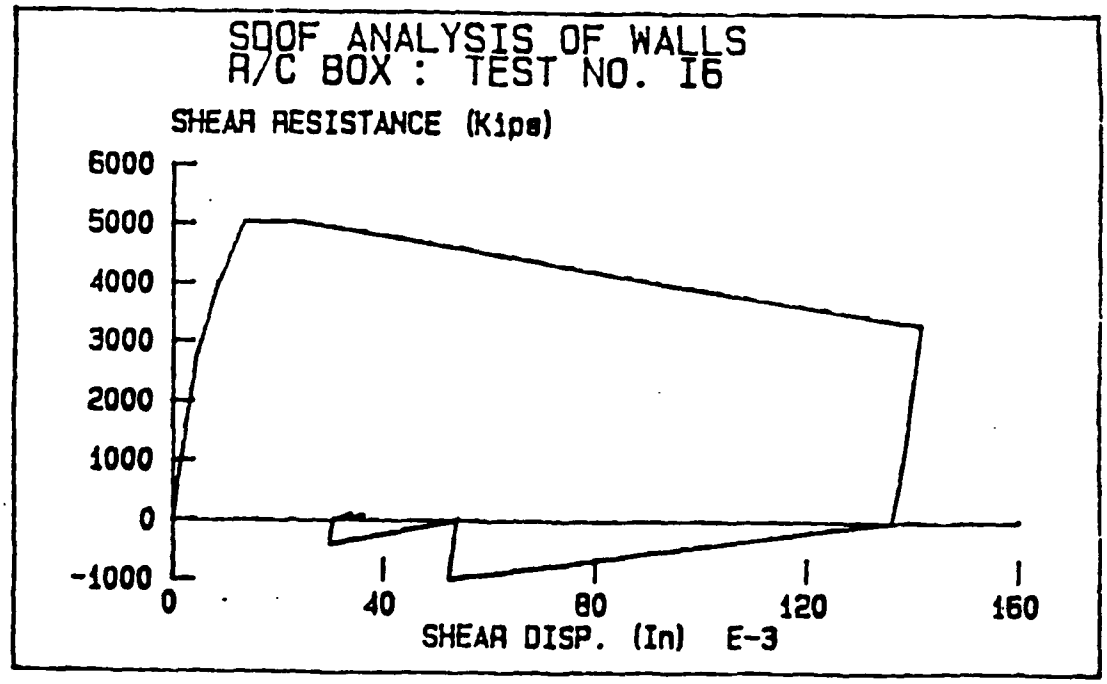

Figure D-29. Base Shear Resistance-Displacement for Wall I-6

(The reverse of this page is blank.)